University of Alberta

Monochloramine penetration in biofilms and nitrification detection in a model chloraminated water distribution system

by

Chun Lu

A thesis submitted to the Faculty of Graduate Studies and Research
in partial fulfillment of the requirements for the degree of

Doctor of Philosophy

Department of Civil and Environmental Engineering

Edmonton, Alberta
Fall 2008

Library and Archives Canada

Published Heritage Branch

395 Wellington Street
Ottawa ON K1A 0N4
Canada

Bibliothèque et Archives Canada

Direction du Patrimoine de l'édition

395, rue Wellington
Ottawa ON K1A 0N4
Canada

Your file Votre référence
ISBN: 978-0-494-46368-0
Our file Notre référence
ISBN: 978-0-494-46368-0

NOTICE:
The author has granted a non-exclusive license allowing Library and Archives Canada to reproduce, publish, archive, preserve, conserve, communicate to the public by telecommunication or on the Internet, loan, distribute and sell theses worldwide, for commercial or non-commercial purposes, in microform, paper, electronic and/or any other formats.

The author retains copyright ownership and moral rights in this thesis. Neither the thesis nor substantial extracts from it may be printed or otherwise reproduced without the author's permission.

AVIS:
L'auteur a accordé une licence non exclusive permettant à la Bibliothèque et Archives Canada de reproduire, publier, archiver, sauvegarder, conserver, transmettre au public par télécommunication ou par l'Internet, prêter, distribuer et vendre des thèses partout dans le monde, à des fins commerciales ou autres, sur support microforme, papier, électronique et/ou autres formats.

L'auteur conserve la propriété du droit d'auteur et des droits moraux qui protège cette thèse. Ni la thèse ni des extraits substantiels de celle-ci ne doivent être imprimés ou autrement reproduits sans son autorisation.

In compliance with the Canadian Privacy Act some supporting forms may have been removed from this thesis.

While these forms may be included in the document page count, their removal does not represent any loss of content from the thesis.

Conformément à la loi canadienne sur la protection de la vie privée, quelques formulaires secondaires ont été enlevés de cette thèse.

Bien que ces formulaires aient inclus dans la pagination, il n'y aura aucun contenu manquant.

Canada

Abstract

Water quality deterioration due to nitrification occurrence in distribution systems has been challenging water utilities using chloramination for disinfection. The growth of nitrifying microorganisms embedded in biofilms in chloraminated water distribution systems (CWDSs) has been blamed for this phenomenon. The objective of this dissertation was to study NH_2Cl penetration in biofilms and nitrification detection in CWDSs by using microelectrodes.

Based on voltammetric experiments, microelectrodes applicable to NH_2Cl measurements were developed. Under polarization potential at -90 mV (vs Ag/AgCl) and pH at neutral, the microelectrodes displayed linear responses to changes of NH_2Cl concentration within ranges (from 0 to 28.0 mg/L as Cl_2) tested. NH_2Cl diffusion coefficient was determined to be 1.7×10^{-6} cm^2/s, which, later in combination with use of NH_2Cl microelectrode, helped make estimations on NH_2Cl flux into biofilms.

Inactivation of NH_2Cl against biofilm microorganisms was investigated using the NH_2Cl microelectrode with focus on the penetration process of NH_2Cl in biofilms grown on different substratum materials including concrete, polyvinylchloride and polycarbonate. It was found that contact time, NH_2Cl concentration and substratum material all could affect NH_2Cl penetration process in biofilms, and thus in turn affected its inactivation process against biofilm microorganisms.

Biofilm tests using microelectrodes to measure oxygen, ammonium, nitrate and pH in biofilms were implemented. This approach was found promising in providing a potential application in nitrification detection in CWDSs. Actively ongoing nitrification was detected by this approach when water nitrite was as low as 0.02 mg-N/L. This

indicates that, compared with 0.05 mg NO_2^--N/L, the often adopted threshold for confirmation of nitrification occurrence in CWDSs, a lower nitrite threshold probably should be proposed in terms of its use in early detection of nitrification in CWDSs.

Microscopic observations on artificial biofilm and oxygen microelectrode measurements on natural biofilms both disclosed that microelectrode tip penetration facilitated mass diffusion in biofilms. This explains why oxygen concentrations in biofilms are sometimes overestimated using microelectrodes in comparison with non-invasive techniques. This study indicates that precaution is needed in dealing with microelectrode fabrication, experimental design, as well as collection, alignment and interpretation of data from microelectrode measurements in biofilms.

Acknowledgements

I would like to express my great gratitude to my supervisors, Dr. Tong Yu and Dr. Daniel W. Smith, without whose academic and financial supports, this dissertation would have been impossible. I also would like to thank Dr. Phillip M. Fedorak, who served as a member of my supervisory committee, for his invaluable advice throughout the dissertation research.

I am grateful to other three professors, Dr. Paul L. Bishop, Dr. Mark R. Loewen and Dr. Stephen A. Craik, who served as members of the final oral examining committee for my dissertation. Their critiques and suggestions are greatly appreciated.

I would especially like to thank the following peoples for their kindness and great help provided to me in the course of implementing this research. Dr. Jingli Luo and Dr. Liang Li of the Department of Chemical & Material Engineering allowed me to use their laboratory to conduct voltammetric experiments. Dr. Octavian Catuneanu and Dr. Ahmed Khidir in the Department of Earth and Atmospheric Sciences and Mr. Rakesh Bhatnagar and Mr. Jack Scott in the Department of Biological Sciences provided me great chances in their laboratories to implement the investigation into the impacts of microsensor tip penetration in biofilms. Mr. Glen Thomas of the Department of Mechanical Engineering saved me a lot of time by loaning me some critical instrument of their laboratory when ours was down and waiting for repair work. Ms. Kathy Semple of the Department of Biological Sciences, Ms. Katarina Pintar and Dr. Robin Slawson of the University of Waterloo gave me very helpful suggestions on MPN tests on nitrifying microorganisms and shared their experience in this particular area.

I would also like to thank staffs and my colleagues in our department, Maria

Demeter, Garry Solonyko, Nick Chernuka, Stefaniya Pavlyshyn, Andrea Fragata, Zhongwei Cheng, Shuying Tan and Mathrani Mukesh. Their kind help made the process of implementing the research project in this department go successfully.

I want to acknowledge the funding sources for my research: the Natural Sciences and Engineering Research Council of Canada (NSERC) and the Canada Foundation for Innovation (CFI).

Finally, I would like to thank my family for their support and encouragement that accompanied me throughout my experience at University of Alberta.

TABLE OF CONTENTS

CHAPTER 1 INTRODUCTION 1

1.1 NITRIFICATION IN CWDSs 1
1.1.1 Aquatic chemistry of chloramines 2
1.1.2 Microbiological nitrification 5
1.1.3 Coupling of chloramination and microbiological nitrification in CWDSs 7
1.2 BIOFILM GROWTH IN CWDSs 7
1.3 MICROBIAL INACTIVATION OF NH_2CL IN BIOFILMS IN CWDSs 9
1.4 DETECTION OF NITRIFICATION IN CWDSs 13
1.5 MICROELECTRODE TECHNIQUES 16
1.6 OBJECTIVES AND OUTLINE OF THE DISSERTATION 19
1.7 REFERENCES 20

CHAPTER 2 MATERIALS AND METHODS 26

2.1 MICROELECTRODES FOR BIOFILM MEASUREMENTS 26
2.1.1 Potentiometric microelectrodes 26
2.1.2 Amperometric microelectrodes 35
2.2 MODEL WATER DISTRIBUTION SYSTEM FOR BIOFILM GROWTH 43
2.3 SET-UP FOR MICROELECTRODE MEASUREMENTS IN BIOFILMS 45
2.4 CHEMICAL AND MICROBIOLOGICAL ANALYSES 46
2.4.1 Chemical analyses 46
2.4.2 Microbiological analyses 47
2.5 REFERENCES 51

CHAPTER 3 DEVELOPMENT OF MICROELECTRODES FOR NH_2CL MEASUREMENTS 52

3.1 INTRODUCTION 52
3.2 MATERIALS AND METHODS 54
3.2.1 Voltammetric experiments 54
3.2.2 The separate microelectrode 56
3.2.3 The combined microelectrode 58
3.3 RESULTS AND DISCUSSIONS 62
3.3.1 Determination of polarization potential 62
3.3.2 Determination of diffusion coefficient 68
3.3.3 Performance of microelectrodes developed 69
3.4 CONCLUSIONS 76
3.5 REFERENCES 77

CHAPTER 4 PENETRATION AND MICROBIAL INACTIVATION OF NH_2CL IN BIOFILMS 78

4.1 Introduction 78
4.2 Materials and Methods 80
4.2.1 Biofilm cultivation 80
4.2.2 Microelectrode measurements in biofilms 81
4.2.3 HPC analyses of biofilms 82
4.2.4 Biofilm thickness estimation 83
4.3 Results and Discussions 83
4.3.1 NH_2Cl transient profiles in biofilms 83
4.3.2 HPC analyses of biofilms 91
4.4 Conclusions 92
4.5 References 93

CHAPTER 5 NITRIFICATION DETECTION USING MICROELECTRODES IN A MODEL CWDS 95

5.1 Introduction 95
5.2 Materials and Methods 97
5.2.1 Model CWDS 97
5.2.2 Biofilm samples 100
5.2.3 Microelectrode measurements in biofilms 100
5.2.4 Analyses of water and biofilm samples 101
5.3 Results and Discussions 102
5.3.1 Operating data of the model CWDS 102
5.3.2 Microbiological analyses 104
5.3.3 Microelectrode measurements in biofilms 105
5.3.4 Impact of biofilm slide material 114
5.4 Conclusions 116
5.5 References 117

CHAPTER 6 IMPACT OF THE PENETRATION OF MICROELECTRODE TIP IN BIOFILMS 120

6.1 Introduction 120
6.2 Materials and Methods 121
6.2.1 Artificial biofilm preparation 121
6.2.2 Set-up of microscopic observation 121
6.2.3 Microelectrode preparation for microscopic observation 122
6.2.4 Static imaging 122
6.2.5 Oxygen profile measurements in biofilm 123
6.3 Results and Discussions 124
6.3.1 Diffusion frontline in biofilm 124
6.3.2 Facilitated diffusion vs microelectrode measurement 127
6.3.3 Oxygen profiles measured in biofilm by microelectrode 130
6.4 Conclusions 136
6.5 References 137

CHAPTER 7 SUMMARY AND RECOMMENDATIONS 139
7.1 SUMMARY 139
7.2 RECOMMENDATIONS ON FUTURE STUDY 143
APPENDICES 144
APPENDIX A - DATA FOR FIGURES IN CHAPTER 2 145
APPENDIX B – DATA FOR FIGURES IN CHAPTER 3 150
APPENDIX C – DATA FOR FIGURES IN CHAPTER 4 183
APPENDIX D – DATA FOR FIGURES IN CHAPTER 5 192
APPENDIX E – DATA FOR FIGURES IN CHAPTER 6 197

LIST OF TABLES

Table 5-1 Biofilm growth conditions monitored using the effluent from the model system during a 1-year study period.....103

Table 6-1 Comparisons between diffusion distances of Rhodamine B 90% diffusion frontline in artificial biofilm with and without microelectrode tip insertion 127

Table 6-2 Comparisons between distances of the facilitated 90% diffusion frontline of Rhodamine B and microelectrode tip movement during its measurements in biofilms at different times 128

Table 6-3 Comparisons of theoretical and facilitated diffusion distances of DO 90% diffusion frontline, and distances of oxygen microelectrode movement during its measurements in biofilms 133

LIST OF FIGURES

Figure 1-1 Coupling of NH_2Cl decomposition and microbiological nitrification 8

Figure 2-1 Calibration curve of a pH microelectrode 33

Figure 2-2 Calibration curve of a nitrate microelectrode.....34

Figure 2-3 Calibration curve of an ammonium microelectrode.....34

Figure 2-4 Calibration curve of a combined oxygen microelectrode.....42

Figure 2-5 Calibration process for a combined oxygen microelectrode 42

Figure 2-6 Biofilm growth reactor used for simulating water distribution system 44

Figure 2-7 Set-up for microelectrode measurements in biofilms.....46

Figure 3-1 Schematic of a three-electrode cell (left) and electric circuit (right) for voltammetric experiment.....56

Figure 3-2 Schematic of a combined microelectrode for NH_2Cl measurement.....59

Figure 3-3 i-E curves for O_2-free NH_2Cl solutions under different pH values.....63

Figure 3-4 i-E curves for pH buffer solution, O_2-free NH_2Cl solution and NH_2Cl solution with DO at pH 3.8 64

Figure 3-5 i-E curves for pH buffer solution, O_2-free NH_2Cl solution and NH_2Cl solution with DO at pH 7.1 65

Figure 3-6 i-E curves for pH buffer solution, O_2-free NH_2Cl solution and NH_2Cl solution with DO at pH 10.1 66

Figure 3-7 i-E curves for O_2-free NH_2Cl solution at different scan rates with linear potential sweep 69

Figure 3-8 Calibration process of a separate microelectrode with continuous inputs of NH_2Cl solutions of seven concentrations (from zero up to 26.2 mg/L as Cl_2) into a flow cell 70

Figure 3-9 Calibration curves of a separate microelectrode using continuous inputs of NH_2Cl solutions of seven concentrations into a flow cell 70

Figure 3-10 Calibration curve of the same microelectrode tested in Figure 3-8 and 3-9 using the same calibration process with 10 days apart between these two tests 71

Figure 3-11 Calibration curve of a combined NH_2Cl microelectrode 74

Figure 4-1 NH_2Cl profiles in the bulk above NH_2Cl-sterilized slides of different materials without biofilm growth..... 84

Figure 4-2 NH_2Cl profile in the bulk above non-sterilized concrete slide without biofilm growth 85

Figure 4-3 Signal profiles of two NH_2Cl microelectrodes measured in bulk and biofilms grown on concrete slides under flowing distilled water condition 85

Figure 4-4 NH_2Cl profiles measured on a patchy biofilms grown on a concrete slide at different contact times 86

Figure 4-5 NH_2Cl profiles measured at a same spot of a patchy biofilm grown on a concrete slide at different contact times minutes 88

Figure 4-6 NH_2Cl profiles measured on a same spot of a patchy biofilm grown on a PVC slide at different contact times 89

Figure 4-7 NH_2Cl profiles measured at a same spot of a patchy biofilm grown on a PC slide at different contact times 90

Figure 5-1 Set-up of a model water distribution system for nitrifying biofilm growth ...98

Figure 5-2 Nitrate and nitrite monitoring data in the model system during a 1-year study period.....103

Figure 5-3 Planktonic nitrifying microorganisms (MPN) and HPC in the model system during the 1-year study period 104

Figure 5-4 Profiles of pH, DO, ammonium and nitrate measured in Biofilm I grown on a concrete slide. 107

Figure 5-5 Profiles of pH, DO, ammonium and nitrate measured in Biofilm II grown on a concrete slide.....109

Figure 5-6 Profiles of pH, DO, ammonium and nitrate measured in Biofilm III grown on a concrete slide 112

Figure 6-1 Microscopic observation of mass diffusion pattern of Rhodamine B in artificial biofilm with penetration of a microelectrode tip 126

Figure 6-2 Time serial microscopic observations of mass diffusion of Rhodamine B in artificial biofilm with penetration of a microelectrode tip 126

Figure 6-3 DO profiles measured under the same spot of a natural biofilm using microelectrode going toward the substratum and retreating back toward the biofilm surface. 131

Chapter 1

Introduction

The major objective of this dissertation research was to study monochloramine (NH_2Cl) penetration in biofilms to inactivate embedded microorganisms and nitrification detection in chloraminated water distribution systems (CWDSs) by using microelectrode techniques. In the drinking water industry, the purpose of adopting chloramination for disinfection is to prevent microbial regrowth in distribution systems, and meanwhile to reduce chlorine disinfection by-products (DBPs). However, episodes of nitrification outbreaks, and the accompanying water quality deterioration, have been observed after introduction of chloramination in many CWDSs. It has been believed that a major culprit behind this phenomenon is the growth of nitrifying microorganisms embedded in biofilms in CWDSs. This chapter reviews the aquatic chemistry of chloramines, microbiological nitrification, biofilm growth, microbial inactivation in biofilms, detection of nitrification occurrence in CWDSs, as well as microelectrode techniques that helped fulfill the objective of this research.

1.1 Nitrification in CWDSs

With increasing public concern on adverse health impacts of chlorine DBPs in drinking water, many utilities have shifted from chlorination to chloramination as secondary disinfection, because disinfection with NH_2Cl is generally believed to produce lower levels of trihalomethanes (THMs) than with free chlorine (Cotruvo, 1981). However, anecdotal occurrences of water quality deterioration with symptoms such as

increased nitrate (NO_3^-), loss of NH_2Cl residual, decreased pH, depleted dissolved oxygen (DO), increases in heterotrophic plate count (HPC) bacteria and total coliform-positive samples in the water have been reported by utilities after their changeover to chloramination (Ike *et al.*, 1988; Wolfe *et al.*, 1988, 1990; Cunliffe, 1991; Skadsen, 1993; Wilczak *et al.*, 1996; Lipponen *et al.*, 2002). It is estimated that in the US, two-thirds of medium and large chloraminating utilities have experienced the same problem (Wilczak *et al.*, 1996). It has been believed that biofilm development and nitrification occurrence in CWDSs attribute to this phenomenon. Some countermeasures have been suggested and practiced by utilities, such as increasing chlorine/ammonia-nitrogen (Cl/N) ratio to reduce excessive ammonia, introducing breakpoint chlorination, shortening system retention time (RT), and introducing a flushing program after observation of those deterioration symptoms. However, these countermeasures may only help in the short term. In other words, an episode of nitrification occurrence in CWDSs may be mitigated, but regarding the long-term effect, there is no satisfactory solution yet. Nitrification will occur again once conditions in CWDSs are favorable.

1.1.1 Aquatic chemistry of chloramines

CWDSs are more often reported than chlorinated ones to face water quality deterioration with symptoms mentioned above. Why? Studies have shown that the unique chemistry of chloramines is one of the major reasons. In a water treatment plant, chloramines are produced by adding free chlorine and ammonia simultaneously or sequentially in water with a certain Cl/N ratio. The reactions taking place in the water can be expressed as the following equations:

$$NH_3 + HOCl \longleftrightarrow NH_2Cl + H_2O \quad (1\text{-}1)$$

$$NH_2Cl + HOCl \longleftrightarrow NHCl_2 + H_2O \quad (1\text{-}2)$$

$$NHCl_2 + HOCl \longleftrightarrow NCl_3 + H_2O \quad (1\text{-}3)$$

Which one is dominant among the three forms, monochloramine (NH_2Cl), dichloramine ($NHCl_2$) and trichloramine (NCl_3), depends on Cl/N ratio, chlorine dose, temperature, alkalinity, and pH. Under typical water treatment conditions, a high Cl/N ratio (e.g. above 5:1 by weight) will result in the formations of all three forms. $NHCl_2$ and NCl_3 are odorous compounds; and for microorganism reduction purpose, NH_2Cl is the desired dominant form as residual chlorine in the distribution system. Therefore, a lower Cl/N ratio (e.g. 3:1 by weight) is usually carefully controlled by utilities. However, the low Cl/N ratio leads to free ammonia in excess in the water, which may become a potential energy source available to ammonia-oxidizing microorganisms (AOM), if any, in CWDSs. Typical NH_2Cl residual for good protection ranges from approximately 1 to 4 mg/L as Cl_2. The US Environmental Protection Agency (USEPA) has promulgated a maximum contaminant level (MCL) for NH_2Cl in drinking water at 4 mg/L as Cl_2.

Although generally believed to be less reactive chemically than free chlorine, NH_2Cl is actually inherently unstable (Valentine *et al.*, 1998). After its application in water, NH_2Cl automatically goes through a complex set of reactions, which accelerates NH_2Cl decomposition and decrease of its microorganism reduction efficacy. The complex aquatic chemistry of NH_2Cl is not fully understood yet, but its auto-decomposition may be expressed using the following two equations showing the overall net stoichiometries (Valentine *et al.*, 1998):

$$4NH_2Cl + 3H_2O \longrightarrow 4Cl^- + 3NH_3 + NO_3^- + 5H^+ \quad (1\text{-}4)$$

$$3NH_2Cl \longrightarrow N_2 + NH_3 + 3Cl^- + 3H^+ \quad (1\text{-}5)$$

It is believed that these are two parallel reaction pathways, and which one is dominant depends on the specific conditions in a given water system.

NH_2Cl also reacts with some co-existing compounds in water. This makes the NH_2Cl concentration decrease even more quickly. It has been found that nitrite (NO_2^-) could increase the rate of NH_2Cl decomposition and thus its loss in water (Leung, 1989; Valentine *et al.*, 1998). Valentine *et al.* (1998) also reported that the presences of bromide and natural organic matter in water might change the product speciation of NH_2Cl decomposition. With the presence of natural organic matter, ammonia is the predominant N-containing product, whereas in the absence of natural organic matter, the primary N-containing decay products are ammonia, nitrogen gas and nitrate, with the first two compounds as the dominant products. Margerum *et al.* (1994) suggested a series of reactions of NH_2Cl oxidation with nitrite as expressed in the following equations:

$$H^+ + NH_2Cl + NO_2^- \longleftrightarrow NH_3 + NO_2Cl \quad (1\text{-}6)$$

$$NO_2Cl + NO_2^- \longleftrightarrow N_2O_4 + Cl^- \quad (1\text{-}7)$$

$$N_2O_4 + OH^- \longrightarrow NO_3^- + NO_2^- + H^+ \quad (1\text{-}8)$$

$$NO_2Cl \longleftrightarrow NO_2^+ + Cl^- \quad (1\text{-}9)$$

$$NO_2^+ + OH^- \longrightarrow NO_3^- + H^+ \quad (1\text{-}10)$$

Consequently, due to the way NH_2Cl is generated in a water plant (i.e. low Cl/N ratio) and the unique chemical properties of NH_2Cl (i.e. auto-decay and ready reactions with nitrite and natural organic matter), adoption of chloramination makes water distribution systems face a troublesome situation – excess of ammonia in the water.

1.1.2 Microbiological nitrification

Microbiological nitrification is a two-step process carried out mainly by two distinct groups of autotrophs, although some heterotrophs and even fungi (Guest and Smith, 2002) have also been reported to be capable of nitrification. These autotrophs get energy from the oxidation of reduced forms of inorganic nitrogen (ammonia and nitrite) and derive most of their cell carbon by reducing carbon dioxide.

The first step of microbiological nitrification is the oxidation of ammonia to nitrite accomplished by AOM that in water environment mainly consists of *Nitrosomonas,* although other genus such as *Nitrosococcus* and *Nitrosospira* are also reported to be present (Koops and Pommerening-Roser, 2001). AOM can take energy from the oxidation process of ammonia with the reaction expressed as

$$NH_4^+ + 1.5O_2 \rightarrow NO_2^- + H_2O + 2H^+ \qquad (1\text{-}11)$$

The second step is the oxidation of nitrite to nitrate by nitrite-oxidizing microorganisms (NOM) that mainly includes members of the genus *Nitrobacter*, although other genus such as *Nitrospira* is also reported to have the same function (Koops and Pommerening-Roser, 2001). The reaction is expressed as

$$NO_2^- + 0.5O_2 \rightarrow NO_3^- \qquad (1\text{-}12)$$

As reflected in Equation (1-11), nitrification leads to pH decrease in a poorly-buffered water due to the production of protons. Decrease in DO in water systems results as nitrification occurs because a significant amount of oxygen is used in the conversion of ammonia to nitrate via nitrite as illustrated in Equation (1-11) and Equation (1-12). From a stoichiometric standpoint, 3 to 4 mg/L of oxygen will be consumed during nitrification of 1 mg/L of ammonia (the exact amount of oxygen depends on how

complete nitrification is in the system). Odell *et al.* (1996) reported that most distribution systems in their survey that experienced nitrification had less than 1 mg/L of ammonia-nitrogen, and nitrification consumed at least 2 mg/L of DO. Utilities with lower DO concentrations in their distribution systems may have less potential for nitrification to occur.

AOM are obligate aerobes and grow slowly with doubling times that can be as long as several days. They grow best when they are in the dark, at a warm temperature (25 to 28°C), pH ranging from 7.5 to 8.5, extended RT and with the presence of free ammonia (Watson *et al.*, 1981; White, 1999). AOM secrete a variety of organic compounds that can enhance the growth of heterotrophs (Watson *et al.*, 1981; Negrin *et al.*, 1990). NOM generally exist in a narrower range of temperature and pH values and have higher requirements for oxygen than AOM. AOM (*Nitrosomonas* species) have a half saturation coefficient for oxygen at around 16 μM, whereas the coefficient for NOM (*Nitrobacter* species) is around 62 μM (Belster, 1979). NOM grow much faster than AOM, and thus the product of AOM activity, nitrite, seldom accumulates in nature unless a specific inhibitor or selective toxin for *Nitrobacter* is present (National Academy of Science, 1978).

Because of these unique features of nitrifiers and the nitrification process they bring about, it has been believed by many investigators that microbiological nitrification is responsible for those water quality deterioration symptoms in CWDSs (Ike *et al.*, 1988; Wolfe *et al.*, 1988, 1990; Cunliffe, 1991; Skadsen, 1993; Lieu *et al.*, 1993; Odell *et al.*, 1996; Wilczak *et al.*, 1996; Lipponen *et al.*, 2002). Factors believed to be contributing to microbiological nitrification occurrence in CWDSs include excessive ammonia and/or

low Cl/N ratio, low NH_2Cl dosage, long RT, and high temperature (Wolfe *et al.*, 1988).

1.1.3 Coupling of chloramination and microbiological nitrification in CWDSs

Due to the way NH_2Cl is generated in a water plant (i.e. low Cl/N ratio with ammonia in excess) and the unique properties of NH_2Cl in water (i.e. auto-decomposition and ready reactions with nitrite and natural organic matter leading to ammonia release), chloramination could be coupled with microbiological nitrification in CWDSs via two chemicals - nitrite and ammonia - as illustrated in Figure 1-1. In other words, addition of NH_2Cl may lead to nitrifying microorganisms growth in CWDSs, and in return, the growth of nitrifying microorganisms may accelerate NH_2Cl decomposition. This coupling effect makes the situation in CWDSs very complicated chemically and biologically. The discoveries of AOM and NOM in biofilms from CWDSs (Ike *et al.*, 1988; Regan *et al.*, 2002; Domingo *et al.*, 2003) have provided some explanation for the belief held by many investigators that chloramination-induced microbiological nitrification is responsible for those symptoms of water quality deterioration in CWDSs.

1.2 Biofilm growth in CWDSs

For water utilities, the primary purpose of applying NH_2Cl and keeping it at a certain concentration in distribution systems is to prevent the finished water from microbial regrowth, and therefore to warrant the finished water to meet relevant quality guidelines. Theoretically, there should be very little chance for nitrification to be brought about by the regrowth of planktonic microorganisms in the finished water. The sessile microorganisms growing on the inner surfaces of the distribution system facilities,

such as pipes and storage reservoirs, started to draw attention after the outbreaks of nitrification in CWDSs. It has been reported that the attachment of nitrifying microorganisms to solid surfaces enhances their growth and renders them more resistant to toxic compounds than freely suspended cells (Powell, 1986). In later studies (Ike *et al.*, 1988; Wolfe *et al.*, 1990; Regan *et al.*, 2002; Domingo *et al.*, 2003), high AOM and NOM population densities were detected in biofilms growing in CWDSs affected by nitrification. These findings indicate that biofilm development makes big contributions to the survival of AOM and NOM in CWDSs.

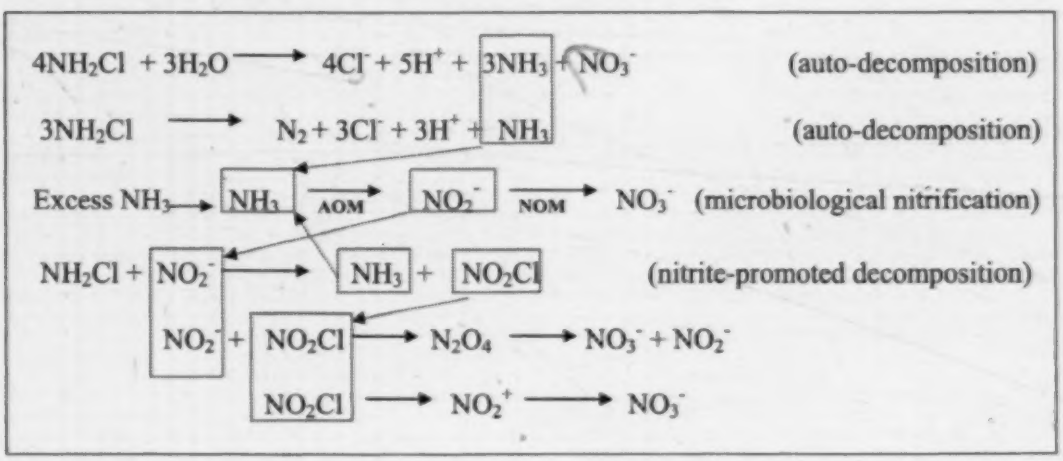
4NH2Cl + 3H2O → 4Cl- + 5H+ + 3NH3 + NO3-
(auto-decomposition)
3NH2Cl → N2 + 3Cl- + 3H+ + NH3
(auto-decomposition)
Excess NH3 → NH3 AOM NO2- NOM NO3-
(microbiological nitrification)
NH2Cl + NO2- → NH3 + NO2Cl
(nitrite-promoted decomposition)
NO2- + NO2Cl → N2O4 → NO3- + NO2-
NO2Cl → NO2+ → NO3-

Figure 1-1 Coupling of NH_2Cl decomposition and microbiological nitrification.

Studies on the direct relationship between chloramination and biofilm development have shown that the practice of chloramination is actually not as effective in controlling biofilm growth as generally expected. Hermanowicz and Filho (1992) used a parameter characterizing bacterial attachment on a rotating disc of polyvinyl

chloride (PVC) and found that NH_2Cl (1 and 4 mg/L) affected bacterial attachment but without avoiding it. It's been reported that biofilms could develop on a concrete surface in the presence of NH_2Cl at 1.06 mg/L as Cl_2 with a concentration of fixed bacteria at 1.4 $\times$ 10^6 total cell/cm^2, and that the extrapolation of study results led to a theoretical concentration of NH_2Cl residual at 8.8 mg/L that would be needed to control biofilm formation (Morin *et al.*, 1999). This value is far beyond the MCL of 4 mg/L and therefore unacceptable by the drinking water industry.

In contrast to controlling biofilm development, the practice of chloramination actually might contribute to biofilm growth in CWDSs due to NH_2Cl decomposition, which leads to a decrease in its disinfection efficacy and release of ammonia, both of which favor the growth of nitrifying microorganisms. Once other environmental conditions in CWDSs are also favorable, activities of nitrifying microorganisms could be stimulated; and nitrifying microorganisms could develop a slime on the walls of the pipe (Geldreich, 1996). Meanwhile, it has been reported that nitrifying microorganisms secrete a variety of organic compounds that can be used by heterotrophs (Negrin *et al.*, 1990; Geldreich, 1996). Geldreich (1996) also suggested that this could be the explanation for heterotrophs density increases in CWDSs. All these kinds of microbial growth ultimately can provide great potential to biofilm development, which in return protect microorganisms from being inactivated by NH_2Cl.

1.3 Microbial inactivation of NH_2Cl in biofilms in CWDSs

Using the combination of microelectrode and fluorescence *in-situ* hybridization with confocal laser-scanning microscopy, Schramm *et al.* (1996) observed that nitrifying

bacteria could be present, in substantially lower numbers though, in the lower anoxic layers, and even occasionally at the bottom of biofilms with thickness at around 200 μm, but nitrification was restricted to a narrow zone of 50 μm on the very top of the biofilms. Nitrifying microorganisms are obligate aerobes, and therefore generally grow in the upper zone near the surface of biofilms where oxygen supply is relatively rich, especially in the case of thick biofilms being developed in distribution systems for very long periods of time. Such an ecological population distribution feature makes nitrifying microorganisms stand at the front line facing a disinfectant, and as a result, they should be more vulnerable to the attack of disinfectant. Consequently, if the presence of nitrifying microorganisms in biofilms is the primary cause for nitrification occurrence in CWDSs, then, the adequacy of currently used NH_2Cl residual concentrations would be questionable. They may be high enough for preventing planktonic microorganisms regrowth, but are they also sufficient to inactivate biofilm microorganisms in CWDSs?

For a disinfectant, the mechanism of its inactivation against biofilm microorganisms is different from that against planktonic cells. In the latter case, disinfectant can directly attack microbial cells, whereas in the case of the former, the disinfectant must first penetrate into the biofilm in order to reach and then attack its targets. This penetration process can be greatly affected by the type and concentration of disinfectant, contact time, biofilm matrix and substratum material. Therefore, a good understanding of the penetration process of disinfectant within biofilms is critical to elucidating how disinfectant, biofilms and pipe material interact with each other and how disinfection efficacy is affected by these interactions.

Most previous studies on disinfection efficacy against biofilm microorganisms

used conventional approaches, in which biofilm samples had to be dispersed and homogenized in suspension in order to conduct viable cell counting. However, this method cannot help elucidate interactions among disinfectant, biofilms and substratum material in the course of disinfectant penetration within biofilms. Investigations using *in-situ* approaches into intact biofilms are crucial to getting a much clearer picture of what really takes place in biofilms during disinfectant penetration.

With the development and application of a chlorine microelectrode, direct observations on penetration of free chlorine in biofilms were conducted (de Beer *et al.*, 1994; Xu *et al.*, 1996; Chen and Stewart, 1996). Results of these studies have disclosed that there is a diffusion-reaction mechanism that affects disinfection efficacy of free chlorine against biofilm microorganisms. de Beer *et al.* (1994) found that free chlorine was reduced by materials in the biofilm matrix during the course of its penetration. The reduction rate of chlorine was strongly dependent on cell density in biofilms (Xu *et al.*, 1996) and the degree of chlorine penetration retardation was proportional to the initial cell density in biofilms (Chen and Stewart, 1996).

Unlike inactivation by free chlorine, which was reported to be affected by substratum surfaces, age of biofilms, encapsulation, and nutrient effects, inactivation by NH_2Cl was reported to be only affected by substratum surfaces (LeChevallier *et al.*, 1988), which remains to be confirmed though. In comparison with free chlorine, NH_2Cl may have a diffusivity in biofilms very close to that of free chlorine, but it is much less reactive chemically with biological matters (Siegrist and Gujer, 1985; van der Wende and Characklis, 1990). NH_2Cl reacts rather specifically with nucleic acids, tryptophane, and sulfur-containing amino acids while having little interaction with polysaccharides;

free chlorine, however, indiscriminately attacks both polysaccharides and cell materials, necessitating a greater dosage because of the chlorine demand in the gelatinous matrix in biofilms (Geldreich, 1996).

Studies have shown that substratum material affects disinfection efficacy of NH_2Cl against biofilm microorganisms (Chen *et al.*, 1993b; LeChevallier *et al.*, 1990; Ollos *et al.*, 1998), and it is believed that this can be attributed to interactions between NH_2Cl and substances associated with substratum material. Woolschlager *et al.* (2001) discovered that NH_2Cl decomposition could be accelerated on concrete surfaces due to the formation of acidified surfaces of aluminosilicates - one major component of concrete - and found that this was the single most influential factor in NH_2Cl decomposition in the distribution system under examination. LeChevallier *et al.* (1993) found that NH_2Cl disinfection efficacy could be affected by high corrosion rates of pipes. Piriou *et al.* (1997) and Vikesland and Valentine (2002) also reported that NH_2Cl reacted with oxidizable species (e.g. Fe (II)) formed from corrosion processes, and this led to undesirable losses in NH_2Cl residual. A typical reaction of this type was suggested as shown by Equation (1-13). This reaction could be catalyzed by a variety of iron oxide surfaces on pipes in distribution systems.

$$NH_2Cl + 2H^+ + 2Fe^{2+} \longrightarrow 2Fe^{3+} + NH_4^+ + Cl^- \qquad (1\text{-}13)$$

After having observed that mild steel corrosion products had retarding impacts on disinfection efficacy of NH_2Cl against homogenized biofilm cells without change in NH_2Cl concentration (3 mg/L) during the whole experimental period (60 minutes at pH 7.0), Chen *et al.* (1993b) suggested that instead of the reaction of NH_2Cl with corrosion products, the binding of corrosion products (ferrous and/or ferric ions) to membrane

proteins bearing electric charges (Stanier *et al.*, 1986) could affect the transport of molecules through the cell membrane and thus affect the disinfection efficacy of NH_2Cl against biofilm microorganisms.

Considering the fact that NH_2Cl decomposition could be promoted by some substances associated with pipe materials (e.g. ferrous iron and aluminosilicates), natural organic matter and nitrite, which could be present due to AOM activity in biofilms in CWDSs, the penetration process of NH_2Cl in biofilms could be greatly weakened; and this could in turn render great reduction of its disinfection efficacy in the course of its penetration in biofilms. In this area, more research needs to be conducted with direct observations on NH_2Cl penetration in intact biofilms in order to help elucidate (1) how NH_2Cl penetrates in natural biofilms of distribution systems, and (2) how the penetration pattern is affected by contact time, NH_2Cl residual concentration and substratum material, on which biofilms grow.

1.4 Detection of nitrification in CWDSs

To avoid violation of water quality regulations, early detection and warning of nitrification in CWDSs is important to utilities. It can help utilities make decisions proactively on implementation of control strategies before an occurrence of measurable water quality deterioration. The convenient, and thus more frequently used method for detection of nitrification occurrence, is to carry out monitoring tests on water in distribution systems. A lot of studies have been conducted in attempts to find correlations between nitrification occurrence and water parameters such as DO, pH, HPC, NH_2Cl residual, ammonia, nitrite, nitrite plus nitrate, identification and population

density of nitrifying microorganisms (Wolfe *et al.*, 1990; Cunliffe, 1991; Lieu *et al.*, 1993; Wilczak *et al.*, 1996; Regan *et al.*, 2002; Pintar *et al.*, 2005), but inconsistent and even contradictory conclusions often resulted. As an important parameter, nitrite has drawn a lot of attention and a critical threshold at 0.05 mg-N/L for determination of nitrification outbreak in CWDSs has been proposed and/or adopted by earlier investigators (Wolfe *et al.*, 1988; Kirmeyer *et al.*, 1995; Wilczak *et al.*, 1996). However, Lieu *et al.* (1993) found that an increase in nitrite lagged behind ammonia-oxidizing bacteria growth by 1 to 3 weeks. Pintar *et al.* (2005) also reported that NH_2Cl residual drop occurred 2 to 3 weeks earlier than ammonia-oxidizing bacteria growth and significant increases in nitrite up to the proposed threshold in full–scale investigations. Given the inconsistency in research findings in this area, Wilczak *et al.* (1996) suggested that the best indicators of nitrification would be a nitrogen balance and the detection of nitrifying bacteria. A recent study (Sathasivan *et al.*, 2005) introduced a method of determining the microbial decay factor "F_m" for NH_2Cl decomposition in distribution systems. This factor is the ratio of the NH_2Cl decay rate due to microbiological agents relative to the chemical decay rate. This approach only used monitoring data on NH_2Cl residual in water and was reported to be more sensitive than traditional indicators. As a result, it was recommended to be a potential tool for utilities to use in early detection of nitrification in CWDSs.

It has been believed that deposits and biofilms grown on surfaces of reservoirs and pipes of distribution systems provide a protective environment for microbial growth; and it is the growth of nitrifying microorganisms in the biofilms and deposits that ultimately leads to the outbreak of nitrification in CWDSs (Ike *et al.*, 1988; Wolfe *et al.*,

1990; Odell *et al.*, 1996). In addition, deposits and biofilms themselves can accelerate NH_2Cl decomposition via chemical reactions between their components and NH_2Cl. Therefore, monitoring tests conducted directly on biofilms, although not as convenient as those on water, become logical choices in searching for more sensitive approaches to early detection of nitrification in CWDSs.

The most commonly used biofilm test for nitrification detection in CWDSs is the detection and enumeration of nitrifying microorganisms using the most probable number (MPN) technique. However, the MPN test normally requires at least 3 weeks of incubation (Matulewich *et al.*, 1975). This time-consuming approach clearly produces data that has very weak relevancy with the operation of the systems involved. In addition, extremely low recovery efficiency (as low as 0.1%) in cultural technique and large variations of test results of the MPN technique (Belser, 1979) make the MPN test play a limited role in providing early detection and warning of nitrification in CWDSs.

To overcome the drawbacks of the MPN technique in detecting nitrifying microorganisms, Regan *et al.* (2002) reported a rapid and sensitive screening approach – the nested-polymerase chain reaction terminal restriction fragment length polymorphorism protocol. This technique helped quickly detect both ammonia-oxidizing bacteria as well as nitrite-oxidizing bacteria in biofilms and deposits in a CWDS without being subject to culturability biases, and thus was recommended to be a presence or absence tool to help water utilities in detecting potential onset of a nitrification episode in CWDSs before other water quality parameters are affected. Detection of the presence of nitrifiers, however, does not necessarily indicate significant potential of nitrification outbreak or significant ongoing nitrification in distribution systems. It may only indicate

that sometime in the past prior to the test, nitrification took place, or there could be no nitrification episode at all if conditions in distribution systems do not allow the detected nitrifiers to proliferate substantially. Therefore, detection of nitrifiers alone is not sufficient for early detection of a nitrification outbreak in CWDSs.

Microbiological nitrification process consists of two biochemical reactions as expressed in Equation (1-11) and (1-12). As a result, a more appropriate approach to elucidate nitrification in distribution systems is to examine, *in-situ* in biofilms, those chemicals such as oxygen, ammonia, nitrite, nitrate and hydrogen ions (protons) that are directly involved in these two biochemical reactions, either as reactants or products. This way, not only the presence but also the status of ongoing nitrification occurring within biofilms can be clearly disclosed. Consequently, such an approach can provide a potential application to early detection and warning of nitrification in CWDSs.

1.5 Microelectrode techniques

Most previous studies on NH_2Cl inactivation against biofilm microorganisms and detection of nitrification in biofilms in CWDSs used some conventional approaches, in which biofilm samples had to be dispersed and homogenized in solution. They were not beyond microbial cell identification and/or enumeration, which plays a limited role in elucidating some fundamental mechanisms associated with NH_2Cl inactivation and nitrification processes taking place in biofilms in CWDSs. Investigations into intact biofilms using *in-situ* measurements are critical to disclosing what is really going on in biofilms under chloraminated conditions, especially with respect to NH_2Cl penetration and nitrification processes in biofilms.

Due to their tiny tips and high spatial resolutions, microelectrodes have been used for *in-situ* investigations into microenvironments such as those in biofilms. They offer a direct way to localize and quantify analytes near and in biofilms. The precisely sited measurements give a great deal of valuable information to assess biofilm processes at the microscopic level.

Microelectrode techniques work on the basis of a linear relationship between the concentration (more precisely, activity or partial pressure) of the analyte and the current or voltage signals of the microelectrode that can be detected by an ammeter or a voltmeter. With *in-situ* measurements using microelectrode techniques, local concentrations of chemicals (e.g. ammonium, nitrate, and DO) and environmental parameters (e.g. pH and redox potential) can be determined immediately, and profiles of these chemicals and parameters can then be constructed. These constructed profiles directly convey three pieces of basic information: concentrations of chemicals at any position measured, concentration gradients, and variations of gradients. Based on these profiles, using proper diffusion coefficients and Fick's Law of Diffusion, mass transports or fluxes and substance transformation or conversion rates (reaction rates) of those chemicals can be calculated. Furthermore, distributions of microenvironmental conditions (i.e. pH, redox potential, aerobic, anaerobic and anoxic conditions) and locations of relevant microbial activities (e.g. nitrification) in biofilms can all be determined. All such information is of great value in helping disclose chemical as well as biological processes occurring in biofilms.

In the past decades, various microelectrodes had been developed. Although the original purposes of some microelectrodes were not for applications to biofilm study,

significant progress has been made in the area of biofilm research thanks to the adoption of microelectrode techniques. de Beer *et al.* (1994) provided direct experimental evidence to disclose the retardation effect of biofilms on chlorine penetration in biofilms using a chlorine microelectrode. Revsbech (1989) developed a combined oxygen microelectrode with a guard cathode, based on which Lu and Yu (2002a, b) evaluated the performance of this type of microelectrode, and conducted a field study to measure oxygen penetration in wastewater biofilms *in-situ*. Study on nitrification in environmental biofilms has been significantly facilitated since the development of the ammonium microelectrode (de Beer and van den Heuvel, 1988a; de Beer *et al.*, 1991), the nitrate microelectrode (de Beer and Sweerts, 1989; Jensen *et al.*, 1993), and the nitrite microelectrode (de Beer *et al.*, 1997). de Beer and van den Heuvel (1988b) directly measured pH gradients in biofilms using a pH microelectrode. With the application of a redox potential microelectrode, Yu (2000) disclosed the phenomenon of stratification of microbial processes and redox potential changes in biofilms. However, there is no microelectrode yet that has the capability to specifically measure NH_2Cl in biofilms. In order to elucidate how NH_2Cl penetrates in biofilms and how its penetration pattern is affected by contact time, biofilm matrix as well as substratum material, the development of a NH_2Cl microelectrode is critical.

Despite the wide use of microelectrodes in studies on microenvironments such as those in biofilms and sediments in aquatic systems, it is not necessarily true that these techniques do not disturb the local microenvironments of their subjects. Some investigators have already noticed that microelectrode techniques cannot be considered totally undisruptive despite their tiny tips (Amann and Kuhl, 1998; Kuhl and Revsbech,

2001). It has been reported that during its profile measurement, the microelectrode tip could introduce impact on the microenvironment around the interface between bulk phase and sediments or biofilms. Glud *et al.* (1994) observed that during the course of the measuring process from the bulk phase to the surface of sediment, an oxygen microelectrode with tip diameter at around 8 μm significantly altered the diffusion boundary layer above the sediment. The thickness of the diffusion boundary layer was reduced by 25 to 45%, and the eroding effect was detected even when the microelectrode tip was situated more than 1 mm above the sediment surface. Glud *et al.* (1998) thus presumably concluded that the similar mechanism could explain why a biofilm, partially (50%) anoxic disclosed by a non-invasive approach, was totally oxic by microelectrode, and thus overestimation of oxygen distribution within biofilms sometimes could result from microelectrode measurements. However, the real mechanism behind this phenomenon has not been fully understood yet, and more direct experimental evidences are needed.

1.6 Objectives and outline of the dissertation

In this dissertation research, a series of investigations were implemented to fulfill the following four specific objectives set up based on the literature review:

(1) To develop a microelectrode capable of measuring NH_2Cl;

(2) To study the penetration of NH_2Cl in biofilms grown on different substratum materials using the newly developed NH_2Cl microelectrode;

(3) To study the feasibility of conducting biofilm tests using microelectrode techniques in nitrification detection in CWDSs; and

(4) To collect more experimental evidences to elucidate the potential impact of the penetration of the microelectrode tip in biofilms during measurement.

Detailed discussions on these investigations have been presented in the following five chapters. Chapter 2 introduces materials and methods generally used throughout the entire dissertation research. The fulfillments of the aforementioned four specific objectives are discussed in Chapter 3, 4, 5 and 6, respectively. Based on the literature review of Chapter 1, a brief introduction is also presented in each of these four chapters to make it possible that each of them can be read as a relatively independent paper without losing context. In the final chapter, Chapter 7, a summary of the dissertation research is provided and recommendations for future study are made.

1.7 References

Amann, R. and Kuhl, M. 1998. In situ methods for assessment of microorganisms and their activities. *Current Opinion in Microbiology*, 1:352-358.

Belser, L. W. 1979. Population ecology of nitrifying bacteria. *Annual Review of Microbiology*, 33:309-333.

Chen, C. I., Griebe, T. and Characklis, W. G. 1993a. Biocide action of monochloramine on biofilm systems of *Pseudomonas aeruginosa*. *Biofouling*, 7:1-17.

Chen, C. I., Griebe, T., Srinivasan, R. and Stewart, P. 1993b. Effects of various metal substrata on accumulation of *Pseudomonas aeruginosa* biofilms and the efficacy of monochloramine as biocide. *Biofouling*, 7:241-251.

Chen, X. and Stewart, P. S. 1996. Chlorine penetration into artificial biofilm is limited by a reaction-diffusion interaction. *Environmental Science and Technology*, 30:2078-2083.

Cotruvo, J. A. 1981. THMs in drinking water. *Environmental Science and Technology*, 15:268.

Cunliffe, D. A. 1991. Bacterial nitrification in chloraminated water supplies. *Applied and Environmental Microbiology*, 57:3399-3402.

de Beer, D. and van den Heuvel, J. C. 1988a. Response of ammonium-selective microelectrodes based on the neutral carrier nonactin. *Talanta*, 35:728-730.

de Beer, D. and van den Heuvel, J. C. 1988b. Gradients in immobilized biological systems. *Analytical Chimica Acta*, 213:259-265.

de Beer, D. and Sweerts, J. P. R. A. 1989. Measurement of nitrate gradients with an ion-selective microelectrode. *Analytical Chimica Acta*, 219:351-356.

de Beer, D., Sweerts, J. P. R. A. and van den Heuvel, J. C. 1991. Microelectrode measurement of ammonium profiles in freshwater sediments. *FEMS Microbiology Ecology*, 86:1-6.

de Beer, D., Srinivasan, R. and Stewart, P. 1994. Direct measurement of chlorine penetration into biofilms during disinfection. *Applied and Environmental Microbiology*, 60:4339-4344.

de Beer, D., Schramm, A., Santegoeds, C. M. and Kuhl, M. 1997. A nitrite microsensor for profiling environmental biofilms. *Applied and Environmental Microbiology*, 63:973-977.

Domingo, J. W. S., Meckes, M. C., Simpson, J. M., Sloss, B. and Reasoner, D. J. 2003. Molecular characterization of bacteria inhabiting a water distribution system simulator. *Water Science and technology*, 47(5):149-154.

Geldreich, E. E. 1996. *Microbial quality of water supply in distribution systems*. Lewis Publishers, CRC Press, Inc., New York.

Guest, R.K. and Smith, D.W. 2002. A potential new role for fungi in a wastewater MBR biological nitrogen reduction system. *Journal of Environmental Engineering and Science*, 1:433-437.

Glud, R. N., Gundersen, J. K., Revsbech, N. P., and Jorgensen, B. B. 1994. Effects on the benthic diffusive boundary layer imposed by microelectrodes. *Limnology and Oceanography*, 39:462-467.

Glud R. N., Santegoeds, C. M., De Beer, D., Hohls, O., and Ramsing, N. B. 1998. Oxygen dynamics at the base of a biofilm studied with planar optrodes. *Aquatic Microbial Ecology*, 14:223-233.

Hermanowicz, S. W. and Filho, F. L. 1992. Disinfection and attachment of bacteria cells. *Water Science and Technology*, 26(3-4):655-664.

Ike, N. R., Wolfe, R. L. and Means, E. G. 1988. Nitrifying bacteria in a chloraminated drinking water system. *Water Science and Technology*, 20(11-12):441-444.

Jensen, K., Revsbech, N. P. and Nielsen, L. P. 1993. Microscale distribution of nitrification activity in sediment determined with a shielded microsensor for nitrate. *Applied and Environmental Microbiology*, 59:3287-3296.

Kirmeyer, G. J., Odell, L. H., Jacangelo, J., Wilczak, A and Wolfe, R. 1995. *Nitrification occurrence and control in chloraminated water systems*. AWWA research Foundation and American Water Works Association, Denver, Colorado, USA.

Koops, H.-P. and Pommerening-Roser, A. 2001. Distribution and ecophysiology of the nitrifying bacteria emphasizing cultured species. *FEMS Microbiology Ecology*, 37:1-9.

Kuhl, M. and Revsbech, N. P. 2001. Biogeochemical microsensors for boundary layer studies. In *The benthic boundary layer: transport processes and biogeochemistry*, Boudreau, B. P. and Jogensen, B. B. (editors). Oxford University Press, Inc., Oxford, New York.

LeChevallier, M. W., Cawthon, C. D. and Lee, R. G. 1988. Factors promoting survival of bacteria in chlorinated water supplies. *Applied and Environmental Microbiology*, 54:649-654.

Lechevallier, M. W., Lowry, C. D. and Lee, R. G. 1990. Disinfecting biofilms in a model distribution system. *Journal AWWA*, 82:87-99.

Lechevallier, M. W., Lowry, C. D., Lee, R. G. and Gibbon, D. L. 1993. Examining the relationship between iron corrosion and the disinfection of biofilm bacteria. *Journal AWWA*, 85:111-123.

Leung, S. W. 1989. *Chemistry and kinetics of chloramine decomposition: nitrite reactions and the formation of an unidentified product*. Ph.D. dissertation, The University of Iowa, Iowa City, Iowa, USA.

Lieu, N. I., Wolfe, R. L. and Means, E. G. III 1993. Optimizing chloramine disinfection for the control of nitrification. *Journal AWWA*, 85:84-90.

Lipponen, M. T. T., Suutari, M. H., and Martikainen, P. J. 2002. Occurrence of nitrifying bacteria and nitrification in Finnish drinking water distribution systems. *Water Research*, 36:4319–4329.

Lu, R. and Yu, T. 2002a. Fabrication and evaluation of an oxygen microelectrode applicable to environmental engineering and science. *Journal of Environmental Engineering and Science*, 1:225-235.

Lu, R. and Yu, T. 2002b. A field study on oxygen penetration in wastewater biofilms, in *Proceedings of Water Environment Federation's 75th Annual Technical Exhibition and Conference(WEFTEC 2002)*, Chicago, Illinois, USA, September 28-October 2, 2002.

Margerum, D. W., Schurter, L. M., Hobson, J. and Moore, E. E. 1994. Water chlorination chemistry: Nonmetal redox kinetics of chloramine and nitrite ion. *Environmental Science and Technology*, 28:331-337.

Matulewich, V. A., Strom, P. F. and Finstein, M. S. 1975. Length of incubation for enumerating nitrifying bacteria present in various environments. *Applied Microbiology*, 29:265-268.

Morin, P., Gauthier, V., Saby, S. and Block, J. C. 1999. Bacterial resistance to chlorine through attachment to particles and pipe surface in drinking water distribution systems, in *the proceedings of the International Conference on Biofilms in Aquatic Systems*, April 13-16, 1997, the University of Warwick, UK. Keevil, C. W., Godfree, A., Holt, D. and Dow, C. (editors), the Royal Society of Chemistry, Cambridge, UK.

National Academy of Science 1978. *Nitrates: An Environmental Assessment*. A report prepared by the Panel on Nitrates of the Coordinating Committee for Scientific and Technical Assessments of Environmental Pollutants. Washington, D.C.

Negrin, J. M., Heyer, W. M. and Cheng, S. 1990. Evaluation of nitrification control strategies at the Los Angeles Department of water and power. *Proceedings of 1990 AWWA Annual Conference*, Cincinnati, Ohio, USA.

Odell, L. H., Kirmeyer, G. J., Wilczak, A., Jacangelo, J. G., Marcinko, J. P. and Wolfe, R. L. 1996. Controlling nitrification in chloraminated systems. *Journal AWWA*, 88:86-98.

Ollos, P. J., Slawson, R. M. and Huck, P. M. 1998. Bench scale investigations of bacterial regrowth in drinking water distribution systems. *Water Science and Technology*, 38(8-9):275-282.

Pintar, K. D. M., Anderson, W. B., Slawson, R. M., Smith, E. F. and Huck, P. M. 2005. Assessment of a distribution system nitrification critical threshold concept. *Journal AWWA*, 97:116-129.

Piriou, P., Kiene, L. and Levi, Y. 1997. Study and modeling of drinking water quality evolution using a pipe loop system. *Proceedings of the annual meeting of the American Water Works Association*, 15-19 June, Atlanta, Georgia, USA.

Powell, S.J. 1986. Laboratory studies of inhibition of nitrification. In *Nitrification* (Prosser, J. I., editor). IRL Press, Washington D.C.

Regan, J. M., Harrington, G. W. and Noguera, D. R. 2002. Ammonia- and nitrite-oxidizing bacterial communities in a pilot-scale chloraminated water distribution system. *Applied and Environmental Microbiology*, 68:73-81.

Revsbech, N. L. 1989. An oxygen microelectrode with a guard cathode. *Limnology and Oceanography*, 34:474-478.

Sathasivan, A., Fisher, I. and Kastl, G. 2005. Simple method for quantifying microbiologically assisted chloramine decay in drinking water. *Environmental Science and Technology*, 39:5407-5413.

Schramm, A., Larsen, L. H., Revsbech, N. P., Ramsing, N. B., Amann, R. and Schleifer, K. H. 1996. Structure and function of a nitrifying biofilm as determinaed by in situ hybridization and the use of microelectrode. *Applied and Environmental Microbiology*, 62:4641-4647.

Siegrist, H. and Gujer, W. 1985. Mass transfer mechanisms in a heterotrophic biofilm. *Water Research*, 19:1369-1378.

Skadsen, J. 1993. Nitrification in a distribution system. *Journal AWWA*, 85:95-103.

Stanier, R.Y., Ingraham, J. L., Wheelis, M. L. and Painter, P. R. 1986. *The microbial world*. 5th edition, Prentice-Hall, Englewood Cliffs, New Jersey.

Valentine, R. L., Ozekin, K. and Vikesland, P. J. 1998. *Chloramine decomposition in distribution system and model waters*. AWWA Research Foundation and American Water Works Association, Denver, Colorado, USA.

van der Wende, E. and Characklis, W.G. 1990. Biofilms in potable water distribution systems, in *Drinking water microbiology – Progress and recent developments*, McFeters, G. A. (editor), Springer-Verlag, New York.

Vikesland, P. J. and Valentine, R. L. 2002. Iron oxide surface-catalyzed oxidation of ferrous iron by monochloramine: Implications of oxide type and carbonate on reactivity. *Environmental Science and Technology*, 36:512-519.

Watson, S. W., Valois, F. W. and Waterbury, J. B. 1981. The family Nitrobacteraceae. In *the Prokaryotes*, Starr, M. P., Stolp, H., Truper, H. G., Balows, A. and Schlegel, H. G. (editors), Springer-Verlag, Berlin.

White, G. C. 1999. *Handbook of chlorination and alternative disinfectants*. 4th edition, John Wiley & Sons, Inc., New York.

Wilczak, A., Jacangelo, J. G., Marcinko, J. P., Odell, L. H., Kirmeyer, G. J. and Wolfe, R. L. 1996. Occurrence of nitrification in chloraminated distribution systems. *Journal AWWA*, 88:74-85.

Wolfe, R. L., Means, E. G. III, Davis, M. K. and Barrett, S. E. 1988. Biological nitrification in covered reservoirs containing chloraminated water. *Journal AWWA*, 80:109-114.

Wolfe, R. L., Lieu, N. I., Izaguirre, G. and Means, E. G. 1990. Ammonia-oxidizing bacteria in a chloraminated distribution system: seasonal occurrence, distribution, and

disinfection resistance. *Applied and Environmental Microbiology*, 56:451-462.

Woolschlager, J., Rittmann, B., Piriou, P., Kiene, L. and Schwartz, B. 2001. Using a comprehensive model to identify the major mechanisms of chloramines decay in distribution systems. *Water Science and Technology: Water Supply*, 1(4):103-110.

Xu, X., Stewart, P. S. and Chen, X. 1996. Transport limitation of chlorine disinfection of *Pseudomonas aeruginosa* entrapped in alginate beads. *Biotechnology and Bioengineering*, 49:93-100.

Yu, T. 2000. *Stratification of microbial processes and redox potential changes in biofilms*. Ph.D. dissertation, University of Cincinnati, Cincinnati, Ohio, USA.

Chapter 2

Materials and Methods

This chapter provides general descriptions on materials and methods commonly used throughout the entire dissertation research including the types, fabrications and calibrations of microelectrodes, the operation of model water distribution systems for biofilm growth, the set-up for chemical concentration profile measurements in biofilms using microelectrodes, as well as conventional chemical and microbiological analyses of water and biofilm samples. Regarding other specialized materials and methods, and some very specific settings and conditions for specific studies, they are introduced in chapters in which they come into use for those particular study purposes.

2.1 Microelectrodes for biofilm measurements

Microelectrodes used in this dissertation research included two groups, the potentiometric and the amperometric electrodes. Working principles, fabrications and calibrations of these microelectrodes are discussed in the following sections.

2.1.1 Potentiometric microelectrodes

Briefly, potentiometric electrodes work on the basis of a linear relationship between the potential difference generated between the working electrode and an external reference electrode and the logarithm of the concentration (more accurately, activity) of the analyte of interest in the sample solution in contact with both the working and external reference electrodes. In this dissertation research, all potentiometric microelectrodes used for pH, ammonium and nitrate measurements were liquid ion-

selective (LIX) membrane microelectrodes. As a result, working principles, fabrications and calibrations of the LIX membrane microelectrodes are introduced in detail here.

2.1.1.1 Working principles of LIX membrane microelectrodes

LIX membrane microelectrodes permit potential measurement of the activity of an ion of interest with presence of other ions in the same sample. A LIX membrane microelectrode system normally includes (1) a galvanic half-cell containing the LIX membrane, the internal filling solution and the internal reference electrode, and (2) another half-cell represented by an external reference electrode in contact with a reference electrolyte. A cell potential, i.e. electromotive force (EMF), is generated when the LIX membrane microelectrode and the external reference electrode are both in contact with the sample solution. The EMF is the sum of a series of local potential differences developed at the solid-liquid, solid-solid and liquid-liquid interfaces of the cell. For ideal LIX membrane microelectrode cell assemblies, the measured EMF expresses a membrane potential that is generated across the LIX membrane, and is directly proportional to the logarithm of the concentration of the selectively transferred ion in the sample. If other potential differences in the cell assembly are assumed to be constant, the EMF of the cell assembly measured via a milli-volt measuring system connected with the working and external reference electrode is given by the Nernst equation:

$$EMF = E_0 + [(2.303R \cdot T/n \cdot F) \cdot \log(\alpha_i)] \qquad (2\text{-}1)$$

where, "EMF" is cell potential; "E_0" is reference potential; "R" is gas constant; "T" is absolute temperature; "n" is charge on the ion; "F" is Faraday constant; and "α_i" is the

activity of the measured ion.

To determine the concentration of the ion of interest in an unknown solution, EMFs in standard solutions of the ion of interest need to be measured first so that EMF (in mV) versus the logarithms of the ionic concentrations can be plotted, leading to a straight-line calibration curve. From this calibration curve, the concentration of the ion of interest in the unknown solution can be read off after the EMF of the sample is measured.

The electrode cell assemblies for three LIX membrane microelectrodes used for pH, ammonium and nitrate measurements, respectively, in this dissertation research were as follows: (1) pH: Reference//sample//pH membrane/pH 7 buffer solution/AgCl,Ag; (2) NH_4^+: Reference//sample//NH_4^+ membrane/0.01M NH_4Cl/AgCl,Ag; and (3) NO_3^-: Reference//sample//NO_3^- membrane/0.05M KCl + 0.05M KNO_3/AgCl,Ag.

2.1.1.2 Fabrication of LIX microelectrodes

The fabrication approach for LIX membrane microelectrodes used in this dissertation research was based on the procedures described by Yu (2000), Li (2001) and de Beer *et al.* (1997), which have improved the performance of some of these microelectrodes, especially with respect to response time, signal stability and tolerance to interference of co-existing ions.

Step 1: Pulling the glass micropipette. Micropipettes were purchased from World Precision Instruments (WPI), Inc. (Sarasota, FL, USA), with a filament inside (Cat.# 1B120F-6). Their outer diameters and lengths were 1.2 mm and 150 mm, respectively. The pulling of the micropipette was conducted on a vertical pipette puller (WPI, PUL-100, microprocessor-controlled) with a trough-shaped heating filament (WPI,

Cat.# 13835).

Step 2: Breaking the tip of the pulled micropipette. The tip of the pulled micropipette was often sealed. It needed to be broken so that in a later step the tip could be filled with ion-selective cocktail. The sealed tip was broken by bumping with a tip-closed Pasteur pipette mounted on a micromanipulator with the aid of a vertical microscope. The diameter of the resultant tip normally was between 1 to 4 μm, depending on the requirements of different types of microelectrodes. For pH and ammonium microelectrodes, tip diameters were normally made at 1 to 2 μm, whereas for nitrate microelectrodes, tip diameters were made at around 3 to 4 μm considering the fact that the cocktail used for the nitrate microelectrode is more viscous.

Step 3: Silanization. The tip of the pulled micropipette from Step 2 was dipped into N,N-dimethyltrimethylsilylamine (Fluka #41716) silanizing agent for around 30 seconds, then the micropipette was transferred to a custom-made holder made from stainless steel and placed in a pre-heated oven at 180 ℃ for at least 24 hours. Once the baking process was finished, the whole set of the holder and micropipettes were put into a desiccator to cool down to room temperature.

Step 4: Back-filling with internal reference solution. The internal reference solution for each type of microelectrode was filled into the micropipette from its back end using a long micro-fill needle (WPI, Cat.# MF28G-5) attached to a syringe. The tip of the needle was inserted down to the shoulder of the micropipette, and the reference solution in the syringe was pushed through the needle such that the tip of the micropipette was filled completely with the solution without any voids. pH 7.0 buffer solution (Fisher Cat# SB107-500), 0.01 M NH_4Cl and 0.05 M KCl + 0.05 M KNO_3 were

used as the internal reference solutions for pH, ammonium and nitrate microelectrode, respectively.

Step 5: Front-filling with liquid membrane. The LIX membrane cocktail for each type of microelectrode was filled into the microelectrode from its tip (front) end. After being back-filled with internal reference solution, the micropipette was immediately inserted into a reservoir of the liquid membrane of that microelectrode using a micromanipulator with the aid of a microscope. LIX membrane cocktails used for each type of microelectrode were as follows: (1) pH: hydrogen ionophore (cocktail B) (Fluka #95293); (2) NH_4^+: ammonium ionophore (cocktail A) (Fluka #09879); and (3) NO_3^-: nitrate ionophore (cocktail A) (Fluka #72549).

During this process, a column of the ion-selective cocktail could be seen formed at the tip with internal reference solution behind it. The front-filling procedure was given a sufficiently long time so that the column of the cocktail could be generated with a length that was around 1000 μm for pH and ammonium microelectrodes, and 500 μm for nitrate microelectrodes.

Step 6: Coating tip with protein layer. After briefly air-drying the membrane for minutes, the tip was inserted, with aid of a vertical microscope, into a cellulose acetate/acetone solution (10%, w/v) for 1 to 2 second(s), and then into a mixture of 1 mL of protein solution containing 10% (w/v) bovine serum albumin (BSA), 50 mM sodium phosphate and 10 μL of 50% glutaraldehyde for several minutes. As a result, a cross-linked, water insoluble protein layer was formed and firmly fixed onto the microelectrode tip. This protein coating effectively shields the hydrophobic liquid membrane surface from interaction with hydrophobic substances in the biofilm matrix,

which was reported by previous investigators (de Beer *et al.*, 1997; Yu, 2000; Li, 2001) to be interfering with the performance of LIX membrane microelectrodes without the protein layer, such as significant and sudden signal drifting, long response time, and leakage of the liquid membrane. Li (2001) reported that the diffusion coefficient in this protein coating is 1000-fold lower than in water. This makes it much more difficult for interfering substances to penetrate the protein layer either because they are too hydrophobic to pass through the protein layer or the pore size of the coating is too small for them to pass through.

Step 7: Assembling outer casing. A Pasteur pipette was used for the outer casing, with both its ends cut according to the length of the microelectrode made above. The microelectrode was inserted into the cut pipette with its tip protruding through the tapered pipette tip at about 2 cm. The connecting area between these two was sealed with silicon glue. After the glue air-dried, 1 M KCl solution was injected into the space between the outer casing and the microelectrode. An Ag/AgCl wire (diameter at 0.25 mm, length at 6 to 7 cm) was then inserted into the KCl solution to be used for connection to the grounding system of the microelectrode measuring system during measurement. Another Ag/AgCl wire (diameter at 0.127 mm, length at about 8 cm) was inserted into the internal reference solution from the end of the microelectrode to serve as the internal reference electrode. If experiments have to be carried out without a Faraday cage, this outer casing configuration can provide effective shielding to reduce external electrical interference. In the case that a Faraday cage is available, like in our laboratory, the merit of this outer casing configuration is not as prominent, and the microelectrode without the outer casing was thus often fabricated and used in biofilm measurements due

to the much lower difficulties in its fabrication.

Step 8: Conditioning microelectrode. As the last step, the completed microelectrode was then stored in conditioning solution until it was needed for calibration and measurement. pH 7.0 buffer (Fisher Cat# SB107-500), 0.02 M NH_4Cl, and 0.1M KCl + 0.1M KNO_3 solutions were used as the conditioning solutions for LIX membrane microelectrodes of pH, ammonium and nitrate, respectively.

2.1.1.3 Calibration of LIX microelectrodes

Before it was used for biofilm measurement, LIX membrane microelectrodes had to be calibrated in order to construct a linear calibration curve. The calibration was done with the LIX membrane microelectrode as the working electrode, and another commercially purchased Ag/AgCl micro-reference electrode (Microelectrodes Inc., Bedford, NH, USA; Cat.# MI-409) as its external reference electrode. Both electrodes were connected to an electrometer (Keithley Instruments Inc., Cleveland, OH, USA, Model 6517A) for voltage measurement. A series of standard solutions at different concentrations for each of these three types of microelectrodes were used to calibrate the corresponding microelectrode. Considering the possible ranges of each of these three parameters to be measured in this dissertation research and the detection limits of the LIX membrane microelectrodes for ammonium and nitrate, which are normally at about 1×10^{-5} M (Li, 2001), standard solutions were chosen as follows: for pH, standard pH buffer solutions of pH 6.00, 8.00 and 10.00 (Fisher's Cat.# SB104B, SB112B and SB116B, respectively) were used; for ammonium and nitrate, solutions of 1×10^{-5}, 1×10^{-4} and 1×10^{-3} M were made from standard NH_4Cl (Fluka Cat.# 09683) and $NaNO_3$

(Fluka Cat.# 72544) solutions, respectively. Calibrations were also conducted in the same water as used in measurements in biofilms using the "standard addition method" (Strobel and Heineman, 1989) to address potential matrix effects. The chemical concentrations in the water were determined using spectrophotometric analytic approaches according to the "Standard Methods" (APHA *et al.*, 1998).

The calibrations were conducted in a Faraday cage to avoid potential electromagnetic interference. Before each reading, the standard solution was thoroughly stirred, and then both the working and reference electrodes were lowered and immersed into the standard solution. The electrode response to each standard solution was taken when the reading was stable. The following figures (Figure 2-1 to Figure 2-3) show examples of calibration curves for pH, ammonium and nitrate microelectrodes obtained.

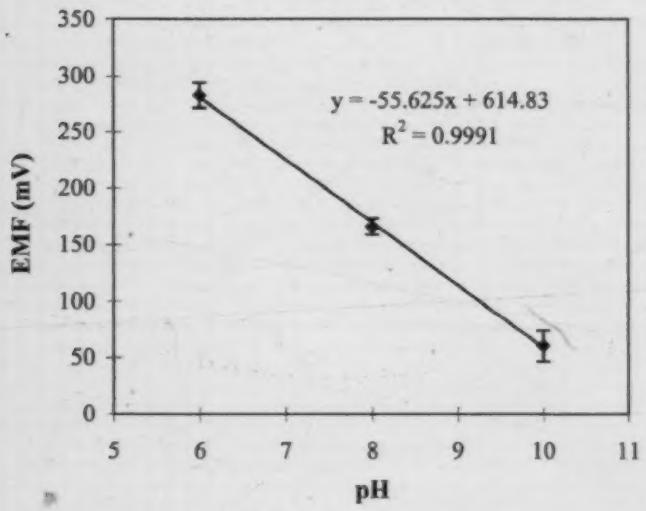

Figure 2-1 Calibration curve of a pH microelectrode.

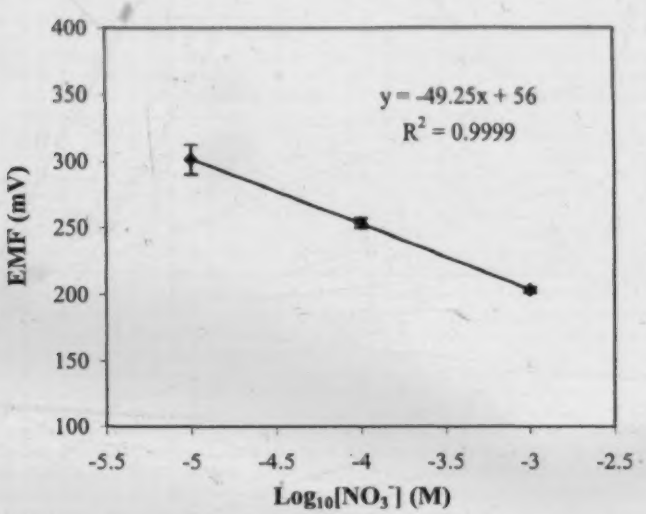

Figure 2-2 Calibration curve of a nitrate microelectrode.

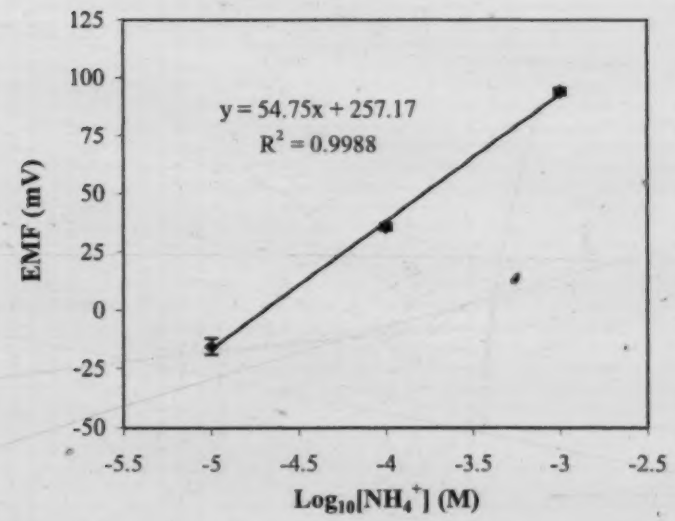

Figure 2-3 Calibration curve of an ammonium microelectrode.

2.1.2 Amperometric microelectrodes

Microelectrodes used in this dissertation research for oxygen and NH_2Cl measurements were both based on an amperometric technique. Because the NH_2Cl microelectrode was newly developed and applied to biofilm study for the first time in this research, a separate chapter (Chapter 3) is arranged to provide detailed discussions on the development of this particular microelectrode. The following sections mainly focus on the working principles of the amperometric technique as well as the fabrication and calibration of the oxygen microelectrode.

2.1.2.1 Working principles of amperometric electrodes

Amperometric electrodes work on the basis of a linear relationship between the current created by electrochemical reaction of an analyte (e.g. oxygen) on the surface of an electrically polarized electrode and the concentration (more accurately, activity or partial pressure) of the analyte in the sample under test. The linear relationship established between the current and the concentration of the analyte in the sample can be expressed as the following equation (Strobel and Heineman, 1989):

$$I = nFADC/\delta \qquad (2\text{-}2)$$

Where, "I" is current, "n" is number of electrons transferred in electrochemical reaction, "F" is Faraday's constant, "A" is surface area of electrode tip, "D" is diffusion coefficient of analyte of interest in solution, "C" is concentration of analyte of interest in bulk solution, "δ" is thickness of diffusion layer. For a given analysis, n, F, A, D and δ can be taken as constant, thus the product of these constants (i.e. $nFAD/\delta$) is a constant factor as well. This factor, often called the calibration factor, can be determined by

implementing a calibration process on the electrode.

2.1.2.2 Fabrication of an oxygen microelectrode

In this dissertation research, a combined oxygen microelectrode with a guard cathode designed by Revsbech (1989) was used. The oxygen microelectrode comprised a working cathode with a glass shaft, a reference anode, a guard cathode, an outer casing, electrolyte and an oxygen permeable silicone membrane. The detailed fabrication procedures for the oxygen microelectrode were introduced elsewhere (Lu and Yu, 2002). Major steps of its fabrication are introduced as follows:

Step 1: Preparation of glass tubing for working cathode shaft. The working cathode shaft consisted of two parts: the white tubing (Schott Glas Export GmbH, Mainz, Germany; Schott 8350, outer diameter: 4.0 mm, wall: 0.5 mm) and the green tubing (Schott 8533, outer diameter: 3.33 mm, inner diameter: 2.69 mm). Each of both glass tubings was heated at the middle over a natural gas burner, and then was pulled by hand until the middle section became around 2.5 mm in diameter for the white or a very fine capillary for the green. These pulled tubings were cut at the middle. For the green tubing, its un-pulled end was further cut off such that only about 1 to 2 cm was left.

Step 2: Etching of working cathode wire. The tip of a piece of platinum (Pt) wire (Aldrich Chem. Co., Milwaukee, WI, USA; Cat.# 35,736-7; 99.99%, diameter: 0.10 mm, length: about 6 cm) was etched in 1 M alkaline (pH > 13) potassium cyanide (KCN) solution under 6 to 7 V voltage supplied by a custom-made power supply with the Pt wire as one electrode and a graphite rod as the other. The Pt wire was moved up and down for several minutes until a tip diameter as small as 1 to 2 μm was obtained. Then,

the Pt wire was rinsed by being immersed, in turn, in three beakers filled with distilled water. Finally, the Pt wire was gently inserted into the pre-made green glass tubing with the etched tip staying in the capillary part.

Step 3: Assembly of working cathode. The pulled end of the pre-made white glass tubing was inserted into the un-pulled end of the green glass tubing with the etched Pt wire. The joint of the white and green tubings was melted together over a fine flame of a butane burner (BernzOmatic, NY, USA; Micro Torch, Model# ST1000TS).

Step 4: Tapering of working cathode tip. First, two stands were prepared: a stand for micromanipulator installation and an extension clamp stand for holding a porcelain socket fixed with a piece of W-shaped canthal wire as a heating loop. Then, the working cathode shaft was hung from its capillary end on the micromanipulator (WPI, Model M3301R). This set-up was adjusted so that the capillary section of the working cathode shaft was placed within the heating loop with the tip of the etched Pt wire within the capillary located at about 1.5 to 2.0 cm above the loop. Heat was then applied until the glass capillary started melting and slowly dropping down to a point where the Pt wire tip was about 0.5 to 1.0 cm above the loop, the voltage was quickly increased so as to make the melting glass less viscous hence coating on the Pt wire. Finally, the whole cathode shaft dropped into a napkin-stuffed beaker underneath. The whole process was monitored with the aid of a horizontal microscope (Carl Zeiss, Jena, Germany; Model: Stemi SV11).

Step 5: Gold-plating of working cathode tip. A gold-plating circuit was prepared by first connecting the negative pole of a 1.5 V battery to the Pt wire in the working cathode shaft. The positive pole of the same battery was then connected to a

piece of Ag wire (99.99%; diameter: 0.25 mm) soldered with a short piece of Pt wire that was inserted into the large end of a Pasteur pipette. The other end of this Pt wire was immersed in an $AuCl_3$ solution (ca. 0.1 M) (Fisher's Cat.# G54-1; $HAuCl_4 \cdot 3H_2O$), which had been sucked into the tip of the Pasteur pipette. The glass coating over the tip of the tapered working cathode was removed by using a micro-dissecting tweezer (Roboz Surgical Instrument Inc., Rockville, MD, USA; Cat.# RS-4905). This step was conducted carefully under a microscope with a built-in scale (Carl Zeiss, Model Axioskop 2 Plus). During the electro-plating process, the naked cathode tip was advanced, through the movement of the microscope stage, into the $AuCl_3$ solution in the Pasteur pipette and stayed there for several seconds, and consequently, a layer of gold on the naked cathode tip was achieved.

Step 6: Preparation of outer casing. The fine section of a Pasteur pipette was heated over a natural gas burner and then pulled by hand until a diameter around 0.5 mm was obtained. Afterwards, the pulled pipette was tapered as in Step 4. As the pipette started dropping, it was moved downward slowly so as to obtain a suitable length and diameter of the casing tip. Finally, the casing dropped into the napkin-stuffed beaker underneath. Sometimes, the casing tip was longer than needed and in that case it could be adjusted at the final assembly stage.

- **Step 7: Preparation of guard cathode.** A piece of white glass tubing was heated and pulled by hand until an inner diameter a little bigger than the Ag wire (Aldrich Chem. Co., Milwaukee, WI, USA, Cat.# 26,555-1; diameter: 0.127 mm) was obtained. The pulled capillary tubing was then cut into 7 to 8 cm long sections. A piece of the Ag wire with a length of about 20 cm was inserted into the prepared capillary with its two ends

extending out of the capillary. One end of the capillary was sealed with Epoxy (Mastercraft Canada, Toronto; 5 minute Epoxy, Resin and Hardener) and then was dried in the air. Later, similar to etching the Pt wire of the working cathode, the tip (about 1 cm in length) of the sealed Ag wire was etched in 0.5 M alkaline KCN solution until a diameter around 1 to 5 μm was obtained.

Step 8: Preparation of reference electrode. A piece of Ag wire (diameter: 0.25 mm) was connected to the negative pole of a 1.5 V AA battery and another piece of the Ag wire with the positive pole of the same battery. Then both of these Ag wires (about 3 to 4 cm in length) were immersed in 1 M HCl solution in a small beaker. In about 1 to 2 minutes, the color of the immersed section of the Ag wire connected with the positive pole became brown, which is the color of AgCl. This AgCl-covered Ag wire was then rinsed with distilled water and later served as the Ag/AgCl reference electrode.

Step 9: Assembly of oxygen microelectrode. The outer casing was fixed on the microscope stage. The working cathode was inserted into the outer casing and pushed carefully toward the tip of the outer casing using the micromanipulator. The distance between the tips of the working cathode and the outer casing was controlled at about 30 to 50 μm. If the distance was too long, a micro-dissecting tweezer could be used to cut the outer casing tip shorter. Another option could be to use a tip-closed Pasteur pipette, mounted on a micromanipulator, to bump the tip of the outer casing to break it shorter. The shaft of the working cathode was then fastened on the microscope stage by the spring clip on the stage. Then, the guard cathode was inserted along the working cathode but stopped behind its tip. Finally, the reference electrode was inserted into the outer casing so that its brown section was kept just within the outer casing. Epoxy was applied

to glue the working, guard and reference electrodes with the outer casing, but an opening was still kept for later addition of electrolyte and glass beads. A tip-closed Pasteur pipette covered with silicone (Dow Corning Co., MI, USA; Silastic Medical Adhensive, Type A) at its tip was mounted on a micromanipulator and was located such that its silicone-covered tip exactly pointed toward the outer casing tip. Then the pipette tip was moved toward the outer casing tip by adjusting the micromanipulator so as to get a membrane with a thickness of 10 to 20 μm within the outer casing tip. The partially finished microelectrode was stored in a test tube overnight to dry the Epoxy and the silicone membrane in the air. Before electrolyte was injected into the outer casing, a piece of Ag wire (Aldrich Chem. Co., Milwaukee, WI, USA; Cat.# 26,555-1; Diameter: 0.127 mm) was inserted into the open end of the working cathode shaft until it contacted the Pt wire. Then, Epoxy was applied to seal the open end of the working cathode shaft. Afterwards, a little electrolyte (a mixture of 0.2 M $KHCO_3$ (50 mL), 0.3 M K_2CO_3 (50 mL), 1.0 M KCl (100 mL) and a little thymol) was first injected into the assembled outer casing, using 1 mL syringe (Becton Dickinson & Co., Franklin Lakes, NJ, USA; Cat.# 309597) with a filter device (Fisher's Cat.# 5-713-401; Puradisc 25 PP, Whatman, 0.2 μm). Then the outer casing was checked under the microscope to see if there were any air bubble(s) within it, especially near the tip. If there was, then the tip was immersed into a beaker of purged water (obtained by boiling water for several minutes) to eliminate bubble(s). After the bubbles were eliminated, a very small amount of glass beads (3M Empore, St. Paul, MN, USA; Filter Aid 400; Diameter 20 to 40 μm;) was added into the outer casing and electrolyte was further injected until the outer casing was full. Finally, Epoxy was applied to completely seal the outer casing and then was dried in the air. The

ultimate tip diameter of the oxygen microelectrode ranged from 15 to 25 μm.

2.1.2.3 Calibration of oxygen microelectrode

After polarization to achieve stable signals, the oxygen microelectrode was calibrated each time before it was used for biofilm measurements. Before calibration, the tip of the oxygen microelectrode was immersed in dstilled water in a custom-made calibration chamber made from Plexiglas, and the microelectrode was connected with an electrometer (Keithley, Model 6517A) that was used to apply a potential of -0.8V (vs Ag/AgCl) as well as to collect current signals generated at the working microelectrode. During a calibration using three points, compressed air with 21% oxygen, a mixed gas with 10.5% oxygen balanced with nitrogen, or nitrogen gas (0% oxygen) was flushed into the calibration chamber through a gas dispersion tube at a flow rate without changing water temperature to generate different conditions with respect to the oxygen concentration in the chamber. Figure 2-4 illustrates a typical calibration curve for a combined oxygen microelectrode (Lu and Yu, 2002). Since it has been observed that such a linear calibration curve could always be achieved from this type of oxygen microelectrode, normally, a 2-point (21% oxygen and oxygen-free) calibration is sufficient for routine use of the oxygen microelectrode. Figure 2-5 illustrates a calibration process for the oxygen microelectrode. As shown in Figure 2-5, the signals corresponding to air-saturated and oxygen-free conditions were at around 280 pA and 7 pA, respectively. This microelectrode had good sensitivity (32.7 pA/mg/L of dissolved oxygen), fast response time (< 1 second) and low stirring effect (<2%).

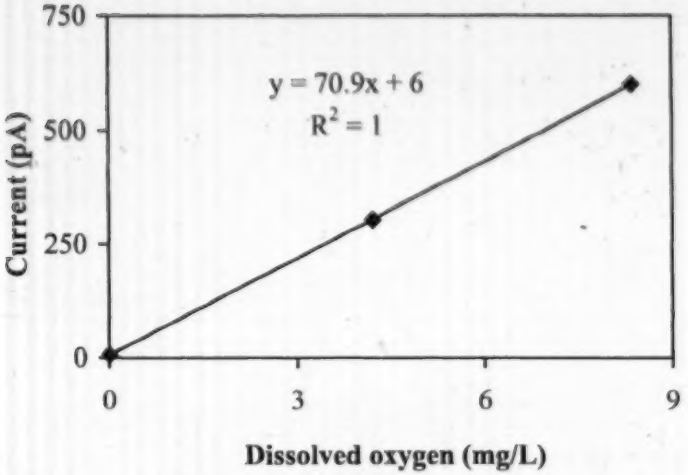

Figure 2-4 Calibration curve of a combined oxygen microelectrode (Lu and Yu, 2002).

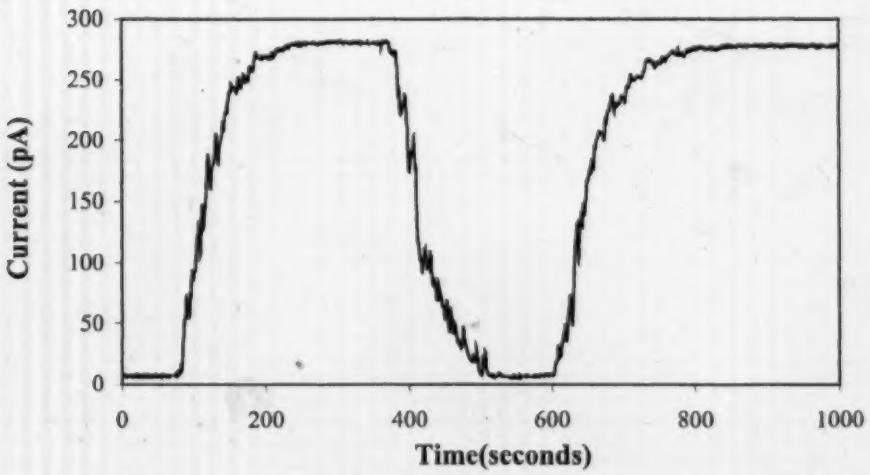

Figure 2-5 A calibration process for a combined oxygen microelectrode.

Before being used for biofilms measurements, the oxygen microelectrode was also calibrated using the water sampled from the biofilm growth system that provided the same water for oxygen measurement in biofilms to take into consideration the potential matrix effect from the water.

2.2 Model water distribution system for biofilm growth

The set-up used to simulate a drinking water distribution system and to promote biofilm growth in such a system is illustrated in Figure 2-6 including an annular reactor (BioSurface Technologies Co., Bozeman, MT, USA, Model 1120JL) and inputs of nutrients and disinfectant with controlled flow rates. The annular reactor consisted of a stationary outer cylinder and an inner drum with 20 slots available for installation of different types of slides made of concrete, polyvinylchloride (PVC), and polycarbonate (PC) as substratum materials for biofilm growth. In this dissertation research, the commercially purchased biofilm slides were cut in half so that the number of slides available for sampling was doubled. The inner drum could rotate at various speeds to create different shear stresses. The retention time (RT) in the reactor could be determined by the dilution rate (or feed flow rate). As a result, this reactor had a capacity to simulate RT and shear force separately within the same system. This provided flexibility to design and operate different combinations of these two factors as desired. The effective volume of the reactor was around 950 mL. With four draft mixing tubes across the inner drum, this reactor could be operated as a complete mixing reactor.

Before being seeded, the assembled model system, including the reactor installed with various slides and tubings, was filled and re-circulated with ethanol (70%) for about

2 cycles. Afterwards, the re-circulation was stopped and the whole system was filled with ethanol overnight before it was rinsed thoroughly with distilled water for about 6 cycles. During the formal operational period, the model system had been aerated by continuously flushing filtered (via a PTFE membrane 0.45 μm filter), compressed air into the feed tank of the system to ensure the system was kept under an aerobic condition. Meanwhile, the system was monitored routinely for chemical and microbiological parameters, including pH, dissolved oxygen (DO), free and total Cl_2, nitrate, nitrite, ammonia, total organic carbon (TOC), heterotrophic plate count (HPC) bacteria, and most probable number (MPN) of nitrifying microorganisms. After biofilms with sufficient thickness became available on the removable slides or certain desired conditions in the model system had been achieved, they were taken out of the reactor and transferred to a special set-up for microelectrode measurement experiments. The model system was operated under room temperature (22 ± 2 °C) all the time.

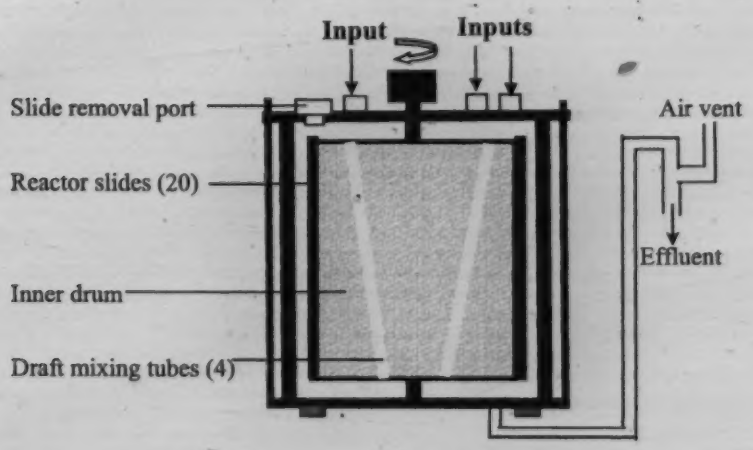

Figure 2-6 Biofilm growth reactor used for simulating water distribution system (modified based on information sheet provided by Biosurface Technologies Co.)

2.3 Set-up for microelectrode measurements in biofilms

All experiments on microelectrode measurements in biofilms were conducted using the set-up illustrated in Figure 2-7. The major part of this set-up was a custom-made flow cell made from transparent Plexiglas. Before the microelectrode measurement in biofilms was started, a stock solution of NH_2Cl with known concentration or water sample collected from the biofilm growth system was pumped into the flow cell at a pre-set flow rate with both the working and the reference electrodes (for the combined oxygen microelectrode, no external reference electrode was needed) immersed in the flowing solution in the flow cell. An arrangement of a peristaltic pump and a speed controller (Cole-Parmer Instrument Co., Vernon Hills, IL, USA, Masterflex model L/S EW-07553-70) was used to provide the pre-set flow rate of the input into the flow cell. After the monitored signals reached a stable status, concentration profiles of chemical species of interest from the bulk phase into the biofilm were then measured using the working microelectrode mounted on an oil hydraulic micromanipulator (Narishige Group, Tokyo, Japan, Cat.# MMO-202N) with a remote three-axis joystick to control movement of the microelectrode. The current or potential signals generated by the working microelectrode during each profile measurement were collected by an electrometer (Keithley, Model 6517A). Positioning of the working microelectrode on each biofilm spot to be measured was performed with the aid of a horizontal binocular microscope (Carl Zeiss, Model Stemi SV11). The entire measuring set-up was installed in a Faraday cage to avoid potential electromagnetic interference on the performance of microelectrodes.

2.4 Chemical and microbiological analyses

Throughout this dissertation research, conventional chemical and microbiological parameters analyzed either on water or biofilm samples included pH, DO, free and total Cl_2, nitrate, nitrite, ammonia, TOC, HPC, and MPN of nitrifying microorganisms. Analytical methods for these parameters generally followed the "Standard Methods" (APHA *et al.*, 1998) and are introduced briefly as follows. For some special parameters such as MPN of nitrifying microorganisms and biofilm thickness that do not have standard analytical methods, more detailed descriptions are presented based on the relevant literature.

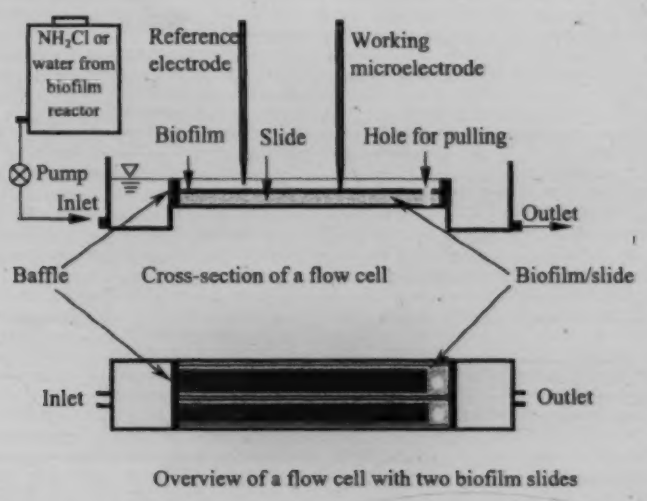

Figure 2-7 Set-up for microelectrode measurements in biofilms.

2.4.1 Chemical analyses

DO. Membrane electrode method using oxygen membrane electrode with DO meter (YSI Inc., Yellow Springs, OH, USA, Model 50B).

pH. Electrometric method using Accumet pH electrode and pH meter (Fisher's Cat.# 13-620-285 and model AR15, respectively).

Free and total Cl_2. DPD colorimetric method using a spectrophotometer (Biochrom Ltd, Cambridge, UK, Biochrom Ultraspec 110 pro UV/Visible) with a wavelength set at 515 nm. A series of standard solutions within the range from 0 to 2.0 mg/L as Cl_2 were tested in parallel each time samples were tested.

Nitrite-N. Colorimetric method using wavelength at 543 nm. Serial standard solutions in the range from 0 to 0.1 mg/L as NO_2^--N were tested in parallel with samples.

Nitrate-N. Colorimetric method using wavelengths at 220 and 275 nm. A series of standard solutions ranging from 0 to 2.0 m/L as NO_3^--N were tested in parallel with samples.

NH_3-N. Phenate colorimetric method using wavelength at 640 nm. Serial standard solutions in the range from 0 to 1.464 mg/L as NH_3-N were tested in parallel with samples.

TOC. Method of UV promoted chemical (persulfate) oxidation followed by infra-red detection. A total organic carbon analyzer (Dohrmann Division, Xertex Corporation, Santa Clara, CA, USA, XERTEX/Dohrmann DC-80) equipped with a linearized non-dispersive infra-red detector was used. Standard solutions of potassium hydrogen phthalate and Na_2CO_3 of 10 mg/L were used for equipment calibration each time samples were tested.

2.4.2 Microbiological analyses

HPC test. Spread plate method with Difco R2A agar (Fisher's Cat.# DF1826171)

as culture medium. Incubation was implemented in a gravity convection incubator (Precision Scientific Group, Chicago, IL, USA, Cat.# 31485). Specific incubation time and temperature are presented in Section 4.2.3 of Chapter 4 and Section 5.2.4 of Chapter 5. For water samples, they were directly used for ten-fold serial dilution preparation; but for biofilm samples, a pre-treatment was implemented as follows. After the biofilm was scraped from a slide using a cell scraper (Corning Inc., Corning, NY, USA, Cat.#3010), it was rinsed with 100 mL autoclaved distilled water or phosphate buffer solution (PBS) into an autoclaved Erlenmeyer flask. The PBS was made by dissolving 0.256 g $NaH_2PO_4 \cdot H_2O$, 1.194 g Na_2HPO_4 and 8.766 g NaCl in 1 L distilled water with ultimate pH at around 7.3. The biofilm suspension was then homogenized on a vortex mixer (Scientific Industries, Inc., Bohemia, NY, USA, Vortex-Genie 2, model # G-560) with a rotation speed at scale 10 for about 3 minutes. The homogenized biofilm suspension was then further treated similarly as water samples for ten-fold serial dilutions (from 1×10^{-1} to 1×10^{-5}) preparation using autoclaved test tubes pre-filled with 9 mL autoclaved distilled water or PBS. Then, 0.1 or 0.5 mL dilute sample at each level was transferred and spread on culture medium in triplicate before incubation. For water samples, the ultimate results of HPC analyses were expressed in colony-forming units (cfu)/mL. For biofilm samples, the length and width of the scraped area on biofilm slides were measured for later HPC density calculation. The ultimate plate count results were expressed as biofilm HPC density in cfu/cm^2.

MPN test for nitrifying microorganisms. There is no standard method currently available for nitrifying microorganisms enumeration. In this dissertation research, the five-tube MPN technique was adopted according to Wolf *et al.* (1988, 1990) and Pintar

and Slawson (2003). Ten-fold serial dilutions (from 1×10^{-1} to 1×10^{-3}) of water or homogenized biofilm samples were made in test tubes, in duplicate, using a modified Soriano & Walker (MSW) culturing medium with the following ingredients (per liter of distilled water): 0.5 g $(NH_4)_2SO_4$, 0.04 g $MgSO_4 \cdot 7H_2O$, 0.04 g $CaCl_2 \cdot 2H_2O$, 0.2 g KH_2PO_4, 0.00016 g ferric citrate, and 0.002 g phenol red. The medium pH was adjusted with NaOH (1 M) to 8.0. Incubation was implemented at 28 °C in the dark for 28 days. After incubation, each test tube was tested for the presence of nitrite or nitrate using cell plate testing with a Corning Costar 24-well cell culture cluster (Fisher's Cat.# CS003526). For the nitrite test, 2 to 3 drops of sample were transferred from each test tube to each cell of the well plate, and then 1 to 2 drop(s) of sulfanilic acid (Fisher's Cat.# A296500) and N,N-dimethyl-α-naphthylamine (Fisher's Cat.# AC204170250) were added into each well with the sample. Culture tubes that exhibited a pink color within 1 minute after addition of the reagents were scored positive for nitrite. For those cultures that were scored negative, a similar procedure was implemented for the nitrate test but with different reagents - diphenylamine (Fisher's Cat.# AC42365) and concentrated H_2SO_4 (98%). Culture tubes that gave a dark blue color within 1 minute were scored positive for nitrate. Ultimately, any culture tube that scored positive for either nitrite or nitrate was scored positive for nitrifying microorganisms, and the MPN was determined accordingly following the approach described in the "Standard Methods" (APHA *et al.*, 1998). Negative and positive controls consisted of distilled water supplemented with MSW medium and MSW medium inoculated with an actively growing culture of nitrifying bacteria (*Nitrosomonas europaea*) (American Type Culture Collection, Rockville, MD, USA, ATCC#19718), respectively. All controls were

incubated under the same conditions as the water and biofilm samples. It has been reported that this MPN procedure has very low recovery efficiencies (0.1 to 5%) (Belser and Mays, 1982), therefore, the result of this technique is more appropriately used for relative comparisons or qualitative presence or absence judgment rather than absolute quantification of nitrifying microorganisms.

Biofilm thickness. Thickness of biofilms grown on slide was estimated using an optical microscopic method with a light microscope (Carl Zeiss, Germany Model Axioskop 2 Plus) as introduced by Bakke and Olsson (1986). Optical thickness (Y_f) of biofilm can be measured directly with microscope by measuring the vertical displacement of the biofilm sample required to move the focal point across the biofilm thickness. However, due to the difference between the refractive indexes in air, water and substratum materials, the actual thickness (L_f) of biofilm (i.e. mechanical thickness) is not the optical thickness. Y_f and L_f are proportional to each other with a proportionality constant, k_f (i.e. $L_f = k_f \cdot Y_f$). Approximated $k_f = n_f/n_m$, where n_f = light refractive index of the biofilm, n_m = refractive index of the medium interfacing the biofilm at its top surface (i.e. the biofilm interface closest to the objective lens). To determine biofilm thickness by light microscopy, knowledge of biofilm refractive index is, therefore, required. Due to the high content of water in biofilms, it is reasonable to assume that its refractive index will be close to that of water, which is 1.333. In the case that the biofilm is tested directly exposed to the air, n_m of the air is taken as unity. As a result, actual biofilm thickness $L_f = 1.333 Y_f$.

2.5 References

American Public Health Association (APHA), American Water Works Association (AWWA), Water Environment Federation (WEF) 1998. *Standard methods for the examination of water and wastewater*, 20th edition. Washington D. C.

Bakke R. and Olsson P. Q. 1986. Biofilm thickness measurements by light microscopy. *Journal of Microbiological Methods*, 5:93-98.

Belser, L. W. and Mays, E. L. 1982. Use of nitrifier activity measurements to estimate the efficiency of viable nitrifier counts in soils and sediments. *Applied and Environmental Microbiology*, 43:945.

de Beer, D., Schramm, A., Santegoeds, C. M. and Kuhl, M. 1997. A nitrite microsensor for profiling environmental biofilms. *Applied and Environmental Microbiology*, 63:973-977.

Li, J. 2001. *Azo dye biodegradation and inhibition effects on aerobic nitrification and anoxic denitrification processes*. Ph.D. dissertation. University of Cincinnati, Cincinnati, Ohio, USA.

Lu, R. and Yu, T. 2002. Fabrication and evaluation of an oxygen microelectrode applicable to environmental engineering and science. *Journal of Environmental Engineering and Science*, 1:225-235.

Pintar, K. D. M. and Slawson, R. M. 2003. Effect of temperature and disinfection strategies on ammonia-oxidizing bacteria in a bench-scale drinking water distribution system. *Water Research*, 37:1805-1817.

Revsbech, N. L. 1989. An oxygen microelectrode with a guard cathode. *Limnology and Oceanography*, 34:474-478.

Strobel, H. A. and Heineman, W. R. 1989. *Chemical instrumentation: a systematic approach*, 3rd edition, John Wiley & Sons, Inc., New York.

Wolfe, R. L., Means, E. G. III, Davis, M. K. and Barrett, S. E. 1988. Biological nitrification in covered reservoirs containing chloraminated water. *Journal AWWA*, 80:109-114.

Wolfe, R. L., Lieu, N. I., Izaguirre, G. and Means, E. G. 1990. Ammonia-oxidizing bacteria in a chloraminated distribution system: seasonal occurrence, distribution, and disinfection resistance. *Applied and Environmental Microbiology*, 56:451- 462.

Yu, T. 2000. *Stratification of microbial processes and redox potential changes in biofilms*. Ph.D. dissertation, University of Cincinnati, Cincinnati, Ohio, USA.

Chapter 3

Development of Microelectrodes For NH_2Cl Measurements

3.1 Introduction

Nitrification outbreaks in chloraminated water distribution systems (CWDSs) have been believed to be due to the activities of nitrifying microorganisms embedded in biofilms growing on facility surfaces in the CWDSs (Wolfe *et al.*, 1988; Cunliffe, 1991; Skadsen, 1993; Wilczak *et al.*, 1996; Lipponen *et al.*, 2002). This indicates that NH_2Cl residual concentrations sufficient to inhibit microbial regrowth in water might not be similarly sufficient to inactivate biofilm microorganisms due to the protection of the biofilm matrix. Conventional analytical approaches using viable cell count play limited roles in helping elucidate how NH_2Cl penetrates in biofilms so as to attack embedded cells. An *in-situ* approach to investigation into intact biofilms is more appropriate and desirable in this regard. Due to their tiny tips and high spatial resolutions, microelectrodes enable us to implement *in-situ* measurements in microenvironments within biofilms. There is, however, no microelectrode currently available for direct NH_2Cl measurement in biofilms.

The study reported in this chapter has developed two types of microelectrodes (the separate and the combined) applicable to direct NH_2Cl measurements. The combined microelectrode comprises both working and reference electrodes that are electrically connected via an internal electrolyte, whereas the separate microelectrode includes the working electrode only. An external reference electrode is needed when the separate microelectrode is used for measurement. Both of these two types of

microelectrodes work on the basis of an amperometric technique, which is based on a linear relationship between electric current created by electrochemical reaction (reduction or oxidation) of an analyte (e.g. NH_2Cl) on the surface of an electrically polarized electrode (i.e. the working electrode) and concentration (more strictly, activity) of the analyte in the sample under test. The linear relationship established between the current generated at the microelectrode and the concentration of the analyte in the sample can be expressed by Equation (2-2) discussed in Chapter 2.

In an amperometric electrode, the current generated at the electrically polarized electrode and measured by a sensitive ammeter is equivalent to the rate of the electrochemical reaction occurring on the surface of the electrode. The rate of the electrochemical reaction is determined by the applied potential and the rate at which the analyte arrives at the electrode (i.e. mass transport rate). Increasing the potential increases the current up to a point termed the "limiting current", beyond which any further increase of the potential does not produce more current. This condition exists because the analyte is consumed as fast as it arrives at the electrode surface and the reaction rate now is determined only by the mass transport rate, which is driven by the analyte concentration gradient existing in a diffusion layer over the electrode surface. As a result, in order for an amperometric electrode to work well for a specific chemical species, it is critical to find the right "polarization potential", under which this specific chemical can undergo an electrochemical reaction on the surface of the electrode, and a linear relationship between the generated current and the concentration of the chemical in question can be established. A good example of an amperometric microelectrode is the one for oxygen measurement as introduced earlier in Chapter 2. NH_2Cl is an oxidant as

well, therefore, it can be reduced on the surface of the working electrode (the cathode) under an appropriate potential applied and thus the resultant current signal can be created and detected.

The following sections in Chapter 3 introduce the development processes of these two types of microelectrodes suitable for NH_2Cl measurements, including the determination of specific polarization potential for NH_2Cl by constructing i-E curves of NH_2Cl, materials selection, fabrication and calibration of the microelectrodes. In addition, determination of the diffusion coefficient of NH_2Cl was also implemented in this study. In combination with microelectrode measurements, this coefficient can be used for estimation of mass transfer or flux of NH_2Cl in biofilms.

3.2 Materials and methods

This section focuses on materials and methods used specifically for the purposes of this particular study on the development of microelectrodes suitable for NH_2Cl measurements. They include those used in voltammetric experiments as well as fabrication and calibration of the separate and combined microelectrodes for NH_2Cl measurements. Detailed descriptions on generally used chemical analyses are presented in Chapter 2.

3.2.1 Voltammetric experiments

A series of voltammetric experiments were implemented in this study in order to construct i-E curves, based on which an appropriate polarization potential and diffusion coefficient of NH_2Cl have been determined. A three-electrode cell arrangement was

used in the voltammetric experiments. The working electrode was a piece of platinum wire (Aldrich Chem. Co., Milwaukee, WI, USA; Cat.# 35,736-7, 99.99%, diameter = 0.1 mm). A piece of similar platinum wire was coiled and used as the counter electrode. The reference electrode was a piece of silver wire (Aldrich Cat.# 32,703-4, 99.99%, diameter = 0.25 mm) coated with silver chloride at its tip part. Each of these three electrodes was sealed into a glass tube (Pasteur pipette). The experimental set-up for the three-electrode cell is shown in Figure 3-1. Linear sweep voltage was applied with a scan rate (SR) at 10 mV/s and a scan increment (SI) at 2 mV/s. The scanning processes were controlled and corresponding results were recorded by a Potentiostat/Galvanostat (EG&G Princeton Applied Research, Oak Ridge, TN, USA; Model 273) connected with a personal computer installed with Model 270/250 Research Electrochemistry Software 4.30 (EG&G Instrument Inc., Oak Ridge, TN, USA). In order to avoid interference from dissolved oxygen (DO), compressed pre-purified N_2 gas was used to purge the NH_2Cl solution under test prior to each test whenever necessary to generate "O_2-free NH_2Cl solution". Corresponding to three tested NH_2Cl solutions with respective concentrations at 0.73 mM, 0.69 mM and 0.92 mM (all as Cl_2), three pH-buffered supporting electrolytes (0.1 M potassium hydrogen phthalate/HCl with pH at 3.8, 0.1 M KH_2PO_4/NaOH with pH at 7.1, and 0.1 M $KHCO_3$/NaOH with pH at 10.1) were adopted, respectively. All solutions used were made using ultra pure water produced by a Maxima Ultra Pure Water system (ELGA LabWater, Bucks, UK) with output water quality of at least 18 MΩ-cm with respect to resistivity.

To determine the diffusion coefficient of NH_2Cl, the same experimental set-up described above was used. The reactive surface area of the working electrode tip was ca.

2.0×10^{-3} cm^2, which was estimated based on tip dimension measurements with the aid of a vertical microscope with built-in scale (Carl Zeiss, Germany; Model Axioskop 2 Plus). The NH_2Cl solution used had a concentration of 3.26 mM as Cl_2 and had been purged with compressed pure N_2 gas just before tests. The supporting electrolyte was 0.25 M KH_2PO_4/NaOH with pH adjusted to 7.0. Linear sweep voltages were applied with SR at 100, 50 and 20 mV/s, respectively, and all with a similar SI at 2 mV/s. All voltammetric experiments were conducted at room temperature (22 °C).

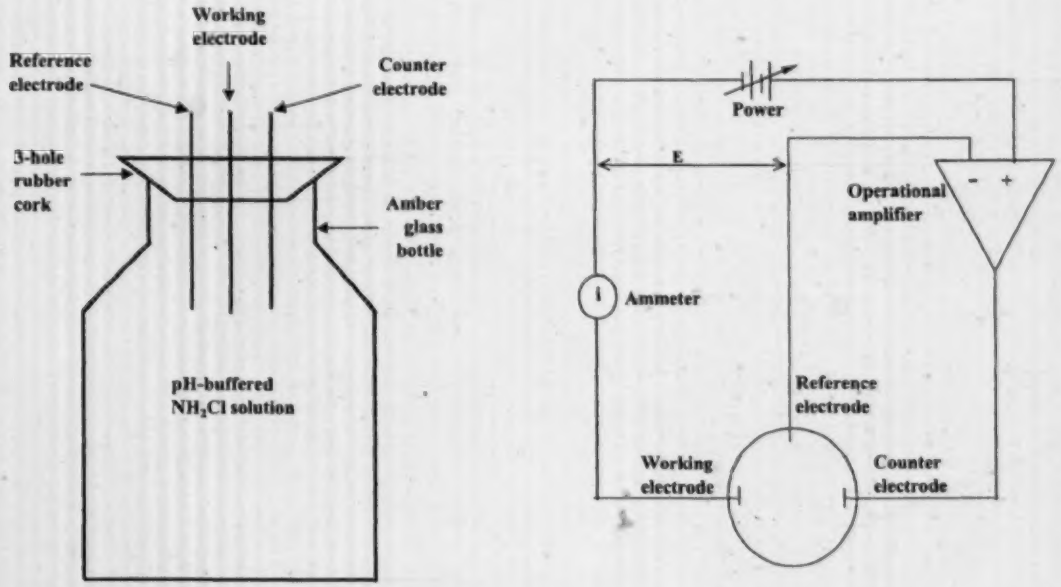

Figure 3-1 Schematic of a three-electrode cell (left) and electric circuit (right) for voltammetric experiment.

3.2.2 The separate microelectrode

Fabrication. A piece of white glass tubing (Schott Glas Export GmbH, Mainz, Germany; Schott 8350, outer diameter: 4.0 mm, wall: 0.5 mm) was pulled by hand under

heat to form a capillary at one end. This tapered tubing was later used as the shaft for the working electrode. A piece of platinum (Pt) wire (Aldrich Cat.# 35,736-7, 99.99%, diameter = 0.10 mm) was soldered with a piece of silver wire (Aldrich Cat.# 32,703-4, 99.99%, diameter = 0.25mm) at one end and the other end of the Pt wire was etched in 1 M alkaline (pH > 13) potassium cyanide (KCN) solution under an applied voltage of around 5 to 6 V (AC) until the diameter of its tip was decreased down to around 2 to 5 μm. This etched Pt wire was then inserted into the previously tapered shaft to ensure that the etched tip stayed in the capillary part. Afterwards, the etched Pt wire was coated with the glass through a tapering process as described previously in Section 2.1.2.2 of Chapter 2. With the aid of a vertical microscope, the tip of the glass-coated Pt wire was exposed using micro-dissecting tweezer; and then the exposed tip was reheated briefly with the heating coil to reseal the lower part of the tip. As a final step, the exposed tip was dipped into 10% (w/v) cellulose acetate (CA)/acetone solution to form a layer of CA film on the tip. When the separate microelectrode was used for NH_2Cl measurement, a separate external reference electrode (usually an Ag/AgCl electrode) was required.

Calibration. A series of NH_2Cl solutions were made with distilled water by diluting a stock solution of NH_2Cl (ca. 150 mg/L as Cl_2) that was generated by a reaction between ammonium chloride (NH_4Cl) (1 M) and sodium hypochlorite (NaOCl) (commercially available at 4 to 6%) with a Cl:N ratio of 3:1 (w/w) to ensure that free chlorine in the solution was negligible, which was the case as the results of tests for free and total chlorine indicated. pH values of these serial NH_2Cl solutions were within the neutral range. All serial NH_2Cl solutions were separately stored in 1-L amber glass bottles. The exact concentration of NH_2Cl in each solution was analyzed just before it

was used for the calibration test.

Before the calibration test, the microelectrode had been kept under polarization in distilled water with applied potential at -90 mv (vs Ag/AgCl) until stable signals were achieved. This polarization potential was selected on the basis of the results of the aforementioned voltammetric experiments and supplied by an electrometer (Keithley, Model 6517A). During the calibration process, distilled water or NH_2Cl stock solution was continuously pumped, with a flow rate of 5 mL/min, into the same set-up as used for microelectrode measurements in biofilms illustrated in Figure 2-7 in Chapter 2 but without biofilm slides installed in the flow cell. The serial NH_2Cl stock solutions were tested in an ascending order with respect to the NH_2Cl concentration in the solutions starting with the distilled water. The current signals generated by the working microelectrode were collected by the electrometer. After stable current signals were achieved for one stock solution, an effluent sample for that solution was collected for NH_2Cl analysis; and meanwhile, the input was switched to another stock solution with the next higher concentration of NH_2Cl. During the entire calibration process, both the working microelectrode and an Ag/AgCl reference electrode (Microelectrodes, Inc., Bedford, NH, USA, MI-409 micro-reference electrode) had been kept immersed in the flowing solution in the flow cell all the time.

3.2.3 The combined microelectrode

Fabrication. The combined microelectrode for NH_2Cl measurement consisted of a working electrode, an internal reference electrode, an outer casing, pH-buffered

electrolyte, and a piece of tip membrane. The configuration of the combined microelectrode is illustrated in Figure 3-2.

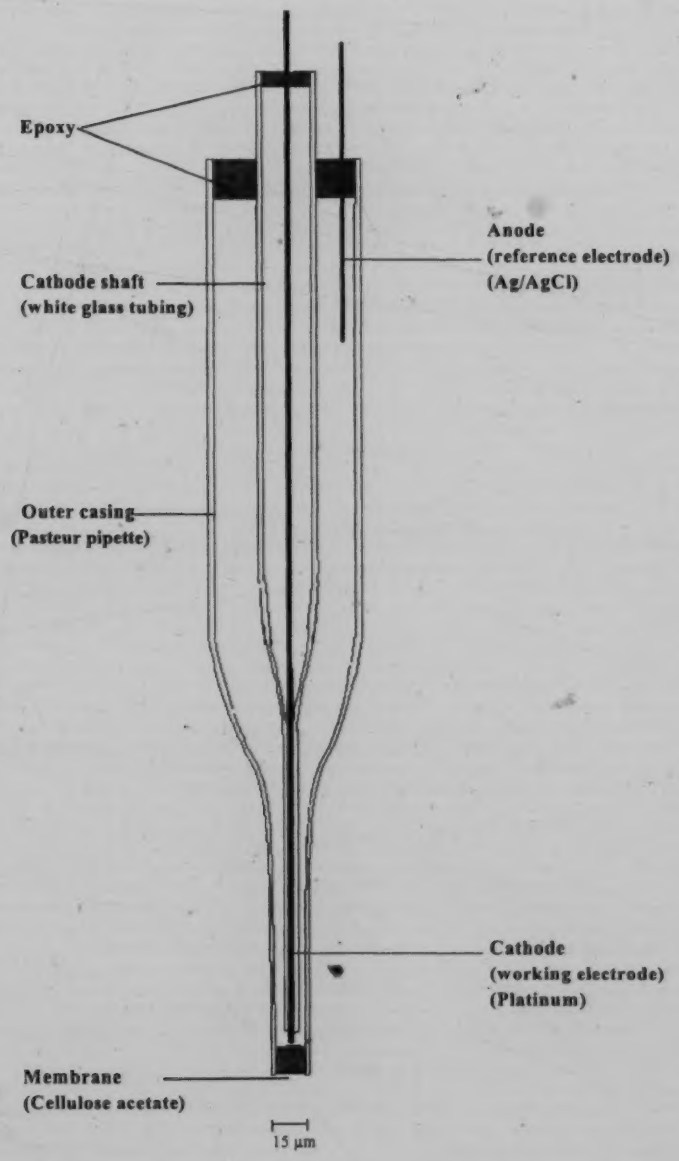

Figure 3-2 Schematic of a combined microelectrode for NH_2Cl measurement.

The major fabrication procedure for this microelectrode was similar to that of previous work on the combined oxygen microelectrode described in Section 2.1.2.2 of Chapter 2. The working electrode was prepared similarly as described earlier for the separate microelectrode for NH_2Cl measurement but without the coating of CA film at its tip. The internal reference electrode was a piece of silver wire (Aldrich Cat.# 32,703-4, 99.99%, diameter: 0.25 mm) coated with silver chloride. The outer casing was made from a Pasteur pipette with a tip diameter at around 15 to 20 μm. A solution of 0.1 M $KHCO_3$/NaOH with pH adjusted to 7.0 was used as the internal electrolyte. This internal electrolyte was selected on the basis of the results of the earlier voltammetric experiments. The tip membrane of the outer casing was made from CA.

It has been reported (Kesting, 1971; Strathmann, 1983; Pinnau and Freeman, 2000) that temperature, relative humidity and compositions of a CA/acetone/non-solvent mixture have significant influence on the formation of CA membrane. In this study, the entire fabrication process was implemented under room temperature (22 °C). The concentration of CA/acetone solution was ca. 0.2 to 0.5% (w/v). The relative humidity was maintained at an appropriate level via controlling the distance between the tip of the outer casing capillary and the tip of an opposing Pasteur pipette filled with ultra pure water mounted on a micromanipulator.

The actual fabrication process was started with the suction of CA/acetone solution into the outer casing capillary. Afterwards, the Pasteur pipette filled with CA/acetone solution mounted on a micromanipulator was immediately replaced with another Pasteur pipette filled with ultra pure water, and the distance between the capillary tip and the opposing pipette tip filled with water was controlled at around 0.2 mm. After

a few minutes, the acetone in the capillary would evaporate leaving behind a porous CA membrane at the tip of the capillary with a thickness at around 30 to 50 μm. The whole process was carefully monitored under a vertical microscope with built-in scale.

To check the quality of the CA membrane formed, a little bit of electrolyte was injected from the back into the outer casing with CA membrane at its tip; and this partially-finished product was stored in a test tube overnight. If there was no leakage at the tip of the capillary, the outer casing with CA membrane would be used for further steps of the fabrication process, i.e. assembly of all components including installation of the working and internal reference electrodes, injection of internal electrolyte and application of epoxy at the end of the outer casing to fasten the working and reference electrodes.

Calibration. A series of NH_2Cl solutions were made similarly as in calibration for the separate microelectrode. All these serial NH_2Cl solutions were separately stored in 60-mL amber glass bottles. Exact concentration of NH_2Cl in each solution was analyzed after calibration tests had been done on that specific solution. Similar to the separate microelectrode, before the beginning of the calibration, the combined microelectrode had been polarized under -90 mV (vs Ag/AgCl) until stable signals were achieved. During the calibration test, the microelectrode was dipped into each NH_2Cl solution in the amber bottle, and the current signals generated by the microelectrode were collected by the electrometer. Calibrations were made in an ascending as well as a descending order with respect to NH_2Cl concentration in the serial solutions. In the latter case, the microelectrode was rinsed with distilled water between tests of the two solutions.

3.3 Results and Discussions

3.3.1 Determination of polarization potential

To find an appropriate polarization potential that can be applied to an electrode to ensure that NH_2Cl is reduced on the surface of the electrode and that a limiting current is achieved was a critical step in developing the desired microelectrode in this study. This goal was achieved by implementing voltammetric experiments to construct an i-E curve (or voltammogram) for NH_2Cl. The constructed i-E curve helped disclose the relationship between different applied potentials (E) and the corresponding current signals (i) created from NH_2Cl reduction on the surface of the working electrode. Based upon the constructed i-E curve, the optimal range of polarization potential for NH_2Cl reduction was then determined.

i-E curves for O_2-free NH_2Cl solutions at three different pH values (i.e. pH 3.8, 7.1 and 10.1) were constructed and illustrated in Figure 3-3. As can be seen in Figure 3-3, pH conditions had substantial impacts on i-E curves for NH_2Cl. In other words, the shape of the i-E curve for NH_2Cl is pH-dependent. The start points of the limiting current plateaus under pH 3.8, 7.1 and 10.1 are around 200 mV, -90 mV and -400 mV vs Ag/AgCl, respectively.

It has been reported (Valentine *et al.*, 1998) that NH_2Cl decomposes and its decomposition rate increases with decreasing pH. Hypochlorous acid (HOCl) can be released from the decomposition process, a hydrolysis process of NH_2Cl, as expressed by the following equation:

$$NH_2Cl + H_2O \rightarrow HOCl + NH_3 \qquad (3\text{-}1)$$

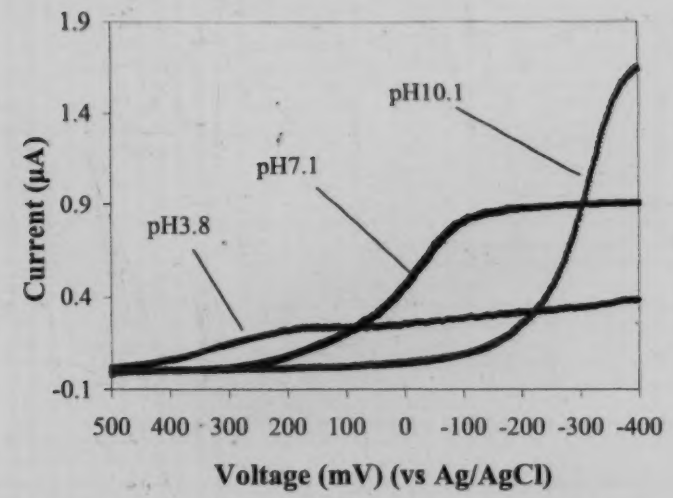

Figure 3-3 i-E curves for O_2-free NH_2Cl solutions under different pH values.

In an earlier study (de Beer *et al.*, 1994) on the penetration of free chlorine in biofilms, a linear relationship was successfully constructed between the free chlorine concentration and the current signal generated from a chlorine microelectrode under a polarization potential at 200 mV (vs Ag/AgCl). This helps further confirm that, under acidic condition with pH 3.8 as illustrated in Figure 3-4, it was free chlorine HOCl rather than NH_2Cl in the O_2-free NH_2Cl solution (Curve 2) that was reduced after the potential was scanned from 500 mV to 200 mV. A limiting current plateau clearly started to be formed for HOCl at 200 mV. Curve 3, which is for the pH buffer solution, illustrates the reduction process of DO as the potential scanning proceeded toward the more negative area. Curve 1, which is for the NH_2Cl solution with DO, illustrates a combined result of Curve 2 and Curve 3 displaying two plateaus formed at different potential ranges for two chemicals, HOCl and DO, respectively. It also can be seen in Figure 3-4 that under

acidic condition, the reduction of oxygen started to interfere with the signals generated from the reduction of HOCl as early as the applied potential was at 500 mV. This interference became more and more substantial as the applied potential was scanned toward the more negative direction, especially after about 180 mV.

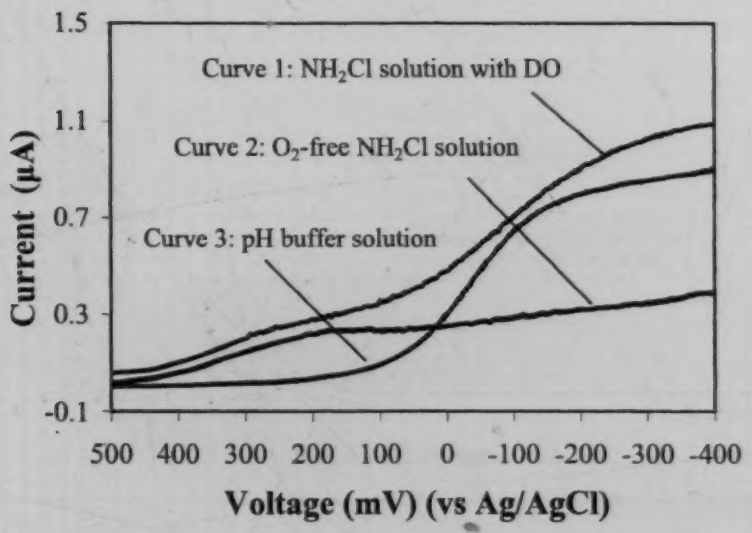

Figure 3-4 i-E curves for pH buffer solution, O_2-free NH_2Cl solution and NH_2Cl solution with DO at pH 3.8.

When pH was in the neutral range, as illustrated in Figure 3-5, NH_2Cl became dominant and thus was reduced when the applied potential was scanned to an appropriate value. At pH 7.1, the potential corresponding to the start point of the limiting current plateau was at around -90 mV, as shown on Curve 2, which depicts an i-E curve for the O_2-free NH_2Cl solution. Curve 3, which is for the pH buffer solution, clearly illustrates the DO reduction process as the potential was scanned from around zero down to -400 mV. Similar to Curve 1 in Figure 3-4 for pH 3.8, Curve 1 in Figure 3-5, which is for the

NH_2Cl solution with DO, also roughly shows a combined result of Curve 2 and Curve 3. From Figure 3-5, it also can be seen that under neutral pH condition, the interference of oxygen reduction with the signals generated from the reduction of NH_2Cl started to become more and more substantial as the applied potential was scanned toward the negative direction, especially after about -80 to -90 mV.

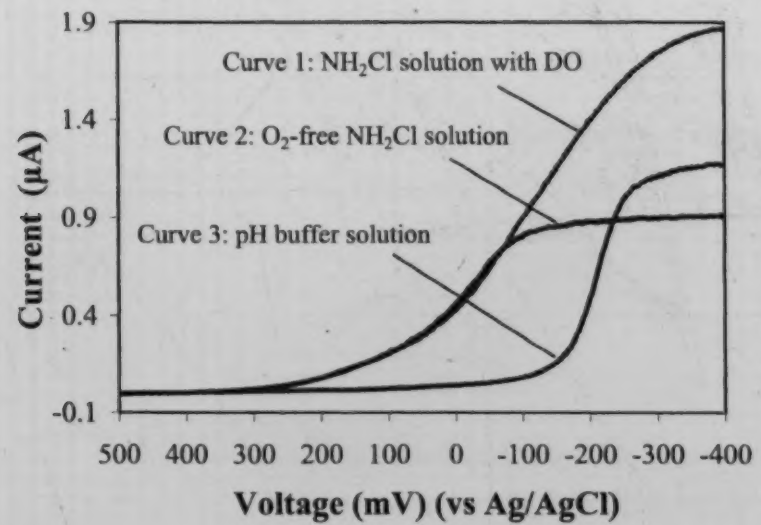

Figure 3-5 i-E curves for pH buffer solution, O_2-free NH_2Cl solution and NH_2Cl solution with DO at pH 7.1.

When pH was within the basic range (i.e. pH 10.1), the potential corresponding to the start point of the limiting current plateau for NH_2Cl was further shifted down to around -390 to -400 mV as shown in Curve 2 in Figure 3-6, which is for the O_2-free NH_2Cl solution. This phenomenon similarly happened to Curve 1 and Curve 3, which are for the NH_2Cl solution with DO and the pH buffer solution, respectively. The reason why the potential corresponding to the start point of the limiting current plateau for

NH_2Cl was so significantly different from that under neutral pH value could not be elucidated in this study. Was it possible that different forms of combined chlorines, in addition to NH_2Cl, co-existed and played roles under basic pH conditions? Or was it just like DO that had different polarization potentials, as shown in Curve 3 in Figure 3-4, Figure 3-5 and Figure 3-6, under different pH conditions? To answer these questions, more research needs to be implemented. However, this was beyond the initial goal of this study.

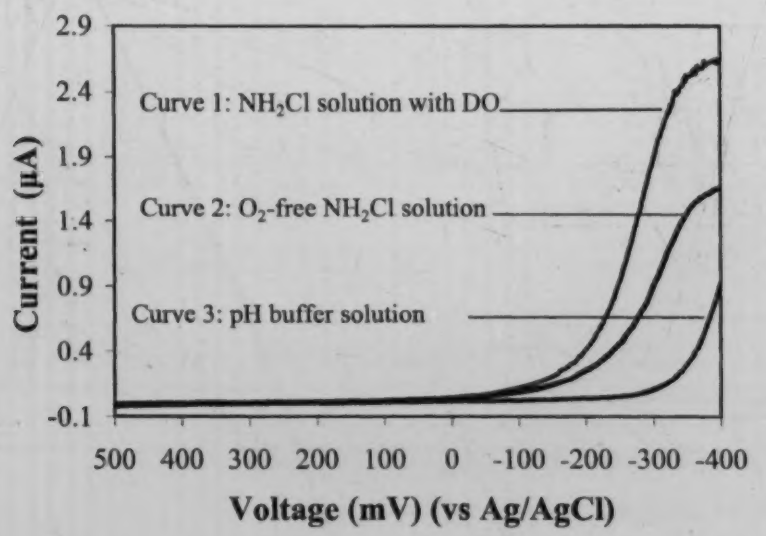

Figure 3-6 i-E curves for pH buffer solution, O_2-free NH_2Cl solution and NH_2Cl solution with DO at pH 10.1.

Under drinking water conditions, pH normally falls into the neutral range. In addition, NH_2Cl is the desired form for microbial inactivation used by water utilities in their water distribution systems. Therefore, based on the curve of pH 7.1 illustrated in Figure 3-3, the potential of -90 mV (vs Ag/AgCl) was chosen as the polarization potential for the microelectrode to be developed for NH_2Cl measurement in this study.

This particularly selected potential can help meet two requirements, i.e. the provision of limiting current from NH_2Cl reduction and minimization of the potential interference from DO reduction under more negative potentials.

It is worth pointing out that in this study, the water conditions in the case of pH 7.1 were carefully controlled so that the monochloramine dominated while the free chlorine was non-detectable in the waters. In reality, however, there are aquatic environments, in which different forms of chlorines (i.e. free chlorine and monochloramine) may co-exist. According to what has been observed in this study, selections of appropriate polarization potentials can potentially help distinguish the co-existing forms of chlorines using the same microelectrode. Under the potential of -90 mV, both free chlorine and monochloramine would be reduced on the surface of the microelectrode tip, and as a result, the current signal generated from the microelectrode would reflect this accordingly. While under the potential of 200 mV, the current signal generated would be largely due to the reduction of free chlorine at the microelectrode tip. Consequently, if it is free chlorine that is of interest in an investigation, then under the potential of 200 mV, potential interference from monochloramine could be minimal. On the contrary, if monochloramine is the subject of interest in a study, then under the potential of –90 mV, the potential interference from free chlorine has to be watched out. In this case, one option is to well control the condition of the water system under test so that monochloramine is the dominating substance in the system, like what was done in this study. Another option is to lump free chlorine and monochloramine together as the subject for test using this microelectrode under this potential, and later on, to distinguish them by switch potential to 200 mV for test on free chlorine.

3.3.2 Determination of diffusion coefficient

One major feature of microelectrode application to microenvironments is that its *in-situ* measurements can help determine the flux of chemicals of interest within the microenvironments. In order to achieve this goal, knowledge of the diffusion coefficient of the chemical of interest is necessary. The purpose of this study was to develop a microelectrode suitable for NH_2Cl penetration studies in biofilms. As a result, the diffusion coefficient of NH_2Cl was determined in the voltammetric experiments as well.

Figure 3-7 illustrates i-E curves of O_2-free NH_2Cl solution at different SRs. A linear relationship between peak currents and square roots of SRs for NH_2Cl can be expressed as follows, according to Bard and Faulkner (2001):

$$i_p = (2.99\times10^5)\cdot n\cdot\sqrt{\alpha\cdot n_a}\cdot A\cdot\sqrt{D}\cdot C\cdot\sqrt{v} \qquad (3\text{-}2)$$

where, i_p is peak current in amperes, n is number of electrons transferred (2e involved in reduction of NH_2Cl to NH_3), α is transfer coefficient (0.5 in most systems), n_a is number of electrons involved in rate-determining step (unity), A is reactive surface area of electrode tip (2.0×10^{-3} cm^2 as determined specifically for the electrode used in this study), D is diffusion coefficient in cm^2/s, C is concentration (3.26 mM as used in this particular experiment), v is scan rate in V/s.

Using equation (3-2) with the experimental data illustrated in Figure 3-7, a diffusion coefficient (D) of NH_2Cl in water at room temperature (22 °C) was calculated to be at around 1.7×10^{-6} cm^2/s. This result might be underestimated due to (1) an overestimated reactive surface area of the working electrode tip based on microscopic determination of its dimensions, and (2) an overestimated NH_2Cl concentration in the test solution due to continuous NH_2Cl auto-decomposition as well as consumption by the

electrochemical reaction occurring on the electrode surface during the whole test process.

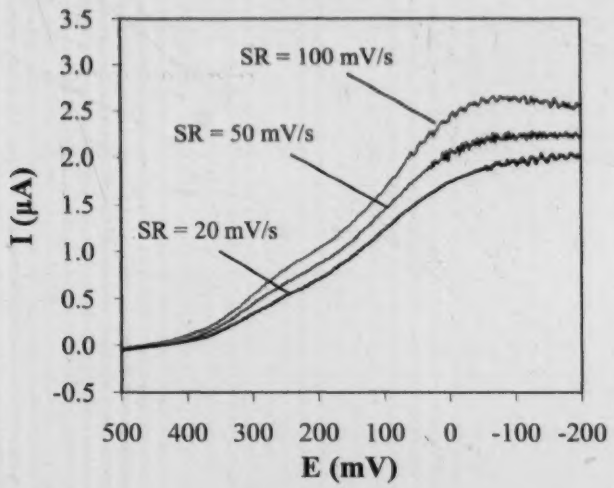

Figure 3-7 i-E curves of O_2-free NH_2Cl solution at different scan rates with linear potential sweep.

3.3.3 Performance of microelectrodes developed

The separate microelectrode. Figure 3-8 illustrates a calibration process for a separate microelectrode with continuous inputs of NH_2Cl at different concentrations from zero (i.e. the blank) up to 26.2 mg/L as Cl_2 into the flow cell, in which both of the working and reference electrodes were immersed. The results indicate that the microelectrode under testing responded well to the changes of NH_2Cl concentrations in the flow cell. The relationship between the signals of the microelectrode and the NH_2Cl concentrations in both the influent and the effluent of the flow cell is plotted in Figure 3-9, which shows a good linearity within the range of NH_2Cl concentrations tested.

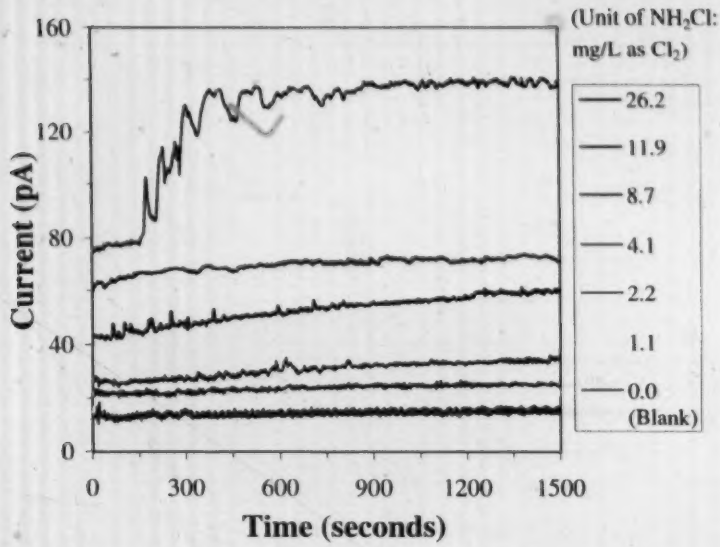

Figure 3-8 Calibration process of a separate microelectrode with continuous inputs of NH_2Cl solutions at seven concentrations (from zero up to 26.2 mg/L as Cl_2) into a flow cell.

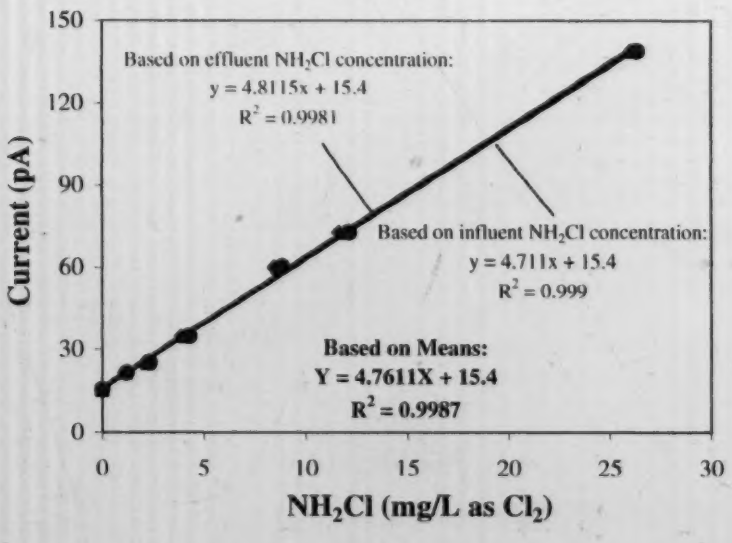

Figure 3-9 Calibration curves of a separate microelectrode using continuous inputs of NH_2Cl solutions of seven concentrations into a flow cell.

Another similar calibration was conducted on the same microelectrode 10 days apart from the test shown in Figures 3-8 and 3-9. The ultimate result (i.e. calibration curve) of this test is illustrated in Figure 3-10. In comparison between Figure 3-9 and Figure 3-10, it is indicated clearly that the microelectrode in question performed stably with respect to the sensitivity (i.e. the slope of the calibration curve) and the linearity (i.e. the R^2 value). The sensitivities were around 4.8 pA and 4.1 pA per mg/L as Cl_2 of NH_2Cl, and the R^2 values were 0.9987 and 0.9984 for these two calibrations, respectively. However, there was a large difference in the residual signals (15.4 pA vs 43.5 pA) of this microelectrode, which indicates an occurrence of signal drifting with the microelectrode during the 10-day period.

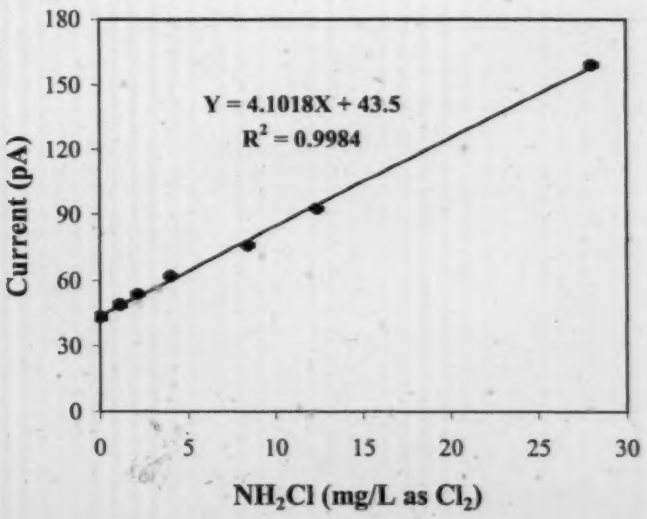

Figure 3-10 Calibration curve of the same microelectrode tested in Figure 3-8 and 3-9 using the same calibration process with 10 days apart between these two tests.

Tests conducted under stagnant as well as flowing solutions indicated that the stirring effect of the separate microelectrode was normally less than 5% under distilled

water conditions and even lower (less than 3%) under a NH_2Cl solution condition. Detection limit and 90% responding time of this microelectrode were observed at 0.45 mg/L as Cl_2 and less than 2 seconds, respectively.

The combined microelectrode. Because of the feature of its measuring circuit, the separate microelectrode could be vulnerable to potential external electromagnetic interference that may exist in the surrounding environment during measurement. In order to improve the measurement using NH_2Cl microelectrode under such a measuring environment, a combined microelectrode was designed in this study, in which the working and reference electrodes were integrated into an outer casing filled with electrolyte. In the combined microelectrode, two important factors needed to be determined to make sure it works properly. They were (1) selection of internal electrolyte and (2) formation of a functional piece of membrane at the tip of the outer casing.

(1) Selection of internal electrolyte. In the combined microelectrode, the internal electrolyte was expected to play two important roles: a medium to complete the measuring circuit between the working and the reference electrodes as well as a medium to be able to provide shielding against potential electromagnetic interference. In addition, consideration was given to the fact that this microelectrode was going to be used to study biofilms in a drinking water environment, which has pH values within the neutral range. Based on the results of the voltammetric experiments conducted earlier, a pH-buffering solution of 0.1 M $KHCO_3$/NaOH with pH adjusted to 7.0 was selected as the internal electrolyte for the combined microelectrode.

(2) Generation of tip membrane. As a frequently adopted membrane material for electrode applications, CA was also selected in this study for membrane generation at the

tip of the combined microelectrode. The critical issue here was to find a proper membrane generation protocol that would warrant a piece of membrane formed at the tip allowing the diffusion of NH_2Cl from the sample under testing into the internal environment (i.e. internal electrolyte) in order for the working electrode to reduce the diffused NH_2Cl on its tip. Test results indicated that the tip membrane of the combined microelectrode generated using the approach introduced in this study was functional.

A calibration curve of a combined microelectrode is illustrated in Figure 3-11. This curve displays a good linear relationship between current signals and NH_2Cl concentrations within the range of NH_2Cl concentrations tested. The relatively large variations in current signals at higher levels of NH_2Cl concentrations might be attributable to the "memory effect" of the microelectrode due to the calibration approach used. This curve was actually an averaged result of four calibration runs, which were run alternately following the low-to-high and then high-to-low orders with regard to NH_2Cl concentrations in the serial solutions under test. Even though the success rate of the combined microelectrode fabrication was often very low, such a linear relationship usually could be observed from those properly fabricated microelectrodes.

Unlike the separate microelectrode, it was observed that the combined microelectrode responded much more sluggishly to the change of NH_2Cl concentration, and as a result, its 90% response time was much longer (even up to minutes had been observed) than that of the separate microelectrode. Detection limit of the combined microelectrode was observed at 0.83 mg/L as Cl_2, which was higher than that of the separate microelectrode. In addition, it was also found difficult to have a combined microelectrode with relatively good long-term performance like that of the separate

microelectrode. This might be attributable to some reasons related with the components of the microelectrode such as deformation or loss of tip membrane.

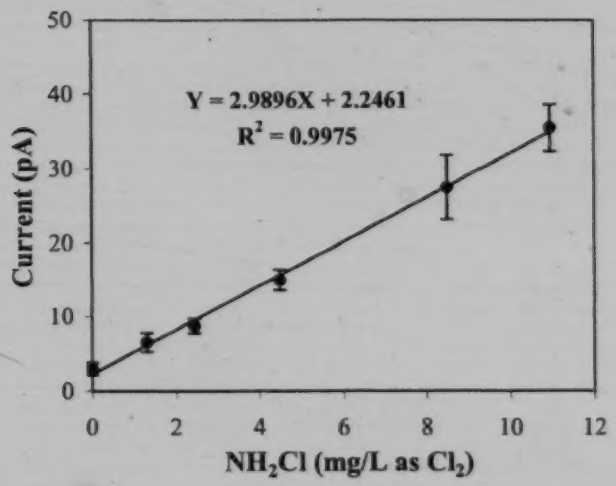

Figure 3-11 Calibration curve of a combined NH_2Cl microelectrode.

Comparison of the microelectrodes. These two types of microelectrodes have their own advantages and disadvantages. The combined microelectrode may be able to, if fabricated properly, provide some degree of protection against potential external electromagnetic interference during its measurement. However, there are a couple of drawbacks with it. Firstly, the degree of difficulty in its fabrication is high, and thus a low success rate of its fabrication is not rare in the laboratory. Secondly, room to increase signal level via enlarging the tip diameter of its working electrode is limited due to its structural features and the requirements of its special application to microenvironments (e.g. biofilms). In other words, a small outer casing tip diameter is preferred and desired for non-disruptive measurements in biofilms, but this requirement

tightly restricts the possibility to increase the tip diameter of the internal working electrode. There are other ways to increase signal level without increasing tip diameter, such as creating a rough surface or increasing the length of the tip of the internal working electrode, but increasing the tip diameter is the easiest. Thirdly, the combined microelectrode responds much slower than that of the separate microelectrode. This might be attributable to (1) the outer casing tip membrane, which was much thicker in comparison with that of the separate, and (2) the existence of the space between the tip membrane and the internal working electrode. Fourthly, the detection limit is higher than that of the separate, which may become a limiting factor in some applications. Last but not least, the lack of long-term stability (i.e. the longevity) of the performance of the microelectrode can become a major concern in some specific applications.

In comparison with the combined microelectrode, the separate microelectrode, as can be perceived, may be more vulnerable to potential external electromagnetic interference. However, it is much easier to make, and often with much higher success rate in fabrication. Meanwhile, the separate microelectrode has more flexibilities in increasing its signal levels, if needed, such as by increasing its tip diameter and hence its reactive surface area thanks to its lack of the structural restriction that exists with the combined microelectrode. More importantly, the separate microelectrode can have much faster responses to the changes of NH_2Cl concentrations and better long-term stability of performance, both of which are difficult to achieve with the combined microelectrode.

As a result, to use the separate or combined microelectrode really depends on specific application requirements. Based on his experience dealing with microelectrodes, the author would recommend that unless a combined microelectrode must be adopted, a

separate microelectrode is generally the choice, especially when measurements are to be conducted under conditions, in which potential external electromagnetic interference in surrounding environment is negligible, or when there is an easier way to minimize the interference to an negligible level, such as using a Faraday cage to install the set-up for microelectrode measurements. This can save time, efforts and funds.

3.4 Conclusions

Based on voltammetric experiments to construct i-E curves for NH_2Cl and evaluation processes of the two newly developed microelectrodes for NH_2Cl measurement, the following conclusions have been made:

(1) It was disclosed that pH had substantial impacts on the shape of i-E curves of NH_2Cl solution. When pH was neutral, the limiting current of NH_2Cl started to be generated from the Pt electrode when the applied potential was at -90 mV (vs Ag/AgCl).

(2) Two types of microelectrodes, the separate and the combined, applicable to direct NH_2Cl measurements were developed. Under the experimentally determined polarization potential (-90 mV vs Ag/AgCl), both types of microelectrodes displayed good linear responses to the changes of NH_2Cl concentration within ranges tested. However, the separate microelectrode generally is the better choice under laboratory environments due to its advantageous characteristics over the combined.

(3) A diffusion coefficient (1.7×10^{-6} cm^2/s) of NH_2Cl in water at room temperature (22 °C) was determined. With this experimentally determined constant, it becomes feasible to estimate flux of NH_2Cl in microenvironments with direct measurements of NH_2Cl profiles using the developed microelectrode.

3.5 References

Bard, A. J. and Faulkner, L. R. 2001. *Electrochemical methods: fundamentals and applications*, 2nd edition, John Wiley & Sons, New York.

Cunliffe, D. A. 1991. Bacterial nitrification in chloraminated water supplies. *Applied and Environmental Microbiology*, 57:3399-3402.

de Beer, D., Srinivasan, R. and Stewart, P. 1994. Direct measurement of chlorine penetration into biofilms during disinfection. *Applied and Environmental Microbiology*, 60:4339-4344.

Kesting, R. E. 1971. *Synthetic polymeric membranes*, McGraw-Hill Book Company, New York.

Lipponen, M. T. T., Suutari, M. H. and Martikainen, P. J. 2002. Occurrence of nitrifying bacteria and nitrification in Finnish drinking water distribution systems. *Water Research*, 36:4319–4329.

Pinnau, I. and Freeman, B. D. 2000. Formation and modification of polymeric membranes: Overview. In *Membrane formation and modification*, American Chemical Society (ACS) symposium series 744, Pinnau, I. and Freeman, B. D. (editors), American Chemical Society, Washington, D.C.

Skadsen, J. 1993. Nitrification in a distribution system. *Journal AWWA*, 85:95-103.

Strathmann, H. 1983. Synthetic membranes and their preparation. In *Synthetic Membranes: Science, Engineering and Applications*, Bungay, P. M., Lonsdale, H. K. and de Pinho, M. N. (editors), NATO ASI Series (Series C: Mathematical and physical sciences), Vol. 181, p1-37.

Valentine, R. L., Ozekin, K. and Vikesland, P. J. 1998. *Chloramine decomposition in distribution system and model waters*. AWWA Research Foundation and American Water Works Association, Denver, Colorado, USA.

Wilczak, A., Jacangelo, J. G., Marcinko, J. P., Odell, L. H., Kirmeyer, G. J. and Wolfe, R. L. 1996. Occurrence of nitrification in chloraminated distribution systems. *Journal AWWA*, 88:74-85.

Wolfe, R. L., Means, E. G. III, Davis, M. K. and Barrett, S. E. 1988. Biological nitrification in covered reservoirs containing chloraminated water. *Journal AWWA*, 80: 109-114.

Chapter 4

Penetration and Microbial Inactivation of NH_2Cl in Biofilms

4.1 Introduction

Outbreaks of nitrification in many chloraminated water distribution systems (CWDSs) has been believed to be attributable to the growth of nitrifying microorganisms embedded in biofilms growing on facility surfaces in the CWDSs (Wolfe *et al.*, 1990; Regan *et al.*, 2003). This indicates that the commonly used NH_2Cl residuals in these CWDSs have not been effectively inactivating biofilm microorganisms. Unlike inactivation against suspended microorganisms, in which a disinfectant usually attacks cells directly, inactivation against biofilm microorganisms is more complicated, because the disinfectant must first penetrate into biofilms in order to reach and then attack its targets. This penetration process can be greatly affected by factors such as disinfectant concentration, contact time, biofilm matrix and substratum material. Therefore, a good understanding of the penetration process of a disinfectant in biofilms is critical to evaluating the effectiveness of the particular disinfectant in inactivating biofilm microorganisms.

Conventional approaches, in which biofilms have to be dispersed and homogenized in solution in order to conduct viable cell counting, play limited roles in helping elucidate how a disinfectant penetrates into biofilms and how the penetration process may be affected by the biofilm matrix and substratum material. Investigations using an *in-situ* approaches into intact biofilms are essential. With the development of a microelectrode specific for free chlorine measurement, direct observations on penetration

of free chlorine in biofilms were conducted (de Beer *et al.*, 1994; Xu *et al.*, 1996; Chen and Stewart, 1996). Results of these studies have provided experimental evidence to disclose the retardation effect of biofilms on free chlorine penetration and a diffusion-reaction mechanism has been proposed.

Inactivation against biofilm microorganisms by NH_2Cl was reported to be affected by the substratum surface; and the mechanism of the resistance of biofilms to NH_2Cl might differ from that of free chlorine (LeChevallier *et al.*, 1988). Woolschlager *et al.* (2001) reported that concrete surfaces could accelerate NH_2Cl decomposition due to the formation of acidified surfaces of aluminosilicates, and this was found to be the single most influential factor in NH_2Cl decomposition in the CWDS studied. Corrosion products on facility surfaces in distribution systems were also reported to have retarding impacts on the effectiveness of NH_2Cl in inactivating embedded cells in biofilms, although different mechanisms have been proposed for this phenomenon (LeChevallier *et al.*, 1993; Piriou *et al.*, 1997; Vikesland and Valentine, 2002; Chen *et al.*, 1993; Stanier *et al.*, 1986). In order to more clearly understand the effectiveness of NH_2Cl in inactivating biofilm microorganisms, it is necessary to elucidate the impacts of different types of biofilm substratum materials (with respect to NH_2Cl demand) on the penetration process of NH_2Cl in biofilms.

Due to the lack of suitable analytical tools, there has been no direct experimental observation yet to elucidate how NH_2Cl penetrates in biofilms. Based on the newly developed microelectrode specifically suitable for NH_2Cl measurement as introduced in Chapter 3, the study of Chapter 4 investigated penetration processes of NH_2Cl in drinking water biofilms as well as impacts of substratum materials on this process.

4.2 Materials and Methods

This section introduces those materials and methods used specifically for the purposes of this particular study on the penetration process of NH_2Cl in biofilms grown on different substratum materials using microelectrode techniques. More detailed descriptions on generally used materials and methods for the operation of the model water distribution system for biofilm growth, chemical and microbiological analyses on water and biofilm samples, fabrication and calibration of microelectrodes, and set-up for microelectrode measurement in biofilms are presented in Chapter 2.

4.2.1 Biofilm cultivation

Biofilms were developed in the annular reactor as described in Section 2.2 of Chapter 2. Three types of sterile slides (polyvinylchloride (PVC), polycarbonate (PC) and concrete) were installed as substratum material for biofilm growth. Because the target biofilms to be promoted to grow for this study were mixed population biofilms similar to those in water distribution systems, flushed wash water sampled during repair work of water mains in a water distribution system was used as the seed for inoculation as well as the feed for biofilm growth after the feed water had been dechlorinated with 0.1 M sodium thiosulfate. This feed water had pH at 7.5, heterotrophic plate count (HPC) concentration at around 6.6×10^5 cfu/mL, and total organic carbon (TOC) ranging from 13 to 450 mg/L, all of which were favorable to biofilm growth. Meanwhile, considering the fact that environmental conditions such as those in slow-flow sections and dead-ends in distribution systems are much more conducive to biofilm development, this experiment simulated such conditions by providing a small shear stress through slow

rotational speed (< 10 rpm) of the inner drum of the reactor and low flow rate (ca. 50 mL/min) of the feed water leading to a retention time (RT) of 19 hours in the reactor. Air was continuously dispersed into the feed tank to ensure the reactor with biofilms was kept under an aerobic condition with dissolved oxygen (DO) at 7.2 to 7.8 mg/L. The reactor had been kept under room temperature (22 ± 2 °C) throughout the entire biofilm growth process.

4.2.2 Microelectrode measurements in biofilms

The separate NH_2Cl microelectrode introduced in Chapter 3 was adopted in this investigation for NH_2Cl profile measurements in biofilms. Prior to its use in NH_2Cl profile measurements on biofilms, the microelectrode had been calibrated as described in Chapter 3. All experiments on NH_2Cl transient profiles in biofilms were conducted using the same set-up illustrated in Figure 2-7 and described in Chapter 2. Before NH_2Cl profile measurements started, a stock solution of NH_2Cl with known concentration had been pumped into the flow cell at a flow rate of 5 mL/min with both the working and reference electrodes being immersed in the flowing solution in the flow cell. After the monitored signals reached a stable status, a biofilm slide sampled from the biofilm growth system was put into the flow cell, and contact time started to be counted. Transient NH_2Cl concentration profiles from the bulk to the biofilm phase were then measured in time series (i.e. NH_2Cl concentration profiles were measured at different contact times on the same biofilm spot or different spots but in the same vicinity) using the working microelectrode mounted on the micromanipulator equipped with a remote 3-D oil hydraulic controller. The effluent from the flow cell was sampled and analyzed immediately to monitor the bulk NH_2Cl concentration in the flow cell.

When HPC analyses of biofilms needed to be conducted in parallel with transient NH_2Cl profile measurements, three pieces of slides of the same material (concrete) with biofilms of similar age and thickness were taken from the annular reactor. One of the three biofilm slides was directly used for HPC analysis without being exposed to NH_2Cl (i.e. contact time t = 0). The remaining two biofilm slides were installed in the flow cell, which was continuously being filled with fresh NH_2Cl solution of 6.7 mg/L as Cl_2. Afterwards, transient NH_2Cl profiles were measured on one of the slides in a time series. The second biofilm slide was taken out of the flow cell after its 60-minute exposure to NH_2Cl, and NH_2Cl residual in the biofilms was briefly neutralized with sodium thiosulfate. Finally, the biofilm was scraped into sterilized distilled water in a flask, homogenized and used for HPC analysis. After all desired transient NH_2Cl profile measurements were completed on the third biofilm slide, this slide was then taken out of the flow cell after its 120-minute exposure to NH_2Cl and treated similarly as the second slide for HPC analysis.

4.2.3 HPC analyses of biofilms

Biofilms on each slide were scraped and rinsed into 100 mL sterile distilled water, and then homogenized on a vortex mixer. The homogenized biofilm suspension was then used to prepare the ten-fold serial dilutions (from 1×10^{-1} to 1×10^{-5}). Each dilution level was spread-plated in triplicate. Incubation was implemented at 25°C for 6 days. The length and width of the scraped area on biofilm slides were measured and the ultimate HPC test results were expressed as biofilm HPC density in cfu/cm^2. More details of HPC analysis are introduced in Section 2.4.2 of Chapter 2.

4.2.4 Biofilm thickness estimation

Biofilm thickness was normally measured either after its use in microelectrode measurements or before biofilm HPC analyses using an optical microscopic method as introduced in Section 2.4.2 of Chapter 2.

4.3 Results and Discussions

4.3.1 NH_2Cl transient profiles in biofilms

Without biofilm growth, the control experiments on NH_2Cl profiles in the bulk solution above NH_2Cl-sterilized slides of concrete, PVC and PC indicated no obvious NH_2Cl concentration gradients for the PVC and PC slides, but a slight gradient formed on the concrete slide as illustrated in Figure 4-1. NH_2Cl concentration near the surface of the concrete slide was about 80% of that in the bulk. In another similar test using a non-sterilized concrete slide, NH_2Cl concentration gradient was much more substantial - NH_2Cl concentration near the slide surface was around 40% of that in the bulk as shown in Figure 4-2. This has confirmed that in comparison with PVC and PC, concrete can be categorized as NH_2Cl-demanding material; and this was the reason leading to NH_2Cl consumption on its surface, and thus the formation of NH_2Cl concentration gradient above its surface. Another control experiment on potential impact of biofilm matrix on microelectrode performance was also conducted. The resultant signal profiles of two NH_2Cl microelectrodes (Figure 4-3) measured in the bulk as well as biofilm grown on concrete slides under flowing distilled water conditions did not show noticeable influence from biofilm matrix on the background signals of the NH_2Cl microelectrodes.

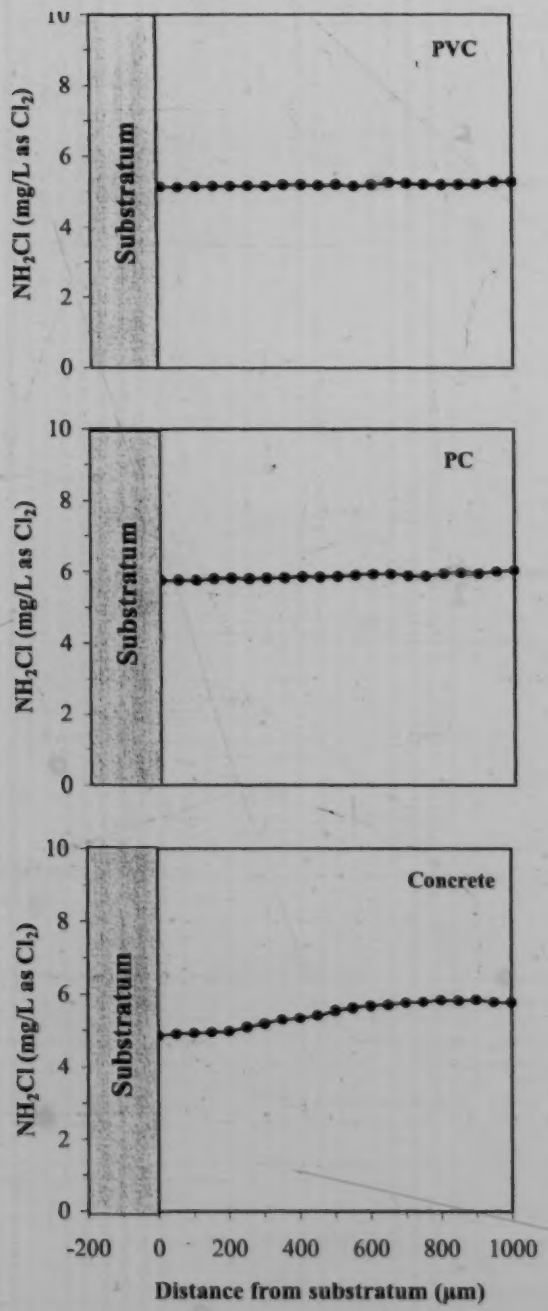

Figure 4-1 NH_2Cl profiles in the bulk above NH_2Cl-sterilized slides of different materials without biofilm growth.

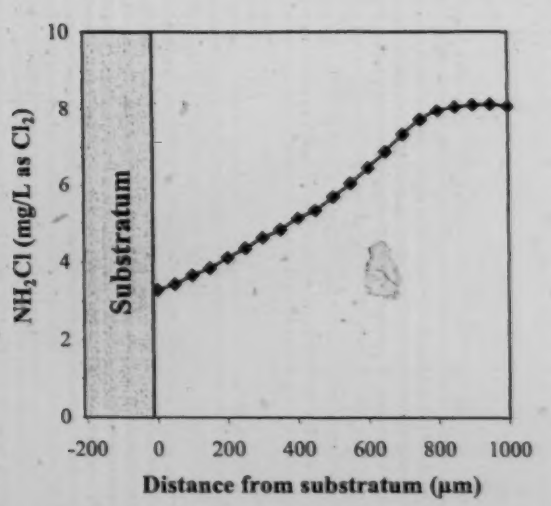

Figure 4-2 NH_2Cl profile in the bulk above non-sterilized concrete slide without biofilm growth.

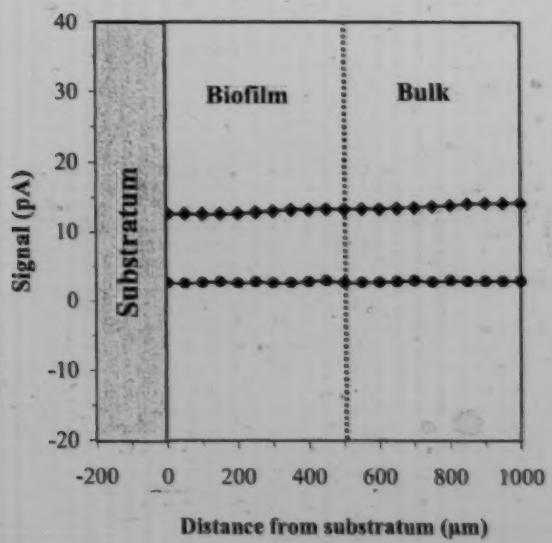

Figure 4-3 Signal profiles of two NH_2Cl microelectrodes measured in bulk and biofilms grown on concrete slides under flowing distilled water condition.

Transient NH_2Cl profiles in biofilms grown on a concrete slide are illustrated in Figure 4-4. These profiles were measured at spots in the vicinity of each other on the biofilms at 15, 45 and 65 minutes, respectively, after the biofilms had been immersed in NH_2Cl solution in the flow cell. NH_2Cl concentration in the stock solution was at 6.6 mg/L as Cl_2. These profiles clearly illustrate the occurrence of NH_2Cl depletion during its penetration in the biofilms; and the degree of the depletion process was greatly affected by contact time. At a contact time of 15 minutes, NH_2Cl concentration near the substratum was around zero, but at 45 and 65 minutes of contact time, NH_2Cl concentrations near the substratum were around 1.4 and 2.1 mg/L as Cl_2, respectively. In addition, the depletion rate in terms of concentration change per unit depth (i.e. the slope of the curve) decreased as contact time increased.

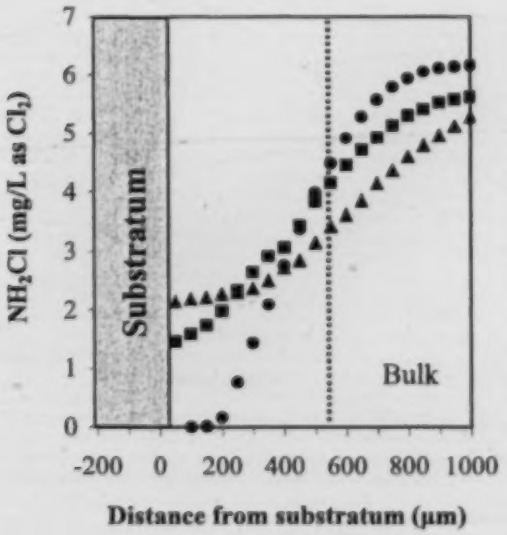

Figure 4-4 NH_2Cl profiles measured on a patchy biofilms grown on a concrete slide at different contact times: (●) 15, (■) 45 and (▲) 65 min.

These sigmoid-shaped NH_2Cl profiles could be explained using a diffusion-reaction mechanism as discussed by de Beer *et al.* (1994) for free chlorine penetration in biofilms. However, the specific types of reactions for free chlorine and NH_2Cl occurring during their penetration processes in biofilms might be significantly different due to their different chemical properties. Unlike free chlorine, which indiscriminately reacts with polysaccharides and cell materials, NH_2Cl may react rather specifically with nucleic acids, tryptophane, and sulfur-containing amino acids while having little interaction with polysaccharides (Geldreich, 1996).

Figure 4-5 illustrates transient NH_2Cl profiles measured on the same spot of a biofilm with a much higher concentration of NH_2Cl (22.3 mg/L as Cl_2). These profiles all indicated full penetration of NH_2Cl within the biofilm during the period of contact time tested. No one partial penetration of NH_2Cl in the biofilm could be observed as in the case of Figure 4-4, in which a much lower concentration of NH_2Cl (6.6 mg/L as Cl_2) was used. This indicates that the bulk concentration of NH_2Cl imposed substantial influence on the penetration process of NH_2Cl in biofilms.

The measured biofilm thickness at the spot where the profiles in Figure 4-5 were measured was around 400 μm, whereas in Figure 4-5 the distance from the substratum to the point where the NH_2Cl concentration started to decrease from the bulk concentration was much greater than 400 μm. It thus can be derived that there was a mass diffusion boundary layer above the biofilm surface. The presence of such a boundary layer disclosed that the real concentration of NH_2Cl on the biofilm surface was actually lower than that in the bulk. For the biofilm illustrated in Figure 4-5, which was exposed to a high NH_2Cl concentration (22.3 mg/L as Cl_2), the NH_2Cl concentrations on the biofilm

surface were about 81% to 92% of that in the bulk for contact times tested. For the biofilm samples illustrated in Figure 4-4, which was exposed to a lower NH_2Cl concentration (6.6 mg/L as Cl_2), this percentage ranged from 55% to 65% for contact times tested. This phenomenon could be explained by the diffusion-reaction mechanism. That is, as NH_2Cl diffused into biofilms, it was consumed within the biofilm; and this consumption in turn led to the formation of a concentration gradient of NH_2Cl above the biofilm. This mechanism helps explain the reason why the NH_2Cl concentration sufficient to inactivate planktonic cells in the bulk is usually not similarly effective in inactivating biofilm microorganisms. In other words, to achieve the same inactivation efficiency, NH_2Cl concentration required for biofilm microorganisms should be higher than that for suspended cells in the bulk.

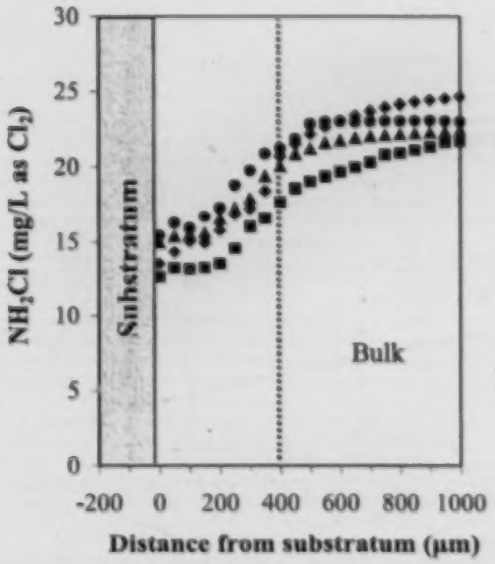

Figure 4-5 NH_2Cl profiles measured at a same spot of a patchy biofilm grown on a concrete slide at different contact times: (◆) 10, (■) 20, (▲) 40 and (●) 70 minutes.

Based on measured profiles and using Fick's first law of diffusion with a diffusion coefficient of 1.7×10^{-6} cm^2/s, which was estimated previously in Chapter 3, NH_2Cl fluxes from the bulk into the biofilms were calculated. The calculated values ranged from 1.7×10^{-8} to 1.1×10^{-7} mol/m^2-s and from 8.7×10^{-9} to 3.2×10^{-8} mol/m^2-s for NH_2Cl concentration of 22.3 and 6.6 mg/L (as Cl_2), respectively. These flux values might be underestimated due to the underestimated diffusion coefficient due to technical limitations as discussed previously in Section 3.3.2 of Chapter 3.

In addition to concrete slides, NH_2Cl transient profiles were also measured in biofilms grown on PVC and PC slides. Unlike concrete, which is believed to be an NH_2Cl-demanding material, these two types of materials are inert in reacting with NH_2Cl, which is confirmed by this study as well (refer to Figure 4-1 and 4-2). Transient NH_2Cl profiles in biofilms grown on PVC and PC slides are illustrated in Figure 4-6 and 4-7, respectively.

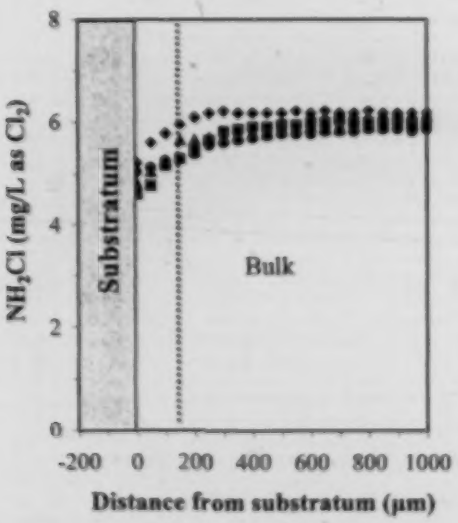

Figure 4-6 NH_2Cl profiles measured on a same spot of a patchy biofilm grown on a PVC slide at different contact times: (◆) 10, (■) 20, (▲) 30 and (●) 45 minutes.

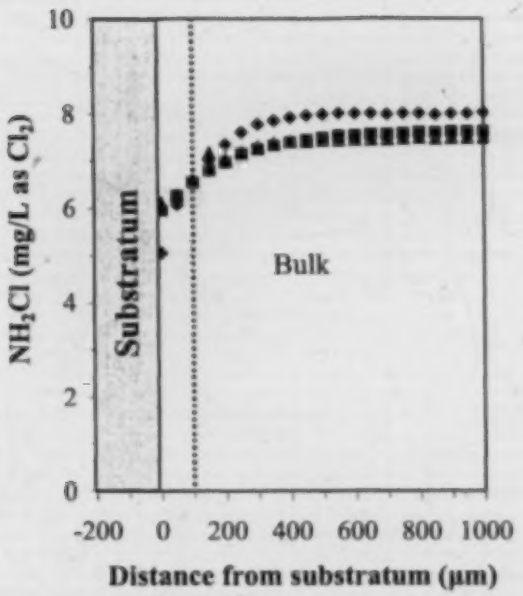

Figure 4-7 NH_2Cl profiles measured at a same spot of a patchy biofilm grown on a PC slide at different contact times: (◆) 5, (■) 15 and (▲) 20 minutes.

As can be seen in both Figure 4-6 and Figure 4-7, full penetration of NH_2Cl in the biofilms grown on these two materials was observed and the contact time was as short as 5 minutes as illustrated in Figure 4-7. These profiles differed from those of concrete slides under comparable NH_2Cl concentrations (6.5 to 6.6 mg/L as Cl_2). There are two possible reasons for this phenomenon: biofilm thickness and substratum material. In Figure 4-4, the average thickness of biofilms was around 540 μm; while in Figure 4-6 and 4-7, the average thickness of biofilms ranged from 110 to 160 μm. Thicker biofilms, as a physical barrier as well as a provider of embedded cells, have a more pronounced retarding effect on the penetration process of NH_2Cl. The type of the substratum material is also important. As was reported by Woolschlager *et al.* (2001) and experimentally supported by this study, concrete has a capacity to react with and thus

consume NH_2Cl, whereas PVC and PC do not. Consequently, during its penetration through the biofilms grown on PVC and PC slides, NH_2Cl could be mainly consumed by its reactions with embedded cells; while in the case of concrete slides, NH_2Cl could be consumed not only by reactions with embedded cells but also by reactions with substratum components (e.g. acidified surfaces of aluminosilicates - one major component of concrete), leading to more rapid depletion. This indicates that the type of substratum materials could have pronounced impact on the penetration process of NH_2Cl in biofilms. It is thus advisable to the drinking water industry that NH_2Cl-demand free materials (such as PVC) rather than NH_2Cl-demanding ones (such as concrete) be used for pipes in CWDSs.

4.3.2 HPC analyses of biofilms

To elucidate the impact of the NH_2Cl penetration process in biofilms on its inactivation process against biofilm bacteria, HPC analyses on biofilms with different contact times were conducted in parallel with transient NH_2Cl profile measurements in biofilms. The biofilms used were grown on concrete slides with similar age and thickness. The concentration of NH_2Cl solution was 6.7 mg/L as Cl_2. Without contact with NH_2Cl, i.e. contact time = 0, HPC density on the biofilm slide was at 4.34×10^7 cfu/cm^2. After exposure to NH_2Cl for 60 minutes, the HPC dropped down to 8.85×10^6 cfu/cm^2, and further down to 6.36×10^5 cfu/cm^2 after 120 minutes of exposure. In combination with the results of transient NH_2Cl profiles measurements, the results of the HPC analyses helped elucidate that the NH_2Cl inactivation against biofilm bacteria was affected by its penetration process within the biofilms. Due to the occurrence of NH_2Cl

depletion, its inactivation against biofilm bacteria was retarded and the efficiency of its inactivation compromised. Only with further supply of NH_2Cl from the bulk and further penetration of NH_2Cl into the biofilms, could NH_2Cl inactivation against biofilm bacteria take place further. For the drinking water industry, to improve inactivation efficiency of NH_2Cl against biofilm microorganisms, measures that can be beneficial to the penetration process of NH_2Cl within biofilms should be considered.

4.4 Conclusions

Transient NH_2Cl profiles in mixed population biofilms grown on slides made from concrete, PVC and PC were measured *in-situ* in time series with respect to contact times ranging from 5 to 70 minutes. Within the timeframes of the tests conducted in this study, the following conclusions have been made:

(1) In biofilms with average thickness at 540 μm and grown on concrete slides, partial penetration of NH_2Cl was observed at a NH_2Cl concentration of 6.6 mg/L as Cl_2 with a contact time of 15 minutes, beyond which full penetrations were observed. With a higher NH_2Cl concentration (22.3 mg/L as Cl_2), only full NH_2Cl penetrations were observed with similarly short contact times. This indicates that contact time and bulk NH_2Cl concentration are two important factors affecting the penetration process of NH_2Cl within biofilms.

(2) Unlike that of concrete slides, full penetrations of NH_2Cl were always observed in thinner biofilms grown on PVC and PC slides under comparable bulk NH_2Cl concentrations and short contact times. This indicates that the type of substratum materials could influence the penetration process of NH_2Cl in biofilms. NH_2Cl-demand

free materials (such as PVC and PC) are more conducive to the penetration process of NH_2Cl in biofilms than NH_2Cl-demanding material (such as concrete).

(3) The elucidation of the presence of a diffusion boundary layer disclosed that the real concentration of NH_2Cl on the biofilm surface was lower than that in the bulk. This observation helps explain why the NH_2Cl concentration sufficient to inactivate planktonic cells in the bulk is usually not similarly effective in inactivating biofilm microorganisms. To achieve same inactivation efficiency, NH_2Cl concentration required for biofilm microorganisms should be higher than that for suspended cells in the bulk.

(4) Biofilm HPC tests in time series with respect to contact time, conducted in parallel with transient NH_2Cl profiles measurements in biofilms, helped elucidate that the penetration process of NH_2Cl in biofilms could affect the inactivation process of NH_2Cl against biofilm microorganisms. Therefore, factors (e.g. bulk NH_2Cl concentration and type of substratum material) that could be conducive to improving the penetration process of NH_2Cl in biofilms could also be beneficial to its inactivation process against biofilm microorganisms. This is of special interest to the drinking water industry with respect to the selection of pipe material for distribution systems.

4.5 References

Chen, C. I., Griebe, T., Srinivasan, R. and Stewart, P. 1993. Effects of various metal substrata on accumulation of *Pseudomonas aeruginosa* biofilms and the efficacy of monochloramine as biocide. *Biofouling*, 7:241-251.

Chen, X. and Stewart, P. S. 1996. Chlorine penetration into artificial biofilm is limited by a reaction-diffusion interaction. *Environmental Science and Technology*, 30:2078-2083.

de Beer, D., Srinivasan, R. and Stewart, P. 1994. Direct measurement of chlorine penetration into biofilms during disinfection. *Applied and Environmental Microbiology*,

60:4339-4344.

Geldreich, E. E., 1996. *Microbial quality of water supply in distribution systems*. Lewis Publishers, CRC Press, Inc., New York.

LeChevallier, M. W., Cawthon, C. D. and Lee, R. G. 1988. Factors promoting survival of bacteria in chlorinated water supplies. *Applied and Environmental Microbiology*, 54:649-654.

Lechevallier, M. W., Lowry, C. D., Lee, R. G. and Gibbon, D. L. 1993. Examining the relationship between iron corrosion and the disinfection of biofilm bacteria. *Journal AWWA*, 85:111-123.

Piriou, P., Kiene, L. and Levi, Y. 1997. Study and modeling of drinking water quality evolution using a pipe loop system. *Proceedings of the annual meeting of the American Water Works Association*, 15-19 June, Atlanta, Georgia, USA.

Regan, J. M., Harrington, G. W. Baribeauc, H., De Leon, R. and Noguera, D. R. 2003. Diversity of nitrifying bacteria in full-scale chloraminated distribution systems. *Water Research*, 37:197-205.

Stanier, R. Y., Ingraham, J. L., Wheelis, M. L. and Painter, P. R. 1986. *The microbial world*, 5th edition, Prentice-Hall, Englewood Cliffs, New Jersey.

Vikesland, P. J. and Valentine, R. L. 2002. Iron oxide surface-catalyzed oxidation of ferrous iron by monochloramine: Implications of oxide type and carbonate on reactivity. *Environmental Science and Technology*, 36:512-519.

Wolfe, R. L., Lieu, N. I., Izaguirre, G. and Means, E. G. 1990. Ammonia-oxidizing bacteria in a chloraminated distribution system: seasonal occurrence, distribution, and disinfection resistance. *Applied and Environmental Microbiology*, 56:451-462.

Woolschlager, J., Rittmann, B., Piriou, P., Kiene, L. and Schwartz, B. 2001. Using a comprehensive model to identify the major mechanisms of chloramines decay in distribution systems. *Water Science and Technology: Water Supply*, 1(4):103-110.

Xu, X., Stewart, P. S. and Chen, X. 1996. Transport limitation of chlorine disinfection of *Pseudomonas aeruginosa* entrapped in alginate beads. *Biotechnology and Bioengineering*, 49:93-100.

Chapter 5

Nitrification Detection Using Microelectrodes In a Model CWDS

5.1 Introduction

Water quality deteriorations due to nitrification outbreak in chloraminated water distribution systems (CWDSs) often make water utilities face potential regulation violations. Early detection and warning of nitrification in CWDSs is important in helping utilities make decisions proactively on implementation of control strategies before outbreak of measurable water quality deterioration. The convenient and thus frequently used method for detection of nitrification occurrence is to carry out monitoring tests on the water in CWDSs. Efforts have been made in attempts to find a correlation between nitrification occurrence and water parameters such as dissolved oxygen (DO), pH, heterotrophic plate count (HPC), NH_2Cl residual, ammonia, nitrite, nitrite plus nitrate, identification and enumeration of nitrifying microorganisms (Wolfe *et al.*, 1990; Cunliffe, 1991; Lieu *et al.*, 1993; Wilczak *et al.*, 1996; Regan *et al.*, 2002; Pintar *et al.*, 2005). However, inconsistent and even contradictory conclusions often resulted. As an important parameter, nitrite has drawn a lot of attention and a critical threshold at 0.05 mg-N/L for determination of nitrification outbreak in CWDSs has been proposed and/or adopted by earlier investigators (Wolfe *et al.*, 1988; Kirmeyer *et al.*, 1995; Wilczak *et al.*, 1996). A newly proposed parameter - the microbial decay factor "F_m" (Sathasivan *et al.*, 2005) - using data on NH_2Cl residual in water in CWDSs was reported to be more sensitive than traditional indicators, and thus was recommended to be a potential tool for utilities to use in early detection of nitrification in CWDSs.

The growth of nitrifying bacteria embedded in biofilms has been blamed for the outbreak of nitrification in CWDSs (Ike *et al.*, 1988; Wolfe *et al.*, 1990; Odell *et al.*, 1996). Therefore, monitoring tests conducted directly on biofilms, although not as convenient as those on water, become logical choices in searching for more sensitive approaches to early detection of nitrification in CWDSs. The commonly used biofilm test is the most probable number (MPN) test on nitrifying microorganisms. However, long incubation time (at least 3 weeks), low recovery efficiency (as low as 0.1%) and large variations of results of MPN tests (Matulewich *et al.*, 1975; Belser, 1979) limit the role this technique plays in early detection of nitrification. A screening approach – the nested-polymerase chain reaction terminal restriction fragment length polymorphorism protocol (Regan *et al.*, 2002) - has overcome the drawbacks of the MPN test. It detected nitrifying bacteria in biofilms quickly without being subject to culturability biases, and thus was recommended as a presence or absence tool for detecting potential onset of a nitrification outbreak. Detection of the presence of nitrifying microorganisms, however, does not necessarily indicate significant potential of nitrification outbreak or actively ongoing nitrification in CWDSs. It may only indicate that sometime in the past, prior to the test, nitrification took place, or there could be no nitrification episode at all if conditions in CWDSs do not allow the detected nitrifying microorganisms to proliferate substantially. Therefore, detection of nitrifying microorganisms alone is not sufficient in helping make early warning of nitrification in CWDSs.

Microbiological nitrification consists of two biochemical reactions as expressed in Equation (1-11) and (1-12) introduced in Chapter 1. Consequently, a more appropriate approach to elucidate nitrification in CWDSs is to examine, *in-situ* in biofilms, those

chemicals such as oxygen, ammonia, nitrite, nitrate and hydrogen ions (protons) that are directly involved in these two biochemical reactions. Due to their tiny tips and high spatial resolutions, microelectrodes are suitable for *in-situ* investigations into microenvironments in biofilms. They provide parameter-specific (e.g. DO, pH, NO_3^-, NH_4^+ and so on) measurements and directly convey three pieces of basic information - concentrations of chemicals of interest at any position measured, concentration gradients and variations of gradients. These data directly disclose status of ongoing nitrification occurring in biofilms. The following sections in Chapter 5 introduce a feasibility study on potential application of the approach of conducting biofilm tests using microelectrodes to nitrification detection in CWDSs based on a 1-year operation of a model CWDS.

5.2 Materials and Methods

This section mainly introduces those materials and methods used specifically for the purposes of the particular study on nitrification detection using microelectrode techniques in a model chloraminated water distribution system. More detailed descriptions on generally used materials and methods for operation of the model system for biofilm growth, chemical and microbiological analyses on water and biofilm samples, fabrications and calibrations of microelectrodes used, and set-up for microelectrode measurement in biofilms are presented in Chapter 2.

5.2.1 Model CWDS

The major components of the set-up used to simulate a CWDS and to promote

nitrifying biofilm growth in such a system are introduced in Chapter 2 and are also illustrated in Figure 5-1. The model system was initially seeded with flushed water sampled in mid-September from a slow-flow or dead-end area of a local distribution system (EPCOR, Edmonton, Alberta) using NH_2Cl as secondary disinfectant. The model system was run in a batch mode with the seed for 24 hours before it was switched to a flow-through mode using the seed as the sole input with a retention time (RT) of 24 hours. After a 9-day, single input, flow-through operation, artificial stock solutions of carbon (C), nitrogen plus phosphorus (N+P), and NH_2Cl were introduced to replace the sole input of seed with flow rates at 0.5, 0.5 and 1.67 mL/min, respectively, to achieve a 6-hour RT (Pintar and Slawson, 2003).

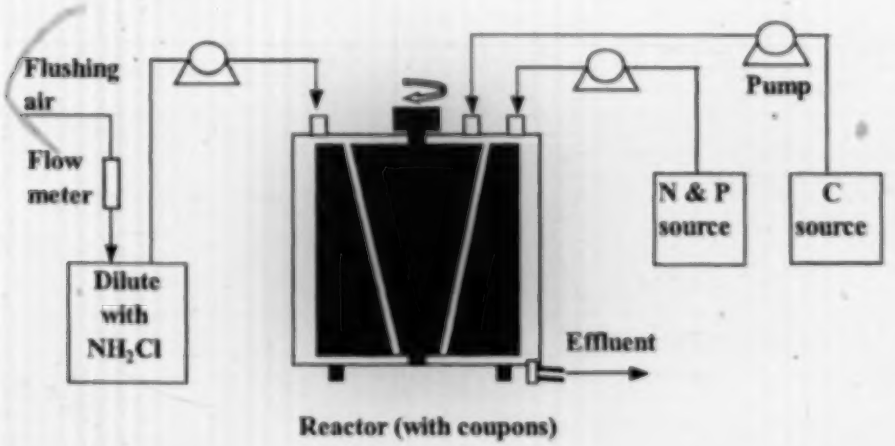

Figure 5-1 Set-up of a model chloraminated water distribution system for nitrifying biofilm growth.

To ensure a C-limiting condition in the system, a C:N:P ratio of 100:25:4 (molar basis) (Ollos *et al.*, 2003) was used. $NaNO_3$ and $KH_2PO_4 + K_2HPO_4$ were used as N and P sources, respectively. Five representative C-containing compounds in drinking water

including sodium acetate, ethanol, proprionaldehyde, parahydroxy-benzoic acid and sodium benzoate (equimolar) were used as the carbon source (Camper, 1996). The ultimate design concentration of C, N and P in the system was 0.6, 0.175 and 0.064 mg/L, respectively.

The primary purpose for running this system was to promote nitrifying biofilm growth under conditions of drinking water distribution systems, thus a low NH_2Cl residual concentration (< 0.2 mg/L as Cl_2) was adopted. This was not intended to represent the residual concentration in a system not experiencing nitrification episodes. Rather, it was chosen to represent the higher end of a typically low NH_2Cl concentration in portions of full-scale systems experiencing nitrification, with low flow rates and long RTs (Pintar *et al.*, 2003). NH_2Cl was made from NH_4Cl (1 M) and NaOCl (4 to 6%) with a Cl/N ratio of 3:1 (w/w) to ensure NH_2Cl to be the dominant disinfectant.

The system was kept at room temperature (22 ± 2 °C) and covered with aluminum foil to ensure a dark environment. Aeration was implemented by flushing filtered air into the seed or diluted NH_2Cl stock solution. A rotational speed of 6 rpm, the lowest available for this particular reactor, was used for mixing. The model system had been routinely monitored for chemical and microbiological parameters.

Initially, the system had been operated under the designed condition for about 8 months, but no obvious nitrification had been detected using water parameters. To increase nitrifying biofilm growth, based on experience from another study (Pintar, 2000), modifications in operation of the model system were made thereafter including an introduction of nitrifying bacteria culture (*Nitrosomonas europaea*) (American Type Culture Collection, Rockville, MD, USA, ATCC#19718) to inoculate the model system

as well as to raise ammonia concentration in the system from 0.23 to 0.72 mg-N/L, and lowering the NH_2Cl residual concentration from 0.14 to 0.04 mg/L as Cl_2. All other operational conditions were kept unchanged.

5.2.2 Biofilm samples

Polyvinylchloride (PVC) slides were installed with concrete slides in the same annular reactor, but there was no visible biofilm developed on the PVC slides even after the 1-year operation of the model system. As a result, in this study, only those biofilms grown the concrete slides were collected for microelectrode measurements. Using the proposed threshold value, 0.05 mg nitrite-N/L, as the primary criterion to judge conditions and to define a nitrification episode in the model system, three types of biofilms grown on the concrete slides were sampled at three different developmental stages for microelectrode measurements. **Biofilm I** was harvested at the first stage when nitrite concentration was around 0.005 mg-N/L. **Biofilm II** was collected at the second stage when a substantial increase in nitrite concentration (up to around 0.02 mg-N/L) had been observed after implementation of the operational modifications (i.e. introduction of nitrifying bacteria and supply of ammonia) in the system. **Biofilm III** was sampled at the third (final) stage when nitrite further increased and finally reached the proposed threshold after a further operational modification, i.e. lowering the NH_2Cl residual, was made.

5.2.3 Microelectrode measurements in biofilms

Concentration profiles measured in biofilms using microelectrodes included those

for oxygen, ammonium, nitrate and pH. Details of fabrications and calibrations of microelectrodes used, and the set-up for conducting all profile measurements in biofilms with these microelectrodes, were introduced in Chapter 2. Stock water sampled from the model system at the time each biofilm slide was harvested was continuously pumped from an amble glass bottle into the transparent Plexiglas flow cell with similar RT (6 hr) as used in the model system.

5.2.4 Analyses of water and biofilm samples

Chemical analyses. Water samples were collected regularly from the model system for chemical analyses. Parameters tested included DO, pH, nitrite, nitrate, ammonium, free and total chlorine, and total organic carbon (TOC). Details of analytical methods for these parameters are described in Section 2.4.1 of Chapter 2.

Microbiological analyses. Microbiological tests conducted included HPC and MPN of nitrifying microorganisms. In addition to regular monitoring tests on effluent from the model system, these tests were also conducted on biofilm samples after their use in microelectrode measurements. Water samples were directly used for HPC and MPN tests, whereas biofilm samples had to be scraped from the slide and rinsed with 100 mL autoclaved phosphate buffer solution (PBS). The biofilm suspension was then homogenized and later treated similarly as water samples. Incubation for HPC tests was implemented at 28° C for 7 days; whereas for MPN tests on nitrifying microorganisms, the incubation period was 28 days. More details of the HPC and MPN tests are introduced in Section 2.4.2 of Chapter 2.

Biofilm thickness measurements. Biofilm thickness was normally measured

either after its use in microelectrode measurements or before biofilm HPC and MPN tests using an optical microscopic method as introduced in Section 2.4.2 of Chapter 2.

5.3 Results and Discussions

5.3.1 Operating data of the model CWDS

Over the 1-year study period, biofilm growth in the model system was under conditions listed in Table 5-1. Figure 5-2 shows nitrate and nitrite monitoring data in the water during the study period. Except for the first 10 days, during which the raw water sampled from the field had been used as the sole input into the model system, nitrate concentrations fluctuated at around 0.18 mg-N/L, which was not largely different from the design concentration via input of $NaNO_3$ as nitrogen source into the model system. Nitrite monitoring data, during the initial 250 days of operation, similarly revealed that nitrite concentrations in the model system were stabilized at around 0.005 mg-N/L. This indicates that during the initial 250-day period, activities of nitrifying microorganisms in the model system were weak. Nitrite concentration started to increase substantially at around the 268th day of the operation, which was about 3 weeks after the implementation of the nitrification-enhancing modifications in the operation of the model system. It finally reached the proposed critical threshold (0.05 mg-N/L) at around the 329th day of the operation. According to the adopted definition for nitrification using the proposed critical threshold, it could be concluded that an episode of nitrification occurred in the model system. However, what was taking place was actually a "partial nitrification", i.e. the second step of nitrification process - conversion of nitrite into nitrate – was weak, based on the nitrate monitoring data in the model system as illustrated in Figure 5-2 as

well as microelectrode measurements in biofilms discussed below.

Table 5-1 Biofilm growth conditions monitored using the effluent from the model system during a 1-year study period.

Parameter	Average	Standard Deviation
DO (mg/L)	6.81	1.12
pH	7. 87	1. 08
NH_3-N (mg/L)	0. 32	0. 21
NH_2Cl (mg/L as Cl_2)	0. 09	0. 09
NO_3-N (mg/L)	0. 18	0. 06
TOC (mg/L)	1. 16	0. 32
HPC (Log_{10} cfu/mL)	4. 95	0. 61

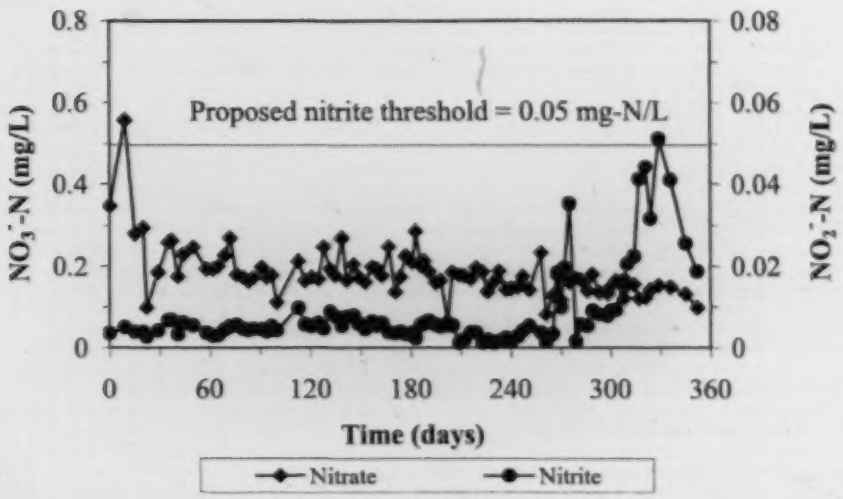

Figure 5-2 Nitrate and nitrite monitoring data in the model system during a 1-year study period.

5.3.2 Microbiological analyses

Figure 5-3 displays results of HPC and MPN enumeration of planktonic microorganisms in the water of the model system. During the entire study period, there was not a clear correlation between the HPC data and development of nitrification. During the initial 250-day period, MPN test only gave one positive result at around the 158th day of the operation. MPN test started to give clearer evidence of the presence of nitrifying microorganisms at around the 263rd day with aforementioned nitrification-enhancing modifications implemented in the model system. However, it generally could not consistently provide such evidence, as illustrated in Figure 5-3, although nitrite monitoring data (Figure 5-2) and microelectrode measurements data in biofilms (discussed below) had indicated otherwise during the last period of the 1-year study. This might be attributable to some technical issues related with the MPN tests for nitrifying microorganisms.

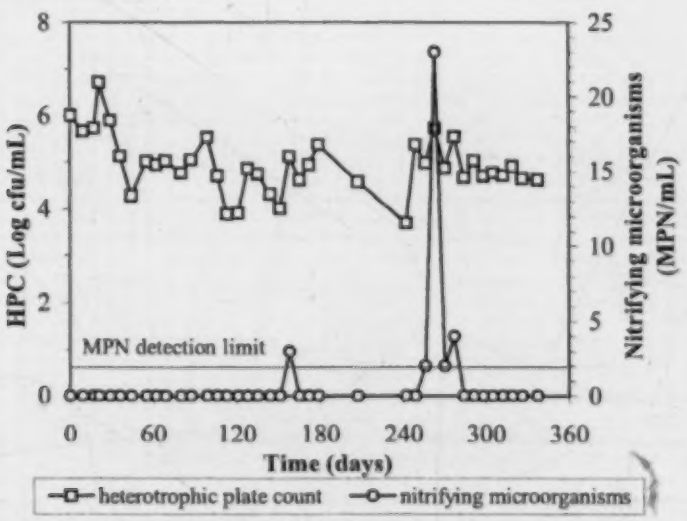

Figure 5-3 Planktonic nitrifying microorganisms (MPN) and HPC in the model system during 1-year study period.

The reason behind the wide use of the MPN test for nitrifying microorganisms is not necessarily because this is the best method, but because it is the only technique available to most investigators. To achieve high counting efficiency, the medium and growth conditions used must allow all nitrifier cells present to grow to a population large enough to be detected; and the cells present must be sufficiently separated from any particulate matter to ensure each cell be individually dispersed and transferred efficiently during the dilution process (Belser, 1979). In reality, these conditions do not necessarily often hold and consequently low recovery efficiency of MPN cultural technique could be as low as between 0.1 to 5 % (Belser and Mays, 1982). Meanwhile, there is also a possibility that over-dilution takes place during serial dilutions preparation process and thus lowers the sensitivity of MPN test in detecting the presence of nitrifying microorganisms. This helps explain why MPN tests responded poorly in this study, when both nitrite monitoring data (Figure 5-2) and microelectrode measurements in biofilms (discussed below) had already indicated actively ongoing nitrification in the system. Besides the above-mentioned technical issues that often lead to underestimations of real population densities of nitrifying microorganisms in the samples under testing, the time lag of obtaining MPN test data for nitrifying microorganisms due to the long incubation time makes conducting MPN test alone insufficient in early detection of nitrification in CWDSs. It is, therefore, important to see if alternatives exist to the observations on other related parameters such as ammonium, nitrate, nitrite, and pH.

5.3.3 Microelectrode measurements in biofilms

Based on the proposed critical nitrite threshold, 0.05 mg N/L, three

developmental stages of the conditions in the model system had been defined including **Stage I, II** and **III** with nitrite concentration at around 0.005, 0.02 and 0.05 mg-N/L, respectively in the water. Accordingly, three types of biofilms (**Biofilm I, II and III** corresponding to these three stages, respectively) were sampled from the model system for microelectrode measurements. This way, how parameter profiles of interest measured using microelectrodes would respond to the condition changes in the model system could be investigated, particularly with respect to the increase in nitrite concentration up to the proposed critical threshold value.

5.3.3.1 Microelectrode measurements in Biofilm I

Figure 5-4 illustrates profiles of DO, pH, ammonium and nitrate measured in **Biofilm I** under conditions with nitrite concentration at 0.005 mg-N/L in the water of the model system. It can be seen in this figure that DO started to decrease near the biofilm surface, but the decrease in DO was not substantial at this time. DO decreased only about 3.1 % from the bulk to the substratum of the biofilm, at which DO was still at a high concentration (around 6.9 mg/L). This indicates that the intensities of microbial activities, both heterotrophic and nitrifying microorganisms, were weak at this stage so that oxygen consumption was not substantial. The biofilm was fully penetrated by DO and thus the entire biofilm was under an aerobic condition. This could be attributed to the carefully maintained high DO concentration in the model system through continuous aeration and the presence of a thin and loose structure of the biofilm. The thickness of the biofilm was less than 100 μm at this stage.

The very weak activities of nitrifying microorganisms in this biofilm could also

be further demonstrated by profiles of nitrate and ammonium, both of which exhibited very slight changes. From the bulk to the substratum of biofilm, nitrate concentrations increased from 0.14 to 0.16 mg-N/L, while ammonium concentrations decreased from 0.17 to 0.15 mg-N/L. Both ammonium and nitrate concentrations were just above the detection limit of the microelectrodes (at around 1×10^{-5} M or 0.14 mg-N/L) (Li, 2001). At the first stage in the model system, although oxygen and ammonia were present throughout the biofilm, the ammonia concentration was obviously too low, with an average only at around 0.23 mg-N/L (or 16 μM as NH_3-N), compared with the half saturation constant (K_{NH3}) value of nitrifying bacteria for ammonia, which is at around 30 to 75 μM (NH_4^+ plus NH_3 at pH 7.8) for strains in the *Nitrosomonas oligotropha* group (Stehr *et al.*, 1995) and 36 to 72 μM as NH_3-N as reported by Metcalf & Eddy (2003). Therefore, although other conditions in the model system at this stage were favorable, the low ammonia concentration was a limiting factor to hinder nitrifying biofilm growth, let alone nitrification occurrence in the model system.

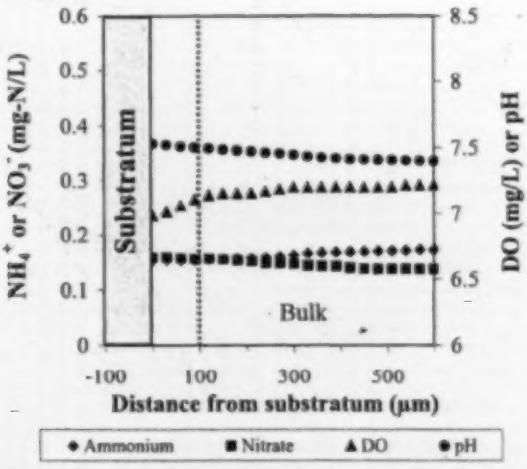

Figure 5-4. Profiles of pH, DO, ammonium and nitrate measured in Biofilm I grown on a concrete slide. Dotted vertical line indicates interface of the bulk and the biofilm.

As anticipated, the pH profile from the bulk to the inside of the biofilm should have been decreasing if there had been nitrification occurring in the biofilm. The observed pH profile, however, illustrated an increasing trend of pH change. Discussion on this issue is made in a later section.

MPN tests conducted at this stage on both water and biofilm could not provide clear evidence of presence of nitrifying microorganisms in the model system. MPN test alone was not sufficiently reliable to help judge presence or absence of nitrifying microorganisms and detect nitrification potential in the system, but its use and testing results at least provided more supporting evidence to the conclusion made based on the results from the microelectrode measurements. That is, under the conditions at the first stage in the model system, the probability of nitrification occurrence was low.

5.3.3.2 Microelectrode measurements in Biofilm II

Based on profile measurements and MPN tests on Biofilm I, and chemical (nitrate and nitrite) and MPN tests on the water of the model system, it was concluded that no vigorous nitrifying microbial activities could be detected in the model system. One major reason for this was the low ammonia concentration. To enhance nitrifying biofilm growth, in addition to an introduction of *Nitrosomonas europaea* to the model system, a supply of ammonia with average concentrations at around 0.72 mg-N/L (52 μM as NH_3-N) was introduced at the second stage of the operation of the model system. Figure 5-5 illustrates profiles of DO, pH, ammonium and nitrate measured in **Biofilm II** grown in the model system with these operational modifications. At the time when Biofilm II was sampled, nitrite concentration in the water of the model system was at 0.019 mg-N/L,

ammonia was 0.72 mg-N/L (52 μM as NH_3-N), and NH_2Cl residual was 0.14 mg/L as Cl_2 with an average input NH_2Cl concentration at 1.03 mg/L as Cl_2.

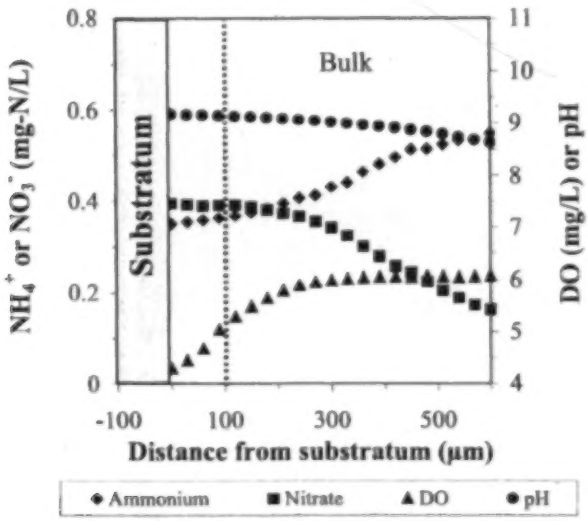

Figure 5-5 Profiles of pH, DO, ammonium and nitrate measured in Biofilm II grown on a concrete slide. Dotted vertical line indicates interface of the bulk and the biofilm.

It is illustrated clearly in Figure 5-5 that DO decrease in Biofilm II became much more substantial than that in Biofilm I. DO dropped from 6.1 to 4.3 mg/L, changing about 29.5 %, from the bulk to the substratum of the biofilm. This indicates that at this stage the intensities of microbial activities were greatly increased in comparison with those in Biofilm I so that oxygen consumption was increased substantially as well. The high DO concentration at the substratum illustrated that Biofilm II was also fully penetrated by DO and thus the entire biofilm was still under aerobic conditions. This could similarly be attributed to the well-maintained aeration in the system and the

presence of thin and loose biofilms. The thickness of the biofilms at the second stage was only around 100 μm.

When considering the profiles of nitrate and ammonium in Figure 5-5, it became clear that ammonia oxidation took place in Biofilm II at a greatly increased rate over Biofilm I. This indicates that the intensities of activities of nitrifying microorganisms in Biofilm II increased largely in comparison with those in Biofilm I. These observations support the explanation that in Biofilm I, low ammonia concentration was a limiting factor to nitrifying microorganisms growth; and once this factor was improved, nitrifying microbial activities were increased substantially, as illustrated in Biofilm II. Ammonium concentration dropped to 0.35 mg-N/L at the substratum from its bulk concentration at 0.55 mg-N/L; meanwhile, nitrate concentration increased from 0.16 mg-N/L in the bulk to around 0.40 mg-N/L at the substratum.

A similar trend of pH change as observed in Biofilm I was also seen in Biofilm II. The pH value increased, rather than decreased, from the bulk to the substratum of the biofilm.

MPN tests conducted at the second stage on both water and biofilm indicated the presence of nitrifying microorganisms in the model system. Population density of nitrifying microorganisms in the water was 2 MPN/mL, while in the biofilm it was 59 MPN/cm^2. These results were consistent with what microelectrode measurements indicated with respect to the presence of nitrifying microorganisms at the second stage. Microelectrode measurements, furthermore, disclosed that nitrification process was proceeding at greatly increased rates at this stage. This rendered a greater potential for significant nitrification in the model system.

It should be pointed out that the observations on the ongoing nitrification taking place with increased rates in biofilms were made under a condition with nitrite concentration as low as 0.02 mg-N/L in the water of the model system. This indicates that, compared with the value of 0.05 mg-N/L for confirmation of nitrification outbreak, a lower critical threshold probably should be proposed for nitrite in terms of its use in early detection of nitrification in CWDSs. Biofilm tests using microelectrodes demonstrated that this technique has the capability to elucidate fundamental phenomena closely associated with nitrification process and, as a result, presents itself a potential tool in detecting nitrification in CWDSs. Although it may be perceived at this time that there will be technical difficulties in adopting this approach to real water distribution systems, further research could demonstrates its feasibility.

5.3.3.3 Microelectrode measurements in Biofilm III

Based on the operational mode at the second stage, one more modification - lowering NH_2Cl residual - was introduced into the model system after the profile measurements on Biofilm II to further enhance activities of nitrifying microorganisms. Figure 5-6 illustrates profiles of DO, pH, ammonium and nitrate measured in **Biofilm III** grown under conditions with nitrite concentration at 0.051 mg-N/L and NH_2Cl residual at 0.04 mg/L as Cl_2 with an average input NH_2Cl concentration of 0.53 mg/L as Cl_2 in the model system.

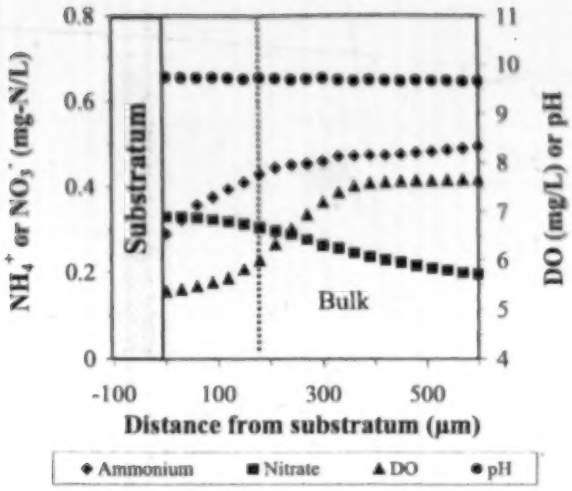

Figure 5-6 Profiles of pH, DO, ammonium and nitrate measured in Biofilm III grown on a concrete slide. Dotted vertical line indicates interface of the bulk and the biofilm.

It can be seen in Figure 5-6 that the degree of DO drop in biofilm III was slightly increased in comparison with that in biofilm II. DO dropped about 30.5 %, from 7.7 mg/L in the bulk to 5.4 mg/L at the substratum of biofilm. The high DO concentration at the substratum indicates that Biofilm III was totally penetrated by DO as well. The thickness of Biofilm III increased to around 180 μm at the third stage, but its structure was not dense yet. Due to their high demand for oxygen, nitrifying microorganisms normally distribute in the upper layers of biofilms. However, using fluorescence *in-situ* hybridization technique in an investigation on distribution of nitrifying bacteria in biofilms with thickness at around 200 μm, Schramm *et al.* (1996) discovered that both ammonia-oxidizing bacteria and nitrite-oxidizing bacteria were not restricted to the upper aerobic zone of the biofilms, but they both were detected in the lower anoxic layers and

even at the substratum of the biofilms. In our study, thickness of biofilms was less than 200 μm and biofilms were fully penetrated by DO at all three stages. As a result, it could be expected that nitrifying microorganisms could be existing at almost any location within the biofilms under such favorable conditions in the model system, except for a special issue related to increased pH and its impact on nitrite-oxidizing microorganisms in Biofilm III. This special issue will be discussed in a later section (Section 5.3.4).

The ammonium profile in Figure 5-6 reveals that ammonium concentration dropped to 0.29 mg-N/L at the substratum of the biofilm from its bulk concentration of 0.55 mg-N/L. Compared with that in Biofilm II, ammonia consumption in Biofilm III was increased, but nitrate generation did not similarly increase. The nitrate profile in Biofilm III reveals that the nitrate concentration increased from 0.17 mg-N/L in the bulk to 0.33 mg-N/L at the substratum of the biofilm. However, when looking into the nitrite monitoring data in the model system, a substantial increase was seen from the second stage to the third stage. This could be attributable to two reasons. Firstly, the lowered NH_2Cl concentration at the third stage led to lowered nitrate generation that otherwise would have taken place through NH_2Cl decomposition reactions; and at the same time it could also promote accumulation of nitrite via decreased nitrite consumption in nitrite-promoted decompositions of NH_2Cl. Secondly, the second step of the nitrification process might be weakened leading to the development of "partial nitrification" in the system. The reason behind this could be the high pH within Biofilm III. Compared with Biofilm II that had pH up to 8.9, Biofilm III had pH increasing up to 9.7 at the substratum as illustrated on the pH profile. This high pH might affect the growth of nitrite-oxidizing microorganisms. As a result, nitrite was accumulated rather than

converted to nitrate, and nitrate generation from this pathway was thus greatly reduced. In the nitrogen cycle, retardation of nitrate generation could also occur due to the presence of anammox bacteria discovered recently (Strous *et al.*, 1999), but under conditions like in this particular study, especially with respect to the high DO concentration throughout the entire biofilms under test, the contribution from anammox reactions to the nitrogen balance in the system under investigation could be neglected. Between the above-mentioned two possible reasons, the second could be the dominating one. More details were discussed below regarding the pH issue.

MPN tests conducted at the third stage on biofilms indicated the presence of nitrifying microorganisms in the model system with a population density at 59 MPN/cm^2, but MPN tests on the water gave negative results.

5.3.4 Impact of biofilm slide material

Based on theory, the expectation for pH profiles in biofilms had been that, due to the nitrification process, which generates protons and consumes alkalinity, pH should have decreased from the bulk to the biofilm phase. The reality in this particular study was, however, that the pH actually increased. This might be attributable to the impact of the slide material used – concrete. According to the manufacturer of the annular reactor used for biofilm growth, the concrete slides were made from water, 110 micron Silica Foundry Sand and Portland Cement and normally has pH at around 12 to 13. As a result, the displayed pH profiles in Figure 5-4 to Figure 5-6 actually were neutralized results between ongoing proton release from the nitrification and alkalinity release from the concrete. It might be that the impact of the former was weaker than that of the latter so

that an increasing pH profile from the bulk to the substratum of biofilm resulted during microelectrode measurements.

From the increases in nitrite concentration monitored in the water of the model system, it seemed reasonable to expect that nitrification should have been more intense in biofilm III than in biofilm II. However, this was not the case. According to profiles measured using microelectrodes, the actual difference between these two scenarios was not as pronounced as had been expected. The impact of concrete slides on pH might have been playing an important role in this regard. It has been reported that the rate of nitrifying bacteria growth is a function of pH, with optimal growth at pH 8.5 (Grady *et al.*, 1999). Harrington *et al.* (2002) reported on pilot studies with chloraminated water that nitrification occurred at all pH conditions ranging from pH 7.9 to 8.9, with the shortest time to onset of nitrification at 8.5 to 8.6; and increased pH resulted in slower growth of nitrifying bacteria. However, in a field survey on CWDSs, nitrification was observed to occur at a range of pH from 7.2 to 9.8 (Odell *et al.*, 1996). Wilczak *et al.* (1996) reported an even wider pH range (6.5 to 9.5), in which nitrification was observed in CWDSs. In our study, the increased pH at 9.7 in Biofilm III might reach the limit and start to inhibit activities of nitrifying microorganisms, especially nitrite-oxidizing microorganisms, which are often much more sensitive to pH change. It has been reported (Belser, 1979) that within a range of 0.1 to 1.0 mg/L, free ammonia was a differential inhibitor of nitrite oxidation. Equilibrium between ammonium and free ammonia is pH dependent. High pH leads to high free ammonia concentrations, which in turn inhibits the growth of nitrite-oxidizing microorganisms and, nitrite accumulation thus results. This could also explain why in Biofilm III ammonia consumption increased

but nitrate generation did not. This indicates that intense "partial nitrification" might be occurring at the third stage in the model system and be one of the major reasons that could be blamed for the increases in nitrite but not in nitrate concentration as illustrated in Figure 5-2. If a nitrite microelectrode had been adopted, the picture may have been elucidated more clearly. However, the reported nitrite microelectrode (de Beer *et al.*, 1997) had a detection limit at around 1×10^{-5} M (or 0.14 mg-N/L) with the presence of chloride ion (Cl^-), which is one of the major products of NH_2Cl decomposition processes, while the actual nitrite concentrations in this particular study were normally below 0.05 mg/L, which was used as a critical threshold for confirmation of a nitrification episode in the model system. Consequently, the existing nitrite microelectrode is not suitable for this particular study. However, this is an area worth being explored in the future.

5.4 Conclusions

Based on the 1-year study on nitrification detection in the nitrifying bacteria-seeded, chloraminated model water distribution system with favorable operational conditions for nitrification, the following conclusions have been made:

(1) Biofilm tests using microelectrodes demonstrated that this technique has the capability to elucidate fundamental phenomena closely associated with nitrification process and, as a result, presents itself a potential tool in detecting nitrification in CWDSs. Although it may be perceived at this time that there will be technical difficulties in adopting this approach to real water distribution systems, further research could demonstrates its feasibility.

(2) Ongoing nitrification was detected by biofilm tests using microelectrodes

when nitrite concentration was as low as 0.02 mg-N/L in the water. This indicates that, compared with the critical threshold of 0.05 mg nitrite-N/L for confirmation of nitrification outbreaks in CWDSs, a lower critical threshold probably should be proposed for nitrite in terms of its use in early detection of nitrification in CWDSs.

5.5 References

Belser, L. W. 1979. Population ecology of nitrifying bacteria. *Annual Review of Microbiology*, 33:309-333.

Belser, L. W. and Mays, E. L. 1982. Use of nitrifier activity measurements to estimate the efficiency of viable nitrifier counts in soils and sediments. *Applied and Environmental Microbiology*, 43:945.

Camper, A. K. 1996. *Factors limiting microbial growth in distribution systems: laboratory and pilot-scale experiments*. AWWA research Foundation and American Water Works Association. Denver, Colorado, USA.

Cunliffe, D. A. 1991. Bacterial nitrification in chloraminated water supplies. *Applied and Environmental Microbiology*, 57:3399-3402.

de Beer, D., Schramm, A., Santegoeds, C. M. and KuHl, M. 1997. A nitrite microsensor for profiling environmental biofilms. *Applied and Environmental Microbiology*, 63:973–977.

Grady, C. P. L Jr., Daigger, G. T. and Lim, H. C. 1999. *Biological wastewater treatment*, 2nd edition. Marcel Dekker Inc., New York.

Harrington, G. W., Noguera, D. R., Kandou, A. I. and Vanhoven, D. J. 2002. Pilot-scale evaluation of nitrification control strategies. *Journal AWWA*, 94:78-89.

Ike, N. R., Wolfe, R. L. and Means, E. G. 1988. Nitrifying bacteria in a chloraminated drinking water system. *Water Science and Technology*, 20(11-12):441-444.

Kirmeyer, G. J., Odell, L. H., Jacangelo, J., Wilczak, A and Wolfe, R. 1995. *Nitrification occurrence and control in chloraminated water systems*. AWWA research Foundation and American Water Works Association. Denver, Colorado, USA.

Li, J. 2001. *Azo dye biodegradation and inhibition effects on aerobic nitrification and anoxic denitrification processes*. Ph.D. dissertation. University of Cincinnati, Cincinnati, Ohio, USA.

Lieu, N. I., Wolfe, R. L. and Means, E. G. III 1993. Optimizing chloramine disinfection for the control of nitrification. *Journal AWWA*, 85:84-90.

Matulewich, V. A., Strom, P. F. and Finstein, M. S. 1975. Length of incubation for enumerating nitrifying bacteria present in various environments. *Applied Microbiology*, 29:265-268.

Metcalf and Eddy 2003. *Wastewater Engineering – treatment and reuse*, 4th edition. McGraw Hill, New York.

Odell, L. H., Kirmeyer, G. J., Wilczak, A., Jacangelo, J. G., Marcinko, J. P. and Wolfe, R. L. 1996. Controlling nitrification in chloraminated systems. *Journal AWWA*, 88:86-98.

Ollos, P. J., Huck, P. M. and Slawson, R. M. 2003. Factors affecting biofilm accumulation in model distribution systems. *Journal AWWA*, 95:87-97.

Pintar, K. D. M. 2000. *Factors influencing nitrifcation in a model chloraminated distribution system*. Master's thesis, University of Waterloo, Waterloo, Ontario, Canada.

Pintar, K. D. M. and Slawson, R. M. 2003. Effect of temperature and disinfection strategies on ammonia-oxidizing bacteria in a bench-scale drinking water distribution system. *Water Research*, 37:1805-1817.

Pintar, K. D. M., Anderson, W. B., Slawson, R. M., Smith, E. F. and Huck, P. M. 2005. Assessment of a distribution system nitrification critical threshold concept. *Journal AWWA*, 97:116-129.

Regan, J. M., Harrington, G. W. and Noguera, D. R. 2002. Ammonia- and nitrite-oxidizing bacterial communities in a pilot-scale chloraminated water distribution system. *Applied and Environmental Microbiology*, 68:73-81.

Sathasivan, A., Fisher, I. and Kastl, G. 2005. Simple method for quantifying microbiologically assisted chloramine decay in drinking water. *Environmental Science and Technology*, 39:5407-5413.

Schramm, A., Larsen, L. H., Revsbech, N. P., Ramsing, N. B., Amann, R. and Schleifer, K-H. 1996. Structure and function of a nitrifying biofilm as determinaed by in situ hybridization and the use of microelectrode. *Applied and Environmental Microbiology*, 62:4641-4647.

Stehr, G., Bottcher, B., Dittberner, P., Rath, G. and Koops, H.-P. 1995. The ammonia-oxidizing nitrifying population of the River Elbe estuary. *FEMS Microbiology Ecology*, 17:177-186.

Strous, M, Fuerst, J. A., Kramer, E. H. M., Logemann, S., Muyzer, G., van de Pas-Schoonen, K. T., Webb, R., Kuenen, J. G. and Jetten, M. S. M. 1999. Missing lithotroph identified as newplanctomycete. *Nature*, 400:446–449.

Wilczak, A., Jacangelo, J. G., Marcinko, J. P., Odell, L. H., Kirmeyer, G. J. and Wolfe, R. L. 1996. Occurrence of nitrification in chloraminated distribution systems. *Journal AWWA*, 88:74-85.

Wolfe, R. L., Means, E. G. III, Davis, M. K. and Barrett, S. E. 1988. Biological nitrification in covered reservoirs containing chloraminated water. *Journal AWWA*, 80:109-114.

Wolfe, R. L., Lieu, N. I., Izaguirre, G. and Means, E. G. 1990. Ammonia-oxidizing bacteria in a chloraminated distribution system: seasonal occurrence, distribution, and disinfection resistance. *Applied and Environmental Microbiology*, 56:451- 462.

Chapter 6

Impact of the penetration of microelectrode tip in biofilms

6.1 Introduction

In the course of experimental investigation into microenvironments, such as those in biofilms, approaches that do not bring in significant impacts on the subjects (e.g. biofilms) are appropriate and desirable. Microelectrodes have been used in studies on biofilms and sediments due to their tiny tips and high spatial resolutions, but their wide uses do not necessarily mean that these techniques do not disturb the local microenvironments of their subjects. Some investigators have already noticed that microelectrodes cannot be considered totally undisruptive despite their tiny tips (Amann and Kuhl, 1998; Kuhl and Revsbech, 2001). Actually, it has been reported that during its profile measurements, the microelectrode could introduce significant impact on the microenvironment around the interface between the bulk and the sediments or biofilms. In a comparative experiment, Glud *et al.* (1994) observed that during the course of its measuring process from the bulk to the surface of sediment, an oxygen microelectrode with tip diameter at 8 μm significantly altered the diffusion boundary layer above the sediment. The thickness of the diffusion boundary layer was reduced by 25 to 45%, and the eroding effect was detected even when the microelectrode tip was situated more than 1 mm above the sediment surface. Glud *et al.* (1998) thus presumably concluded that the similar mechanism could explain why biofilms, partially (50%) anoxic disclosed by non-invasive approaches using planar optodes, was totally oxic by the microelectrode technique, and thus overestimation of dissolved oxygen (DO) distribution within biofilms

could result from microelectrode measurements. However, the real mechanism behind this phenomenon has not been fully understood yet. More experimental evidence is needed in order to more clearly elucidate what really happens within biofilms with the insertion of a microelectrode tip. Chapter 6 introduces a preliminary investigation implemented in an effort to collect direct experimental evidence to elucidate what kind of impact a microelectrode tip could bring in by its penetration and how significant the impact, if any, could be on microelectrode measurements within biofilms.

6.2 Materials and Methods

6.2.1 Artificial biofilm preparation

Due to the complexity of real biofilms with respect to their morphology, compositions and structures, well-defined model systems of biofilms could be very useful in helping determine the impacts of a single factor on fundamental properties in biofilms. Study has shown that an artificial biofilm model is suited to simulate important biofilm matrix properties (Strathmann *et al.*, 2000). As a result, an artificial biofilm was adopted in this study. This biofilm was made from 0.5% (w/v) agar (Sigma Cat. # A6686), which was dissolved under heating in distilled water. Before it cooled down to solidify, the agar (about 0.3 mL) was poured into 0.5 mL transparent tubes with a flat cap (Thermowell™ Tube, Cat. # 6530, Corning Inc., Corning, NY, USA).

6.2.2 Set-up of microscopic observation

A Nikon Polarizing Microscope (Nikon Inc., Instrument Group, Melville, NY, USA, Model ECLIPSE E600 POL) was used in this experiment with the following

features: Eyepiece - CFI 10×/22CM (Nikon); Objective - magnification and numerical aperture ranging from minimum (4×/0.10p, ∞/- WD30) to maximum (40×/0.65p, ∞/- WD0.65); Illumination - internal Koehler-type diascopic illumination optics; Photo switch - five-level fine adjustment selector; Lamp rating – 100 w halogen lamp (OSRAM HCX64623 or PHILIPS 7724). A Nikon digital camera (COOLPIX990, 3.34 Mega pixels) with MDC lens was installed on the microscope. A micromanipulator (World Precision Instrument, Inc., Sarasota, FL., USA, Model M3301) with resolution of 10 μm was arranged to stand beside the microscope to hold as well as to position the microelectrode during the microscopic observations in this experiment.

6.2.3 Microelectrode preparation for microscopic observation

A separate microelectrode for oxygen measurement was used in the microscopic observation and imaging experiments. It consisted of an etched Pt wire coated with white glass and a naked tip. The fabrication procedure for this microelectrode followed the procedure described in Section 2.1.2.2 of Chapter 2 for the working cathode of the combined oxygen microelectrode but without the step of gold-plating at its tip. This microelectrode had diameters of 2, 9 and 12 μm at locations of 0, 100 and 200 μm behind its tip.

6.2.4 Static imaging

Before implementation of the formal static imaging process, the entire microscopic observation set-up was arranged such that a right zooming area could be approximately pre-set to achieve a clear view on the microelectrode tip penetration into

the artificial biofilms. During the formal imaging experiment, a drop of an indicator dye, Rhodamine B (1%, w/v), was added onto the surface of the artificial biofilms in the transparent tube. Then the tube was quickly fastened on the stage of the microscope. Afterwards, the microelectrode, held on the micromanipulator, was pushed and penetrated into the artificial biofilm until its tip just came into the view of the microscope. From this point, the microelectrode was further moved forward up to a distance of 1000 μm, which was controlled by the micromanipulator. At this moment, there was no Rhodamine B penetrating into the view yet. Once the pink tracer diffused into the view, the time started to be counted, and the microscopic pictures in time series were taken as well.

6.2.5 Oxygen profile measurements in biofilm

To take advantage of its stable performance, the combined oxygen microelectrode as introduced in Section 2.1.2 of Chapter 2 was used to measure DO profiles in a natural, mixed population biofilm grown on a concrete slide. This biofilm was sampled from a well-aerated model drinking water distribution system as described in Section 5.2.1 of Chapter 5. The tip diameter of the oxygen microelectrode was at around 20 μm. Using a combination of time interval and step size at 3 seconds and 20 μm, respectively, DO profiles were measured on the same biofilm spot when the microelectrode was moved from the biofilm surface toward the substratum as well as when the microelectrode was retreated back toward the biofilm surface. The positioning of the microelectrode tip on the biofilm surface was implemented with the aid of a microscope. Detailed information on the calibration process of the oxygen microelectrode and the set-up for microelectrode

measurements in biofilms is presented in Section 2.1.2.3 and Section 2.3 of Chapter 2, respectively.

6.3 Results and Discussions

6.3.1 Diffusion frontline in biofilm

In a uniform aqueous medium, mass diffusion of a chemical of interest (solute) can be described by the following model using 95.5% diffusion frontline according to Strobel and Heineman (1989):

$$L_{95.5} = (8 \cdot D \cdot t_{95.5})^{1/2} \quad (6\text{-}1)$$

where, $L_{95.5}$ is distance between origin and 95.5% diffusion frontline of solute at time $t_{95.5}$ (cm), D is diffusion coefficient of solute in aqueous medium (cm^2/s), and $t_{95.5}$ is time (seconds). The "95.5% diffusion frontline of solute" is defined as the line to which about 95.5% of the solute molecule population has diffused from the origin.

In particular, a model has been recommended for describing mass diffusion of a solute in biofilms as follows using the 90% diffusion frontline (Stewart, 2003):

$$L_{90} = (D_e \cdot t_{90}/1.03)^{1/2} \quad (6\text{-}2)$$

where, L_{90} is the distance between origin and 90% diffusion frontline of solute at time t_{90} (cm), D_e is effective diffusion coefficient of solute in biofilms (cm^2/s).

According to either of the above models, in the same direction within the aqueous medium or biofilm, the diffusion frontline (either 90% or 95.5%) of a solute theoretically should be advancing uniformly from its origin. In other words, from a three-dimensional perspective, a specific diffusion frontline of a solute should be in a plane perpendicular to the diffusion direction of the solute. What about the situation in which the biofilm is

penetrated with a microelectrode tip? Figure 6-1 illustrates such a case, in which the tracer Rhodamine B had diffused for 5 minutes within the artificial biofilm with the insertion of an oxygen microelectrode tip with diameters of 2, 9 and 12 μm at locations of 0, 100 and 200 μm behind its tip.

As can be seen in Figure 6-1, the mass diffusion pattern was totally changed from the theoretically expected for the scenario without microelectrode penetration. The 90% diffusion frontline, which was constructed approximately based on the intensities of the pink tracer shown on Figure 1, was actually not uniform on the same plane perpendicular to the direction of microelectrode penetration. A curved line as indicated in Figure 6-1 was developed. From a three-dimensional perspective, it can be perceived that the 90% diffusion frontline was formed as a cone-shaped surface (contour) with its top on the microelectrode. This cone-shaped surface clearly indicated a facilitating effect of the penetration of the microelectrode tip on the mass diffusion of Rhodamine B along the direction of the microelectrode penetration in the artificial biofilm. The closer to the microelectrode, the more significant this facilitating effect was.

According to Equation (6-2), in the case of no microelectrode penetration, the theoretical distance (L_{90}) of the 90% diffusion frontline of Rhodamine B after 5-minute diffusion should have been at around 104 μm using an effective diffusion coefficient of 3.7×10^{-7} cm^2/s for Rhodamine B in biofilms (Rani *et al.*, 2005). However, according to Figure 6-1, it appears obvious that the distance from the left edge of the microscopic picture to the real 90% diffusion frontline of Rhodamine B along the microelectrode was much larger than 104 μm. It was approximately 494 μm, which was estimated based on Figure 6-1. It was about 4.8 times greater than that of the theoretical value in the

scenario without microelectrode penetration.

Time serial pictures of mass diffusion of Rhodamine B in the artificial biofilm with the insertion of the microelectrode tip were also taken in this investigation and illustrated in Figure 6-2. Based on these microscopic pictures, quantitative comparisons between theoretically and experimentally estimated diffusion distances of the 90% diffusion frontline of Rhodamine B along the direction of microelectrode penetration at different times were made and listed in Table 6-1.

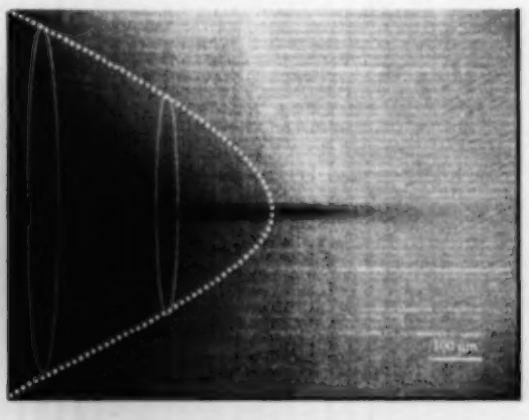

Figure 6-1 Microscopic observation of mass diffusion pattern of Rhodamine B in artificial biofilm with penetration of a microelectrode tip.

Figure 6-2 Time serial microscopic observations of mass diffusion of Rhodamine B in artificial biofilm with penetration of a microelectrode tip.

In Table 6-1, $L_{f\text{-}RB}$ is the facilitated diffusion distance of the 90% diffusion frontline with microelectrode penetration. It is experimentally estimated from time-serial images. $L_{t\text{-}RB}$ is the theoretical diffusion distance of the 90% diffusion frontline without microelectrode penetration. It is determined by Equation (6-2) using an effective diffusion coefficient in biofilm at 3.7×10^{-7} cm^2/s. As can be seen in Table 6-1, for Rhodamine B, the values of $L_{f\text{-}RB}$ were all larger than those of $L_{t\text{-}RB}$. This indicates that the penetration of microelectrode tip greatly facilitated the mass diffusion of Rhodamine B in the direction of microelectrode penetration. It also can be seen that this facilitating effect seems to be independent of diffusion time. The ratio between $L_{f\text{-}RB}$ and $L_{t\text{-}RB}$ are all close to each other at around 4.8 to 4.9 at different diffusion times from 1 to 5 minutes.

Table 6-1 Comparisons between diffusion distances of Rhodamine B 90% diffusion frontline in artificial biofilm with and without microelectrode tip insertion.

t_{90} (min)	$L_{t\text{-}RB}$ (μm)	$L_{f\text{-}RB}$ (μm)	Ratio ($L_{f\text{-}RB}/L_{t\text{-}RB}$)
1	46	227	4.9
2	66	320	4.9
3	80	392	4.9
4	93	450	4.8
5	104	494	4.8

Notes: (i)$L_{t\text{-}RB}$=theoretical diffusion distance of 90% diffusion frontline without microelectrode tip insertion, determined by equation (6-2) using $D_e=3.7 \times 10^{-7}$ cm^2/s; (ii)$L_{f\text{-}RB}$=facilitated diffusion distance of 90% diffusion frontline with microelectrode tip insertion, experimentally estimated from images taken in time series.

6.3.2 Facilitated diffusion vs microelectrode measurement

In order to determine if such a diffusion-facilitating effect has substantial impact

on microelectrode measurements within biofilms, which is something that we are more interested in with respect to application of microelectrode techniques to biofilm study, comparisons have been made in Table 6-2 between distances of the facilitated 90% diffusion frontline of Rhodamine B and microelectrode tip movement during its profile measurements in biofilms at different times.

Table 6-2 Comparisons between distances of the facilitated 90% diffusion frontline of Rhodamine B and microelectrode tip movement during its measurements in biofilms at different times.

t_{90} (min)	$L_{f\text{-}RB}$ (μm)	$L_{m3\text{-}30}$ (μm)	$L_{m6\text{-}30}$ (μm)	$L_{m6\text{-}50}$ (μm)
1	227	600	300	500
2	320	1200	600	1000
3	392	1800	900	1500
4	450	2400	1200	2000
5	494	3000	1500	2500

Note: $L_{m3\text{-}30}$, $L_{m6\text{-}30}$ and $L_{m6\text{-}50}$ are distances microelectrode tip moves during its measurements in biofilm with combinations of time interval and step size at 3 s/30 μm, 6 s/30 μm and 6 s/50 μm, respectively.

In microelectrode measurements, two parameters have to be pre-set: step size of the microelectrode tip movement and the time interval between step movements that is used for valid signal generation by the microelectrode and data collection by the data acquisition system. In Table 6-2, step sizes of 30 and 50 μm and time intervals of 3 and 6 seconds were employed for demonstration purposes. As can be seen in Table 6-2, at all times from 1 to 5 minutes, the distances passed by the facilitated 90% diffusion frontline

of Rhodamine B are smaller than those to be passed by microelectrode tip with any of these three combinations of step size and time intervals (i.e. 3 s/30 μm, 6 s/30 μm and 6 s/50 μm). This indicates that the facilitated 90% diffusion frontline would always be staying behind the microelectrode tip at each corresponding time during its profile measurements within biofilms. This demonstrates that the diffusion-facilitating effect of the microelectrode tip penetration does not affect profile measurements in biofilms using microelectrode, because the real working area of the microelectrode is at its tip. However, this conclusion is only valid under this particularly discussed condition.

There are many factors that may affect mass diffusion in biofilms and the selection of the speed of microelectrode tip movement during its profile measurements in biofilms. Factors such as diffusion coefficients of chemicals of interest, hydraulic conditions, biofilm compositions and structures, consumption or generation due to chemical reactions and microbial activities occurring in biofilms all will affect mass diffusion in biofilms. Chemicals with larger diffusion coefficients than that of Rhodamine B can be expected to move faster than Rhodamine B. Hydraulic conditions, especially those of local environments surrounding biofilms can affect the thickness of the diffusion boundary layer, which in turn determines the concentration gradient, the driving force, for mass diffusion from the bulk water into biofilms. Biofilm compositions and structures determine biofilm density, which in turn affects the mass diffusion of chemicals in biofilms.

Factors that affect the selection of the overall speed of the microelectrode tip movement during profile measurements include step size, step moving speed, response time of the microelectrode, and data collecting speed of the data acquisition system. As a

result, it is reasonable to expect that the degrees of the significance of the impact that the penetration of microelectrode tip may bring about on microelectrode measurements in biofilms may vary under different sets of conditions. This area is worth further investigation, results of which will be useful in guiding experimental design as well as data analysis and interpretation in biofilm study using microelectrode techniques.

6.3.3 Oxygen profiles measured in biofilm by microelectrode

Earlier studies (Glud *et al.*, 1994, 1998) have already investigated the impact of the movement of an oxygen microelectrode tip on the microenvironment around the interface between the bulk and the sediments or biofilms. It was found that the thickness of the diffusion boundary layer above the interface was greatly eroded by the microelectrode tip as it moved from the bulk toward the interface. In order to make comparison with what was achieved in the microscopic observations discussed earlier, in this study, oxygen profile measurements using the microelectrode was implemented only in the biofilm phase, i.e. the DO profiles were measured directly starting from the biofilm surface. Figure 6-3 illustrates two DO profiles measured on the same biofilm spot using a time interval of 3 seconds and a step size of 20 μm. The biofilm under test was sampled from a well-aerated model drinking water distribution system. The bottom (the first) profile was measured first, when the microelectrode was moved from the biofilm surface toward the substratum of the biofilm. The top (the second) profile was measured right after, when the microelectrode was retreated back toward the biofilm surface.

According to the theory of diffusion-reaction mechanism, DO profiles like these two illustrated in Figure 6-3 are the combined results of a continuous mass diffusion

process of DO from the bulk phase into the biofilm and a continuous consumption process of DO by aerobic microorganisms embedded in the biofilms. As disclosed in Figure 6-3, substantial oxygen concentration decreases occurred only within the upper layers (ranging from the surface to a depth at around 40 to 60 μm) of the biofilm; while in the deeper layers, oxygen concentration decreased gradually. This could be attributable to the substrate-limiting drinking water environment in the model system for biofilm growth, especially within the deeper layers of the biofilm. The substrate-limiting condition largely prohibited microbial activities and growth, and thus substantially decreased oxygen consumption within the deeper layers of the biofilm. Consequently, mass diffusion rather than microbial consumption was the dominating mechanism responsible for DO distributions within the deeper layers of the biofilm.

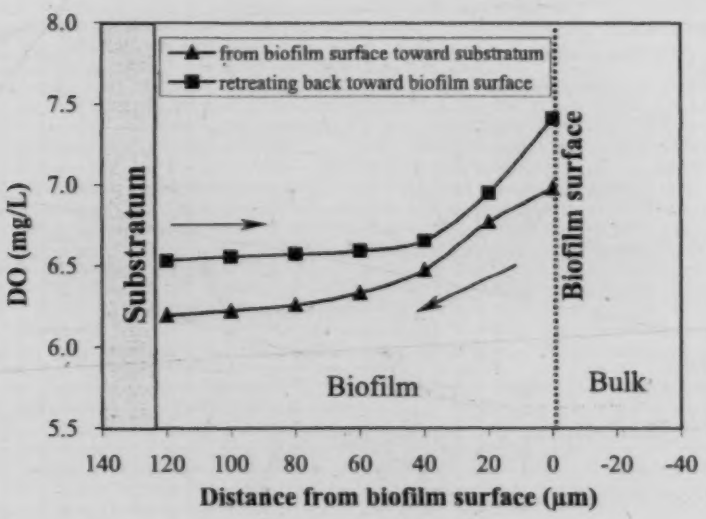

Figure 6-3 DO profiles measured under the same spot of a drinking water biofilm using microelectrode going toward the substratum and retreating back toward the biofim surface.

In Figure 6-3, it is clearly demonstrated that DO concentrations on the second profile are all higher than those on the first profile at each corresponding depth under the same biofilm spot, although these two DO profiles were actually measured by the same microelectrode on the same spot of the biofilm, all of which seem to make it nearly legitimate for these two profiles to be called "duplicates". The disparity between the two DO measurements on the biofilm surface could be explained by the eroding effect on the diffusion boundary layer from the movement of the microelectrode tip during its measurements (Glud *et al.*, 1994). The disparities between other DO measurements at each measured depth could be attributable to the impact of the microelectrode tip penetration within biofilms, as discussed earlier, during the first profile measurement. Taking oxygen diffusion coefficient in water (D_{aq}) at 2.42×10^{-5} cm^2/s at 25°C (Lide, 2006 - 2007) and $D_e/D_{aq} = 0.57$ (Stewart, 2003) led to $D_e = 1.38 \times 10^{-5}$ cm^2/s for effective diffusion coefficient of oxygen in biofilms, which is nearly 37 times larger than that of Rhodamine B. Based on the estimated D_e, theoretical diffusion distances of the 90% diffusion frontline of oxygen at different times without microelectrode penetration could be estimated. The estimated values are listed in Table 6-3. Meanwhile, assuming the experimentally determined ratio of $L_{f\text{-}RB}/L_{t\text{-}RB} = 4.85$ (refer to Table 6-1) could be applied to $L_{f\text{-}O}/L_{t\text{-}O}$, the ratio between diffusion distances of the facilitated and theoretical 90% diffusion frontlines of oxygen in biofilm, comparisons between distances of the facilitated 90% diffusion frontline of oxygen (with microelectrode penetration) and oxygen microelectrode tip movement during its profile measurements at different times could be made and listed in Table 6-3 as well.

Table 6-3 Comparisons of theoretical and facilitated diffusion distances of DO 90% diffusion frontline, and distances of oxygen microelectrode movement during its measurements in biofilms.

t_{90} (s)	$L_{t\text{-}O}$ (μm)	$L_{f\text{-}O}$ (μm)	$L_{m3\text{-}20}$ (μm)
3	64	310	20
6	90	439	40
9	111	537	60
12	128	620	80
15	143	693	100
18	157	760	120

Notes: (i)$L_{t\text{-}O}$=theoretical diffusion distance of DO 90% diffusion frontline without microelectrode penetration, determined by equation (6-2) using $De=1.4 \times 10^{-5}$ cm^2/s; (ii)$L_{f\text{-}O}$=facilitated diffusion distance of DO 90% diffusion frontline with microelectrode penetration assuming $L_{f\text{-}O}/L_{t\text{-}O}=L_{f\text{-}RB}/L_{t\text{-}RB}=4.85$ as determined experimentally; (iii)$L_{m3\text{-}20}$=distances passed by oxygen microelectrode tip during its profile measurements in biofilm with time interval and step size at 3 s and 20 μm, respectively.

As can be seen in Table 6-3, unlike in the situation of Rhodamine B, which has effective diffusion coefficient much smaller than that of oxygen in biofilms, all values of $L_{f\text{-}O}$ for oxygen are larger than those of $L_{m3\text{-}20}$, which is the distance the oxygen microelectrode tip would pass during its profile measurements with a combination of time interval and step size at 3 seconds and 20 μm, respectively, as used in the measurements of those two DO profiles shown in Figure 6-3. This indicates that during the first DO profile measurement using the DO microelectrode, unlike Rhodamine B, DO from the bulk phase was actually immediately following rather than staying far away behind the tip of the microelectrode along its way toward the substratum of biofilm. The insertion of the oxygen microelectrode might actually generate a channel structure around the microelectrode, as illustrated by the cone-shape diffusion in Figure 6-2, that

greatly facilitated oxygen transport from the bulk phase into the biofilms. This resulted in disturbance (more specifically, increase) in local DO concentration at each depth the microelectrode passed during its first profile measurement; and the increased DO concentrations finally were detected and reflected on the second DO profile that was constructed when the microelectrode was retreated backward to the biofilm surface. Therefore, if these two DO profile measurements were taken as "duplicates", and the ultimate results were derived accordingly, i.e. a DO profile consisting of average DO concentration at each measured depth based on these two DO profiles, then, overestimation of DO concentration at each depth would inevitably result. This observation indicates that more precautions need to be applied when dealing with the experimental design of profile measurements as well as the collection, alignment and interpretation of profile data from microelectrode measurements within biofilms.

The extent of such an effect may not always be similar during profile measurements using microelectrode. Types of chemicals of interest, dimensions and shapes of microelectrodes used, compositions, structures and morphology of biofilms as well as hydrodynamics of the aquatic environment surrounding biofilms all will play a role in this regard. However, the example illustrated herein has provided direct experimental evidence indicating the presence of such an impact, i.e. mass diffusion–facilitating effect of microelectrode tip penetration, on microelectrode measurements in natural biofilms that otherwise is often neglected solely based on a convenient assumption that impact of tiny microelectrode tip could be negligible. This example has raised an awareness of the existence of this kind of impact; and in some case, it may become imperative to take it into consideration from fabrication of microelectrode,

experimental design, preparation and implementation of microelectrode measurement to final data analysis and interpretations.

Although the insertion of the microelectrode tip could bring about mass diffusion-facilitating effect in biofilms, it needs to be noted that the practice of using microelectrodes in biofilm measurements is still valid. The distribution status of a specific substance such as DO in biofilms is determined mainly by a diffusion–reaction mechanism; and a pseudo-steady state is normally established in biofilms at the time when the profile is measured with microelectrode. Therefore, the initial profile measurement using microelectrode, if implemented properly, will still be able to reflect the status of the substance of interest in a biofilm. The mass diffusion-facilitating effect brought in by the insertion of the microelectrode tip may mainly play its role in the subsequent profile measurements on the same spot of the biofilms.

In most cases in biofilm studies using microelectrodes, minimizing or even eliminating such kind of impact from the penetration of microelectrode tip is desired. New progress has been made that can help achieve this goal to various degrees. One is to use a microoptode array (Holst *et al.*, 1997) that can be used to measure oxygen concentrations at different depths simultaneously so that physical impacts brought in by insertion of the microelectrode tip on the local DO concentrations measurements can be avoided. However, the results measured by this approach at one certain moment actually provide DO concentrations under different spots of a same piece of biofilm. Therefore, considering the heterogeneous nature of biofilms, it would be doubtful that DO profile constructed on the basis of a set of DO concentration data measured using this approach at different depth under different biofilm spots would properly reflect the real DO

distribution in the biofilm under test. In addition, from the perspective of each spot of the biofilm penetrated by one microoptode of the array, this approach cannot be claimed as being undisruptive and non-destructive yet.

Another approach much closer to being non-disruptive and non-destructive, the planar optodes approach, has been developed (Glud *et al.*, 1996, 1998) and successfully used for simultaneous, two-dimensional measurements of oxygen distributions in biofilms vertically as well as horizontally (e.g. on the base of biofilms). In this approach, the planar optodes initially have to be inserted vertically in parallel to the vertical profile of biofilm or sediment to be observed or to be placed horizontally on the substratum of biofilms before being used for biofilm attachment and growth. This means that an initial disturbance during installation of the planar optodes inevitably would take place, but during later DO profile measurements, no further physical disturbance would be introduced. This approach is thus more suited for investigation into DO changes during growing processes of biofims or condition shifting processes of environment surrounding biofilms under test.

6.4 Conclusions

Based on microscopic observations on microelectrode tip penetration in artificial biofilm as well as microelectrode measurements in natural biofilm, the following conclusions have been made:

(1) Microscopic observations have disclosed that microelectrode tip penetration in biofilm substantially facilitated mass diffusion of Rhodamine B in the artificial biofilm

with respect to the movement of its diffusion frontline, especially along the direction of microelectrode tip penetration.

(2) DO profiles measured on the same spot of the natural biofilm have also demonstrated such a diffusion-facilitating effect of microelectrode tip penetration taking place in real profile measurements using a microelectrode. This observation has provided an explanation on why oxygen concentrations in biofilms are sometimes overestimated using microelectrodes in comparison with non-invasive technique using planar optodes.

(3) Although the validity of the practice of using microelectrodes in biofilm study can still be held, the potential impact of microelectrode tip penetration in biofilms should not be neglected simply for convenience. More precautions and efforts are needed when dealing with fabrication of microelectrodes, experimental design of profile measurements as well as collection, alignment and interpretation of profile data from microelectrode measurements within biofilms.

(4) Whether or not the observed diffusion-facilitating effect is an issue of concern to microelectrode measurements in biofilms cannot be simply generalized. The evaluation has to be made based on specific factors related to biofilms, chemicals, microelectrodes as well as measuring approaches used. This preliminary study has shed some light on this particular issue in an effort to draw more attention so that more in-depth investigations can be implemented in the future.

6.5 References

Amann, R. and Kuhl, M. 1998. In situ methods for assessment of microorganisms and their activities. *Current Opinion in Microbiology*, 1:352-358.

Glud, R. N., Gundersen, J. K., Revsbech, N. P., and Jorgensen, B. B. 1994. Effects on the benthic diffusive boundary layer imposed by microelectrodes. *Limnology and Oceanography*, 39:462-467.

Glud, R. N., Ramsing, N. B., Gundersen, J. K., and Klimant, I. 1996. Planar optrodes, a new tool for fine scale measurements of two dimensional O_2 distribution in benthic microbial communities. *Marine Ecology Progress Series*. 140:217-226.

Glud, R. N., Santegoeds, C. M., de Beer, D., Hohls, O., and Ramsing, N. B. 1998. Oxygen dynamics at the base of a biofilm studied with planar optrodes. *Aquatic Microbial Ecology*, 14:223-233.

Holst G., Glud, R. N., Kuhl, M., and Klimant, I. 1997. A microoptodes array for fine-scale measurement of oxygen distribution. *Sensors and Actuators B (Chemical)*. 38-39:122-129.

Kuhl, M. and Revsbech, N. P. 2001. Biogeochemical microsensors for boundary layer studies. In *The benthic boundary layer: transport processes and biogeochemistry*, Boudreau, B. P. and Jogensen, B. B. (editors). Oxford University Press, Inc., Oxford, New York, p180-210.

Lide, D. R. (editor-in-chief) 2006-2007. *CRC Handbook of Chemistry and Physics*, 87th edition, CRC Press, New York, p6-196

Rani, S. A., Pitts, B. and Stewart, P. S. 2005. Rapid diffusion of fluorescent tracers into staphylococcus epidermidis biofilms visualized by time lapse microscopy. *Antimicrobial Agents and Chemotherapy*, 49:728–732.

Stewart, P.S. (2003). Diffusion in biofilms. *Journal of Bacteriology*, 185(5):1485-1491.

Strathmann, M., Griebe, T. and Flemming H.-C. 2000. Artificial biofilm model – a useful tool for biofilm research. *Applied Microbiology and Biotechnology*, 54:231-237.

Strobel, H. A. and Heineman, W. R. 1989. *Chemical instrumentation: a systematic approach*, 3rd edition, John Wiley & Sons, Inc., New York.

Chapter 7

Summary and Recommendations

Water quality deterioration due to nitrification outbreaks and early detection of nitrification occurrence in water distribution systems have been challenging many water utilities using chloramination for disinfection. It has been believed that it is the growth of nitrifying microorganisms embedded in biofilms in chloraminated water distribution systems (CWDSs) that leads to this phenomenon. After having developed the microelectrode suitable for NH_2Cl measurement, this dissertation research continued to investigate microbial inactivation of NH_2Cl against biofilm microorganisms by focusing on the penetration process of NH_2Cl in biofilms grown on different substratum materials. Meanwhile, a new approach to the detection of nitrification occurrence in CWDSs was investigated in an effort to determine if this proposed approach of conducting biofilm tests using microelectrodes could provide potential application in the drinking water industry. Finally, a preliminary study was also implemented in this dissertation research to elucidate potential impacts of the penetration of a microelectrode tip during its measurement in biofilms. A summary about these research works is made in the following section. In addition, recommendations on future study in relevant areas are also made at the end of this chapter.

7.1 Summary

The development of a microelectrode capable of measuring NH_2Cl was introduced in Chapter 3 of this dissertation. As the most important step, polarization

potential specifically for NH_2Cl was determined based on the voltammetric experiments to construct i-E curves of NH_2Cl under different pH values. It was disclosed that pH had substantial impacts on i-E curves of NH_2Cl. When pH was neutral, the limiting current started to be generated from the Pt electrode when the applied potential was at -90 mV (vs Ag/AgCl). Two types of microelectrodes, the separate and the combined, applicable to NH_2Cl measurements were developed. Under the experimentally determined polarization potential of -90 mV (vs Ag/AgCl), both types of microelectrodes displayed good linear responses to the changes of NH_2Cl concentration within the ranges tested. However, the separate microelectrode was found to be the better choice under laboratory environments due to its advantageous characteristics over the combined microelectrode. In addition, a diffusion coefficient of 1.7×10^{-6} cm^2/s was determined for NH_2Cl. This experimentally determined constant, in combination with the use of NH_2Cl microelectrode, later helped make estimations on NH_2Cl flux into biofilms.

In Chapter 4, an investigation was discussed to elucidate, by using the newly developed NH_2Cl microelectrode, how NH_2Cl penetrates in biofilm and thus its microbial inactivation against biofilm microorganisms. Partial penetrations of NH_2Cl were observed in biofilms of 540 μm thick, grown on concrete slides with the NH_2Cl concentration at 6.6 mg/L as Cl_2 within contact time of 15 minutes, beyond which full penetrations were observed. In comparison, only full penetrations were observed at a higher NH_2Cl concentration (22.3 mg/L as Cl_2) with similarly short contact time. This indicates that contact time and bulk NH_2Cl concentration are two important factors affecting the penetration process of NH_2Cl in biofilms. Unlike that of concrete slides, full penetrations of NH_2Cl were always observed in thinner biofilms grown on

polyvinylchloride (PVC) and polycarbonate (PC) slides with comparably short contact times and low bulk NH_2Cl concentrations. This indicates that the type of substratum materials could influence the penetration process of NH_2Cl in biofilms. NH_2Cl-demand free materials (such as PVC and PC) are more conducive to NH_2Cl penetration in biofilms than NH_2Cl-demanding material (such as concrete). This study also elucidated that a mass diffusion boundary layer existed above the biofilm surface and NH_2Cl concentration decreased across the diffusion boundary layer from the bulk phase to the biofilm surface. This observation helps explain why the NH_2Cl concentration sufficient to inactivate planktonic cells in the bulk is usually not similarly effective in inactivating biofilm microorganisms. To achieve same inactivation efficiency, NH_2Cl concentration required for biofilm microorganisms should be higher than that for suspended cells in the bulk. Biofilm heterotrophic plate count (HPC) tests in time series with respect to contact time, conducted in parallel with transient NH_2Cl profiles measurements in biofilms, helped elucidate that the penetration process of NH_2Cl in biofilms could affect its inactivation process against biofilm microorganisms. Therefore, factors that could be conducive to improving the penetration process of NH_2Cl in biofilms (e.g. bulk NH_2Cl concentration and type of substratum material) could also be beneficial to its inactivation process against biofilm microorganisms. This is of special interest to the drinking water industry with respect to the selection of pipe material for CWDSs.

Based on a 1-year operation of a nitrifying bacteria-seeded, chloraminated model water distribution system with favorable operational conditions for nitrification, Chapter 5 introduced a new approach to the detection of nitrification by conducting biofilm tests using microelectrodes to measure profiles of dissolved oxygen (DO), ammonium, nitrate

and pH that are directly involved in nitrification processes occurring in biofilms. This approach was found to have the capability to elucidate some fundamental phenomena closely associated with nitrification process, and therefore, presents itself a potential tool in detecting nitrification in CWDSs. It was also observed that actively ongoing nitrification in the model CWDS could be detected by biofilm tests using microelectrodes when water nitrite concentration was as low as 0.02 mg-N/L. This indicates that compared with the often adopted critical threshold of 0.05 mg NO_2^--N/L for confirmation of nitrification occurrence in CWDSs, a lower critical threshold probably should be proposed for nitrite with respect to its use in early detection of nitrification in CWDSs.

Finally, in Chapter 6, microscopic observations were conducted and disclosed that the penetration of a microelectrode tip into biofilm substantially facilitated mass diffusion of Rhodamine B in an artificial biofilm with respect to the movement of its diffusion frontline, especially along the direction of the penetration of the microelectrode tip. DO profiles measured on the same spot of a natural biofilm also disclosed such an effect taking place in actual profile measurements using microelectrode. This observation explains why oxygen concentrations in biofilms are sometimes overestimated using microelectrodes in comparison with non-invasive technique using planar optodes. Although the validity of the practice of using microelectrodes in biofilm study can still be held, experimental results of this study have indicated that the potential impact of microelectrode tip penetration in biofilms should not be neglected simply for convenience. Whether or not this effect is an issue of concern to microelectrode measurements in biofilms, however, cannot be simply generalized. The evaluation should be made based on specific factors related to biofilms, chemicals, microelectrode

as well as measuring approaches used. More efforts and precautions are needed when dealing with fabrication of microelectrodes, experimental design of profile measurements as well as collection, alignment and interpretation of profile data from microelectrode measurements in biofilms. This preliminary study has shed some light on this particular issue in an effort to draw more attention so that more in-depth investigations can be implemented in the future.

7.2 Recommendations on future study

Due to the complex aquatic chemistry of NH_2Cl and the coupling of NH_2Cl decomposition process and microbiological nitrification process in CWDSs, a combined use of microelectrodes that are capable of measuring parameters (DO, pH, ammonium, nitrite, nitrate, NH_2Cl) directly involved in these processes is important in elucidating, more clearly, what takes place within biofilms and its relationship with the outbreak of nitrification in CWDSs. In order to fulfill this goal, further research work on improvements of the performance of some of the required microelectrodes, especially with respect to the detection limits of the NH_2Cl and nitrite microelectrodes, is strongly recommended.

Considering the impacts, as observed in this study, of the penetration of the microelectrode tip during its profile measurements in biofilms, more in-depth research in this area should also be recommended.

Appendices

Appendix A - Data for Figures in Chapter 2

Appendix B - Data for Figures in Chapter 3

Appendix C - Data for Figures in Chapter 4

Appendix D - Data for Figures in Chapter 5

Appendix E - Data for Figures in Chapter 6

Appendix A - Data for Figures in Chapter 2

Data for Figure 2-1:

pH	EMF (mV) (vs Ag/AgCl)		
	Test 1	Test 2	Average
6.0	291	275	283
8.0	171	161	166
10.0	70	51	60.5

Data for Figure 2-2:

Log_{10} (NO_3^-, M)	EMF (mV) (vs Ag/AgCl)		
	Test 1	Test 2	Average
-5.0	310	294	302
-4.0	256	251	253.5
-3.0	205	202	203.5

Data for Figure 2-3:

Log_{10} (NH_4^+, M)	EMF (mV) (vs Ag/AgCl)		
	Test 1	Test 2	Average
-5.0	-13	-18	-15.5
-4.0	37	35	36
-3.0	95	93	94

Data for Figure 2-5:

Time (s)	Signal (pA)	Time (s)	Signal (pA)	Time (s)	Signal (pA)	Time (s)	Signal (pA)	Time (s)	Signal (pA)	Time (s)	Signal (pA)	Time (s)	Signal (pA)	Time (s)	Signal (pA)	Time (s)	Signal (pA)
0	8	29.5	7	59	7	88.5	65	118	165	147.5	222	177	253	206.5	270	236	279
0.5	8	30	7	59.5	7	89	70	118.5	172	148	232	177.5	257	207	268	236.5	279
1	8	30.5	6	60	7	89.5	72	119	180	148.5	234	178	260	207.5	267	237	279
1.5	8	31	6	60.5	7	90	71	119.5	184	149	237	178.5	261	208	269	237.5	280
2	8	31.5	7	61	7	90.5	66	120	188	149.5	239	179	260	208.5	270	238	279
2.5	8	32	6	61.5	6	91	63	120.5	187	150	238	179.5	260	209	272	238.5	279
3	7	32.5	7	62	7	91.5	63	121	179	150.5	239	180	261	209.5	273	239	279
3.5	7	33	6	62.5	7	92	62	121.5	172	151	240	180.5	260	210	272	239.5	279
4	7	33.5	6	63	7	92.5	58	122	168	151.5	241	181	260	210.5	270	240	279
4.5	6	34	7	63.5	7	93	57	122.5	167	152	243	181.5	260	211	269	240.5	279
5	7	34.5	7	64	7	93.5	55	123	165	152.5	247	182	257	211.5	268	241	279
5.5	7	35	7	64.5	7	94	57	123.5	159	153	245	182.5	257	212	269	241.5	279
6	7	35.5	6	65	7	94.5	65	124	160	153.5	245	183	258	212.5	271	242	279
6.5	6	36	6	65.5	6	95	73	124.5	168	154	244	183.5	260	213	273	242.5	280
7	7	36.5	7	66	7	95.5	71	125	175	154.5	242	184	262	213.5	272	243	280
7.5	6	37	7	66.5	7	96	72	125.5	179	155	242	184.5	265	214	271	243.5	280
8	7	37.5	7	67	7	96.5	80	126	181	155.5	243	185	266	214.5	271	244	280
8.5	7	38	6	67.5	7	97	86	126.5	180	156	243	185.5	267	215	275	244.5	279
9	7	38.5	7	68	7	97.5	88	127	180	156.5	243	186	270	215.5	275	245	279
9.5	7	39	7	68.5	7	98	91	127.5	182	157	243	186.5	269	216	274	245.5	279
10	7	39.5	7	69	7	98.5	90	128	184	157.5	243	187	273	216.5	274	246	280
10.5	7	40	7	69.5	7	99	86	128.5	186	158	243	187.5	272	217	275	246.5	280
11	7	40.5	6	70	7	99.5	86	129	188	158.5	244	188	270	217.5	275	247	280
11.5	7	41	6	70.5	7	100	89	129.5	191	159	241	188.5	270	218	275	247.5	280
12	7	41.5	7	71	7	100.5	93	130	196	159.5	240	189	269	218.5	274	248	281
12.5	6	42	6	71.5	7	101	94	130.5	201	160	239	189.5	269	219	274	248.5	279
13	7	42.5	7	72	7	101.5	93	131	205	160.5	243	190	269	219.5	274	249	279
13.5	7	43	6	72.5	7	102	94	131.5	204	161	245	190.5	269	220	275	249.5	278
14	7	43.5	7	73	7	102.5	98	132	198	161.5	249	191	269	220.5	276	250	279
14.5	7	44	7	73.5	8	103	106	132.5	189	162	251	191.5	268	221	275	250.5	280
15	6	44.5	7	74	7	103.5	111	133	185	162.5	252	192	268	221.5	275	251	279
15.5	7	45	7	74.5	8	104	116	133.5	182	163	252	192.5	268	222	276	251.5	280
16	7	45.5	7	75	8	104.5	121	134	181	163.5	249	193	268	222.5	275	252	279
16.5	6	46	6	75.5	8	105	123	134.5	186	164	247	193.5	269	223	275	252.5	280
17	6	46.5	7	76	9	105.5	118	135	191	164.5	245	194	269	223.5	276	253	279
17.5	7	47	8	76.5	10	106	124	135.5	195	165	244	194.5	270	224	276	253.5	280
18	7	47.5	7	77	7	106.5	133	136	195	165.5	244	195	269	224.5	276	254	281
18.5	7	48	7	77.5	8	107	133	136.5	197	166	244	195.5	268	225	274	254.5	281
19	6	48.5	7	78	9	107.5	128	137	199	166.5	244	196	267	225.5	275	255	280
19.5	7	49	7	78.5	8	108	115	137.5	200	167	248	196.5	267	226	275	255.5	280
20	7	49.5	7	79	8	108.5	106	138	202	167.5	250	197	268	226.5	276	256	281
20.5	7	50	6	79.5	8	109	111	138.5	202	168	249	197.5	268	227	277	256.5	281
21	7	50.5	6	80	9	109.5	120	139	203	168.5	252	198	268	227.5	277	257	279
21.5	6	51	6	80.5	9	110	134	139.5	206	169	255	198.5	269	228	277	257.5	279
22	7	51.5	6	81	11	110.5	143	140	211	169.5	255	199	270	228.5	276	258	280
22.5	6	52	7	81.5	15	111	144	140.5	215	170	251	199.5	270	229	276	258.5	280
23	7	52.5	7	82	13	111.5	147	141	214	170.5	251	200	270	229.5	278	259	280
23.5	6	53	7	82.5	11	112	147	141.5	212	171	251	200.5	270	230	278	259.5	280
24	7	53.5	7	83	13	112.5	133	142	210	171.5	251	201	270	230.5	277	260	280
24.5	7	54	7	83.5	16	113	129	142.5	209	172	249	201.5	269	231	277	260.5	280
25	6	54.5	6	84	21	113.5	133	143	212	172.5	248	202	269	231.5	278	261	280
25.5	7	55	8	84.5	29	114	129	143.5	218	173	250	202.5	269	232	278	261.5	280
26	7	55.5	7	85	35	114.5	132	144	222	173.5	253	203	268	232.5	278	262	280
26.5	6	56	7	85.5	43	115	143	144.5	223	174	253	203.5	268	233	277	262.5	280
27	6	56.5	8	86	53	115.5	147	145	223	174.5	252	204	268	233.5	279	263	280
27.5	6	57	7	86.5	48	116	145	145.5	223	175	253	204.5	268	234	278	263.5	280
28	6	57.5	7	87	51	116.5	144	146	222	175.5	252	205	267	234.5	278	264	280
28.5	6	58	7	87.5	54	117	148	146.5	224	176	251	205.5	267	235	279	264.5	280
29	7	58.5	7	88	55	117.5	156	147	228	176.5	250	206	270	235.5	279	265	280

Data for Figure 2-5 (Cont'):

Time (s)	Signal (pA)	Time (s)	Signal (pA)	Time (s)	Signal (pA)	Time (s)	Signal (pA)	Time (s)	Signal (pA)	Time (s)	Signal (pA)	Time (s)	Signal (pA)	Time (s)	Signal (pA)	Time (s)	Signal (pA)
265.5	280	295	281	324.5	281	354	280	383.5	252	413	115	442.5	78	472	32	501.5	7
266	281	295.5	281	325	281	354.5	280	384	241	413.5	110	443	75	472.5	31	502	9
266.5	281	296	281	325.5	281	355	280	384.5	235	414	105	443.5	70	473	32	502.5	19
267	280	296.5	281	326	281	355.5	280	385	241	414.5	103	444	69	473.5	30	503	23
267.5	281	297	281	326.5	281	356	281	385.5	244	415	102	444.5	72	474	31	503.5	21
268	281	297.5	282	327	281	356.5	280	386	237	415.5	105	445	71	474.5	39	504	17
268.5	280	298	282	327.5	281	357	280	386.5	230	416	104	445.5	68	475	45	504.5	14
269	280	298.5	282	328	280	357.5	281	387	224	416.5	103	446	66	475.5	47	505	14
269.5	280	299	282	328.5	281	358	280	387.5	222	417	100	446.5	63	476	42	505.5	19
270	280	299.5	281	329	281	358.5	280	388	227	417.5	94	447	63	476.5	37	506	26
270.5	280	300	282	329.5	281	359	280	388.5	230	418	92	447.5	64	477	36	506.5	25
271	280	300.5	282	330	280	359.5	280	389	227	418.5	96	448	63	477.5	37	507	19
271.5	279	301	280	330.5	281	360	280	389.5	223	419	103	448.5	60	478	36	507.5	14
272	279	301.5	281	331	281	360.5	281	390	224	419.5	104	449	57	478.5	33	508	12
272.5	279	302	281	331.5	281	361	281	390.5	231	420	106	449.5	55	479	32	508.5	10
273	279	302.5	282	332	280	361.5	277	391	231	420.5	110	450	53	479.5	31	509	9
273.5	279	303	282	332.5	280	362	278	391.5	228	421	108	450.5	54	480	29	509.5	8
274	279	303.5	281	333	279	362.5	281	392	228	421.5	109	451	57	480.5	28	510	8
274.5	280	304	282	333.5	280	363	281	392.5	231	422	112	451.5	62	481	27	510.5	8
275	280	304.5	282	334	281	363.5	282	393	237	422.5	105	452	66	481.5	26	511	7
275.5	280	305	282	334.5	280	364	282	393.5	238	423	101	452.5	65	482	24	511.5	8
276	280	305.5	281	335	281	364.5	281	394	231	423.5	100	453	69	482.5	23	512	8
276.5	280	306	281	335.5	281	365	281	394.5	232	424	97	453.5	59	483	23	512.5	7
277	280	306.5	281	336	280	365.5	281	395	234	424.5	96	454	53	483.5	22	513	7
277.5	280	307	281	336.5	280	366	281	395.5	229	425	97	454.5	49	484	21	513.5	8
278	281	307.5	281	337	280	366.5	281	396	222	425.5	103	455	47	484.5	21	514	7
278.5	280	308	280	337.5	280	367	281	396.5	216	426	103	455.5	44	485	20	514.5	7
279	280	308.5	280	338	280	367.5	282	397	213	426.5	101	456	43	485.5	20	515	6
279.5	281	309	280	338.5	280	368	282	397.5	210	427	99	456.5	48	486	19	515.5	7
280	280	309.5	280	339	280	368.5	281	398	195	427.5	95	457	61	486.5	20	516	6
280.5	280	310	281	339.5	280	369	281	398.5	180	428	95	457.5	63	487	19	516.5	7
281	281	310.5	281	340	280	369.5	282	399	175	428.5	108	458	59	487.5	19	517	7
281.5	281	311	281	340.5	280	370	281	399.5	174	429	109	458.5	52	488	19	517.5	7
282	280	311.5	281	341	281	370.5	281	400	175	429.5	95	459	52	488.5	19	518	7
282.5	281	312	281	341.5	281	371	281	400.5	179	430	92	459.5	54	489	22	518.5	6
283	281	312.5	281	342	281	371.5	281	401	187	430.5	105	460	51	489.5	24	519	6
283.5	280	313	281	342.5	280	372	280	401.5	185	431	103	460.5	47	490	24	519.5	6
284	280	313.5	281	343	280	372.5	278	402	186	431.5	94	461	43	490.5	21	520	6
284.5	281	314	281	343.5	281	373	275	402.5	191	432	90	461.5	45	491	20	520.5	6
285	281	314.5	281	344	280	373.5	273	403	192	432.5	86	462	47	491.5	18	521	6
285.5	281	315	281	344.5	280	374	274	403.5	192	433	84	462.5	46	492	19	521.5	6
286	281	315.5	281	345	280	374.5	275	404	189	433.5	82	463	43	492.5	20	522	6
286.5	281	316	280	345.5	280	375	273	404.5	188	434	81	463.5	42	493	20	522.5	6
287	282	316.5	281	346	280	375.5	272	405	193	434.5	81	464	45	493.5	22	523	7
287.5	282	317	281	346.5	280	376	272	405.5	199	435	84	464.5	49	494	30	523.5	7
288	282	317.5	281	347	280	376.5	272	406	203	435.5	86	465	46	494.5	26	524	7
288.5	281	318	280	347.5	280	377	274	406.5	196	436	85	465.5	42	495	23	524.5	8
289	281	318.5	280	348	280	377.5	273	407	188	436.5	82	466	40	495.5	22	525	9
289.5	281	319	280	348.5	280	378	271	407.5	181	437	78	466.5	39	496	21	525.5	9
290	281	319.5	281	349	280	378.5	270	408	176	437.5	75	467	38	496.5	20	526	8
290.5	282	320	281	349.5	280	379	271	408.5	180	438	72	467.5	35	497	15	526.5	8
291	281	320.5	280	350	280	379.5	272	409	179	438.5	70	468	34	497.5	12	527	7
291.5	281	321	280	350.5	281	380	273	409.5	157	439	69	468.5	35	498	11	527.5	8
292	281	321.5	281	351	281	380.5	274	410	145	439.5	69	469	34	498.5	10	528	8
292.5	281	322	281	351.5	280	381	274	410.5	134	440	74	469.5	33	499	9	528.5	7
293	281	322.5	281	352	280	381.5	273	411	125	440.5	83	470	32	499.5	9	529	7
293.5	282	323	281	352.5	280	382	266	411.5	119	441	84	470.5	33	500	8	529.5	7
294	281	323.5	281	353	281	382.5	262	412	116	441.5	82	471	35	500.5	8	530	7
294.5	282	324	280	353.5	281	383	262	412.5	117	442	79	471.5	35	501	8	530.5	6

Data for Figure 2-5 (Cont'):

Time (s)	Signal (pA)	Time (s)	Signal (pA)	Time (s)	Signal (pA)	Time (s)	Signal (pA)	Time (s)	Signal (pA)	Time (s)	Signal (pA)	Time (s)	Signal (pA)	Time (s)	Signal (pA)	Time (s)	Signal (pA)
531	6	560.5	6	590	7	619.5	39	649	165	678.5	223	708	244	737.5	265	767	272
531.5	6	561	6	590.5	7	620	36	649.5	167	679	224	708.5	245	738	266	767.5	272
532	6	561.5	6	591	6	620.5	35	650	166	679.5	224	709	247	738.5	267	768	273
532.5	6	562	7	591.5	8	621	38	650.5	166	680	224	709.5	250	739	266	768.5	273
533	6	562.5	6	592	7	621.5	46	651	168	680.5	224	710	251	739.5	265	769	273
533.5	6	563	6	592.5	7	622	54	651.5	171	681	227	710.5	254	740	264	769.5	274
534	6	563.5	7	593	7	622.5	56	652	173	681.5	229	711	254	740.5	264	770	274
534.5	6	564	7	593.5	7	623	56	652.5	173	682	230	711.5	251	741	265	770.5	273
535	6	564.5	6	594	8	623.5	60	653	176	682.5	231	712	249	741.5	265	771	273
535.5	6	565	6	594.5	7	624	62	653.5	177	683	230	712.5	249	742	265	771.5	273
536	6	565.5	7	595	7	624.5	62	654	175	683.5	233	713	250	742.5	265	772	272
536.5	6	566	6	595.5	7	625	67	654.5	173	684	236	713.5	251	743	265	772.5	272
537	6	566.5	6	596	7	625.5	73	655	172	684.5	237	714	251	743.5	262	773	271
537.5	6	567	6	596.5	7	626	72	655.5	177	685	237	714.5	251	744	261	773.5	271
538	6	567.5	6	597	7	626.5	65	656	182	685.5	237	715	251	744.5	260	774	271
538.5	6	568	6	597.5	7	627	56	656.5	184	686	233	715.5	251	745	261	774.5	272
539	6	568.5	6	598	7	627.5	50	657	184	686.5	228	716	251	745.5	261	775	272
539.5	6	569	6	598.5	7	628	48	657.5	181	687	225	716.5	250	746	261	775.5	271
540	6	569.5	6	599	8	628.5	48	658	179	687.5	223	717	251	746.5	262	776	272
540.5	6	570	6	599.5	8	629	57	658.5	177	688	225	717.5	251	747	262	776.5	274
541	5	570.5	6	600	7	629.5	61	659	181	688.5	226	718	252	747.5	262	777	276
541.5	6	571	6	600.5	8	630	72	659.5	189	689	227	718.5	252	748	263	777.5	272
542	6	571.5	6	601	8	630.5	79	660	195	689.5	227	719	252	748.5	264	778	271
542.5	6	572	6	601.5	8	631	88	660.5	195	690	229	719.5	252	749	264	778.5	270
543	6	572.5	6	602	7	631.5	99	661	193	690.5	231	720	252	749.5	264	779	270
543.5	5	573	6	602.5	8	632	108	661.5	193	691	230	720.5	253	750	264	779.5	271
544	6	573.5	6	603	9	632.5	113	662	196	691.5	229	721	253	750.5	264	780	272
544.5	6	574	6	603.5	10	633	117	662.5	199	692	228	721.5	253	751	265	780.5	272
545	6	574.5	6	604	11	633.5	121	663	200	692.5	229	722	253	751.5	265	781	272
545.5	5	575	7	604.5	14	634	124	663.5	201	693	230	722.5	253	752	264	781.5	272
546	6	575.5	6	605	17	634.5	127	664	201	693.5	231	723	253	752.5	264	782	273
546.5	6	576	7	605.5	18	635	130	664.5	203	694	230	723.5	252	753	264	782.5	272
547	7	576.5	7	606	18	635.5	132	665	203	694.5	230	724	252	753.5	264	783	272
547.5	6	577	6	606.5	18	636	130	665.5	205	695	230	724.5	253	754	264	783.5	270
548	6	577.5	7	607	18	636.5	119	666	206	695.5	230	725	252	754.5	266	784	270
548.5	6	578	7	607.5	19	637	107	666.5	207	696	233	725.5	252	755	268	784.5	270
549	6	578.5	6	608	22	637.5	102	667	207	696.5	234	726	252	755.5	269	785	271
549.5	6	579	6	608.5	29	638	109	667.5	206	697	235	726.5	252	756	269	785.5	270
550	6	579.5	6	609	31	638.5	119	668	205	697.5	236	727	253	756.5	269	786	269
550.5	6	580	6	609.5	26	639	129	668.5	205	698	236	727.5	253	757	269	786.5	270
551	6	580.5	6	610	21	639.5	133	669	206	698.5	236	728	255	757.5	268	787	271
551.5	5	581	6	610.5	21	640	136	669.5	206	699	236	728.5	257	758	266	787.5	272
552	5	581.5	6	611	32	640.5	136	670	205	699.5	236	729	257	758.5	266	788	273
552.5	6	582	7	611.5	26	641	135	670.5	205	700	235	729.5	257	759	265	788.5	274
553	6	582.5	6	612	23	641.5	141	671	205	700.5	235	730	258	759.5	265	789	274
553.5	6	583	7	612.5	23	642	141	671.5	204	701	235	730.5	259	760	266	789.5	274
554	5	583.5	7	613	25	642.5	132	672	204	701.5	234	731	261	760.5	267	790	273
554.5	5	584	7	613.5	27	643	129	672.5	201	702	231	731.5	263	761	268	790.5	274
555	7	584.5	7	614	32	643.5	138	673	201	702.5	231	732	264	761.5	268	791	275
555.5	6	585	7	614.5	33	644	147	673.5	200	703	233	732.5	265	762	269	791.5	274
556	6	585.5	7	615	34	644.5	149	674	204	703.5	237	733	266	762.5	270	792	274
556.5	6	586	7	615.5	36	645	146	674.5	210	704	240	733.5	266	763	270	792.5	274
557	6	586.5	7	616	39	645.5	140	675	216	704.5	242	734	267	763.5	270	793	274
557.5	6	587	7	616.5	42	646	139	675.5	218	705	244	734.5	267	764	270	793.5	275
558	6	587.5	7	617	43	646.5	147	676	217	705.5	244	735	267	764.5	270	794	275
558.5	6	588	7	617.5	41	647	150	676.5	213	706	245	735.5	266	765	271	794.5	275
559	6	588.5	6	618	42	647.5	150	677	215	706.5	245	736	265	765.5	271	795	275
559.5	6	589	7	618.5	46	648	154	677.5	220	707	245	736.5	265	766	272	795.5	275
560	6	589.5	7	619	43	648.5	159	678	222	707.5	244	737	265	766.5	272	796	274

Data for Figure 2-5 (Cont'):

Time (s)	Signal (pA)	Time (s)	Signal (pA)	Time (s)	Signal (pA)	Time (s)	Signal (pA)	Time (s)	Signal (pA)	Time (s)	Signal (pA)	Time (s)	Signal (pA)	Time (s)	Signal (pA)	Time (s)	Signal (pA)
796.5	275	819.5	276	842.5	278	865.5	279	888.5	279	911.5	278	934.5	279	957.5	278	980.5	278
797	275	820	276	843	278	866	278	889	278	912	278	935	278	958	278	981	278
797.5	275	820.5	276	843.5	277	866.5	278	889.5	278	912.5	278	935.5	278	958.5	278	981.5	278
798	276	821	277	844	278	867	278	890	278	913	278	936	279	959	278	982	278
798.5	276	821.5	276	844.5	278	867.5	278	890.5	278	913.5	278	936.5	278	959.5	278	982.5	278
799	276	822	276	845	277	868	277	891	278	914	278	937	278	960	278	983	278
799.5	276	822.5	276	845.5	278	868.5	277	891.5	278	914.5	278	937.5	279	960.5	278	983.5	277
800	276	823	277	846	279	869	278	892	278	915	278	938	278	961	278	984	277
800.5	277	823.5	276	846.5	278	869.5	278	892.5	278	915.5	278	938.5	278	961.5	278	984.5	277
801	276	824	275	847	278	870	278	893	279	916	279	939	279	962	278	985	277
801.5	275	824.5	275	847.5	277	870.5	278	893.5	278	916.5	278	939.5	278	962.5	279	985.5	277
802	275	825	276	848	278	871	279	894	278	917	279	940	278	963	279	986	277
802.5	276	825.5	276	848.5	278	871.5	278	894.5	277	917.5	278	940.5	278	963.5	279	986.5	277
803	275	826	277	849	279	872	278	895	278	918	278	941	278	964	279	987	277
803.5	275	826.5	276	849.5	278	872.5	278	895.5	278	918.5	278	941.5	279	964.5	278	987.5	278
804	276	827	276	850	278	873	278	896	279	919	277	942	279	965	278	988	278
804.5	276	827.5	276	850.5	277	873.5	278	896.5	279	919.5	277	942.5	279	965.5	279	988.5	278
805	277	828	275	851	278	874	277	897	278	920	278	943	279	966	279	989	278
805.5	276	828.5	275	851.5	278	874.5	278	897.5	277	920.5	277	943.5	279	966.5	278	989.5	278
806	277	829	275	852	278	875	278	898	277	921	278	944	278	967	278	990	278
806.5	276	829.5	275	852.5	278	875.5	278	898.5	278	921.5	278	944.5	278	967.5	278	990.5	279
807	277	830	276	853	277	876	278	899	278	922	278	945	278	968	279	991	278
807.5	277	830.5	276	853.5	278	876.5	278	899.5	278	922.5	278	945.5	279	968.5	278	991.5	277
808	277	831	275	854	278	877	278	900	278	923	278	946	278	969	278	992	278
808.5	276	831.5	275	854.5	278	877.5	278	900.5	278	923.5	277	946.5	278	969.5	277	992.5	278
809	276	832	276	855	278	878	278	901	278	924	278	947	278	970	277	993	278
809.5	276	832.5	276	855.5	278	878.5	278	901.5	278	924.5	277	947.5	278	970.5	277	993.5	278
810	276	833	276	856	278	879	278	902	279	925	278	948	278	971	277	994	278
810.5	277	833.5	277	856.5	278	879.5	278	902.5	278	925.5	278	948.5	278	971.5	277	994.5	278
811	277	834	277	857	278	880	278	903	278	926	278	949	278	972	277	995	278
811.5	277	834.5	276	857.5	278	880.5	278	903.5	279	926.5	278	949.5	279	972.5	277	995.5	278
812	277	835	277	858	278	881	278	904	278	927	278	950	278	973	277	996	279
812.5	276	835.5	276	858.5	277	881.5	278	904.5	279	927.5	279	950.5	278	973.5	278	996.5	278
813	277	836	277	859	278	882	278	905	278	928	278	951	278	974	279	997	279
813.5	276	836.5	277	859.5	278	882.5	278	905.5	278	928.5	279	951.5	278	974.5	278	997.5	278
814	276	837	277	860	278	883	278	906	279	929	278	952	279	975	279	998	278
814.5	275	837.5	278	860.5	278	883.5	279	906.5	279	929.5	278	952.5	279	975.5	278	998.5	278
815	275	838	277	861	278	884	278	907	279	930	279	953	278	976	277	999	278
815.5	275	838.5	277	861.5	278	884.5	278	907.5	279	930.5	278	953.5	278	976.5	278	999.5	278
816	275	839	277	862	278	885	278	908	279	931	279	954	278	977	278	1000	278
816.5	275	839.5	278	862.5	278	885.5	278	908.5	279	931.5	279	954.5	278	977.5	278		
817	275	840	277	863	278	886	279	909	279	932	278	955	278	978	278		
817.5	275	840.5	278	863.5	279	886.5	278	909.5	278	932.5	278	955.5	278	978.5	278		
818	276	841	279	864	278	887	278	910	278	933	279	956	277	979	278		
818.5	276	841.5	277	864.5	278	887.5	278	910.5	278	933.5	279	956.5	278	979.5	278		
819	276	842	277	865	278	888	278	911	279	934	278	957	278	980	278		

Appendix B – Data for Figures in Chapter 3

Data for Figure 3-3:

Voltage (mV)	Current (μA) NH_2Cl-pH 3.8	NH_2Cl-pH 7.1	NH_2Cl-pH 10.1	Voltage (mV)	Current (μA) NH_2Cl-pH 3.8	NH_2Cl-pH 7.1	NH_2Cl-pH 10.1
500	0.019	-0.006	-0.004	386	0.069	0.004	0.002
498	0.019	-0.006	-0.004	384	0.070	0.004	0.003
496	0.020	-0.006	-0.003	382	0.071	0.004	0.003
494	0.021	-0.006	-0.004	380	0.073	0.004	0.004
492	0.021	-0.006	-0.004	378	0.075	0.005	0.005
490	0.021	-0.006	-0.004	376	0.076	0.004	0.004
488	0.022	-0.006	-0.003	374	0.078	0.005	0.005
486	0.022	-0.005	-0.003	372	0.079	0.006	0.006
484	0.023	-0.005	-0.003	370	0.081	0.006	0.005
482	0.024	-0.005	-0.003	368	0.083	0.006	0.006
480	0.024	-0.004	-0.002	366	0.084	0.006	0.007
478	0.025	-0.004	-0.002	364	0.086	0.007	0.006
476	0.025	-0.004	-0.001	362	0.088	0.006	0.006
474	0.026	-0.004	-0.001	360	0.090	0.007	0.007
472	0.027	-0.005	-0.001	358	0.091	0.007	0.007
470	0.027	-0.004	0.000	356	0.094	0.007	0.008
468	0.028	-0.004	0.000	354	0.095	0.007	0.008
466	0.029	-0.004	0.001	352	0.097	0.008	0.008
464	0.029	-0.003	0.000	350	0.099	0.008	0.007
462	0.030	-0.003	0.001	348	0.102	0.008	0.007
460	0.031	-0.003	0.001	346	0.104	0.009	0.007
458	0.031	-0.002	0.001	344	0.106	0.009	0.007
456	0.032	-0.002	0.002	342	0.107	0.009	0.007
454	0.032	-0.002	0.001	340	0.110	0.010	0.006
452	0.033	-0.002	0.002	338	0.112	0.009	0.006
450	0.034	-0.001	0.002	336	0.114	0.010	0.006
448	0.034	-0.001	0.002	334	0.116	0.010	0.005
446	0.035	-0.001	0.002	332	0.118	0.011	0.005
444	0.036	-0.001	0.001	330	0.120	0.011	0.005
442	0.036	-0.001	0.002	328	0.122	0.012	0.005
440	0.037	-0.001	0.002	326	0.123	0.012	0.005
438	0.038	-0.001	0.002	324	0.125	0.013	0.005
436	0.039	-0.001	0.002	322	0.127	0.013	0.005
434	0.040	0.000	0.003	320	0.129	0.013	0.005
432	0.041	0.000	0.001	318	0.131	0.014	0.004
430	0.042	-0.001	0.003	316	0.132	0.015	0.005
428	0.043	-0.001	0.002	314	0.134	0.015	0.005
426	0.044	0.000	0.002	312	0.136	0.015	0.004
424	0.046	0.000	0.003	310	0.137	0.016	0.005
422	0.047	0.000	0.002	308	0.138	0.016	0.005
420	0.048	0.000	0.003	306	0.141	0.017	0.005
418	0.049	0.000	0.004	304	0.143	0.017	0.005
416	0.050	0.000	0.003	302	0.144	0.018	0.006
414	0.051	0.000	0.003	300	0.146	0.018	0.006
412	0.053	0.000	0.003	298	0.148	0.019	0.007
410	0.054	0.001	0.003	296	0.149	0.020	0.007
408	0.055	0.001	0.003	294	0.151	0.020	0.007
406	0.056	0.001	0.003	292	0.152	0.021	0.008
404	0.057	0.001	0.003	290	0.154	0.021	0.007
402	0.059	0.002	0.003	288	0.156	0.023	0.008
400	0.060	0.002	0.002	286	0.158	0.023	0.008
398	0.061	0.002	0.003	284	0.159	0.024	0.008
396	0.062	0.002	0.002	282	0.161	0.025	0.008
394	0.064	0.002	0.002	280	0.163	0.025	0.008
392	0.065	0.003	0.002	278	0.164	0.026	0.008
390	0.066	0.003	0.002	276	0.166	0.027	0.009
388	0.067	0.003	0.002	274	0.167	0.028	0.009

Data for Figure 3-3 (Cont'):

Voltage (mV)	Current (μA) NH_2Cl-pH 3.8	NH_2Cl-pH 7.1	NH_2Cl-pH 10.1	Voltage (mV)	Current (μA) NH_2Cl-pH 3.8	NH_2Cl-pH 7.1	NH_2Cl-pH 10.1
272	0.169	0.029	0.010	152	0.233	0.133	0.018
270	0.170	0.030	0.010	150	0.234	0.136	0.019
268	0.172	0.031	0.010	148	0.235	0.138	0.018
266	0.174	0.031	0.010	146	0.233	0.141	0.019
264	0.175	0.033	0.010	144	0.234	0.144	0.019
262	0.177	0.034	0.010	142	0.233	0.147	0.019
260	0.178	0.035	0.011	140	0.231	0.149	0.019
258	0.180	0.036	0.011	138	0.233	0.151	0.019
256	0.181	0.037	0.011	136	0.234	0.153	0.019
254	0.182	0.038	0.010	134	0.235	0.156	0.018
252	0.184	0.040	0.010	132	0.234	0.158	0.019
250	0.186	0.040	0.010	130	0.235	0.161	0.018
248	0.188	0.042	0.010	128	0.234	0.164	0.018
246	0.187	0.042	0.010	126	0.234	0.166	0.019
244	0.189	0.043	0.011	124	0.236	0.169	0.019
242	0.191	0.045	0.011	122	0.235	0.172	0.018
240	0.191	0.046	0.011	120	0.236	0.175	0.018
238	0.195	0.047	0.011	118	0.240	0.178	0.019
236	0.195	0.049	0.010	116	0.239	0.180	0.018
234	0.197	0.050	0.012	114	0.239	0.183	0.018
232	0.198	0.051	0.011	112	0.239	0.189	0.019
230	0.200	0.053	0.011	110	0.235	0.193	0.019
228	0.201	0.055	0.011	108	0.232	0.194	0.019
226	0.202	0.056	0.012	106	0.232	0.194	0.019
224	0.204	0.057	0.012	104	0.232	0.198	0.020
222	0.205	0.059	0.011	102	0.233	0.202	0.020
220	0.206	0.060	0.012	100	0.235	0.204	0.020
218	0.208	0.062	0.011	98	0.232	0.210	0.020
216	0.210	0.064	0.011	96	0.231	0.217	0.021
214	0.213	0.065	0.012	94	0.235	0.220	0.021
212	0.215	0.067	0.012	92	0.235	0.218	0.022
210	0.217	0.069	0.012	90	0.233	0.220	0.021
208	0.218	0.071	0.012	88	0.234	0.224	0.022
206	0.220	0.073	0.012	86	0.236	0.226	0.022
204	0.220	0.074	0.012	84	0.236	0.232	0.023
202	0.220	0.077	0.012	82	0.236	0.235	0.024
200	0.218	0.079	0.012	80	0.234	0.242	0.024
198	0.219	0.081	0.012	78	0.231	0.242	0.024
196	0.219	0.083	0.012	76	0.234	0.247	0.025
194	0.219	0.085	0.012	74	0.238	0.255	0.025
192	0.222	0.087	0.013	72	0.237	0.259	0.027
190	0.226	0.089	0.013	70	0.236	0.265	0.027
188	0.227	0.092	0.013	68	0.235	0.269	0.027
186	0.227	0.094	0.013	66	0.231	0.277	0.028
184	0.228	0.096	0.014	64	0.234	0.277	0.028
182	0.229	0.099	0.013	62	0.236	0.275	0.028
180	0.230	0.101	0.014	60	0.237	0.283	0.029
178	0.230	0.104	0.014	58	0.241	0.286	0.030
176	0.233	0.106	0.015	56	0.242	0.292	0.030
174	0.234	0.108	0.014	54	0.241	0.295	0.030
172	0.233	0.111	0.015	52	0.241	0.302	0.030
170	0.232	0.113	0.015	50	0.240	0.303	0.031
168	0.233	0.115	0.016	48	0.237	0.304	0.030
166	0.233	0.117	0.016	46	0.239	0.314	0.032
164	0.232	0.120	0.016	44	0.240	0.319	0.033
162	0.233	0.123	0.016	42	0.242	0.325	0.032
160	0.234	0.125	0.016	40	0.241	0.329	0.032
158	0.235	0.127	0.017	38	0.243	0.338	0.033
156	0.232	0.129	0.018	36	0.243	0.342	0.034
154	0.235	0.131	0.018	34	0.241	0.347	0.033

Data for Figure 3-3 (Cont'):

Voltage (mV)	Current (μA) NH_2Cl-pH 3.8	NH_2Cl-pH 7.1	NH_2Cl-pH 10.1	Voltage (mV)	Current (μA) NH_2Cl-pH 3.8	NH_2Cl-pH 7.1	NH_2Cl-pH 10.1
32	0.244	0.352	0.034	-88	0.281	0.784	0.082
30	0.245	0.358	0.034	-90	0.283	0.789	0.083
28	0.247	0.365	0.034	-92	0.281	0.790	0.084
26	0.248	0.370	0.035	-94	0.283	0.793	0.086
24	0.245	0.379	0.036	-96	0.283	0.796	0.088
22	0.245	0.381	0.036	-98	0.284	0.799	0.089
20	0.247	0.389	0.036	-100	0.284	0.799	0.090
18	0.246	0.392	0.036	-102	0.287	0.809	0.092
16	0.246	0.399	0.037	-104	0.287	0.814	0.093
14	0.246	0.407	0.038	-106	0.287	0.814	0.095
12	0.245	0.414	0.038	-108	0.289	0.819	0.095
10	0.245	0.422	0.039	-110	0.291	0.821	0.098
8	0.246	0.431	0.039	-112	0.293	0.828	0.099
6	0.247	0.439	0.040	-114	0.297	0.828	0.100
4	0.248	0.446	0.040	-116	0.294	0.827	0.102
2	0.252	0.450	0.040	-118	0.292	0.828	0.104
0	0.254	0.458	0.041	-120	0.289	0.828	0.106
-2	0.255	0.465	0.041	-122	0.292	0.833	0.108
-4	0.253	0.472	0.042	-124	0.291	0.836	0.109
-6	0.252	0.480	0.043	-126	0.292	0.836	0.111
-8	0.252	0.486	0.043	-128	0.292	0.837	0.113
-10	0.254	0.497	0.043	-130	0.292	0.842	0.117
-12	0.257	0.504	0.045	-132	0.294	0.844	0.119
-14	0.257	0.510	0.044	-134	0.297	0.844	0.120
-16	0.257	0.521	0.045	-136	0.298	0.846	0.123
-18	0.260	0.531	0.046	-138	0.299	0.851	0.125
-20	0.261	0.541	0.047	-140	0.300	0.854	0.129
-22	0.261	0.548	0.047	-142	0.303	0.851	0.131
-24	0.260	0.553	0.048	-144	0.302	0.852	0.134
-26	0.261	0.562	0.049	-146	0.301	0.852	0.137
-28	0.262	0.571	0.049	-148	0.300	0.852	0.140
-30	0.263	0.579	0.050	-150	0.298	0.856	0.143
-32	0.264	0.583	0.051	-152	0.300	0.857	0.146
-34	0.260	0.592	0.052	-154	0.303	0.857	0.149
-36	0.258	0.602	0.052	-156	0.304	0.855	0.152
-38	0.260	0.609	0.053	-158	0.305	0.856	0.156
-40	0.262	0.617	0.054	-160	0.307	0.860	0.159
-42	0.264	0.624	0.055	-162	0.309	0.858	0.163
-44	0.265	0.636	0.056	-164	0.310	0.859	0.166
-46	0.267	0.648	0.057	-166	0.308	0.859	0.169
-48	0.269	0.656	0.058	-168	0.306	0.866	0.173
-50	0.269	0.664	0.059	-170	0.309	0.864	0.176
-52	0.270	0.677	0.059	-172	0.308	0.867	0.180
-54	0.272	0.680	0.060	-174	0.308	0.867	0.183
-56	0.273	0.688	0.061	-176	0.308	0.870	0.183
-58	0.272	0.692	0.062	-178	0.308	0.874	0.186
-60	0.273	0.700	0.064	-180	0.310	0.873	0.199
-62	0.269	0.708	0.064	-182	0.311	0.874	0.200
-64	0.267	0.713	0.066	-184	0.313	0.873	0.207
-66	0.270	0.718	0.068	-186	0.311	0.875	0.211
-68	0.274	0.729	0.069	-188	0.312	0.871	0.221
-70	0.277	0.733	0.069	-190	0.313	0.870	0.223
-72	0.279	0.739	0.071	-192	0.315	0.874	0.230
-74	0.280	0.745	0.072	-194	0.318	0.875	0.237
-76	0.280	0.752	0.073	-196	0.318	0.877	0.240
-78	0.281	0.754	0.075	-198	0.316	0.877	0.247
-80	0.278	0.761	0.076	-200	0.319	0.878	0.253
-82	0.279	0.767	0.078	-202	0.318	0.878	0.261
-84	0.279	0.771	0.078	-204	0.319	0.879	0.262
-86	0.281	0.777	0.080	-206	0.318	0.879	0.265

Data for Figure 3-3 (Cont'):

Voltage (mV)	Current (μA) NH_2Cl-pH 3.8	NH_2Cl-pH 7.1	NH_2Cl-pH 10.1	Voltage (mV)	Current (μA) NH_2Cl-pH 3.8	NH_2Cl-pH 7.1	NH_2Cl-pH 10.1
-208	0.318	0.877	0.276	-306	0.347	0.902	0.972
-210	0.317	0.878	0.282	-308	0.346	0.902	0.991
-212	0.317	0.876	0.289	-310	0.347	0.900	1.021
-214	0.319	0.880	0.288	-312	0.349	0.900	1.042
-216	0.320	0.880	0.302	-314	0.349	0.901	1.071
-218	0.320	0.882	0.307	-316	0.351	0.902	1.094
-220	0.322	0.882	0.318	-318	0.351	0.903	1.119
-222	0.323	0.881	0.329	-320	0.352	0.901	1.147
-224	0.325	0.884	0.330	-322	0.351	0.897	1.171
-226	0.327	0.880	0.341	-324	0.353	0.897	1.194
-228	0.326	0.882	0.352	-326	0.354	0.896	1.213
-230	0.325	0.884	0.359	-328	0.352	0.897	1.240
-232	0.325	0.884	0.364	-330	0.356	0.900	1.256
-234	0.325	0.885	0.374	-332	0.358	0.902	1.281
-236	0.326	0.888	0.385	-334	0.358	0.904	1.305
-238	0.329	0.886	0.394	-336	0.362	0.907	1.331
-240	0.327	0.889	0.408	-338	0.362	0.908	1.353
-242	0.326	0.888	0.416	-340	0.360	0.902	1.372
-244	0.329	0.888	0.432	-342	0.362	0.903	1.393
-246	0.330	0.886	0.438	-344	0.361	0.903	1.408
-248	0.330	0.887	0.452	-346	0.363	0.905	1.424
-250	0.330	0.889	0.463	-348	0.364	0.906	1.445
-252	0.328	0.889	0.468	-350	0.365	0.907	1.457
-254	0.329	0.888	0.480	-352	0.366	0.907	1.481
-256	0.330	0.887	0.496	-354	0.367	0.904	1.493
-258	0.332	0.889	0.514	-356	0.370	0.904	1.506
-260	0.331	0.887	0.528	-358	0.371	0.906	1.519
-262	0.334	0.890	0.540	-360	0.373	0.905	1.528
-264	0.336	0.894	0.558	-362	0.377	0.905	1.542
-266	0.337	0.892	0.571	-364	0.378	0.908	1.549
-268	0.338	0.893	0.585	-366	0.376	0.909	1.558
-270	0.337	0.895	0.595	-368	0.378	0.903	1.567
-272	0.335	0.895	0.615	-370	0.380	0.902	1.581
-274	0.339	0.895	0.632	-372	0.384	0.904	1.587
-276	0.339	0.894	0.655	-374	0.382	0.905	1.591
-278	0.339	0.896	0.675	-376	0.384	0.906	1.600
-280	0.341	0.898	0.696	-378	0.386	0.907	1.607
-282	0.342	0.897	0.715	-380	0.385	0.909	1.611
-284	0.341	0.895	0.728	-382	0.383	0.906	1.613
-286	0.340	0.892	0.743	-384	0.383	0.906	1.620
-288	0.340	0.892	0.759	-386	0.387	0.907	1.626
-290	0.340	0.894	0.775	-388	0.386	0.906	1.630
-292	0.341	0.896	0.805	-390	0.386	0.907	1.642
-294	0.343	0.894	0.826	-392	0.388	0.911	1.645
-296	0.344	0.900	0.855	-394	0.385	0.912	1.649
-298	0.345	0.895	0.876	-396	0.387	0.907	1.650
-300	0.346	0.897	0.900	-398	0.389	0.907	1.649
-302	0.345	0.897	0.927	-400	0.387	0.910	1.649
-304	0.346	0.899	0.951				

Data for Figure 3-4:

Voltage (mV)	Current (μA) at pH 3.8			Voltage (mV)	Current (μA) at pH 3.8		
	NH_2Cl with DO	O_2-free NH_2Cl	pH 3.8 buffer		NH_2Cl with DO	O_2-free NH_2Cl	pH 3.8 buffer
500	0.057	0.019	0.003	386	0.112	0.069	0.010
498	0.058	0.019	0.004	384	0.114	0.070	0.010
496	0.058	0.020	0.004	382	0.116	0.071	0.010
494	0.059	0.021	0.004	380	0.118	0.073	0.010
492	0.060	0.021	0.004	378	0.119	0.075	0.011
490	0.061	0.021	0.004	376	0.121	0.076	0.011
488	0.061	0.022	0.004	374	0.123	0.078	0.011
486	0.061	0.022	0.004	372	0.125	0.079	0.011
484	0.061	0.023	0.004	370	0.127	0.081	0.011
482	0.062	0.024	0.004	368	0.129	0.083	0.012
480	0.062	0.024	0.004	366	0.131	0.084	0.012
478	0.062	0.025	0.004	364	0.133	0.086	0.013
476	0.062	0.025	0.004	362	0.135	0.088	0.012
474	0.063	0.026	0.004	360	0.138	0.090	0.013
472	0.063	0.027	0.005	358	0.140	0.091	0.014
470	0.064	0.027	0.005	356	0.142	0.094	0.013
468	0.064	0.028	0.005	354	0.144	0.095	0.014
466	0.064	0.029	0.005	352	0.146	0.097	0.014
464	0.065	0.029	0.005	350	0.148	0.099	0.014
462	0.065	0.030	0.005	348	0.149	0.102	0.014
460	0.066	0.031	0.006	346	0.152	0.104	0.015
458	0.066	0.031	0.005	344	0.154	0.106	0.015
456	0.066	0.032	0.005	342	0.156	0.107	0.015
454	0.068	0.032	0.005	340	0.159	0.110	0.015
452	0.068	0.033	0.006	338	0.160	0.112	0.016
450	0.069	0.034	0.006	336	0.163	0.114	0.016
448	0.069	0.034	0.006	334	0.164	0.116	0.016
446	0.070	0.035	0.006	332	0.167	0.118	0.016
444	0.071	0.036	0.006	330	0.169	0.120	0.016
442	0.072	0.036	0.006	328	0.172	0.122	0.016
440	0.073	0.037	0.006	326	0.174	0.123	0.017
438	0.074	0.038	0.006	324	0.175	0.125	0.017
436	0.075	0.039	0.006	322	0.178	0.127	0.017
434	0.076	0.040	0.006	320	0.181	0.129	0.017
432	0.077	0.041	0.007	318	0.182	0.131	0.018
430	0.078	0.042	0.006	316	0.184	0.132	0.017
428	0.080	0.043	0.007	314	0.187	0.134	0.017
426	0.081	0.044	0.007	312	0.188	0.136	0.018
424	0.083	0.046	0.007	310	0.191	0.137	0.018
422	0.085	0.047	0.007	308	0.193	0.138	0.018
420	0.086	0.048	0.007	306	0.194	0.141	0.018
418	0.087	0.049	0.008	304	0.196	0.143	0.019
416	0.088	0.050	0.008	302	0.199	0.144	0.018
414	0.090	0.051	0.008	300	0.201	0.146	0.019
412	0.092	0.053	0.009	298	0.202	0.148	0.019
410	0.093	0.054	0.008	296	0.207	0.149	0.018
408	0.095	0.055	0.008	294	0.218	0.151	0.019
406	0.096	0.056	0.009	292	0.220	0.152	0.019
404	0.098	0.057	0.009	290	0.217	0.154	0.019
402	0.100	0.059	0.009	288	0.217	0.156	0.019
400	0.101	0.060	0.009	286	0.217	0.158	0.020
398	0.102	0.061	0.010	284	0.221	0.159	0.020
396	0.103	0.062	0.009	282	0.225	0.161	0.019
394	0.106	0.064	0.009	280	0.226	0.163	0.020
392	0.108	0.065	0.010	278	0.228	0.164	0.020
390	0.108	0.066	0.010	276	0.227	0.166	0.020
388	0.110	0.067	0.010	274	0.225	0.167	0.020

Data for Figure 3-4 (Cont'):

Voltage (mV)	Current (μA) at pH 3.8			Voltage (mV)	Current (μA) at pH 3.8		
	NH_2Cl with DO	O_2-free NH_2Cl	pH 3.8 buffer		NH_2Cl with DO	O_2-free NH_2Cl	pH 3.8 buffer
272	0.229	0.169	0.020	152	0.305	0.233	0.055
270	0.230	0.170	0.020	150	0.308	0.234	0.056
268	0.232	0.172	0.021	148	0.311	0.235	0.057
266	0.233	0.174	0.021	146	0.310	0.233	0.058
264	0.236	0.175	0.021	144	0.312	0.234	0.059
262	0.239	0.177	0.021	142	0.313	0.233	0.060
260	0.240	0.178	0.022	140	0.316	0.231	0.062
258	0.240	0.180	0.022	138	0.317	0.233	0.063
256	0.247	0.181	0.022	136	0.320	0.234	0.064
254	0.248	0.182	0.023	134	0.319	0.235	0.065
252	0.248	0.184	0.024	132	0.320	0.234	0.067
250	0.246	0.186	0.024	130	0.320	0.235	0.068
248	0.245	0.188	0.024	128	0.321	0.234	0.069
246	0.248	0.187	0.025	126	0.324	0.234	0.071
244	0.249	0.189	0.025	124	0.328	0.236	0.072
242	0.247	0.191	0.025	122	0.330	0.235	0.073
240	0.250	0.191	0.026	120	0.333	0.236	0.075
238	0.251	0.195	0.026	118	0.334	0.240	0.076
236	0.253	0.195	0.026	116	0.331	0.239	0.078
234	0.256	0.197	0.027	114	0.331	0.239	0.080
232	0.256	0.198	0.028	112	0.333	0.239	0.081
230	0.255	0.200	0.028	110	0.334	0.235	0.083
228	0.257	0.201	0.028	108	0.335	0.232	0.085
226	0.261	0.202	0.029	106	0.335	0.232	0.087
224	0.263	0.204	0.029	104	0.338	0.232	0.089
222	0.263	0.205	0.030	102	0.343	0.233	0.091
220	0.263	0.206	0.030	100	0.353	0.235	0.092
218	0.266	0.208	0.031	98	0.354	0.232	0.094
216	0.270	0.210	0.031	96	0.351	0.231	0.096
214	0.269	0.213	0.032	94	0.353	0.235	0.099
212	0.269	0.215	0.033	92	0.353	0.235	0.101
210	0.269	0.217	0.033	90	0.355	0.233	0.104
208	0.269	0.218	0.034	88	0.356	0.234	0.106
206	0.273	0.220	0.034	86	0.360	0.236	0.108
204	0.278	0.220	0.035	84	0.361	0.236	0.112
202	0.279	0.220	0.035	82	0.366	0.236	0.114
200	0.280	0.218	0.036	80	0.372	0.234	0.116
198	0.280	0.219	0.037	78	0.370	0.231	0.118
196	0.277	0.219	0.037	76	0.371	0.234	0.122
194	0.282	0.219	0.038	74	0.371	0.238	0.125
192	0.281	0.222	0.039	72	0.372	0.237	0.128
190	0.282	0.226	0.040	70	0.375	0.236	0.131
188	0.283	0.227	0.041	68	0.379	0.235	0.133
186	0.288	0.227	0.042	66	0.378	0.231	0.138
184	0.288	0.228	0.042	64	0.381	0.234	0.140
182	0.287	0.229	0.043	62	0.389	0.236	0.144
180	0.290	0.230	0.044	60	0.388	0.237	0.148
178	0.292	0.230	0.045	58	0.390	0.241	0.151
176	0.294	0.233	0.045	56	0.392	0.242	0.155
174	0.289	0.234	0.046	54	0.397	0.241	0.158
172	0.289	0.233	0.048	52	0.401	0.241	0.161
170	0.293	0.232	0.048	50	0.402	0.240	0.166
168	0.301	0.233	0.049	48	0.403	0.237	0.169
166	0.301	0.233	0.049	46	0.409	0.239	0.173
164	0.300	0.232	0.050	44	0.411	0.240	0.177
162	0.300	0.233	0.050	42	0.412	0.242	0.181
160	0.299	0.234	0.051	40	0.413	0.241	0.186
158	0.302	0.235	0.052	38	0.413	0.243	0.192
156	0.304	0.232	0.053	36	0.416	0.243	0.196
154	0.304	0.235	0.055	34	0.425	0.241	0.200

Data for Figure 3-4 (Cont'):

Voltage (mV)	Current (μA) at pH 3.8			Voltage (mV)	Current (μA) at pH 3.8		
	NH_2Cl with DO	O_3-free NH_2Cl	pH 3.8 buffer		NH_2Cl with DO	O_3-free NH_2Cl	pH 3.8 buffer
32	0.430	0.244	0.206	-88	0.676	0.281	0.605
30	0.432	0.245	0.212	-90	0.680	0.283	0.614
28	0.432	0.247	0.215	-92	0.686	0.281	0.618
26	0.436	0.248	0.220	-94	0.690	0.283	0.625
24	0.440	0.245	0.229	-96	0.695	0.283	0.630
22	0.443	0.245	0.233	-98	0.696	0.284	0.635
20	0.442	0.247	0.238	-100	0.701	0.284	0.641
18	0.444	0.246	0.244	-102	0.708	0.287	0.643
16	0.446	0.246	0.251	-104	0.713	0.287	0.654
14	0.452	0.246	0.256	-106	0.716	0.287	0.657
12	0.456	0.245	0.262	-108	0.719	0.289	0.658
10	0.464	0.245	0.267	-110	0.725	0.291	0.667
8	0.469	0.246	0.275	-112	0.733	0.293	0.669
6	0.470	0.247	0.279	-114	0.735	0.297	0.673
4	0.474	0.248	0.288	-116	0.738	0.294	0.680
2	0.475	0.252	0.295	-118	0.742	0.292	0.685
0	0.477	0.254	0.301	-120	0.746	0.289	0.685
-2	0.480	0.255	0.307	-122	0.751	0.292	0.691
-4	0.488	0.253	0.313	-124	0.758	0.291	0.697
-6	0.491	0.252	0.322	-126	0.763	0.292	0.697
-8	0.497	0.252	0.325	-128	0.766	0.292	0.704
-10	0.500	0.254	0.336	-130	0.771	0.292	0.707
-12	0.504	0.257	0.341	-132	0.776	0.294	0.710
-14	0.511	0.257	0.347	-134	0.779	0.297	0.713
-16	0.514	0.257	0.358	-136	0.781	0.298	0.718
-18	0.519	0.260	0.363	-138	0.785	0.299	0.723
-20	0.519	0.261	0.366	-140	0.790	0.300	0.726
-22	0.523	0.261	0.374	-142	0.796	0.303	0.728
-24	0.529	0.260	0.384	-144	0.801	0.302	0.733
-26	0.535	0.261	0.393	-146	0.808	0.301	0.735
-28	0.539	0.262	0.397	-148	0.812	0.300	0.740
-30	0.544	0.263	0.406	-150	0.816	0.298	0.742
-32	0.547	0.264	0.413	-152	0.820	0.300	0.743
-34	0.554	0.260	0.415	-154	0.821	0.303	0.747
-36	0.555	0.258	0.427	-156	0.822	0.304	0.749
-38	0.559	0.260	0.436	-158	0.827	0.305	0.750
-40	0.563	0.262	0.443	-160	0.833	0.307	0.756
-42	0.567	0.264	0.450	-162	0.839	0.309	0.758
-44	0.572	0.265	0.458	-164	0.841	0.310	0.758
-46	0.577	0.267	0.467	-166	0.841	0.308	0.760
-48	0.581	0.269	0.472	-168	0.846	0.306	0.760
-50	0.585	0.269	0.480	-170	0.854	0.309	0.764
-52	0.592	0.270	0.485	-172	0.857	0.308	0.769
-54	0.599	0.272	0.493	-174	0.859	0.308	0.772
-56	0.603	0.273	0.500	-176	0.860	0.308	0.772
-58	0.606	0.272	0.507	-178	0.864	0.308	0.773
-60	0.612	0.273	0.517	-180	0.868	0.310	0.776
-62	0.614	0.269	0.522	-182	0.873	0.311	0.778
-64	0.617	0.267	0.524	-184	0.877	0.313	0.779
-66	0.627	0.270	0.531	-186	0.881	0.311	0.782
-68	0.631	0.274	0.541	-188	0.885	0.312	0.784
-70	0.634	0.277	0.545	-190	0.889	0.313	0.788
-72	0.637	0.279	0.553	-192	0.893	0.315	0.788
-74	0.637	0.280	0.562	-194	0.892	0.318	0.791
-76	0.638	0.280	0.569	-196	0.894	0.318	0.794
-78	0.643	0.281	0.573	-198	0.897	0.316	0.794
-80	0.653	0.278	0.580	-200	0.903	0.319	0.794
-82	0.663	0.279	0.587	-202	0.906	0.318	0.795
-84	0.671	0.279	0.591	-204	0.911	0.319	0.800
-86	0.675	0.281	0.599	-206	0.916	0.318	0.801

Data for Figure 3-4 (Cont'):

Voltage (mV)	Current (μA) at pH 3.8			Voltage (mV)	Current (μA) at pH 3.8		
	NH_2Cl with DO	O_2-free NH_2Cl	pH 3.8 buffer		NH_2Cl with DO	O_2-free NH_2Cl	pH 3.8 buffer
-208	0.920	0.318	0.800	-306	1.031	0.347	0.855
-210	0.922	0.317	0.807	-308	1.033	0.346	0.856
-212	0.922	0.317	0.805	-310	1.034	0.347	0.860
-214	0.919	0.319	0.805	-312	1.037	0.349	0.857
-216	0.923	0.320	0.809	-314	1.041	0.349	0.857
-218	0.928	0.320	0.810	-316	1.039	0.351	0.861
-220	0.933	0.322	0.810	-318	1.037	0.351	0.860
-222	0.935	0.323	0.811	-320	1.040	0.352	0.860
-224	0.937	0.325	0.815	-322	1.041	0.351	0.862
-226	0.938	0.327	0.812	-324	1.046	0.353	0.865
-228	0.942	0.326	0.816	-326	1.048	0.354	0.864
-230	0.947	0.325	0.817	-328	1.047	0.352	0.868
-232	0.948	0.325	0.819	-330	1.047	0.356	0.870
-234	0.952	0.325	0.818	-332	1.049	0.358	0.869
-236	0.955	0.326	0.817	-334	1.050	0.358	0.870
-238	0.959	0.329	0.822	-336	1.052	0.362	0.870
-240	0.962	0.327	0.820	-338	1.056	0.362	0.873
-242	0.964	0.326	0.822	-340	1.059	0.360	0.873
-244	0.968	0.329	0.826	-342	1.060	0.362	0.874
-246	0.971	0.330	0.826	-344	1.061	0.361	0.876
-248	0.975	0.330	0.827	-346	1.062	0.363	0.877
-250	0.976	0.330	0.829	-348	1.061	0.364	0.875
-252	0.976	0.328	0.830	-350	1.061	0.365	0.876
-254	0.978	0.329	0.831	-352	1.063	0.366	0.877
-256	0.981	0.330	0.832	-354	1.066	0.367	0.880
-258	0.983	0.332	0.834	-356	1.067	0.370	0.879
-260	0.985	0.331	0.838	-358	1.070	0.371	0.879
-262	0.989	0.334	0.837	-360	1.069	0.373	0.882
-264	0.988	0.336	0.835	-362	1.073	0.377	0.882
-266	0.990	0.337	0.840	-364	1.072	0.378	0.879
-268	0.992	0.338	0.838	-366	1.074	0.376	0.882
-270	0.994	0.337	0.839	-368	1.076	0.378	0.886
-272	0.993	0.335	0.843	-370	1.076	0.380	0.882
-274	0.997	0.339	0.844	-372	1.077	0.384	0.885
-276	1.000	0.339	0.843	-374	1.079	0.382	0.887
-278	1.003	0.339	0.842	-376	1.078	0.384	0.887
-280	1.005	0.341	0.846	-378	1.081	0.386	0.886
-282	1.007	0.342	0.845	-380	1.084	0.385	0.890
-284	1.010	0.341	0.847	-382	1.082	0.383	0.893
-286	1.014	0.340	0.847	-384	1.085	0.383	0.889
-288	1.013	0.340	0.850	-386	1.082	0.387	0.894
-290	1.014	0.340	0.848	-388	1.084	0.386	0.895
-292	1.014	0.341	0.845	-390	1.085	0.386	0.892
-294	1.018	0.343	0.851	-392	1.087	0.388	0.895
-296	1.021	0.344	0.850	-394	1.088	0.385	0.898
-298	1.024	0.345	0.851	-396	1.088	0.387	0.900
-300	1.027	0.346	0.853	-398	1.088	0.389	0.897
-302	1.027	0.345	0.854	-400	1.088	0.387	0.898
-304	1.028	0.346	0.853				

Data for Figure 3-5:

Voltage (mV)	Current (μA) at pH 7.1			Voltage (mV)	Current (μA) at pH 7.1		
	NH_2Cl with DO	O_2-free NH_2Cl	pH 7.1 buffer		NH_2Cl with DO	O_2-free NH_2Cl	pH 7.1 buffer
500	-0.007	-0.006	0.000	386	0.002	0.004	0.003
498	-0.007	-0.006	0.000	384	0.003	0.004	0.004
496	-0.006	-0.006	0.000	382	0.004	0.004	0.004
494	-0.006	-0.006	0.000	380	0.004	0.004	0.004
492	-0.006	-0.006	0.000	378	0.004	0.005	0.004
490	-0.006	-0.006	0.001	376	0.004	0.004	0.004
488	-0.006	-0.006	0.001	374	0.005	0.005	0.004
486	-0.005	-0.005	0.001	372	0.004	0.006	0.003
484	-0.005	-0.005	0.001	370	0.005	0.006	0.004
482	-0.005	-0.005	0.001	368	0.005	0.006	0.004
480	-0.004	-0.004	0.001	366	0.006	0.006	0.004
478	-0.004	-0.004	0.001	364	0.006	0.007	0.004
476	-0.004	-0.004	0.002	362	0.006	0.006	0.004
474	-0.004	-0.004	0.002	360	0.007	0.007	0.005
472	-0.004	-0.005	0.001	358	0.007	0.007	0.004
470	-0.003	-0.004	0.002	356	0.008	0.007	0.004
468	-0.004	-0.004	0.001	354	0.008	0.007	0.004
466	-0.004	-0.004	0.001	352	0.009	0.008	0.004
464	-0.003	-0.003	0.002	350	0.009	0.008	0.004
462	-0.003	-0.003	0.002	348	0.009	0.008	0.004
460	-0.003	-0.003	0.002	346	0.010	0.009	0.005
458	-0.002	-0.002	0.002	344	0.011	0.009	0.004
456	-0.002	-0.002	0.002	342	0.010	0.009	0.004
454	-0.002	-0.002	0.002	340	0.011	0.010	0.005
452	-0.001	-0.002	0.002	338	0.011	0.009	0.005
450	-0.002	-0.001	0.002	336	0.012	0.010	0.004
448	-0.001	-0.001	0.002	334	0.013	0.010	0.005
446	-0.001	-0.001	0.002	332	0.013	0.011	0.006
444	-0.001	-0.001	0.002	330	0.013	0.011	0.005
442	0.000	-0.001	0.002	328	0.013	0.012	0.005
440	0.000	-0.001	0.002	326	0.014	0.012	0.005
438	0.000	-0.001	0.002	324	0.014	0.013	0.006
436	0.001	-0.001	0.002	322	0.015	0.013	0.006
434	0.000	0.000	0.003	320	0.015	0.013	0.006
432	0.001	0.000	0.003	318	0.016	0.014	0.006
430	0.001	-0.001	0.002	316	0.016	0.015	0.006
428	0.001	-0.001	0.002	314	0.016	0.015	0.007
426	0.001	0.000	0.003	312	0.017	0.015	0.008
424	0.001	0.000	0.002	310	0.017	0.016	0.007
422	0.001	0.000	0.002	308	0.017	0.016	0.007
420	0.001	0.000	0.002	306	0.018	0.017	0.007
418	0.001	0.000	0.002	304	0.019	0.017	0.007
416	0.001	0.000	0.002	302	0.019	0.018	0.007
414	0.001	0.000	0.002	300	0.019	0.018	0.008
412	0.001	0.000	0.002	298	0.019	0.019	0.008
410	0.001	0.001	0.002	296	0.020	0.020	0.007
408	0.001	0.001	0.003	294	0.020	0.020	0.008
406	0.001	0.001	0.002	292	0.021	0.021	0.008
404	0.002	0.001	0.003	290	0.022	0.021	0.008
402	0.002	0.002	0.003	288	0.022	0.023	0.008
400	0.002	0.002	0.003	286	0.023	0.023	0.009
398	0.002	0.002	0.003	284	0.023	0.024	0.009
396	0.002	0.002	0.004	282	0.024	0.025	0.009
394	0.002	0.002	0.003	280	0.025	0.025	0.009
392	0.002	0.003	0.003	278	0.025	0.026	0.009
390	0.003	0.003	0.004	276	0.026	0.027	0.010
388	0.003	0.003	0.003	274	0.026	0.028	0.010

Data for Figure 3-5 (Cont'):

Voltage (mV)	Current (μA) at pH 7.1			Voltage (mV)	Current (μA) at pH 7.1		
	NH_2Cl with DO	O_2-free NH_2Cl	pH 7.1 buffer		NH_2Cl with DO	O_2-free NH_2Cl	pH 7.1 buffer
272	0.027	0.029	0.009	152	0.130	0.133	0.015
270	0.028	0.030	0.010	150	0.134	0.136	0.016
268	0.029	0.031	0.010	148	0.136	0.138	0.016
266	0.029	0.031	0.010	146	0.139	0.141	0.017
264	0.031	0.033	0.011	144	0.141	0.144	0.017
262	0.031	0.034	0.011	142	0.144	0.147	0.017
260	0.033	0.035	0.011	140	0.146	0.149	0.017
258	0.034	0.036	0.012	138	0.149	0.151	0.017
256	0.035	0.037	0.011	136	0.152	0.153	0.017
254	0.036	0.038	0.012	134	0.154	0.156	0.017
252	0.037	0.040	0.012	132	0.157	0.158	0.017
250	0.038	0.040	0.012	130	0.159	0.161	0.018
248	0.040	0.042	0.012	128	0.162	0.164	0.018
246	0.041	0.042	0.012	126	0.164	0.166	0.018
244	0.042	0.043	0.013	124	0.167	0.169	0.019
242	0.043	0.045	0.013	122	0.170	0.172	0.018
240	0.044	0.046	0.013	120	0.173	0.175	0.019
238	0.046	0.047	0.013	118	0.175	0.178	0.019
236	0.047	0.049	0.013	116	0.178	0.180	0.019
234	0.048	0.050	0.013	114	0.181	0.183	0.020
232	0.050	0.051	0.013	112	0.185	0.189	0.019
230	0.051	0.053	0.013	110	0.188	0.193	0.021
228	0.052	0.055	0.013	108	0.192	0.194	0.020
226	0.054	0.056	0.014	106	0.194	0.194	0.021
224	0.055	0.057	0.014	104	0.198	0.198	0.021
222	0.057	0.059	0.013	102	0.198	0.202	0.022
220	0.058	0.060	0.014	100	0.201	0.204	0.022
218	0.059	0.062	0.015	98	0.205	0.210	0.023
216	0.061	0.064	0.014	96	0.209	0.217	0.023
214	0.063	0.065	0.014	94	0.214	0.220	0.023
212	0.064	0.067	0.015	92	0.217	0.218	0.023
210	0.067	0.069	0.014	90	0.222	0.220	0.024
208	0.068	0.071	0.014	88	0.224	0.224	0.024
206	0.070	0.073	0.015	86	0.228	0.226	0.024
204	0.072	0.074	0.015	84	0.232	0.232	0.024
202	0.073	0.077	0.015	82	0.234	0.235	0.025
200	0.075	0.079	0.015	80	0.235	0.242	0.025
198	0.077	0.081	0.015	78	0.238	0.242	0.026
196	0.079	0.083	0.015	76	0.243	0.247	0.026
194	0.081	0.085	0.015	74	0.249	0.255	0.026
192	0.083	0.087	0.014	72	0.253	0.259	0.027
190	0.085	0.089	0.014	70	0.257	0.265	0.027
188	0.087	0.092	0.015	68	0.259	0.269	0.027
186	0.089	0.094	0.014	66	0.260	0.277	0.027
184	0.092	0.096	0.014	64	0.267	0.277	0.028
182	0.094	0.099	0.014	62	0.271	0.275	0.028
180	0.096	0.101	0.014	60	0.272	0.283	0.029
178	0.098	0.104	0.014	58	0.275	0.286	0.029
176	0.101	0.106	0.015	56	0.278	0.292	0.030
174	0.103	0.108	0.015	54	0.282	0.295	0.030
172	0.106	0.111	0.014	52	0.289	0.302	0.030
170	0.108	0.113	0.015	50	0.294	0.303	0.031
168	0.110	0.115	0.015	48	0.298	0.304	0.031
166	0.113	0.117	0.016	46	0.300	0.314	0.032
164	0.115	0.120	0.015	44	0.305	0.319	0.032
162	0.118	0.123	0.015	42	0.309	0.325	0.032
160	0.120	0.125	0.016	40	0.316	0.329	0.032
158	0.123	0.127	0.016	38	0.320	0.338	0.033
156	0.125	0.129	0.016	36	0.326	0.342	0.034
154	0.128	0.131	0.016	34	0.328	0.347	0.034

Data for Figure 3-5 (Cont'):

Voltage (mV)	Current (μA) at pH 7.1			Voltage (mV)	Current (μA) at pH 7.1		
	NH_2Cl with DO	O_2-free NH_2Cl	pH 7.1 buffer		NH_2Cl with DO	O_2-free NH_2Cl	pH 7.1 buffer
32	0.336	0.352	0.034	-88	0.834	0.784	0.071
30	0.345	0.358	0.034	-90	0.844	0.789	0.072
28	0.352	0.365	0.034	-92	0.858	0.790	0.074
26	0.354	0.370	0.035	-94	0.868	0.793	0.075
24	0.359	0.379	0.035	-96	0.876	0.796	0.077
22	0.362	0.381	0.035	-98	0.885	0.799	0.078
20	0.368	0.389	0.035	-100	0.893	0.799	0.080
18	0.370	0.392	0.036	-102	0.904	0.809	0.082
16	0.377	0.399	0.036	-104	0.911	0.814	0.084
14	0.385	0.407	0.036	-106	0.918	0.814	0.085
12	0.392	0.414	0.037	-108	0.935	0.819	0.087
10	0.399	0.422	0.037	-110	0.946	0.821	0.089
8	0.403	0.431	0.037	-112	0.954	0.828	0.091
6	0.416	0.439	0.037	-114	0.965	0.828	0.093
4	0.419	0.446	0.038	-116	0.975	0.827	0.097
2	0.424	0.450	0.038	-118	0.986	0.828	0.098
0	0.432	0.458	0.038	-120	0.997	0.828	0.101
-2	0.439	0.465	0.039	-122	1.006	0.833	0.104
-4	0.445	0.472	0.040	-124	1.015	0.836	0.106
-6	0.451	0.480	0.041	-126	1.022	0.836	0.109
-8	0.456	0.486	0.041	-128	1.032	0.837	0.113
-10	0.467	0.497	0.041	-130	1.045	0.842	0.115
-12	0.471	0.504	0.042	-132	1.057	0.844	0.119
-14	0.480	0.510	0.042	-134	1.067	0.844	0.123
-16	0.492	0.521	0.043	-136	1.076	0.846	0.127
-18	0.498	0.531	0.044	-138	1.082	0.851	0.130
-20	0.505	0.541	0.044	-140	1.096	0.854	0.134
-22	0.511	0.548	0.044	-142	1.107	0.851	0.138
-24	0.519	0.553	0.045	-144	1.118	0.852	0.143
-26	0.529	0.562	0.045	-146	1.129	0.852	0.148
-28	0.534	0.571	0.046	-148	1.134	0.852	0.153
-30	0.543	0.579	0.046	-150	1.148	0.856	0.158
-32	0.555	0.583	0.047	-152	1.159	0.857	0.164
-34	0.563	0.592	0.047	-154	1.169	0.857	0.170
-36	0.571	0.602	0.048	-156	1.183	0.855	0.176
-38	0.586	0.609	0.049	-158	1.189	0.856	0.183
-40	0.591	0.617	0.049	-160	1.198	0.860	0.189
-42	0.601	0.624	0.050	-162	1.210	0.858	0.195
-44	0.607	0.636	0.050	-164	1.220	0.859	0.203
-46	0.617	0.648	0.051	-166	1.228	0.859	0.212
-48	0.628	0.656	0.052	-168	1.241	0.866	0.223
-50	0.633	0.664	0.052	-170	1.249	0.864	0.232
-52	0.645	0.677	0.053	-172	1.259	0.867	0.240
-54	0.655	0.680	0.055	-174	1.270	0.867	0.257
-56	0.666	0.688	0.055	-176	1.282	0.870	0.268
-58	0.681	0.692	0.056	-178	1.292	0.874	0.279
-60	0.688	0.700	0.057	-180	1.296	0.873	0.297
-62	0.698	0.708	0.057	-182	1.308	0.874	0.311
-64	0.706	0.713	0.058	-184	1.322	0.873	0.326
-66	0.714	0.718	0.059	-186	1.329	0.875	0.349
-68	0.725	0.729	0.061	-188	1.342	0.871	0.363
-70	0.737	0.733	0.061	-190	1.348	0.870	0.381
-72	0.749	0.739	0.062	-192	1.357	0.874	0.397
-74	0.757	0.745	0.064	-194	1.365	0.875	0.420
-76	0.766	0.752	0.064	-196	1.376	0.877	0.442
-78	0.777	0.754	0.066	-198	1.390	0.877	0.462
-80	0.789	0.761	0.066	-200	1.396	0.878	0.486
-82	0.801	0.767	0.067	-202	1.402	0.878	0.504
-84	0.811	0.771	0.069	-204	1.410	0.879	0.525
-86	0.820	0.777	0.070	-206	1.420	0.879	0.552

Data for Figure 3-5 (Cont'):

Voltage	Current (μA) at pH 7.1			Voltage	Current (μA) at pH 7.1		
(mV)	NH_2Cl with DO	O_2-free NH_2Cl	pH 7.1 buffer	(mV)	NH_2Cl with DO	O_2-free NH_2Cl	pH 7.1 buffer
-208	1.431	0.877	0.580	-306	1.751	0.902	1.118
-210	1.441	0.878	0.600	-308	1.757	0.902	1.114
-212	1.450	0.876	0.625	-310	1.761	0.900	1.120
-214	1.456	0.880	0.651	-312	1.766	0.900	1.123
-216	1.465	0.880	0.674	-314	1.770	0.901	1.125
-218	1.475	0.882	0.701	-316	1.776	0.902	1.127
-220	1.482	0.882	0.727	-318	1.782	0.903	1.128
-222	1.489	0.881	0.747	-320	1.785	0.901	1.128
-224	1.498	0.884	0.770	-322	1.788	0.897	1.136
-226	1.507	0.880	0.797	-324	1.791	0.897	1.139
-228	1.518	0.882	0.813	-326	1.796	0.896	1.138
-230	1.525	0.884	0.836	-328	1.800	0.897	1.139
-232	1.535	0.884	0.854	-330	1.802	0.900	1.141
-234	1.540	0.885	0.872	-332	1.803	0.902	1.144
-236	1.548	0.888	0.893	-334	1.806	0.904	1.149
-238	1.555	0.886	0.910	-336	1.807	0.907	1.147
-240	1.565	0.889	0.925	-338	1.811	0.908	1.145
-242	1.571	0.888	0.941	-340	1.816	0.902	1.148
-244	1.577	0.888	0.952	-342	1.818	0.903	1.151
-246	1.582	0.886	0.964	-344	1.822	0.903	1.148
-248	1.591	0.887	0.978	-346	1.822	0.905	1.153
-250	1.598	0.889	0.989	-348	1.826	0.906	1.152
-252	1.602	0.889	0.997	-350	1.831	0.907	1.150
-254	1.610	0.888	1.010	-352	1.833	0.907	1.158
-256	1.618	0.887	1.017	-354	1.833	0.904	1.155
-258	1.624	0.889	1.024	-356	1.833	0.904	1.154
-260	1.631	0.887	1.032	-358	1.839	0.906	1.154
-262	1.636	0.890	1.041	-360	1.839	0.905	1.159
-264	1.644	0.894	1.048	-362	1.844	0.905	1.161
-266	1.650	0.892	1.055	-364	1.844	0.908	1.158
-268	1.654	0.893	1.058	-366	1.844	0.909	1.158
-270	1.664	0.895	1.057	-368	1.847	0.903	1.158
-272	1.666	0.895	1.060	-370	1.851	0.902	1.165
-274	1.672	0.895	1.067	-372	1.854	0.904	1.166
-276	1.681	0.894	1.074	-374	1.855	0.905	1.172
-278	1.683	0.896	1.079	-376	1.853	0.906	1.174
-280	1.692	0.898	1.082	-378	1.859	0.907	1.170
-282	1.696	0.897	1.082	-380	1.860	0.909	1.171
-284	1.701	0.895	1.091	-382	1.862	0.906	1.173
-286	1.706	0.892	1.094	-384	1.867	0.906	1.170
-288	1.710	0.892	1.098	-386	1.862	0.907	1.167
-290	1.715	0.894	1.094	-388	1.864	0.906	1.175
-292	1.723	0.896	1.098	-390	1.867	0.907	1.176
-294	1.723	0.894	1.105	-392	1.868	0.911	1.174
-296	1.735	0.900	1.105	-394	1.870	0.912	1.170
-298	1.738	0.895	1.108	-396	1.867	0.907	1.174
-300	1.744	0.897	1.111	-398	1.870	0.907	1.174
-302	1.747	0.897	1.110	-400	1.876	0.910	1.176
-304	1.748	0.899	1.116				

Data for Figure 3-6:

Voltage (mV)	Current (μA) at pH 10.1			Voltage (mV)	Current (μA) at pH 10.1		
	NH_2Cl with DO	O_2-free NH_2Cl	pH 10.1 buffer		NH_2Cl with DO	O_2-free NH_2Cl	pH 10.1 buffer
500	-0.020	-0.004	-0.010	386	-0.004	0.002	-0.003
498	-0.019	-0.004	-0.009	384	-0.004	0.003	-0.003
496	-0.019	-0.003	-0.010	382	-0.004	0.003	-0.002
494	-0.018	-0.004	-0.009	380	-0.003	0.004	-0.003
492	-0.017	-0.004	-0.009	378	-0.003	0.005	-0.003
490	-0.017	-0.004	-0.009	376	-0.002	0.004	-0.002
488	-0.017	-0.003	-0.008	374	-0.002	0.005	-0.002
486	-0.016	-0.003	-0.008	372	-0.002	0.006	-0.002
484	-0.016	-0.003	-0.008	370	-0.002	0.005	-0.002
482	-0.016	-0.003	-0.008	368	-0.001	0.006	-0.001
480	-0.016	-0.002	-0.008	366	-0.001	0.007	-0.002
478	-0.015	-0.002	-0.008	364	0.000	0.006	-0.002
476	-0.015	-0.001	-0.008	362	0.000	0.006	-0.003
474	-0.015	-0.001	-0.008	360	0.000	0.007	-0.002
472	-0.015	-0.001	-0.008	358	0.000	0.007	-0.002
470	-0.014	0.000	-0.008	356	0.000	0.008	-0.002
468	-0.014	0.000	-0.008	354	0.001	0.008	-0.002
466	-0.014	0.001	-0.007	352	0.001	0.008	-0.002
464	-0.014	0.000	-0.007	350	0.001	0.007	-0.002
462	-0.013	0.001	-0.006	348	0.002	0.007	-0.002
460	-0.014	0.001	-0.007	346	0.001	0.007	-0.002
458	-0.013	0.001	-0.006	344	0.001	0.007	-0.001
456	-0.012	0.002	-0.006	342	0.002	0.007	-0.002
454	-0.013	0.001	-0.006	340	0.001	0.006	-0.001
452	-0.012	0.002	-0.006	338	0.002	0.006	-0.001
450	-0.012	0.002	-0.006	336	0.002	0.006	-0.001
448	-0.012	0.002	-0.005	334	0.002	0.005	-0.001
446	-0.012	0.002	-0.005	332	0.002	0.005	-0.001
444	-0.011	0.001	-0.005	330	0.002	0.005	0.000
442	-0.011	0.002	-0.005	328	0.002	0.005	-0.001
440	-0.011	0.002	-0.005	326	0.002	0.005	-0.001
438	-0.011	0.002	-0.005	324	0.002	0.005	-0.001
436	-0.011	0.002	-0.005	322	0.003	0.005	0.000
434	-0.010	0.003	-0.005	320	0.003	0.005	0.000
432	-0.010	0.001	-0.005	318	0.003	0.004	0.000
430	-0.010	0.003	-0.005	316	0.004	0.005	0.001
428	-0.009	0.002	-0.005	314	0.003	0.005	0.000
426	-0.009	0.002	-0.005	312	0.004	0.004	0.001
424	-0.008	0.003	-0.004	310	0.004	0.005	0.001
422	-0.008	0.002	-0.004	308	0.004	0.005	0.001
420	-0.008	0.003	-0.004	306	0.004	0.005	0.001
418	-0.008	0.004	-0.004	304	0.005	0.005	0.001
416	-0.007	0.003	-0.004	302	0.005	0.006	0.001
414	-0.007	0.003	-0.004	300	0.005	0.006	0.001
412	-0.007	0.003	-0.004	298	0.005	0.007	0.002
410	-0.006	0.003	-0.004	296	0.005	0.007	0.002
408	-0.006	0.003	-0.003	294	0.005	0.007	0.002
406	-0.006	0.003	-0.004	292	0.005	0.008	0.002
404	-0.006	0.003	-0.004	290	0.006	0.007	0.002
402	-0.006	0.003	-0.004	288	0.006	0.008	0.003
400	-0.006	0.002	-0.003	286	0.005	0.008	0.003
398	-0.006	0.003	-0.003	284	0.005	0.008	0.003
396	-0.005	0.002	-0.003	282	0.006	0.008	0.003
394	-0.005	0.002	-0.004	280	0.006	0.008	0.003
392	-0.005	0.002	-0.003	278	0.006	0.008	0.004
390	-0.004	0.002	-0.003	276	0.006	0.009	0.004
388	-0.004	0.002	-0.003	274	0.006	0.009	0.003

Data for Figure 3-6 (Cont'):

Voltage (mV)	Current (μA) at pH 10.1			Voltage (mV)	Current (μA) at pH 10.1		
	NH_2Cl with DO	O_2-free NH_2Cl	pH 10.1 buffer		NH_2Cl with DO	O_2-free NH_2Cl	pH 10.1 buffer
272	0.006	0.010	0.004	152	0.014	0.018	0.007
270	0.006	0.010	0.004	150	0.015	0.019	0.007
268	0.005	0.010	0.004	148	0.015	0.018	0.008
266	0.005	0.010	0.004	146	0.016	0.019	0.008
264	0.006	0.010	0.004	144	0.016	0.019	0.008
262	0.006	0.010	0.004	142	0.016	0.019	0.008
260	0.006	0.011	0.004	140	0.017	0.019	0.009
258	0.006	0.011	0.005	138	0.017	0.019	0.008
256	0.006	0.011	0.005	136	0.017	0.019	0.008
254	0.006	0.010	0.005	134	0.017	0.018	0.009
252	0.006	0.010	0.005	132	0.018	0.019	0.009
250	0.006	0.010	0.005	130	0.018	0.018	0.008
248	0.006	0.010	0.004	128	0.018	0.018	0.009
246	0.007	0.010	0.004	126	0.018	0.019	0.009
244	0.007	0.011	0.005	124	0.019	0.019	0.010
242	0.007	0.011	0.004	122	0.019	0.018	0.010
240	0.007	0.011	0.005	120	0.019	0.018	0.010
238	0.008	0.011	0.005	118	0.020	0.019	0.010
236	0.008	0.010	0.005	116	0.019	0.018	0.010
234	0.008	0.012	0.005	114	0.021	0.018	0.010
232	0.008	0.011	0.005	112	0.020	0.019	0.010
230	0.008	0.011	0.005	110	0.021	0.019	0.011
228	0.009	0.011	0.005	108	0.021	0.019	0.011
226	0.009	0.012	0.005	106	0.021	0.019	0.011
224	0.010	0.012	0.005	104	0.022	0.020	0.011
222	0.010	0.011	0.005	102	0.022	0.020	0.011
220	0.010	0.012	0.005	100	0.022	0.020	0.012
218	0.010	0.011	0.005	98	0.023	0.020	0.011
216	0.010	0.011	0.005	96	0.023	0.021	0.012
214	0.011	0.012	0.005	94	0.024	0.021	0.011
212	0.011	0.012	0.005	92	0.024	0.022	0.012
210	0.011	0.012	0.005	90	0.025	0.021	0.012
208	0.011	0.012	0.004	88	0.025	0.022	0.012
206	0.011	0.012	0.005	86	0.025	0.022	0.012
204	0.012	0.012	0.005	84	0.025	0.023	0.013
202	0.011	0.012	0.005	82	0.026	0.024	0.013
200	0.011	0.012	0.005	80	0.026	0.024	0.013
198	0.012	0.012	0.005	78	0.027	0.024	0.013
196	0.012	0.012	0.005	76	0.027	0.025	0.013
194	0.013	0.012	0.005	74	0.027	0.025	0.013
192	0.012	0.013	0.005	72	0.027	0.027	0.013
190	0.011	0.013	0.005	70	0.027	0.027	0.013
188	0.011	0.013	0.005	68	0.027	0.027	0.013
186	0.011	0.013	0.005	66	0.027	0.028	0.013
184	0.012	0.014	0.005	64	0.027	0.028	0.014
182	0.012	0.013	0.005	62	0.027	0.028	0.013
180	0.012	0.014	0.005	60	0.028	0.029	0.013
178	0.012	0.014	0.005	58	0.028	0.030	0.013
176	0.012	0.015	0.005	56	0.028	0.030	0.013
174	0.011	0.014	0.006	54	0.029	0.030	0.014
172	0.012	0.015	0.006	52	0.029	0.030	0.014
170	0.012	0.015	0.005	50	0.030	0.031	0.014
168	0.013	0.016	0.006	48	0.030	0.030	0.015
166	0.013	0.016	0.006	46	0.031	0.032	0.014
164	0.013	0.016	0.006	44	0.032	0.033	0.015
162	0.013	0.016	0.006	42	0.032	0.032	0.014
160	0.014	0.016	0.007	40	0.032	0.032	0.015
158	0.014	0.017	0.007	38	0.033	0.033	0.015
156	0.014	0.018	0.007	36	0.034	0.034	0.015
154	0.014	0.018	0.008	34	0.034	0.033	0.015

Data for Figure 3-6 (Cont'):

Voltage (mV)	Current (μA) at pH 10.1			Voltage (mV)	Current (μA) at pH 10.1		
	NH_2Cl with DO	O_2-free NH_2Cl	pH 10.1 buffer		NH_2Cl with DO	O_2-free NH_2Cl	pH 10.1 buffer
32	0.035	0.034	0.015	-88	0.105	0.082	0.022
30	0.036	0.034	0.015	-90	0.107	0.083	0.022
28	0.036	0.034	0.016	-92	0.109	0.084	0.023
26	0.037	0.035	0.016	-94	0.111	0.086	0.022
24	0.038	0.036	0.016	-96	0.113	0.088	0.023
22	0.039	0.036	0.016	-98	0.116	0.089	0.023
20	0.039	0.036	0.016	-100	0.118	0.090	0.023
18	0.040	0.036	0.016	-102	0.120	0.092	0.024
16	0.041	0.037	0.016	-104	0.123	0.093	0.024
14	0.041	0.038	0.016	-106	0.126	0.095	0.024
12	0.042	0.038	0.017	-108	0.128	0.095	0.024
10	0.043	0.039	0.017	-110	0.131	0.098	0.024
8	0.044	0.039	0.017	-112	0.134	0.099	0.025
6	0.045	0.040	0.018	-114	0.136	0.100	0.025
4	0.046	0.040	0.018	-116	0.140	0.102	0.025
2	0.046	0.040	0.018	-118	0.143	0.104	0.025
0	0.047	0.041	0.018	-120	0.146	0.106	0.026
-2	0.048	0.041	0.018	-122	0.149	0.108	0.026
-4	0.049	0.042	0.018	-124	0.153	0.109	0.027
-6	0.050	0.043	0.018	-126	0.157	0.111	0.026
-8	0.050	0.043	0.019	-128	0.161	0.113	0.027
-10	0.051	0.043	0.019	-130	0.164	0.117	0.028
-12	0.052	0.045	0.019	-132	0.167	0.119	0.028
-14	0.053	0.044	0.019	-134	0.171	0.120	0.028
-16	0.053	0.045	0.019	-136	0.175	0.123	0.028
-18	0.055	0.046	0.019	-138	0.179	0.125	0.029
-20	0.055	0.047	0.020	-140	0.183	0.129	0.029
-22	0.057	0.047	0.019	-142	0.187	0.131	0.029
-24	0.058	0.048	0.020	-144	0.193	0.134	0.030
-26	0.059	0.049	0.019	-146	0.196	0.137	0.030
-28	0.059	0.049	0.020	-148	0.202	0.140	0.030
-30	0.060	0.050	0.019	-150	0.206	0.143	0.031
-32	0.062	0.051	0.019	-152	0.212	0.146	0.031
-34	0.063	0.052	0.019	-154	0.218	0.149	0.032
-36	0.064	0.052	0.020	-156	0.223	0.152	0.032
-38	0.065	0.053	0.020	-158	0.232	0.156	0.032
-40	0.065	0.054	0.019	-160	0.242	0.159	0.032
-42	0.067	0.055	0.020	-162	0.250	0.163	0.033
-44	0.068	0.056	0.020	-164	0.253	0.166	0.033
-46	0.069	0.057	0.020	-166	0.260	0.169	0.034
-48	0.070	0.058	0.020	-168	0.262	0.173	0.034
-50	0.071	0.059	0.020	-170	0.268	0.176	0.035
-52	0.073	0.059	0.020	-172	0.275	0.180	0.035
-54	0.074	0.060	0.020	-174	0.285	0.183	0.036
-56	0.076	0.061	0.020	-176	0.297	0.183	0.036
-58	0.078	0.062	0.020	-178	0.301	0.186	0.036
-60	0.079	0.064	0.021	-180	0.308	0.199	0.037
-62	0.081	0.064	0.021	-182	0.312	0.200	0.038
-64	0.083	0.066	0.021	-184	0.322	0.207	0.038
-66	0.084	0.068	0.021	-186	0.336	0.211	0.038
-68	0.086	0.069	0.021	-188	0.345	0.221	0.039
-70	0.088	0.069	0.021	-190	0.353	0.223	0.039
-72	0.090	0.071	0.021	-192	0.365	0.230	0.039
-74	0.092	0.072	0.021	-194	0.374	0.237	0.039
-76	0.093	0.073	0.022	-196	0.388	0.240	0.039
-78	0.095	0.075	0.022	-198	0.398	0.247	0.040
-80	0.097	0.076	0.022	-200	0.415	0.253	0.040
-82	0.099	0.078	0.022	-202	0.432	0.261	0.040
-84	0.101	0.078	0.022	-204	0.444	0.262	0.040
-86	0.103	0.080	0.022	-206	0.458	0.265	0.041

Data for Figure 3-6 (Cont'):

Voltage	Current (μA) at pH 10.1			Voltage	Current (μA) at pH 10.1		
(mV)	NH_2Cl with DO	O_2-free NH_2Cl	pH 10.1 buffer	(mV)	NH_2Cl with DO	O_2-free NH_2Cl	pH 10.1 buffer
-208	0.467	0.276	0.041	-306	2.000	0.972	0.120
-210	0.486	0.282	0.041	-308	2.035	0.991	0.125
-212	0.497	0.289	0.042	-310	2.045	1.021	0.129
-214	0.518	0.288	0.043	-312	2.105	1.042	0.134
-216	0.535	0.302	0.043	-314	2.125	1.071	0.138
-218	0.552	0.307	0.043	-316	2.150	1.094	0.144
-220	0.571	0.318	0.044	-318	2.195	1.119	0.150
-222	0.587	0.329	0.044	-320	2.215	1.147	0.156
-224	0.608	0.330	0.045	-322	2.255	1.171	0.163
-226	0.627	0.341	0.046	-324	2.250	1.194	0.169
-228	0.650	0.352	0.046	-326	2.300	1.213	0.176
-230	0.674	0.359	0.047	-328	2.295	1.240	0.183
-232	0.696	0.364	0.047	-330	2.345	1.256	0.190
-234	0.719	0.374	0.047	-332	2.400	1.281	0.200
-236	0.742	0.385	0.048	-334	2.380	1.305	0.213
-238	0.764	0.394	0.049	-336	2.395	1.331	0.221
-240	0.793	0.408	0.050	-338	2.410	1.353	0.233
-242	0.818	0.416	0.051	-340	2.435	1.372	0.240
-244	0.849	0.432	0.052	-342	2.445	1.393	0.250
-246	0.877	0.438	0.052	-344	2.445	1.408	0.262
-248	0.908	0.452	0.054	-346	2.505	1.424	0.274
-250	0.939	0.463	0.055	-348	2.480	1.445	0.290
-252	0.971	0.468	0.055	-350	2.505	1.457	0.300
-254	1.006	0.480	0.057	-352	2.515	1.481	0.315
-256	1.038	0.496	0.058	-354	2.520	1.493	0.331
-258	1.073	0.514	0.059	-356	2.535	1.506	0.343
-260	1.105	0.528	0.060	-358	2.530	1.519	0.358
-262	1.137	0.540	0.061	-360	2.560	1.528	0.376
-264	1.173	0.558	0.063	-362	2.550	1.542	0.394
-266	1.209	0.571	0.064	-364	2.540	1.549	0.416
-268	1.250	0.585	0.066	-366	2.590	1.558	0.430
-270	1.287	0.595	0.068	-368	2.570	1.567	0.456
-272	1.334	0.615	0.069	-370	2.580	1.581	0.477
-274	1.370	0.632	0.072	-372	2.575	1.587	0.499
-276	1.407	0.655	0.074	-374	2.585	1.591	0.525
-278	1.446	0.675	0.076	-376	2.630	1.600	0.553
-280	1.484	0.696	0.078	-378	2.600	1.607	0.579
-282	1.522	0.715	0.080	-380	2.605	1.611	0.607
-284	1.565	0.728	0.083	-382	2.620	1.613	0.638
-286	1.612	0.743	0.086	-384	2.620	1.620	0.669
-288	1.649	0.759	0.089	-386	2.630	1.626	0.699
-290	1.687	0.775	0.091	-388	2.630	1.630	0.724
-292	1.728	0.805	0.094	-390	2.630	1.642	0.758
-294	1.767	0.826	0.098	-392	2.640	1.645	0.791
-296	1.807	0.855	0.101	-394	2.620	1.649	0.820
-298	1.844	0.876	0.105	-396	2.640	1.650	0.854
-300	1.885	0.900	0.108	-398	2.625	1.649	0.888
-302	1.920	0.927	0.112	-400	2.645	1.649	0.922
-304	1.965	0.951	0.116				

Data for Figure 3-7:

Voltage	Current (μA)			Voltage	Current (μA)			Voltage	Current (μA)		
(mV)	SR=100	SR=50	SR*=20	(mV)	SR=100	SR=50	SR=20	(mV)	SR=100	SR=50	SR=20
500	-0.038	-0.056	-0.044	380	0.164	0.116	0.083	260	0.762	0.624	0.492
498	-0.035	-0.052	-0.044	378	0.170	0.123	0.088	258	0.780	0.634	0.503
496	-0.035	-0.050	-0.042	376	0.174	0.129	0.091	256	0.786	0.646	0.505
494	-0.033	-0.049	-0.041	374	0.180	0.133	0.096	254	0.797	0.652	0.515
492	-0.030	-0.048	-0.040	372	0.185	0.138	0.100	252	0.805	0.660	0.530
490	-0.027	-0.047	-0.039	370	0.193	0.144	0.105	250	0.807	0.665	0.533
488	-0.026	-0.044	-0.038	368	0.199	0.151	0.110	248	0.822	0.680	0.543
486	-0.024	-0.042	-0.036	366	0.212	0.158	0.114	246	0.828	0.687	0.542
484	-0.022	-0.039	-0.035	364	0.216	0.164	0.119	244	0.841	0.686	0.548
482	-0.020	-0.039	-0.033	362	0.223	0.169	0.125	242	0.850	0.691	0.561
480	-0.016	-0.038	-0.033	360	0.232	0.176	0.130	240	0.854	0.700	0.569
478	-0.014	-0.034	-0.031	358	0.239	0.183	0.135	238	0.869	0.712	0.573
476	-0.012	-0.032	-0.030	356	0.250	0.190	0.141	236	0.873	0.719	0.577
474	-0.009	-0.030	-0.029	354	0.254	0.197	0.147	234	0.886	0.728	0.588
472	-0.007	-0.030	-0.027	352	0.268	0.208	0.152	232	0.899	0.737	0.596
470	-0.003	-0.028	-0.025	350	0.275	0.219	0.158	230	0.901	0.741	0.603
468	0.000	-0.024	-0.024	348	0.282	0.222	0.165	228	0.907	0.752	0.600
466	0.001	-0.022	-0.023	346	0.291	0.230	0.170	226	0.915	0.759	0.606
464	0.004	-0.020	-0.021	344	0.295	0.237	0.176	224	0.926	0.768	0.618
462	0.007	-0.019	-0.019	342	0.308	0.248	0.182	222	0.935	0.773	0.629
460	0.010	-0.017	-0.018	340	0.320	0.257	0.188	220	0.943	0.778	0.636
458	0.014	-0.013	-0.017	338	0.329	0.266	0.194	218	0.950	0.786	0.632
456	0.016	-0.010	-0.015	336	0.344	0.271	0.208	216	0.961	0.796	0.643
454	0.018	-0.009	-0.014	334	0.348	0.281	0.217	214	0.967	0.802	0.654
452	0.021	-0.007	-0.011	332	0.360	0.288	0.224	212	0.978	0.810	0.667
450	0.025	-0.005	-0.010	330	0.373	0.298	0.229	210	0.986	0.820	0.664
448	0.028	0.000	-0.008	328	0.383	0.308	0.232	208	0.996	0.829	0.674
446	0.031	0.002	-0.006	326	0.398	0.323	0.244	206	1.008	0.836	0.685
444	0.033	0.003	-0.004	324	0.402	0.325	0.251	204	1.011	0.846	0.693
442	0.036	0.005	-0.003	322	0.412	0.337	0.259	202	1.019	0.857	0.702
440	0.040	0.007	-0.001	320	0.424	0.351	0.263	200	1.027	0.861	0.701
438	0.044	0.011	0.001	318	0.436	0.361	0.272	198	1.039	0.872	0.710
436	0.046	0.015	0.004	316	0.452	0.373	0.282	196	1.048	0.877	0.719
434	0.049	0.017	0.006	314	0.460	0.376	0.292	194	1.059	0.883	0.733
432	0.052	0.018	0.007	312	0.471	0.382	0.295	192	1.067	0.893	0.736
430	0.057	0.021	0.010	310	0.482	0.398	0.297	190	1.076	0.903	0.746
428	0.061	0.026	0.011	308	0.493	0.404	0.309	188	1.088	0.919	0.759
426	0.063	0.029	0.013	306	0.509	0.416	0.317	186	1.101	0.922	0.765
424	0.067	0.031	0.016	304	0.520	0.426	0.331	184	1.109	0.932	0.775
422	0.069	0.032	0.018	302	0.532	0.437	0.332	182	1.118	0.947	0.781
420	0.074	0.036	0.020	300	0.542	0.449	0.338	180	1.125	0.953	0.792
418	0.078	0.041	0.023	298	0.550	0.457	0.349	178	1.135	0.967	0.806
416	0.080	0.044	0.025	296	0.567	0.475	0.357	176	1.147	0.974	0.817
414	0.085	0.046	0.028	294	0.578	0.481	0.367	174	1.158	0.980	0.826
412	0.088	0.048	0.030	292	0.585	0.486	0.367	172	1.169	0.992	0.826
410	0.094	0.052	0.033	290	0.600	0.493	0.375	170	1.177	0.997	0.843
408	0.097	0.058	0.036	288	0.614	0.501	0.387	168	1.193	1.010	0.853
406	0.100	0.061	0.039	286	0.627	0.512	0.397	166	1.204	1.018	0.867
404	0.105	0.064	0.042	284	0.638	0.522	0.405	164	1.215	1.032	0.870
402	0.108	0.067	0.044	282	0.646	0.530	0.409	162	1.229	1.043	0.879
400	0.114	0.071	0.048	280	0.660	0.540	0.417	160	1.239	1.054	0.891
398	0.119	0.076	0.050	278	0.673	0.554	0.427	158	1.253	1.070	0.904
396	0.122	0.080	0.054	276	0.681	0.562	0.438	156	1.261	1.082	0.910
394	0.128	0.084	0.057	274	0.689	0.569	0.435	154	1.273	1.086	0.917
392	0.131	0.087	0.061	272	0.701	0.578	0.444	152	1.286	1.104	0.931
390	0.138	0.092	0.063	270	0.710	0.588	0.457	150	1.298	1.108	0.948
388	0.143	0.099	0.067	268	0.724	0.595	0.467	148	1.314	1.124	0.955
386	0.147	0.103	0.071	266	0.735	0.602	0.473	146	1.327	1.135	0.966
384	0.152	0.107	0.075	264	0.744	0.608	0.475	144	1.337	1.144	0.975
382	0.157	0.112	0.079	262	0.754	0.616	0.488	142	1.349	1.163	0.985

* SR: Scan rate (mV/s).

Data for Figure 3-7 (Cont'):

Voltage	Current (μA)			Voltage	Current (μA)			Voltage	Current (μA)		
(mV)	SR=100	SR=50	SR=20	(mV)	SR=100	SR=50	SR=20	(mV)	SR=100	SR=50	SR=20
140	1.367	1.174	1.002	26	2.275	1.945	1.638	-88	2.635	2.195	1.970
138	1.384	1.187	1.010	24	2.225	1.910	1.643	-90	2.645	2.265	1.930
136	1.398	1.204	1.017	22	2.265	1.970	1.654	-92	2.605	2.210	1.940
134	1.409	1.213	1.033	20	2.280	1.950	1.664	-94	2.640	2.200	1.965
132	1.422	1.225	1.045	18	2.315	1.935	1.671	-96	2.615	2.240	1.955
130	1.434	1.239	1.055	16	2.345	1.960	1.683	-98	2.655	2.235	1.960
128	1.453	1.252	1.067	14	2.355	1.970	1.690	-100	2.645	2.195	1.970
126	1.466	1.263	1.073	12	2.380	1.995	1.701	-102	2.650	2.200	1.920
124	1.478	1.275	1.087	10	2.370	2.045	1.704	-104	2.615	2.215	1.940
122	1.495	1.285	1.100	8	2.385	1.975	1.710	-106	2.610	2.235	1.965
120	1.510	1.305	1.114	6	2.370	1.985	1.724	-108	2.600	2.250	1.945
118	1.529	1.320	1.122	4	2.380	2.060	1.730	-110	2.640	2.220	1.990
116	1.541	1.333	1.134	2	2.390	1.965	1.735	-112	2.640	2.220	2.000
114	1.557	1.346	1.146	0	2.400	2.020	1.742	-114	2.645	2.250	1.955
112	1.571	1.361	1.160	-2	2.455	2.075	1.747	-116	2.660	2.230	1.965
110	1.587	1.375	1.171	-4	2.470	2.070	1.754	-118	2.590	2.190	1.935
108	1.607	1.389	1.182	-6	2.490	2.055	1.760	-120	2.585	2.245	1.925
106	1.618	1.405	1.192	-8	2.440	2.055	1.772	-122	2.590	2.235	1.980
104	1.631	1.415	1.210	-10	2.440	2.050	1.775	-124	2.620	2.210	2.010
102	1.651	1.425	1.220	-12	2.465	2.085	1.788	-126	2.660	2.270	2.000
100	1.664	1.445	1.230	-14	2.500	2.105	1.788	-128	2.590	2.230	2.005
98	1.688	1.457	1.240	-16	2.520	2.045	1.795	-130	2.620	2.245	1.970
96	1.699	1.470	1.252	-18	2.540	2.095	1.801	-132	2.610	2.250	1.935
94	1.717	1.486	1.272	-20	2.515	2.150	1.807	-134	2.625	2.200	1.985
92	1.730	1.496	1.278	-22	2.530	2.075	1.812	-136	2.600	2.240	1.990
90	1.750	1.519	1.293	-24	2.500	2.120	1.815	-138	2.595	2.265	2.000
88	1.772	1.534	1.304	-26	2.515	2.160	1.820	-140	2.580	2.215	2.040
86	1.785	1.540	1.315	-28	2.545	2.150	1.823	-142	2.600	2.230	2.005
84	1.801	1.561	1.331	-30	2.555	2.085	1.832	-144	2.580	2.265	1.990
82	1.812	1.571	1.342	-32	2.575	2.125	1.838	-146	2.615	2.225	1.985
80	1.828	1.583	1.353	-34	2.575	2.125	1.844	-148	2.610	2.210	1.950
78	1.853	1.598	1.364	-36	2.580	2.170	1.846	-150	2.605	2.230	1.965
76	1.866	1.607	1.381	-38	2.570	2.170	1.852	-152	2.590	2.230	2.005
74	1.885	1.624	1.389	-40	2.590	2.125	1.861	-154	2.545	2.250	2.015
72	1.898	1.638	1.404	-42	2.570	2.195	1.863	-156	2.555	2.235	2.030
70	1.930	1.654	1.413	-44	2.560	2.175	1.867	-158	2.590	2.220	2.025
68	1.930	1.667	1.423	-46	2.580	2.120	1.866	-160	2.635	2.255	1.985
66	1.975	1.682	1.438	-48	2.585	2.175	1.877	-162	2.600	2.230	1.980
64	1.995	1.696	1.447	-50	2.640	2.200	1.880	-164	2.590	2.205	1.995
62	1.995	1.705	1.456	-52	2.615	2.170	1.882	-166	2.540	2.225	2.000
60	2.025	1.723	1.467	-54	2.625	2.145	1.886	-168	2.545	2.250	2.030
58	2.050	1.730	1.479	-56	2.590	2.205	1.908	-170	2.565	2.230	2.020
56	2.030	1.742	1.491	-58	2.605	2.190	1.872	-172	2.565	2.230	2.020
54	2.030	1.758	1.502	-60	2.590	2.210	1.900	-174	2.590	2.225	2.020
52	2.050	1.767	1.510	-62	2.630	2.195	1.891	-176	2.550	2.245	1.990
50	2.070	1.779	1.527	-64	2.635	2.170	1.880	-178	2.575	2.265	1.995
48	2.120	1.793	1.535	-66	2.650	2.245	1.920	-180	2.650	2.225	2.000
46	2.125	1.808	1.544	-68	2.660	2.190	1.917	-182	2.580	2.215	2.020
44	2.165	1.818	1.553	-70	2.630	2.160	1.945	-184	2.540	2.235	2.040
42	2.150	1.832	1.562	-72	2.600	2.240	1.945	-186	2.535	2.230	2.035
40	2.165	1.847	1.573	-74	2.610	2.230	1.925	-188	2.545	2.210	2.030
38	2.160	1.857	1.579	-76	2.630	2.200	1.950	-190	2.520	2.245	2.010
36	2.175	1.866	1.592	-78	2.660	2.200	1.920	-192	2.550	2.255	2.010
34	2.215	1.874	1.604	-80	2.645	2.190	1.910	-194	2.575	2.235	2.000
32	2.220	1.886	1.607	-82	2.630	2.195	1.925	-196	2.580	2.230	2.030
30	2.260	1.902	1.621	-84	2.645	2.240	1.920	-198	2.555	2.210	2.025
28	2.250	1.890	1.625	-86	2.640	2.190	1.920	-200	2.530	2.230	2.025

Data for Figure 3-8:

Time (s)	Current signal (pA)							Time (s)	Current signal (pA)						
	C0*	C1*	C2*	C3*	C4*	C5*	C6*		C0	C1	C2	C3	C4	C5	C6
1	12.4	15.6	21.8	25.6	43.6	59.4	74.3	57	12.5	15.6	21.1	25.8	42.4	63.2	77.7
2	13.2	16	22.3	26.9	43.5	60.3	74.5	58	13	14.6	21.5	26	42.8	63.6	77.6
3	14.1	13.1	22.3	26.9	43.7	60.4	74.9	59	13.3	14.9	22	26.2	42.6	63.5	77.6
4	13.6	16.5	20.4	26.7	43.4	60.8	74.8	60	12.8	15.7	21.6	25.8	43.3	63.2	77.6
5	12.8	15.8	22.9	27.2	42.7	61.1	74.9	61	12.7	15.2	21.7	25.7	43.7	64.4	77.3
6	14.3	14.3	21.8	26.6	42.9	61.4	75.4	62	13.9	14.9	21.7	26.2	44.7	64.5	77.2
7	13.1	16.1	21.1	26.6	43.7	61.5	75.3	63	12.5	16	21.9	25.9	45.8	64.5	77.1
8	13	15.7	22.5	28	43.6	62	75.3	64	11.7	15.3	21.8	24.3	46.9	64.5	77
9	14.1	14.3	21.4	26.7	43.5	61.8	76.2	65	13.6	14.7	22.1	25.9	47.6	64.3	77.1
10	14.3	16	21.8	26.3	43.6	62.3	76.4	66	12.6	16.5	21.7	25.6	46.3	64	77.1
11	13.3	16.8	22.4	27.5	43.5	62.7	76.3	67	11.1	15.2	21.1	25.2	46.2	64	77.1
12	12.2	15.3	21.7	27	43.3	62.7	76.4	68	12.9	14.9	22	26.8	44.7	63.5	77
13	16.6	15.6	21.5	26.4	42.6	62.9	75.3	69	12.5	16.6	21.8	25.3	44	63.4	77.3
14	14.7	16.5	23	27.4	43.2	63	76.5	70	10.9	15.3	21.8	25.9	43.7	63.7	77.7
15	14	14.9	21.4	26.9	42.7	62.8	76.6	71	13.4	15.5	21.9	25.9	43.3	63.8	77.6
16	13.7	15.1	21.1	25.2	42.6	63	76.6	72	13	17.1	21.7	25.2	43.3	63.9	77.8
17	10.5	16.5	22.4	24.2	42.8	63.1	76.4	73	11.8	15.5	21.5	25.7	43.3	63.5	77.5
18	13.9	15.2	21.4	25.1	42.8	63.3	76.2	74	12	14	21.6	25.6	42.5	63.3	77.2
19	14.2	15	21.4	25.4	43.2	63.6	75.8	75	13.9	17.3	21.6	25	42.4	63.5	77.4
20	18.3	16.6	22.4	26.6	42.8	63	75.4	76	11.9	15.2	21	25.7	42.9	64	77.6
21	14.7	15.3	21.2	25.9	43.1	63.1	75.1	77	12	14.8	21.7	24.9	42.2	63.8	77.2
22	13.9	15.7	20.9	25.9	42.3	63.3	76.8	78	13.4	17.3	21	24.3	42.8	64	78.3
23	14.7	16.7	22.5	26.5	42.6	63.1	75.8	79	11.7	14.5	21.8	24.8	44	64.5	78
24	13.5	15.8	21.4	26.3	43.1	63.2	76	80	11	15.5	21.5	25.1	44	64.2	77.6
25	13.4	15	22.4	25.9	43.2	63.2	75.9	81	12.8	16.5	20.1	23.9	44.9	64.5	77.6
26	14.4	16.5	21.9	26.7	43.9	63.4	75.7	82	11.5	15.2	22.2	24.8	44.6	64.8	77.6
27	13.9	15.2	21.8	26.5	42.9	63.1	76	83	11.6	15	21	25.1	44.2	64.3	77.5
28	13	14.7	21.8	25.3	43.5	63.2	76.3	84	12.6	16.4	20.7	24.9	44.1	64.8	77.2
29	13.9	16.8	22.3	26.2	43.1	63.1	76.2	85	12.8	14.9	21.7	25.6	44.4	64.9	77.6
30	13.7	15.4	21.7	25.9	43.2	63.1	76.4	86	11.9	15.5	20.8	25.2	43	65.1	77.5
31	12.5	14.4	20.7	25.5	42.8	63.4	76.5	87	12.8	16.3	20.7	25.6	42.8	65	77.5
32	14	16.9	22.1	25.8	42.6	62.8	76	88	13.8	15.2	22.1	25.7	42.3	65.3	77.7
33	14.2	15.3	21.5	25.9	43	62.7	76.1	89	12.7	15.3	21.1	25.9	42.2	65	77.4
34	13.6	13.5	20.8	25.9	42.9	62.9	76	90	12.6	16.1	21.2	25.1	42.9	64.8	76.8
35	13.7	17.1	21.8	27.1	42.6	62.1	75.8	91	13.3	14.9	22.4	25.6	43	65.1	77.7
36	15.4	14.9	21.5	26.4	42.1	61.4	76.3	92	12.9	15.1	21	25.5	42.3	64.7	77
37	13.7	14.3	21.5	26.2	42.2	61.3	77.5	93	11.5	15.9	20.7	25.3	42.5	64.7	77.2
38	13.1	17	21.8	26.9	42	61.4	77.3	94	13.2	15	22.1	25.6	43.1	65.1	77.7
39	14.5	14.5	21.4	26.2	42	61	77.1	95	12.6	15.6	21.2	25.4	42.8	65.2	77.8
40	12.9	14.5	20.7	26.1	41.7	61.1	77	96	12.4	16	21.1	25.4	42.9	64.7	77.7
41	11.7	16.9	22	27	42.5	61.5	77	97	12.9	15.1	22.3	25.6	43.8	65.1	77.4
42	13.4	15.2	21.2	26	42.7	61.8	77.2	98	13.5	15.5	21	25.5	43.7	65.1	77.8
43	12.1	13.8	21.6	26.3	42.8	61.5	77.1	99	12.3	15.5	21.2	25.2	44.2	64.6	77.9
44	11.7	17.9	21.9	26.6	43.6	61.8	77.2	100	12.2	14.7	21.8	25.3	46.1	64.9	77.4
45	13.1	14.8	21.1	25.8	43.4	61.7	77.3	101	13.9	15.7	21.1	25.5	47.6	65.3	78.1
46	13.2	14.1	21.2	25.9	43.4	61.9	77.5	102	11.9	16.3	20.6	24.9	48.1	65.2	77.9
47	12.1	17.4	21.6	26.7	42.4	62.4	77.6	103	11.7	15.1	21.4	25.2	48	65	77.8
48	13.1	15.1	21	25.9	42.5	62.5	77.6	104	13.4	15.9	21.3	25.7	47.2	65	77.8
49	14.4	14.8	20.7	26.1	42.8	62.8	77.8	105	12.9	16.5	21.2	24.7	46.7	64.8	77.8
50	12.9	17.2	21.9	26.5	42.6	62.8	77.8	106	11.5	14.5	21.7	25.6	45.8	64.9	77.5
51	12.8	14.9	21.2	26.2	42.6	62.7	77.6	107	12.8	15.5	21.1	25.8	45.8	65.3	77.5
52	13.9	14	21.4	26.1	42.6	63	78	108	12.8	15.9	20.6	25.3	45.9	64.5	77.7
53	13	17	21.7	26.2	42.6	62.8	78	109	11.8	15.2	21.9	25.8	45.8	65	78.1
54	12	15	21.2	25.9	42.5	62.9	77.6	110	12.7	14.9	21.4	26.1	45.7	65	78
55	13.4	14	21.3	25.4	42.4	63	77.5	111	13.5	15.9	21.2	25.8	45.6	65.1	78.5
56	13.2	16.2	21.9	26.3	41.8	63.2	77.9	112	11.9	14	21.8	25.8	46	65.4	78

Data for Figure 3-8 (Cont'):

Time (s)	Current signal (pA)							Time (s)	Current signal (pA)						
	C0	C1	C2	C3	C4	C5	C6		C0	C1	C2	C3	C4	C5	C6
113	12.3	15.5	21.3	25.6	45.7	65.1	77.7	169	13.7	16.2	22	26.3	44.6	66.5	97.6
114	14.2	16.3	21.2	25.1	45.5	65.2	77.8	170	13.8	15.3	22.8	25.8	45.4	66.8	99.6
115	12.5	13.9	21.8	25.8	45.3	65.3	78	171	12.4	17.1	23.3	27	45	66.7	101.4
116	11.5	15.5	21.4	26.2	45.3	65.4	77.8	172	14	16.1	22.3	26.3	45.3	66.3	102.2
117	13.6	16.7	21.2	25.3	45.4	65.8	77.8	173	14.4	14.4	22	25.5	46	67	102.1
118	12.5	15.4	21.8	26.7	44.8	65.4	77.9	174	13.1	16.4	21.8	27	45	66.8	100.9
119	11.3	14.5	21.1	25.8	45.3	65.5	77.8	175	13.9	15.4	21.4	25.8	45.7	66.3	99.3
120	12.6	16.9	21.4	26.2	46	65.2	77.5	176	15	14.9	21.8	25.7	45.9	66.4	97.1
121	12.1	15.1	21.7	26.8	47.1	65.1	77.9	177	13.8	15.8	21.4	26.8	45.9	66.7	95.3
122	11.8	14.7	21	25.8	47.4	65.2	78.2	178	13.5	15.6	21.4	26.4	46.2	66.8	93.9
123	12.7	17.3	21.7	26.6	46.7	65.2	77.5	179	15	14.2	22.5	26.1	47.8	66.8	93
124	14	15.3	21.7	26.6	45.7	65.1	78.9	180	14.1	16.7	21.5	27.1	48.7	66.4	91.8
125	13.2	15.5	21	26.5	46.1	65.4	78.6	181	12.9	16.8	21.3	26.3	49.1	66.6	91.1
126	12.7	17.5	21.1	25.7	46.1	65.6	78.3	182	14.4	14.6	22.5	25.4	48.2	66.9	90.3
127	14.4	15	21.4	26.4	44.7	65	78.8	183	14.1	16	21.3	26.8	47	66.9	89.8
128	12.6	14.7	21.2	26	44.9	65.1	78.2	184	13.6	16	21.6	26.2	46.8	66.6	88.8
129	12.2	17.2	21.8	26.1	44.7	65.3	78.2	185	14	15.4	22.1	25.6	47.1	66.5	88.6
130	13.7	15	21.9	26.5	44.6	65.2	78	186	14.8	15	21.5	26.4	48.4	66.7	88.3
131	13.3	14.3	21.1	26	44.8	65.2	78.2	187	13.3	16.8	21.8	26	49.2	66.6	87.8
132	12.1	17	22.1	25.9	45	65.7	78	188	13.9	15.6	22.2	25.7	49.6	66.5	87.8
133	13.6	15.5	21.9	26.9	44.4	65.6	78.1	189	15.1	15.8	21.7	26.5	49.5	66.2	88.1
134	14	14.9	20.9	26.1	45.4	65.9	78	190	13.8	17.5	21	26	49.5	66.5	87.5
135	13.2	17.1	21.4	26.1	45.2	66.5	78.4	191	13.8	15	22.1	26.1	49.2	66.5	87.6
136	13.8	16	21.3	26.4	45.5	65.4	78.5	192	15.7	15.4	21.3	26.7	47.5	66.2	87.3
137	14.2	15.1	21.2	26.5	45.5	66.2	78	193	14.2	16.8	21.2	26.3	46.3	66.4	86.6
138	13.2	17.4	22.3	26	45.2	66.3	78.2	194	13.4	15.4	21.8	27	46.2	66.6	86.7
139	12.9	15.4	21.2	26.7	45.3	65.8	78.5	195	14.7	15	20.8	26.1	46.4	66.7	86.9
140	15	15.1	20.8	26.4	44.7	66.4	78	196	14.7	17.2	21.6	25.9	45.8	66.5	88.1
141	12.9	17.1	22.2	25.7	45	66.4	77.9	197	13.4	15.8	21.7	27.5	45.5	66.7	87.5
142	12.4	15.4	21.3	26.5	44.7	66.2	78.3	198	14	14.3	21.6	26.7	45	66.7	87
143	13.6	14.8	21.1	25.8	45.4	66.1	78.5	199	14.3	16.8	22	26	45.4	66.7	87
144	14.1	17.2	22	25.9	44.6	66.8	78.1	200	13.6	15.7	22.7	27.1	45.2	66.9	86.6
145	12.7	15.9	21.5	26.3	44.7	66.4	78.4	201	13.6	14.5	22	26.1	45.4	66.7	86.4
146	13.6	14.5	20.7	25.7	44.1	66.5	78.7	202	14.7	15.5	21.9	26.2	44.9	66.9	86.6
147	14.2	17.7	22.3	25.9	44.2	66.7	78.4	203	13.9	15.4	21.7	27.1	45	67.1	87.3
148	12.7	15.3	21.5	26.7	44.9	66.8	78.4	204	13	14.6	21	26.2	45.5	66.5	88.5
149	13.4	15	20.5	25.6	44.9	66.7	78	205	14.9	15.6	21.5	26.2	45.1	66.8	89.9
150	14.5	17.5	22	25.5	44.5	66.5	77.5	206	13	16	21.8	27	45.5	66.6	91.5
151	12.6	15.3	21.1	26.6	44.7	66.9	78.1	207	12.5	14.7	20.7	26.1	45.4	66.9	93.3
152	12.7	15.2	21	26.1	44.8	66.6	79.1	208	13.6	15.1	21	26.2	46.3	67.1	95.6
153	14.7	17.2	22	25.8	44.6	66.8	80	209	14	16.3	21.4	26.8	46	66.9	98.7
154	13.3	15.4	21.5	26.2	44.9	66.7	79.7	210	12.5	14.2	21.1	26.5	46.3	66.8	101.2
155	11.5	14.4	21.3	26	44.8	66.9	79.8	211	13.1	14.1	21	26.2	46.5	67.1	103.1
156	13.8	17.7	22.1	26.2	44.5	66.6	80	212	14.5	15.9	21.3	27.2	46.5	66.7	105.1
157	12.7	15.2	21.2	26.8	44.5	66.7	80.3	213	12.8	14.8	21.1	26.8	46.8	67.1	106.3
158	12.1	14.6	21	26	44.5	66.7	80.6	214	12.8	14	20.9	26.5	47.1	67.1	107.2
159	13.1	17.4	22.1	26.4	43.4	67	80.9	215	14.3	16.6	21.4	26.9	47.4	66.7	108.4
160	13.6	14.9	21.1	26.5	43.7	67	81.1	216	12.8	16	21	26.5	47.2	67	109.1
161	13	14.8	21.2	25.7	44.3	66.7	81.2	217	12.1	13.6	20.7	26.9	47.7	67.1	109.9
162	13.3	17.8	22.1	26.2	44.3	67.1	81.3	218	13.7	17.3	21.1	27.5	47.3	66.9	110.2
163	14.5	14.7	21.1	25.9	44.4	66.8	81.7	219	13.3	15	21	27	46	67	110.4
164	12.9	14.6	21.4	26.4	44.9	66.9	82.9	220	11.5	14.6	21.1	26.9	45.7	67.1	110.6
165	13.3	17.3	21.7	26.7	44.8	67	84.8	221	13.1	17.5	21.5	27.3	45.7	66.6	110.9
166	14.6	15.5	21	26.5	45	66.6	87.3	222	13.3	15.4	21.1	26.3	46.3	67.1	111.5
167	13	14.8	21.6	26.3	45.4	66.5	91.2	223	12.7	14.9	21.5	27.1	46.4	67.3	112.2
168	12.4	17.5	21.6	25.9	44.7	66.6	94.3	224	12.8	17.1	21.5	26.5	46.1	67.1	112.6

Data for Figure 3-8 (Cont'):

Time (s)	Current signal (pA)							Time (s)	Current signal (pA)						
	C0	C1	C2	C3	C4	C5	C6		C0	C1	C2	C3	C4	C5	C6
225	14.2	15.9	21.2	26.1	46.1	66.9	113.7	281	13.5	16.6	22.4	27.4	48.6	67.9	106.3
226	12.9	13.8	21.5	26.5	46.3	67.5	113.9	282	13.3	16.2	22.1	27.1	47.5	68	108.9
227	12.9	16.1	21.5	27	46.4	67.4	113.6	283	15.4	15.7	21.6	27.8	48	68.1	111
228	14.5	16	20.9	26.9	46.3	67.4	112.8	284	13.3	16.7	21.9	26.9	47.8	68	113.4
229	12.7	15.3	21.1	27.4	46.4	67.3	110.6	285	13.5	15.4	21.7	27.1	47.4	67.9	115.5
230	12.2	16	21.7	28.2	46.7	67.3	108.6	286	15	15.9	22	27.2	47.6	68.1	116.7
231	14.6	16	20.8	27.6	46.3	67.5	106.1	287	14.4	17.4	22.1	27.1	47.6	68	118.9
232	14	15.7	21.8	27.6	46.4	67.1	103	288	13.5	16	21.9	26.9	47.6	68.2	120.4
233	12.8	15.8	21.1	27.5	46.4	68	100.3	289	14.6	15.7	21.7	27.2	47.8	68.3	122.2
234	13.7	15.6	20.5	27	46.3	67.8	102.6	290	14.6	17	22	27.1	48	68.3	123.6
235	14.5	15.2	21.3	27.5	46.6	67.9	103.9	291	14.1	16.3	21.8	25.9	47.6	68.2	124.5
236	12.9	16	21.4	26.4	46.9	67.5	102.3	292	15.1	15.2	21.8	27.3	47.8	68.7	125.3
237	13.8	16.5	20.3	26.4	47.2	67.9	103.4	293	15.7	17.6	22.1	26.7	47.4	68.3	126.6
238	15.1	15.1	21.7	26.5	46.3	67.7	103.5	294	14.2	15.8	21.7	26.6	46.5	68.4	127.1
239	14.3	14.9	21.2	26.9	46.6	67.6	103.4	295	15.2	15.3	21.6	27	48.7	68.2	127.9
240	14.1	16.4	20.6	26.2	47.2	67.6	103.7	296	15.9	17	21.9	26.6	48.1	68.1	128.1
241	15.1	15.2	22	26.7	46.2	67.9	104.2	297	15.1	15.9	21.8	26.4	47.9	67.8	129.5
242	14.1	14.9	21.5	26.7	46.6	68	105.3	298	14.6	14.7	21	27	48.1	67.4	129.5
243	13.4	16.6	20.6	26.2	46.7	68	105.8	299	15.7	16.2	22	26.7	47.7	67.5	129.8
244	15	15.7	21.2	27	46.2	67.9	105.9	300	14.8	15.7	21.9	27.3	47.6	67.6	130.1
245	14.2	15.7	21	26.7	46.4	68	105.2	301	14.2	14.1	21.2	28.2	47.6	67.9	130.1
246	13.9	16.5	20.3	26.7	46.7	68.1	104.3	302	15.5	16.1	22.8	27.4	47.7	67.7	129.5
247	13.8	15.7	21	26.9	46.4	67.9	104	303	14.5	16.3	21.9	27.9	47.3	67.8	129.5
248	14.7	14.2	20.8	27	46.8	68.3	104	304	13.5	14.8	22	27.6	45.7	67.3	129
249	13.9	17	20.6	26.6	48.2	68	105.3	305	14.7	15.9	22.5	27.1	47.2	67.6	127.8
250	14	15.2	21.6	26.9	50.4	68	105.5	306	14.2	16.8	21.7	27.7	50.1	67.4	126.7
251	15	15	21.6	27	52.2	68	105.7	307	13.5	15.8	21.3	27.8	47.6	67.6	126.2
252	13.8	17.1	20.9	27	52.1	68.1	106	308	14.2	15.4	22.5	27	47.2	67.3	126
253	13.2	16.2	21.2	27.9	51	68.1	106.4	309	14.6	16.8	21.9	26.8	46.9	67.2	126.7
254	14.5	15	21.5	27	49.5	68.2	106.8	310	13.4	16	21.1	27.3	46.8	67.1	126.6
255	13.2	17.2	20.9	26.5	48.9	68.2	107.7	311	14	16.2	22.5	26.7	47.1	66.8	126.9
256	12.6	16.2	21.5	27.8	48	68.3	108.3	312	15.1	17.5	21.8	26.5	46.8	67.5	127.3
257	14.3	14.8	21.8	26.8	47.5	68.3	108.9	313	13.5	16.1	21.5	26.8	46.6	67.7	127.4
258	13.9	16	21.4	26	47.2	68.3	109.5	314	13.9	15	22.5	26.4	46.9	67.5	126.6
259	12.5	15.8	21.6	27.2	47.4	68.2	110.3	315	15.1	17.6	21.6	27.3	46.9	67.5	126.3
260	13.5	14.4	21.9	26.8	46.9	68.4	111.1	316	13.4	16	20.8	27.1	47	67.4	125.6
261	13.8	15.9	21.1	26.3	47.4	68.4	111.6	317	12.6	14.9	22	27.3	47.2	67.3	125.6
262	12.9	16.5	20.6	27.7	47.4	68.4	112.3	318	14.7	15.6	22.1	26.6	46.9	67.2	124.8
263	13.1	15.8	21.8	26.4	47.1	68.3	112.9	319	13.2	15.9	21.3	27.1	47	67.1	124.4
264	14	15.8	21.8	26	47	68.5	113.5	320	12.2	14	22.1	26.7	47.3	67.2	123.8
265	12.9	17.1	21.3	27.5	47.1	68.2	114.5	321	14	15.1	21.7	27.1	47.2	66.6	122.9
266	13.1	15.3	22.6	26.8	46.9	68.7	115.3	322	13.5	16.1	21.5	27.2	47.5	66.9	122.5
267	14.8	15.2	22.2	26.6	47.1	68.4	115.8	323	12.7	14.8	22.3	26.2	47.6	66.9	122.9
268	13.2	17.1	22.6	27.6	46.9	68.2	114.6	324	13.6	15.5	21.8	27.2	48.2	66.9	122.8
269	12.5	15.8	22.8	26.9	47.2	68.5	112.8	325	13.3	16.2	21	26.7	47.8	67	122.5
270	14.4	14.1	22.3	26.9	47.1	68.4	111.1	326	12.7	15.7	22.2	26.7	47.8	66.9	122
271	12.7	16.9	22.4	27.8	47.7	68.2	109.4	327	13.5	14.6	22	26.5	47.9	67.4	122
272	12.2	15.9	23	26.9	47	68.5	109.7	328	13.7	16.9	21.8	27	47.5	67.4	121.4
273	13.6	14.2	22.4	26.8	46.8	68.6	109.9	329	12.5	15.6	21.1	27.6	48.3	67.1	121.3
274	14	16.9	22.5	28.1	47.5	68.2	111.2	330	13.1	15.4	21.9	27.8	48	67.1	120.5
275	12.1	15.7	22.7	27	46.9	68.1	112.6	331	14.8	17.6	21.6	27.3	47.8	67	120.3
276	13.6	14.2	21.8	26.8	46.8	68.2	114.1	332	13.1	16.1	21.1	26.3	47.8	66.7	119.3
277	13.7	15.8	22.3	27.7	47.7	68.3	113.3	333	13	15.8	22.1	28.5	48	66.7	119.3
278	13.3	16	22.4	27	48.6	68	110.4	334	14.6	17.6	21.8	28.3	47.7	66.3	119.3
279	14	15	21.5	26.7	48.5	68	105.5	335	12.7	15.9	21.4	28.8	47.4	66.8	118.7
280	14.6	15.8	21.7	28	48.8	67.9	103.3	336	12.6	15	22.6	29.4	47.8	67.3	118.6

Data for Figure 3-8 (Cont'):

Time (s)	Current signal (pA)							Time (s)	Current signal (pA)						
	C0	C1	C2	C3	C4	C5	C6		C0	C1	C2	C3	C4	C5	C6
337	14.6	16.1	21.8	28.8	47.6	66.9	118.7	393	12.9	17.1	22.2	28.7	48.6	68.4	133.5
338	13.5	16.4	21.2	29	48	67.1	119.2	394	14.8	16.4	23.1	28	49	68.4	133.6
339	12.3	14.8	23.1	29.1	47.9	66.8	118.6	395	13.3	16.6	22.6	27.8	48.8	68.7	133.5
340	14.3	16	22.5	28.3	47.6	67	119.2	396	12.9	17.2	22.1	28.4	48.7	68.7	134.2
341	13.5	16.9	22	27.6	47.2	66.7	120	397	14.2	16.3	23.3	27.9	48.2	68.3	134.1
342	12.7	15.5	23	29	47.4	67.3	120.2	398	13.4	15.3	22.2	27.8	49	68.4	134.7
343	13.7	16.3	22.8	27.9	47.9	67.3	120.4	399	12.3	17.1	22	28.6	48.5	68.3	135.3
344	14.4	16.4	22.4	27.8	47.6	67.2	121.3	400	13.8	15.7	23.1	28.6	48.6	68.4	135.8
345	12.4	15.8	22.1	28.5	47.3	67.8	121.7	401	13.8	15.2	22.3	28.8	48.7	68.4	135.6
346	13.7	16.4	22.7	27.7	48.1	67.7	122.7	402	12.8	17.2	22.1	29.7	48.5	68.2	135.8
347	14.5	17.3	22	27.8	48.2	67.5	123.3	403	14.2	16	23	28.8	49.4	68.4	135.8
348	13	16.2	21.5	28	47.7	67.6	124.3	404	13.8	16.1	22.7	28.9	49	68.4	135.8
349	13.6	16.3	22.4	27.9	48.7	68.1	125.7	405	13.1	17.8	21.8	29.2	48.5	68.4	135.9
350	14.9	16.9	21.6	27.2	47.5	68.3	126.2	406	13.8	16.2	23	28.9	49.1	68.4	136
351	13.2	16.1	21.7	28.4	47.8	68.3	127.2	407	14.6	15.3	22.3	28.3	48.9	68.2	135.9
352	13	16.1	23.1	27.4	48.8	68.4	128.2	408	13.1	17.3	22.2	28.6	48.5	68.3	135.9
353	15	17.1	22	27	48.3	68.9	128.5	409	13.3	16.2	22.8	28.4	48.4	68.5	136.1
354	13.1	16.3	21.2	28	48.1	68.9	128.6	410	15	15.8	22.1	27.7	49.4	68.4	136.3
355	12.8	16.2	21.7	27.3	48.1	68.6	129	411	13.4	17.3	22.3	28.8	48.6	68.6	136.3
356	14.6	17.1	21.7	27.3	48.6	68.9	129.7	412	13.3	16.4	22.6	27.6	49.5	68.6	136.4
357	13.4	16.7	21.5	28.2	48.1	68.8	130.4	413	15.2	15.9	22.2	27.9	49.5	68.6	136
358	12.7	16.2	22.3	27.7	48.2	69	130.8	414	13.4	17.4	22.1	28.1	48.9	68.6	135.9
359	13.8	17.5	22.3	26.8	48.4	69.1	131	415	13.5	16.1	22.8	27.5	49.5	68.6	136.2
360	13.7	16	21.8	27.8	48.2	69.3	131.4	416	15.2	15.3	21.9	27.4	50.1	68.7	135.3
361	12.9	16	22.4	27.4	48.2	69.1	132.3	417	13.7	17.7	21.5	27.4	50.2	68.6	134.7
362	13.5	17.1	22.4	27.3	48.6	69.2	132.4	418	12.4	16.5	22.8	26.9	50.5	68.6	134.8
363	14.7	15.8	22.3	27.6	48.4	69.3	132.6	419	14.8	15.8	22.4	27.1	50.6	68.4	134
364	13.1	16	22.2	27.2	47	69.4	133.4	420	13.5	16.9	22.2	27.6	51.1	68.3	133.1
365	13.3	16.6	22.6	27.3	48.3	69.5	133.4	421	12.6	16.5	22.9	27.6	50.7	68.8	133.1
366	14.8	15.4	22.3	27.5	48.5	69.6	133.7	422	14.2	15.5	22.1	28.7	50.6	68.7	132.6
367	13.2	15	22.8	27	48.3	69.8	133.8	423	13.7	17	21.8	29.4	50.3	68.3	132.3
368	13.1	16.9	22.8	26.3	48.6	69.2	134.3	424	12.9	16.9	23.2	29.1	49.4	68.8	131.5
369	15	15.6	22.4	27.5	48.5	69.2	134.3	425	13.9	15.3	22.5	30	50	68.4	131.5
370	13.4	16	22.6	27	48.6	69.3	134.2	426	13.8	17	23	29.4	50	68.8	131.2
371	13.2	16.9	22.6	26.8	48.9	69.4	134.4	427	13.3	16.4	23.2	29	49.3	68.5	130.6
372	15.2	15.8	22.3	27.9	48.3	69.4	135.3	428	13.8	15.1	22.6	29.3	49.3	68.9	129.9
373	13.8	16.2	22.8	27.3	49.4	69.7	135.1	429	14.9	16	23.1	29.3	50.2	68.6	129.7
374	12.8	17.4	23.1	27.1	48.7	69.3	135.3	430	13.3	16.5	23.2	28.7	48.9	68.2	129.6
375	14.7	15.8	23	28.1	48.5	69.6	135.7	431	13.8	14.9	22.8	28.6	49.5	68.4	129.3
376	13.2	15.9	23.1	27	49.3	69.3	136	432	15.3	15.8	22.5	28.8	49.5	68.4	129.6
377	12.9	17.4	23.1	27	48.4	69.1	135.4	433	13.5	16.8	23.2	28.7	49	68.3	129.3
378	14.3	16.2	22.6	27.5	48.7	69.5	136.2	434	13.2	15.6	22.7	29.1	49.6	68.7	129.3
379	13.6	15.3	23.7	27	49.4	69	136.3	435	15.3	16.4	23.1	28.7	49.4	68.3	129.6
380	12.6	17.3	22.9	26.8	49	69.1	136	436	13.8	16.8	23.3	28.2	49	68.1	129.2
381	13.9	16	22	27.6	49	69.6	135.7	437	12.9	16.1	22.8	28.4	49.6	67.9	128.3
382	14.1	15	23.5	26.8	48.8	69.4	135.7	438	15.2	16.5	23.3	28.3	49.2	68.1	128
383	13	16.8	23	26.8	49.3	69.2	135.4	439	13.7	16.9	23	27.7	49.4	67.5	128.3
384	13.9	16.4	22.5	27.3	49.5	69	135.1	440	12.6	16.3	22.3	28.1	49.6	67.6	127.5
385	14.3	15.3	23.5	27.2	49.6	69.1	134.6	441	14.7	16.9	23.2	28.1	49.5	67.6	127.1
386	12.9	17.2	22.3	26.6	51.6	68.4	134.4	442	14.1	18	22.9	27.6	49.7	68.1	127
387	13.7	16.9	22.2	27.9	52.8	68.7	134.7	443	13.1	17.6	22.6	28.5	50.1	67.7	127
388	14.7	15.7	23.7	27.3	53	68.9	134.1	444	14	17.5	23.9	27.9	50.3	67.7	126.7
389	13.5	16	22.7	26.8	52.2	68.8	134.2	445	14.5	18.6	22.9	28	50.2	67.6	126
390	13.4	16.6	22.2	28.1	50.4	68.7	134	446	12.9	17.5	22.4	28	50	67.5	125.5
391	15.1	15.7	22.7	27.4	49.7	68.7	134	447	14	17.4	23.8	27.9	49.8	67.4	124.6
392	13.2	16.1	21.9	28	48.7	68.6	133.7	448	14.8	19.5	22.7	27.6	50.4	67.2	124.7

Data for Figure 3-8 (Cont'):

Time (s)	Current signal (pA)							Time (s)	Current signal (pA)						
	C0	C1	C2	C3	C4	C5	C6		C0	C1	C2	C3	C4	C5	C6
449	13.5	17.9	22.1	27.5	50.3	67.1	124.5	505	14.3	16.4	22.7	29.9	50.8	69.5	135.1
450	13.8	17	23.5	28.8	50.5	67.3	124.5	506	13.7	18	23	29.3	50.6	69.4	135.5
451	14.9	19	22.8	27.8	50.8	67.4	124.4	507	13.9	16.9	23.1	29.2	50.4	69.7	135.4
452	13.7	17.2	22.7	27.6	50.3	67.6	125.2	508	15.3	15.7	22.5	29.6	50.5	69.6	135.1
453	13.2	17	23.2	27.6	50.7	67	125.5	509	13.8	18.2	23.1	28.9	51	69.5	135.2
454	15.8	18	22.5	27.4	50.7	67.7	125.7	510	13.6	16.7	23	28.6	50.3	69.2	134.7
455	13.4	17.1	22.3	28.2	50.1	67.6	125.9	511	15.7	15.9	22.5	29.6	50.7	69.1	134.6
456	13.4	16.1	23.4	28.3	50.5	67.4	125.6	512	13.5	17.1	23.1	29.4	50.8	69.5	134.4
457	14.9	18.3	22.6	28.2	50.9	67.5	125.1	513	13.2	16.4	23.3	29	50.3	69.2	134.4
458	13.7	17.1	22.3	27.7	49.9	67.7	125.4	514	14.5	16.2	22.2	29.8	50.6	69.1	134.3
459	13.3	16	22.9	28.5	50.7	67.6	125.3	515	13.9	17.3	23.2	29.5	50.8	69.3	134.3
460	14.6	17.2	22.5	28.1	50.6	67.7	124.4	516	12.8	17.1	22.8	29.2	50.5	69.2	134.9
461	13.3	16.7	22	28.7	50.1	67.6	124.1	517	14.5	15.5	22.2	28.6	50.5	69.3	135.2
462	13.2	15.9	23.1	28.4	50.6	67.8	123.9	518	14.2	17.5	22.6	28.1	50.9	68.9	135.8
463	14.4	16.8	22.3	27.5	50.7	67.3	123.9	519	12.6	16.9	22.6	28.1	50.6	69	136.3
464	14.3	17.4	22.7	29.2	50.1	67.7	124.4	520	14.2	15.7	22.2	28.5	50.6	69.2	136.6
465	13.1	16.6	23	28.1	50.2	68.1	124.6	521	14.3	16.7	22.4	27.9	51.3	69.3	136.8
466	14.2	16.5	22.8	28	50.1	68.1	124.7	522	12.9	17.2	22.9	29.2	51.5	69.3	136.7
467	15	17.2	22.9	28.6	50.1	68.5	125.5	523	13.2	16.3	21.9	29	50.7	69	136.6
468	13.7	16.8	22.7	27.9	49.8	68.8	126.4	524	15.1	17	22.8	28.3	51	69.4	136.5
469	14	16.3	22.2	27.9	50.5	68.2	127.8	525	13	17.6	22.5	29.6	51.5	69	136.7
470	15.1	17.5	22.4	28.7	50	68.5	128.7	526	13	17.3	22	28.8	50.5	69.2	137.5
471	14.1	16.9	22.9	28.5	49.9	68.6	129.4	527	15.1	16.7	22.7	28.3	51.1	69.4	137.2
472	13.6	16.6	22.6	27.9	50.6	68.7	130.3	528	13.1	17.7	22.8	29.2	51.4	69.5	137.3
473	15.1	18.1	22	29.5	50.2	68.7	132	529	12.9	17	22.4	28.4	50.8	69.4	137.6
474	13.8	16.8	23	28.7	49.5	69.1	132.1	530	15.4	16.7	23	28.7	51.1	69.6	137.2
475	12.8	16.8	22.4	28.7	50.9	68.9	133.2	531	13.1	18.1	22.4	29.2	51	69.9	137.4
476	14.9	18	22.8	29.7	50.1	68.9	133.6	532	13	17	22.3	28.5	50.9	69.7	137.3
477	13.8	16.4	23.2	29.4	50.3	68.9	133	533	14.5	17.5	23	29	51.3	69.9	137.1
478	13	16.3	23	30.3	50.4	68.9	134.3	534	13.8	18.2	22.5	29.8	51.1	69.7	137.1
479	14.4	18.1	23.2	30.5	49.8	69.1	134.6	535	12.6	17.9	22.3	29.7	51.4	70	137
480	14.5	16.7	23.3	29.4	50.3	68.9	134.6	536	14.3	16.7	23.2	29.4	51.2	69.9	137.1
481	13.1	16.5	23	29.3	50.9	68.9	134.8	537	14.4	19.1	22.6	30.4	50.9	70.2	137.2
482	14.3	18.1	22.9	30	50	69.2	134.6	538	13.1	17.5	22.1	29.6	51.3	70.3	136.6
483	14.8	17	23.3	29.1	50.9	68.6	134.5	539	14	16.9	23.8	29.7	51.2	69.8	136.5
484	13.3	16.4	22.9	29.2	51	68.5	134.7	540	14.5	18.4	22.7	30	51.3	69.9	136.4
485	14.4	18.5	22.5	29.4	50.4	68.3	135.1	541	14	17.3	22.2	29.3	51.5	70.2	136.3
486	14.9	16.2	23.3	29.4	50.5	68.3	135.4	542	14	17.7	23.7	29.3	50.4	69.7	136.3
487	13.6	15.6	22.9	28.9	51	68.8	135.2	543	15.5	19.3	22.9	30	51.7	70	135.4
488	13.5	18.3	22.7	29.4	50.3	69.4	135.6	544	13.9	17.5	22.6	29.7	51.3	70	134.7
489	15.6	16.4	23.4	29.1	51	68.8	135.8	545	13.8	16.8	23.2	29.3	51.1	69.9	133.8
490	13.5	15.8	22.6	28.5	51.1	69.5	135.4	546	15.8	19.1	22.7	30.3	51.4	70	132.6
491	13	17	22.9	29.3	50.5	69.3	135.6	547	13.7	17.3	22.3	30	51.4	69.8	132
492	15	16.3	23.9	28.7	51	69	135.2	548	13.1	16.8	23.1	29.9	51.3	69.7	131.6
493	13.3	15.1	23.7	28.3	51.2	69.3	134.8	549	14.9	18.3	22.9	30.5	51.3	69.4	130.7
494	12.8	17.2	23.5	28.5	50.6	69.1	135.1	550	14.3	17.6	22.7	30	51.4	69.9	130.7
495	15	17.3	23	28.3	51.1	68.9	134.7	551	13.5	17.1	23.5	30.6	50.8	69.6	130.4
496	13.3	15.6	22.8	28.7	50.8	68.9	134.7	552	14.6	18	22.9	30.3	51.8	69.6	129.9
497	12.9	17.3	22.9	28.8	51	69.2	135.3	553	14.5	17.3	22.9	29.6	51.7	69.6	129.3
498	14.4	16.5	23.1	28.5	51.4	69.4	135.5	554	13.1	16.4	23	29.4	51.2	69.5	129.5
499	13.5	15.8	22.7	29.3	50.9	69	136	555	14.5	18.5	22.3	29.4	51.3	69.6	129.6
500	12.3	17	22.2	28.5	51	68.9	135.5	556	14.5	17.1	23	29	51.2	69.5	129.3
501	14.1	16.6	23.4	28.7	50.1	69.5	135.3	557	14.5	16.4	22.4	29.3	50.9	69.6	129.9
502	13.9	16.2	22.6	29.5	50.8	69.2	135.4	558	13.8	17.6	22.3	28.6	51.6	69.6	129.3
503	12.8	17.5	23.1	29.1	50.4	69.3	135.3	559	15.1	17.7	22.6	28.7	51	69.5	129.8
504	13.7	17.5	23.1	28.6	50.5	69.4	135.1	560	13.6	16.9	22.4	29.1	51.2	69.2	130

Data for Figure 3-8 (Cont'):

Time (s)	Current signal (pA)							Time (s)	Current signal (pA)						
	C0	C1	C2	C3	C4	C5	C6		C0	C1	C2	C3	C4	C5	C6
561	13.6	18.1	21.9	29.1	51	70.1	130	617	13.1	18.5	23.2	34.3	51.5	70.8	134
562	15.2	17.5	23.3	28.1	51.4	69.5	129.8	618	13.9	17.5	23.5	33.8	51.6	70.1	134.1
563	13.4	16.3	22.9	28.8	51.1	69.3	129.4	619	14.4	17.2	24	35	51.1	70.3	134.4
564	13.2	18.6	23.4	29.3	50.7	69.4	129.7	620	13.4	18.5	23.9	34.1	51.2	70.4	134.7
565	15.5	17.4	24.1	29.1	51.1	69.8	129.5	621	14.1	17.6	24.5	33.8	51.7	70.9	134.9
566	13.2	16.5	23.2	29.9	51.4	69.8	129.1	622	14.7	17.8	24.2	32.2	51.5	70.5	135.4
567	12.9	17.6	23	29.8	50.9	69.3	129.7	623	13.9	18.4	24.2	31.4	51.9	70.6	135.2
568	14.6	17.4	23.4	29.7	51	69.4	129.5	624	13.6	16.9	24.3	32.1	51.4	70.7	134.4
569	14.1	16.8	22.7	30.7	51.5	69.2	129.1	625	15.7	17.5	24.2	32.6	52.9	70.9	134.3
570	12.6	17.5	22.5	30.3	50.7	69.5	129.5	626	13.8	18.8	23.7	32.6	52.4	70.8	134.1
571	14.1	17.8	23	30.1	51.3	69.2	129.3	627	13.7	16.9	24.4	32.3	52.9	71	134.1
572	14.1	16.7	22.6	30.8	51.2	69.3	129.4	628	15.7	17.2	24.5	32.9	52.6	70.9	134.6
573	13	17.5	22.7	30.5	51.1	69.5	130.1	629	13.7	18.5	24	32.8	52.2	70.7	134.9
574	14	17.9	23.1	30.6	51.3	69.4	130.8	630	14	17.6	24.8	33	52.5	70.7	135
575	15.1	17	22.8	31.5	51.8	69.7	130.9	631	15.9	16.9	24.4	33.3	52.5	70.6	135.2
576	13.8	16.6	23.1	31.2	51.2	70.2	130.9	632	14	18.3	24.1	33.1	52.1	70.6	135.4
577	14	17.9	23	30.5	51.4	69.3	130.7	633	13.4	17.7	24.6	33	51.7	70.9	136
578	15.2	17.2	22.5	31.9	51.5	69.5	130.7	634	15.5	16.9	24	32.9	52.6	71	136.6
579	14	17.8	23	31.2	51.7	69.4	130.7	635	13.9	18.3	23	32.5	52.4	71	137.2
580	13.4	18.2	22.9	30.4	51.7	69.4	130.4	636	13.1	17.4	23.8	32.6	52.5	71.2	137
581	15.1	17.5	22.5	31.4	51.9	69.2	130.9	637	14.8	16.6	23.5	32.2	52.2	71.1	137.3
582	13.6	18	22.8	30.6	51.6	69.6	131.4	638	13.6	17.1	23.2	31.8	52.6	70.9	136.2
583	13.3	18.3	22.6	30	51.4	69.4	131.4	639	12.5	17.9	23.5	31.8	52.7	70.7	135.6
584	14.8	17.3	21.9	31.1	52.1	69.3	131.7	640	14.6	16.9	23.7	31.1	52.5	71.2	136.1
585	14.5	17.6	23.5	32.1	51.4	69.4	131.6	641	14.3	17.6	22.8	31.2	52.6	71.3	136.2
586	13.4	18.4	23	32.7	51.3	69.7	131.8	642	14.6	18	24.5	31.6	52.2	71.2	136.4
587	14.8	17.6	22.1	33.9	51.6	69.6	132.5	643	15.6	16.8	23.3	31.5	51.8	71.3	136.3
588	14.8	17.9	23.7	33.1	51.4	69.5	132.7	644	13.8	17.7	22.8	31.6	52.3	71.2	136.1
589	13.3	18.6	23	32.6	51.8	69.8	133	645	13.6	18.3	23.5	31.6	52.8	70.7	136.8
590	15.1	17.9	22.3	32.2	52	70.1	133.6	646	14.9	17.8	23.3	30.8	52.1	70.9	136.8
591	14.6	17.9	23.4	31.4	52.6	70.3	133.3	647	14	17	23.2	30.4	52.2	70.9	137
592	14.1	18.8	22.7	30.9	53.1	70.1	133.6	648	13.7	18.7	23.5	31	52.9	70.7	137.1
593	14.5	17.5	23.2	30.4	54	70.2	134.2	649	14.5	18.1	23.6	30.5	51.8	70.9	136.6
594	14.9	17.2	24.1	29.7	54.4	70.2	134.3	650	14.8	17.1	22.8	29.7	52.2	71	136.7
595	13.9	18.1	22.9	30	54.1	70.3	134.1	651	13.9	18.9	24.4	30.3	52.3	71.3	136.6
596	14.2	17.4	22.9	30	53.5	70.3	134.3	652	14	17.6	23.2	29.4	52.1	71.2	136.5
597	15.7	17	23.5	30	53.1	70.1	134.7	653	15.4	17.6	23	28.9	52.6	70.9	136.4
598	13.6	19.1	22.9	30	52.8	69.9	135.2	654	14.3	19	23.8	30	52.2	70.9	136.7
599	14.4	17.9	22.6	29.8	52.8	70.2	135	655	13.2	18	23.2	29.1	52.3	71.1	136.5
600	15.3	17.4	23.2	29.7	51.8	70.4	134.4	656	15.5	17.1	23.5	29.4	51.9	70.8	136.3
601	13.3	18.9	22.8	30	51.5	70.6	134.5	657	13.9	18.8	24.4	29.7	52.4	71.1	136.3
602	13.6	18.2	22.6	29.9	52	70.3	134.1	658	13.3	17.3	23.2	29.3	52.3	71	136.1
603	15.7	17.3	23	30	51.8	70.5	133.7	659	15	16.4	23.1	28.7	51.8	70.7	135.9
604	13.1	18.6	22.6	30.1	52	70.4	134.1	660	14.4	18.8	24	29.7	52.7	70.5	135.8
605	13.5	18	22.6	30.2	51.4	70.5	134.2	661	13.4	18.2	22.7	29.1	53.1	70.4	135.6
606	15.2	17	23	30.1	51.6	70.3	133.9	662	15	16.9	23.2	28.9	53	70.8	135.5
607	13.9	18	22.7	31	51.5	70.2	133.7	663	14.3	18.7	23.7	29.6	53.2	71	135.6
608	13.1	17.6	23.6	30.9	51.7	70.6	133.4	664	13.1	17.7	23.5	29.2	53.5	71	135.7
609	15.1	16.7	23.3	31.1	51.6	70.4	133.2	665	14.8	17.7	23.3	29.9	53.2	70.6	135.8
610	13.7	17.6	23.5	32.3	50.7	70.1	133.2	666	14.6	18.4	24.6	29.8	53.6	70.5	135.7
611	13.4	18.1	23.1	32.4	51.4	70.7	133.2	667	12.9	17.8	23.7	29.4	53.1	70.3	135.6
612	14.5	17	22.8	33	51.4	70	133.4	668	14.4	16.6	24	29.9	53	70.2	135.4
613	13.5	18	23.5	33.9	51.4	69.9	133.6	669	15.1	18.1	24.4	30	52.6	70.2	135.3
614	13	18	23.4	33.3	51.4	70.1	133.9	670	13.4	17.8	23.8	30	52.5	70.4	136
615	14	17.5	23.6	33.7	51.7	70.1	134.9	671	14.5	17	23.8	29.7	52.9	70.8	135.7
616	14.1	17.6	23.7	34.1	51.1	70.9	134.2	672	15.5	18	24.6	30.3	52.8	70.6	136

Data for Figure 3-8 (Cont'):

Time (s)	Current signal (pA)							Time (s)	Current signal (pA)						
	C0	C1	C2	C3	C4	C5	C6		C0	C1	C2	C3	C4	C5	C6
673	13.9	18.1	23.5	30.3	52.9	70.8	136.2	729	15.6	18.2	23.2	30.2	53.6	71.3	131.7
674	14.5	16.9	23.5	30.3	53.1	70.6	136.3	730	13.8	20.3	23.8	29.8	53.4	71.2	132
675	15.4	18.1	24.2	30.3	52.4	70.8	135.2	731	14.3	18.6	23.8	30.4	53.6	71.2	131.4
676	14	18.5	23.1	30.8	53.1	71.2	135.3	732	15.3	18.4	23.4	29.9	53.8	71	131.1
677	14.6	17.5	24	31.9	53.1	70.8	136.3	733	14.4	19.6	24.1	31	53.4	71.1	130.8
678	15.7	17.8	23.1	32.1	52.6	71	136.8	734	13.7	18.2	24.1	30.9	53.4	71.3	130.7
679	14.2	18.2	24.4	31.3	53.4	70.7	137	735	16	17.6	23.9	30.2	53.6	70.9	130.6
680	13.8	17.7	23.4	31.1	53.5	70.9	136.9	736	14	18.8	24	31.6	54	70.8	130.2
681	15.1	18.1	23.5	30.4	52.9	71.2	136.9	737	13.6	18.5	23.9	31.4	53.9	70.2	130.2
682	14.2	18.6	24.1	29.6	53.3	71.1	136.8	738	15.6	17.4	24.2	31.7	53.7	70.1	130.5
683	13.4	16.6	23.6	30.4	52.7	71.6	136.9	739	14.1	17.6	23.8	32.1	53.9	70.3	130
684	15.1	18.7	23.4	30.1	53.1	71.2	137.4	740	13.4	18	24	30.9	54	70.4	130
685	14.4	18.4	24	30.4	52.9	70.7	137.2	741	15	18	23.7	30.7	54	70.2	130.5
686	13.6	17.6	23.3	29.4	52.7	71.2	137.2	742	14.5	18	22.8	31.6	53.6	70.3	130.3
687	14.7	18.1	22.6	30.1	53.3	71.2	137.5	743	13.9	18.3	24.2	30.7	53.1	70.4	130.2
688	14.4	18.3	23.7	29.6	52.1	71.4	137.4	744	15.1	18.4	23.7	30.8	53.6	70.5	130.8
689	13.4	16.9	23	30	52.7	71.5	136.9	745	15.1	17.9	24	31.3	53.2	70.3	132
690	13.8	17.9	22.9	30.5	53.6	71.2	137.6	746	13.9	19.3	24.3	31	52.9	70.4	132.5
691	15	17.8	23.3	29.5	52.6	70.9	137.1	747	15.1	18.4	23.7	31.2	52.9	70	132.7
692	13.8	16.4	23	31.3	52.7	70.9	137.2	748	15.8	18	24	31.7	52.7	70.9	132.7
693	14.1	18.1	23	30.3	52.9	71.1	136.9	749	14.6	19.6	23.9	31.5	53.3	70.7	132.5
694	15.5	18.1	23.5	30.1	53.2	70.8	137.4	750	14.7	18.8	23.6	31.1	52.9	70.5	132.9
695	13.7	16.9	23.3	30.7	52.4	70.8	137.6	751	15.9	18.6	23.2	31.6	53.5	70.8	133.2
696	14	17.6	22.9	30.6	52.8	70.8	137	752	14.8	19.6	24.2	31.5	53.8	70.7	133.2
697	15.4	18.6	22.8	30.1	52.9	70.7	137.7	753	14.8	19	23.4	31.5	53	70.7	133.7
698	14.1	17.6	23.4	31.7	52.7	70.5	137.3	754	15.9	17.6	24.1	31.7	53.3	70.7	133.8
699	13.1	17.9	22.9	30.4	52.9	70.4	136.8	755	14.4	19.9	24.3	31.5	53.9	70.4	133.6
700	16.3	18.4	23.4	30.4	53.3	70.4	136.9	756	14.3	18.5	23.5	31.8	53.2	70.4	133.5
701	14	18.4	23.1	31.3	52.5	70.4	136.4	757	15.5	17.7	24.5	31.7	53.5	70.1	134.2
702	13.3	18.3	22.9	30.3	52.6	70.2	136.1	758	14.2	19	23.8	31.4	53.8	70.1	134
703	15.2	18.3	23.6	30.3	53.2	70.6	136.2	759	13.4	18	23.1	30.9	53.2	70.5	134.2
704	14	17.7	23.8	31.8	53.2	71.1	136	760	15.3	17.5	23.8	31.5	53.7	70.6	134.1
705	13.4	17.6	23.4	30.7	53.2	71.2	136.2	761	14.5	18.9	23.4	31.1	53.6	70.7	134.2
706	14.8	18.9	23	31.1	54.8	70	136.1	762	13.6	18.4	23.1	31.6	53.8	70.6	134.3
707	14	17.9	23.9	32	55.7	70.3	135.8	763	14.8	17.4	23.5	31.4	54.2	70.8	134.2
708	13.7	17.7	23.5	31	56.5	70.4	135.5	764	14.8	18.9	23.4	30.8	54.2	70.3	134
709	15	19	23.6	31.2	56.5	70.6	135.3	765	13.3	18.4	23.4	31.4	54.3	70.5	134
710	15.4	18.2	24	31.9	55.3	70.4	134.4	766	14.8	17.6	24.3	31.2	54.2	70.8	133.6
711	13.8	18.3	23.2	31.3	54.8	70.6	134	767	14.7	18.2	23.1	31.9	54.8	70.3	133.1
712	14.6	19.2	23.6	31.3	55.1	70.5	134.1	768	14.1	19.5	23.1	31.2	55.3	70.2	133.2
713	15.6	18.7	23.8	32	54.6	70.7	133.9	769	14.6	18	23.6	30.5	55	70.9	132.7
714	14.3	17.7	22.9	31.7	54.2	70.8	133.7	770	15.7	18.3	23.8	30.7	55	70	133.3
715	14.4	19.5	24	31.1	53.9	70.7	133.6	771	14.2	19.5	23.5	31.3	55	70.2	133.2
716	15.6	18.6	23.6	31.4	53.8	71	132.8	772	14.7	18.5	24.7	31.1	55.1	70.2	133.8
717	14.6	18.1	23.4	30.7	53.3	71.3	133	773	16.1	18.6	23.9	30.3	54.6	70.2	133.8
718	14	19.7	24	30.2	53.3	71.2	132.6	774	14.1	19.6	23.7	32.2	54.5	70.9	134.2
719	15.9	18.3	23.6	30.8	53.7	71.2	133.2	775	14.9	17.9	24	30.9	53.7	70.1	134.4
720	14.5	18.6	23	30.2	53.5	70.8	133	776	16	17.8	23.6	30.2	54.2	70.4	134.2
721	13.8	19.4	24.5	29.7	53.5	71.2	133.7	777	14.3	19.5	23.4	31.4	54.2	70.4	134.3
722	15.2	18.6	23.4	30.2	53.7	71.4	133.5	778	14	18.2	23.6	30.7	53.6	70.3	134.9
723	14.2	17.4	23.4	30	53.4	71.3	132.7	779	15.8	17.4	23.6	31.3	53.3	70	135
724	14	19.7	23.2	30.2	53.5	71.3	133.1	780	14.8	19	23.3	31.9	53.5	70.9	135.8
725	14.5	18.4	23.2	30.2	53.5	70.9	132.8	781	13.2	18.8	23.7	30.9	54.3	70.1	135.8
726	14.7	18.3	23.1	30	54.1	71.2	132.6	782	15.1	17.6	23.6	30.9	53.5	70.8	136
727	14	19.9	24.1	29	53	71.7	132.5	783	14.4	18.8	22.8	31.6	54	70.9	136.3
728	14.5	18.5	23.6	30.2	53.8	71.3	132.2	784	13.7	19.2	24.3	31.2	53.8	70.9	136.2

Data for Figure 3-8 (Cont'):

Time (s)	Current signal (pA)							Time (s)	Current signal (pA)						
	C0	C1	C2	C3	C4	C5	C6		C0	C1	C2	C3	C4	C5	C6
785	14.7	17.9	23.6	31.2	53.3	70.8	136.1	841	13.8	18.9	24.5	32.2	54.8	70.5	135.8
786	15	18.8	23.3	31.4	53.6	70.7	135.6	842	15.1	18.7	24.4	31.9	54.1	70.1	135.5
787	14.4	19.2	23.7	31.6	54.5	70.9	136	843	14.8	20.2	24.5	32.3	54.4	70.6	135.5
788	14.7	18.5	23.4	31.9	53.2	70.5	136.7	844	13.6	18.8	25.3	31.7	54.8	70.3	134.8
789	15.4	18.6	23.1	31.8	53.7	70.6	136.2	845	15.2	17.8	24	31.8	54.8	70.4	134.7
790	14.7	19.6	24.6	31.2	54.2	70.2	136.7	846	15.1	19.8	24.2	32.1	55.1	70.5	135.3
791	14.5	19.2	24.1	31.3	54.1	70.3	136.2	847	13.9	19	25	31.7	55.3	71	135.8
792	15.6	18.6	23	31.6	55.1	70.7	136.4	848	14.7	18.3	24.4	31.5	54.3	70.3	135.9
793	14.2	20	24.7	31.5	55	70.9	136.2	849	15.3	19.2	24.3	31	54.6	70	136
794	13.8	18.6	23.9	31.2	54.3	70.8	136.6	850	14.2	18.7	24.7	31.8	55.3	70.4	136.1
795	15.4	18.4	23.4	31.5	54.7	71	136.9	851	14.5	18.4	24.3	31.3	54.8	70.7	136.4
796	14.4	20	24.3	31.7	54.3	70.9	136.3	852	15.4	18.6	23.7	31.4	54.7	70.1	135.9
797	13.8	18.7	23.7	31.5	55.2	70.7	135.8	853	13.8	19.4	24.6	31.9	54.6	70.7	136.3
798	15.2	17.6	23.3	32.2	54.9	70.7	135.7	854	14.4	19.1	24.6	31.3	54.7	70.6	136.9
799	14.9	19.8	24.3	32.2	54.6	70.6	135.5	855	15.9	18.9	24	32.5	54.4	70.8	136.6
800	13.6	18	23.7	31.4	54.6	70.6	135.4	856	14.1	19.7	24.6	31.6	55	70.3	136.3
801	15.3	17.3	23.6	32.4	55	70.9	135	857	14	19	23.9	31.4	54.6	70.5	136.5
802	15.1	18.8	24.8	31.5	55	70	134.7	858	15.6	18.5	23.7	32.2	54.8	70.3	136.8
803	13.9	18.1	23.9	31.5	55.5	70.1	134.5	859	14.4	20	24.5	31.7	55.3	70.5	136.5
804	14.5	17.8	23.3	32.1	56.4	70.2	133.9	860	13.3	18.8	24.1	31.9	55	71.6	137
805	15.4	18.9	24.7	31.4	55	70.1	133.3	861	15.2	18.7	24.1	32.4	54.6	71.1	137
806	13.9	18.6	24	31.7	55.7	69.9	132.9	862	14.7	20.1	24.7	31.9	54.7	70.8	136.4
807	14.6	18.4	23.9	32.1	55.3	70.1	132.8	863	13.5	19.4	24.3	30.9	54.7	70.8	136.6
808	15.5	18.4	24.1	31.8	55.1	70.3	132.4	864	15.2	18.1	23.3	32.6	54.5	70.9	136.6
809	13.9	19	23.5	31.2	55.3	70.2	132.5	865	14.7	20	24.4	32	54.9	70.1	136.1
810	14.5	18.1	23.2	32.8	54.6	70.3	132.6	866	13.9	18.8	23.8	32.1	54.8	70.2	136.1
811	16	18.6	24.7	33	54.5	70.7	133.3	867	14.8	18.2	23.8	32.9	54.5	70.2	136.3
812	14	19.6	23.9	32.8	54	70.8	132.5	868	14.4	19.3	24.5	32.1	54.7	70.4	136.8
813	14.3	18.4	23.9	32.1	54.6	70.1	133.4	869	14.2	18.8	23.6	32.1	54.8	70.2	137.3
814	16	18.5	24.4	33.6	54.5	70.3	134.3	870	14.4	18.4	24.3	33	54.8	70	137.6
815	14.7	19.3	24.2	33.1	54.1	70.5	134.4	871	15.1	20.4	24.5	31.8	54.2	70	137.5
816	13.8	18.8	24.5	33.5	54.1	70.3	134.7	872	13.8	19.2	23.8	31.3	54.4	70.4	137.7
817	15.4	18.1	25.1	34.1	54.4	70.4	135	873	14.8	18.4	23.7	32.4	54.5	70.9	137.6
818	14.4	19.5	25	33.9	54.3	70.8	135.4	874	15.9	19.9	24.6	31.9	54.5	70.3	137.6
819	13.5	18.8	24.3	34.2	53.9	70.3	134.8	875	14.2	19.2	24	32.8	54.8	70.2	139.2
820	14.9	18	25.6	34.1	55.1	70.7	135.1	876	14.7	18	24.2	33	54.5	70.9	138.5
821	14.1	19.1	24.5	33.7	54.7	71.9	135.2	877	15.6	19.5	24.6	32.4	54.6	70.8	138.4
822	13.9	18.6	24.2	33	54.6	71.1	135.5	878	14.8	19.4	24.1	32.3	54.5	70.1	138.4
823	14.9	18.8	24	34	55	70.8	135.3	879	14.5	18.8	24.5	32.8	54.7	70.8	138.3
824	15.3	18.9	23.8	32.9	55.1	71.8	135.2	880	15.9	19.4	24.6	32.2	54.4	70.3	138.4
825	14	19.7	23.5	32.3	55.1	71.6	135.3	881	14.5	19.3	23.9	32.3	54.5	70.3	138.4
826	14.5	18.3	24.6	33.1	54.3	70.8	135.4	882	14.2	18.9	24.1	32.8	54.9	70.4	138.2
827	15.9	18.2	23.8	32	55.1	71.5	135.6	883	16.1	19.5	24.6	31.8	54.3	70.6	138.8
828	14.1	19.6	23.1	32.1	54.9	71.1	135.3	884	14.3	19.9	24.1	31.8	54.4	70.1	138.4
829	14.3	18.3	24.8	32.4	54.5	70.6	135.1	885	14.8	19.4	24.3	32.3	54.9	70	137.8
830	15.9	18.6	23.6	31.7	54.5	71.2	134.9	886	16.1	19.3	24.7	32	54.3	70.4	138
831	14.7	19.7	23.6	31.2	54.6	71.4	134.7	887	14.4	20.2	24.4	31.7	54.5	70.3	138
832	14.4	18.9	23.7	31.8	54.9	70.7	135.2	888	14.4	19.5	23.9	32.3	55.1	70.2	138.1
833	16	18.2	23.9	31.5	54.3	70.7	135	889	16	19.1	24.9	32.3	54.4	70.2	138
834	15	19.9	23.4	31.3	54.3	71.5	134.9	890	15.1	20.3	24.5	31.3	54.5	71.9	138.9
835	13.9	18.9	24.8	31.7	54.1	70.8	135	891	13.8	19.9	24.1	32.3	55.6	72.2	138.9
836	16.2	18.6	24.5	31.7	53.9	71.4	135.7	892	15.8	19.7	24.9	32.2	55	72.2	138.5
837	14.1	20.3	24.5	32.1	53.9	71.3	135.5	893	14.9	20.5	24.6	31.7	55.3	71.5	138.7
838	13.7	19	25	32.2	54.8	70.7	135.1	894	14.1	20.1	24.6	32.2	55.1	71.4	138.4
839	15	19.4	24.6	31.5	54.6	70.3	135.1	895	15.8	19.1	24.9	31.8	55.2	71.9	138.5
840	14.6	20.6	24.1	31.6	54.8	71.2	135.5	896	15	20.6	24.3	31.7	55.5	71.8	138.1

Data for Figure 3-8 (Cont'):

Time (s)	Current signal (pA)							Time (s)	Current signal (pA)						
	C0	C1	C2	C3	C4	C5	C6		C0	C1	C2	C3	C4	C5	C6
897	14.3	19.4	24.2	32.3	55	71	137.9	953	14.1	19.4	24.1	32.8	55.5	72.2	137.3
898	15.6	19.2	25.1	32.1	55.5	71.2	138.1	954	14.6	19.8	24	32.8	55.4	71.9	136.9
899	15.5	20.5	24.7	32.1	55.1	71.7	138	955	16.4	19.9	24.1	32.7	55.7	72.1	137.1
900	14.6	19.1	23.6	32.7	55.8	71	138.2	956	14.4	19.1	24.7	32.8	55.8	71.9	137.4
901	15	18.7	25.1	32	56.1	70.7	138.9	957	14.6	19.1	23.9	32.6	55.2	72	137.8
902	15.6	20.5	24.1	32.4	55.3	71.1	138.5	958	16.1	20.1	24.1	32.2	55.5	71.7	137.3
903	14.3	19.6	24.1	32.9	55.1	71.1	139.1	959	14.5	19.6	25.2	32.9	56	72.2	137.7
904	15	17.9	25.2	32.3	55.3	70.4	138.8	960	14.5	19	24.6	32.2	55.7	72.5	137.7
905	15.9	19.8	24.2	33.1	55.2	70.8	138.7	961	16.2	20.2	24.1	32.4	55.4	72.4	139.1
906	15.1	19.4	24	33.1	55	70.8	138.3	962	14.5	19.7	24.7	32.7	55.2	71.6	138.8
907	15	18.3	25.1	32.9	55.2	70.2	137.9	963	14.4	19.7	24.2	32.6	55.1	72.4	138
908	15.9	19.1	24.6	32.9	54.8	70.1	137.5	964	16.2	20.6	23.8	32.7	55.2	72.3	138.2
909	14.9	19.5	23.9	33.3	54.8	70.4	137.6	965	15	20.1	24.5	33.3	55.6	71.9	138.3
910	14.6	18.9	25	32.8	54.8	70.3	138.3	966	14.3	19.2	24.5	32.8	56	71.9	138.5
911	16.4	19	24.5	33	54.9	70.1	138.1	967	16.1	20.6	23.8	32.4	55.1	72.2	138.7
912	14.4	19.5	24	32.4	55.1	70.7	137.9	968	14.8	19.3	24.3	33.1	55.6	71.8	138.9
913	14	18.9	25.4	31.9	54.9	70	138.1	969	13.9	19	25	32.2	56.2	71.8	138.2
914	15.7	19.1	24	32.6	55.4	70.4	137.7	970	16	20.7	24.9	32	55.6	72.2	138.3
915	14.2	20	24.3	32.7	55.1	70	137.2	971	15.4	19.7	23.7	33.5	55.1	72.1	138.1
916	14	18.7	25.2	32.2	55.5	70.9	137.6	972	14.3	19.1	25.3	32.3	55.5	72.3	137.9
917	15.6	18.7	24.3	32.6	55.3	70.4	137.5	973	15.7	20.1	24.4	32.5	56	72	138
918	14.2	20.2	24.2	32.2	55	70.5	137.1	974	14.4	19.5	24.3	33.5	56	72.1	137.8
919	13.3	19.2	25.2	31.9	55.5	70.6	137.4	975	13.9	18.4	25.2	32.3	55.8	71.9	138.3
920	15.1	18.8	24.5	32.3	55.5	71.1	137.2	976	14.7	20.6	24.4	32.1	56.1	71.9	138.3
921	14.8	20.4	24.4	32.2	55	71.5	137	977	14.9	19.2	24.4	33.5	55.6	72	138.3
922	13.5	19.5	24.9	32.1	55.3	71.1	137	978	13.9	18.5	25.3	32.8	55.5	71.9	139
923	14.9	19.5	24.5	32.7	55.2	71.7	137.4	979	14.7	20.4	24.3	32.9	55.7	71.6	138.8
924	15.4	20.5	24.5	32.3	55.3	72.2	137.3	980	15.5	19.3	23.8	33.4	55.8	71.9	138.6
925	14.2	19.4	25.3	32.5	54.9	71.9	137.5	981	14.5	18.7	25.2	32.8	55.1	72.1	138.4
926	14.7	18.7	24.6	32.2	55.2	71.6	137.5	982	14.9	19.9	24.4	32.7	55	71.7	138.6
927	15.3	20.2	23.9	32.5	55.4	72	137.1	983	15.4	19.2	23.7	33.3	56.1	72.1	138.5
928	14.3	19	24.9	32.1	55.7	72	137.2	984	15	18.2	24.6	32.7	55.3	72.1	138.3
929	14.7	18.7	23.7	32.8	55.4	72.2	136.9	985	14.6	20.3	24.6	32.4	55.4	72.1	138.5
930	15.9	19.1	23.3	32.8	55.2	71.7	137.2	986	16.3	19.6	24.4	33.4	55.9	71.9	138.7
931	14.7	19.3	23.8	32.1	54.8	72.2	136.7	987	14.8	18.9	24.8	32.6	55.5	72.2	138.6
932	14.6	18	24.1	32.1	55.5	72.2	136.8	988	14.4	20	23.2	32.7	56	72.1	138.1
933	16.2	19.7	23.7	32.3	55.6	72	137.3	989	16.2	19.9	23.3	33	56.1	71.7	138.3
934	14.6	19.5	24.2	31.9	55.2	72.4	137.4	990	14.6	19.6	24.9	32.6	56	72	139.1
935	14.2	18.2	24.4	31.5	54.9	72.4	137.9	991	14.3	19.8	25.1	32.5	55.6	71.9	139
936	15.5	19.7	23.1	32.2	55.4	71.9	138	992	15.6	19.8	24.2	33.2	55.5	72.1	138.8
937	14.9	19	25.2	31.7	55.6	72	137.8	993	14.6	19.9	24.4	32.9	55.6	71.7	138.6
938	13.7	18.1	24	32	55.4	72.4	137.6	994	13.6	19.9	25	32.1	55.6	72	138.4
939	15.6	19.5	24.1	32.3	56	72.6	137.9	995	15.3	20.3	24.2	32.8	55.6	71.8	138.8
940	15.2	19.5	23.8	31.3	55	72.2	137.6	996	14.6	19.5	23.9	32.5	55.9	71.6	138.4
941	14	18.6	24.2	32.3	55.6	72.5	137	997	13.6	20	23.3	32.4	56.4	71.5	138.8
942	15.6	19.7	23.5	32.3	56	72.7	137.4	998	15	20.1	25.7	32.9	55.7	71.8	138.7
943	15.2	19.6	24	31.8	55.4	72.3	137.4	999	14.6	19.5	24.6	32.8	55.9	71.5	139
944	14.3	18.1	24.7	32.3	55.8	72.3	136.9	1000	13.8	20.1	24.9	32.9	56	71.5	139
945	14.9	19.9	24	32.4	55.1	73.2	137.3	1001	15.1	20.1	24.4	33.2	55.7	72.1	138.9
946	15.6	19.6	24.6	32.1	55.4	72.4	137.9	1002	15	19.8	23.8	32.7	56	71.7	138.9
947	14.3	18.4	24.7	32.3	55.2	72.1	138.1	1003	14.2	19.9	24.3	32.4	56.2	71.3	139.2
948	14.9	19.5	23.9	32.5	55.8	72.4	138	1004	15.2	19.9	24.4	32.9	55.6	71.3	139.4
949	16.1	20.1	24.6	32.3	55.6	72.7	137.8	1005	15.1	19.4	24.1	32.3	55.6	71.7	139.2
950	14	19.2	24.5	32.3	54.8	72.2	138	1006	14.3	19.2	23.1	32.1	56.2	71.1	139.1
951	14.7	19.3	24.3	33	55.5	71.8	137.5	1007	14.8	19.9	24.1	32.6	56.4	70.7	138.8
952	15.4	19.7	24.5	32.8	55.6	72.4	137.2	1008	15.7	19.1	23.8	32.2	56.3	71.3	139.6

Data for Figure 3-8 (Cont'):

Time (s)	Current signal (pA)							Time (s)	Current signal (pA)						
	C0	C1	C2	C3	C4	C5	C6		C0	C1	C2	C3	C4	C5	C6
1009	13.9	19.6	24.2	32	55.5	71	139.2	1065	13.9	21.7	24.9	32.9	56.3	72	139.4
1010	14.6	19.7	24.4	33.1	56.1	70.9	139.3	1066	16.4	20.2	24.6	33.2	57	71.8	138.7
1011	15.8	18.9	23.8	32.1	56.2	71	139	1067	14.6	20.2	24.1	32.8	56.4	71.8	138.4
1012	14.8	19	24.6	32.1	55.6	71.3	139.5	1068	14.4	21.2	24.3	32.8	56.5	71.8	138.4
1013	14.7	19.7	24.3	33.3	56.4	70.9	139.5	1069	15.9	20.1	24.4	33.1	56.6	71.9	138.4
1014	16	19	24.1	32.2	55.4	70.8	138.8	1070	14.7	19.9	23.8	32.6	56.3	71.9	137.9
1015	14.5	19.2	23.8	32.4	55.5	71.3	138.6	1071	13.7	21.3	24.1	33.2	56.4	72.2	137.3
1016	14	20.3	25.4	33.2	56.2	70.9	138.6	1072	16	20.3	24.4	33	56.8	71.9	137
1017	16.1	19.7	24.3	32.5	56.4	70.4	138.4	1073	14.9	19.4	23.7	32.9	56.5	72.2	137.1
1018	14.4	19.4	23.3	32.8	56	70.9	138.6	1074	14	21.2	24.8	32.5	56.6	71.9	137.6
1019	14.4	20.6	24.3	33	55.6	71.1	138.4	1075	15.9	19.4	24.2	32.9	56.4	71.9	137.8
1020	15.6	19.4	24.6	32.4	56.1	70.8	138.7	1076	14.9	19.1	24.1	32.8	56.3	71.9	138.2
1021	14.5	19.9	24.1	32.6	55.9	71.2	137.9	1077	14.1	20.5	24.1	33.2	56.2	71.6	138.5
1022	13.8	20.7	24.1	33.4	56.1	71.2	138.2	1078	15.1	20.1	24.3	32.9	55.6	71.9	138.6
1023	16	19.2	24.7	32.7	56.1	71.4	138.1	1079	15	19	23.9	32.8	56	71.9	138.7
1024	14.7	19	24.3	32.7	56	71	138.1	1080	14.3	19	23.8	33.1	56.5	72.3	138.5
1025	13.7	20.3	24.6	33.2	56.3	71.6	138.9	1081	15.6	20.5	24.5	33.2	56.3	72.1	138.2
1026	15.9	19.6	25.1	32.8	56.3	72.2	138.2	1082	15.7	19.2	23.9	33.2	56.6	71.8	137.9
1027	15.1	19.3	24.6	33	56.3	71.4	138.1	1083	14.7	19.6	24.4	34.2	56.3	72.2	137.6
1028	14	20.4	24.5	33.5	55.8	71.8	138.3	1084	15.4	20.5	24.5	33.9	56.2	72.2	137.7
1029	15.8	19.5	24.9	33.2	55.9	71.8	138	1085	15.9	19.2	24.2	34	56.7	71.7	139
1030	14.9	19.4	24.3	33	56.2	71.7	138.5	1086	14.6	19.8	23.9	34.5	56.5	72	139.4
1031	14.1	21.2	24.6	33	55.9	71.7	138.2	1087	14.9	20.7	24.8	33.4	56.6	71.8	139.3
1032	15.7	20.1	24.6	32.7	55.7	72	138	1088	16.2	20.1	24.3	33.5	56.5	72.1	139.1
1033	15	19.9	24.6	33.5	55.7	72.2	138.3	1089	14.5	19.8	24.7	34.1	57.1	72.1	139.2
1034	14.1	21	24.7	32.8	56.5	71.8	138.5	1090	14.9	20.6	24.6	33.5	56.9	72.1	139.5
1035	15.9	19.9	25.1	32.9	56.1	72	138.5	1091	16.2	19.8	24.2	33.4	56.7	72.2	139.7
1036	15.2	19.4	24.5	33.1	55.5	71.9	138.4	1092	14.5	20.3	24.3	33.8	56.7	71.9	139.7
1037	14.1	20.9	24.2	33.3	55.8	72.6	138	1093	14.9	20.7	24.8	32.9	57.1	72	139.5
1038	15.2	20	24.6	32	55.7	71.9	138.1	1094	16.3	19.7	24.2	33.2	56.7	71.9	139.1
1039	14.9	18.9	24.2	33.2	55.5	72.1	137.9	1095	13.9	20.3	24.1	34	56.8	72	139
1040	14	21	23.8	32.8	56.3	72.1	137.1	1096	14.2	20.9	25.1	32.8	57.1	71.8	139.2
1041	15	20	24.9	32.4	55.6	72.2	137.7	1097	15.8	19.7	24.4	32.9	56.5	72.2	138.7
1042	15.2	19	24.5	32.9	55.8	72.4	136.6	1098	14.1	20	24.5	33.7	57	71.9	138.8
1043	14.3	20.1	24.5	32.7	57	72.2	136.7	1099	14.3	21.2	24.3	33.3	57.1	71.6	138.8
1044	15.2	19.5	24.9	33.1	56.3	71.9	136.5	1100	16	20.2	23.6	33	56.6	71.9	138.8
1045	15.4	19.2	24.6	33.2	56.2	72	136.8	1101	14.4	19.8	23.3	33.9	56.9	71.9	138.6
1046	14.7	19.7	24.2	32.8	56.7	71.9	137.1	1102	14.4	20.9	25	33.1	56.6	71.5	138.6
1047	15	20.2	25.2	32.4	56.7	71.9	136.5	1103	16.1	20.2	26.1	33.3	57.4	71.5	138.9
1048	15.9	19.1	24.4	33.2	56.7	72	136	1104	14.2	20.1	25.4	34	57.2	72	137.9
1049	14.3	20.3	24.2	33	56.7	72.2	136.5	1105	14.3	21.3	23.8	33.2	56.7	71.9	137.7
1050	15	20.2	25.1	32.5	56.9	72.2	136.6	1106	16.2	20.6	24	33.3	57	72.1	137.4
1051	16	19.2	24.3	33.1	55.6	71.7	137.4	1107	14.1	20.3	25.9	33.7	56.5	72.2	137.3
1052	14.2	20	24	32.6	56.5	72.1	137.3	1108	14.3	20.9	25.6	32.8	57.3	72.2	137.2
1053	14.9	20.2	25.1	32.5	56.6	72.2	137	1109	15.7	19.9	25.1	33	57.6	72	136.7
1054	15.5	19.4	24.2	33.3	56.4	71.9	137.6	1110	14.5	20.3	24.9	33.4	56.5	72.6	136.9
1055	14.3	20	24.3	32.4	56.2	71.6	137.7	1111	14.2	20.7	25.1	32.7	56.8	72.6	137
1056	14.3	20.7	25.3	32.6	56	72.2	137.5	1112	15.8	20.4	24.7	32.8	57.5	71.9	137.4
1057	15.8	20.2	24.7	33.1	56.3	71.9	138.7	1113	14.8	20.5	25	33.6	57.2	72.1	137.4
1058	14.4	19.9	24	32.5	55.8	72.1	138.7	1114	13.7	21.1	24	33.2	57.1	72.3	137.3
1059	14.6	20.8	24.6	33	55.8	72.3	138.6	1115	15.8	20.8	25.6	32.8	57.3	72.1	138.1
1060	16.4	19.8	24.5	32.7	56.2	72.1	138.7	1116	14.5	20.6	26.4	33.6	57.1	72.3	138.1
1061	14.3	19.9	24.1	32.6	56.2	71.5	139.1	1117	13.9	21.3	24.9	32.9	57.1	72.6	138.3
1062	14.1	21.2	25	33	56.4	71.8	139.2	1118	14.9	20.7	24.5	33	57.5	72.7	138.7
1063	16.2	19.6	23.9	33.4	56.9	72.3	139.2	1119	14.3	20.6	23.7	33.6	56.8	72.1	138.3
1064	14.4	19.9	24.2	33.2	56.2	71.9	139.8	1120	13.4	21.1	24.9	33.2	57.2	72.4	138.4

Data for Figure 3-8 (Cont'):

Time (s)	Current signal (pA)							Time (s)	Current signal (pA)						
	C0	C1	C2	C3	C4	C5	C6		C0	C1	C2	C3	C4	C5	C6
1121	15	20.8	24.8	32.9	57.2	72.9	138.4	1177	15.3	20.3	24.6	33.4	56.9	70.8	139.5
1122	14.8	20.6	24.5	34	56.9	72.2	138.2	1178	15	19.7	25.7	33.1	57.1	71	139.4
1123	14.3	20.8	25	33.1	56.9	72.2	138.1	1179	14.7	21.3	24	33.2	56.8	70.8	139.8
1124	15.1	20.1	24.3	33	57	72.5	138.1	1180	14.9	20.3	24.5	33.2	56.9	70.8	139.9
1125	14.7	20.1	24.6	34	57	72.1	137.8	1181	15.5	19.6	26.6	33.6	57.1	71.1	139.8
1126	13.8	21	25.1	33.1	57.7	72	137.8	1182	14.4	20.7	25.2	33.5	56.5	71.4	139.6
1127	14.7	20.6	24.3	32.9	56.9	72.4	137.5	1183	15	20.7	24.9	33	57.3	71.1	139.3
1128	15.3	20.6	24.3	33.6	57.1	72	137.8	1184	16.3	19.8	25.4	33.7	57	71.7	139.6
1129	14.2	21.2	25.4	33.3	56.6	71.7	138.2	1185	14.6	20.7	24.8	33.4	57.2	71.9	139.4
1130	14.6	20	24.8	33.3	57.2	72	137.7	1186	15.2	20.3	24.3	33	57.4	71.6	138.9
1131	15.4	20.7	24.8	33.9	57.3	72.1	138.4	1187	16.1	19.7	25.1	33.5	57.1	71.8	138.7
1132	14.1	20.8	25.6	33.1	56.3	71.8	138.4	1188	15.1	20.6	24.4	33.5	57.3	71.6	139.3
1133	14.7	20.2	24.5	32.8	57	71.7	137.9	1189	14.8	20.3	24.4	32.9	57.8	71.3	139.1
1134	15.5	20.3	24	33.8	57.2	72.1	138.1	1190	16.3	19.4	24.2	33.1	57.1	71.4	139.7
1135	13.8	20.9	25.5	33	57	71.9	138	1191	14.6	21.2	26	32.9	57.2	71.7	139.8
1136	14.7	20.1	24.6	33.2	56.9	71.7	138.7	1192	14.5	20.4	25.6	32.8	57	71	139.5
1137	16	20.8	24.8	33.5	57.3	71.9	138.6	1193	16.3	19.5	24.5	33.1	57.1	71.1	139.7
1138	14.8	20.4	25.5	33.1	56.1	71.8	138.1	1194	14.8	21.4	24.1	33	57.6	71	139.7
1139	14.9	20.1	24.3	33.2	56.7	71.2	138.7	1195	14.6	20.3	25.1	32.3	58.4	71.5	139.4
1140	15.9	20.7	24.1	33.2	56.8	71.2	138.4	1196	16	20.1	24.6	33.1	57.5	71.4	139.1
1141	14.9	20.5	24	33.5	57	71.5	138.9	1197	14.3	21.7	26.2	33.4	57.5	71.2	138.5
1142	14.7	19.9	24.4	33	56.7	71.2	138.8	1198	14.1	20.5	24.7	32.7	58	71.5	138.3
1143	16.4	20.3	24.1	33.4	56.1	71.1	138.3	1199	16.3	20.5	24.2	33.3	57.2	71.4	138.5
1144	14.9	20.5	24.5	33.1	57.1	71.1	138.6	1200	14.2	21.7	25.5	33.2	57.9	71.3	138.1
1145	14.7	19.5	24.7	33.2	56.6	71.1	139	1201	14.2	20.3	25.1	33	57.4	71.5	138.2
1146	16.3	20	24.4	33.3	56.8	70.9	139.5	1202	15.8	20.3	24.3	33.2	57.3	71.1	138.2
1147	14.7	20.7	24.5	33	56.6	70.5	138.9	1203	14.6	21.9	25.5	33.2	57.8	71.4	138.8
1148	13.9	19.9	24.7	33.5	57	70.8	138.9	1204	13.9	21.1	24.6	33.2	57.5	71.6	139
1149	15.3	20.1	24.5	33.5	57.1	70.7	138.8	1205	16	20.6	24.6	33.7	57.4	71.2	138.7
1150	14.8	20.2	24.2	33	57.4	70.7	138.7	1206	14.5	21.9	25.1	33.8	57.4	71.3	138.8
1151	13.8	19.9	25.1	32.9	57	70.5	138.9	1207	14	20.5	24.6	33.8	57.7	71.6	138.5
1152	15.6	20	24.8	33.4	57.3	70.5	139.2	1208	16.3	20.7	24.4	33.6	57.1	71.4	138.5
1153	15.6	20.4	24.4	33.3	57.5	70.6	139.6	1209	14.5	21.4	25.7	33.6	57.3	71.5	137.9
1154	13.9	19.6	25	32.6	57.2	70.6	140.1	1210	14.4	20.8	25	33	57.6	71.5	138.2
1155	15.5	20.2	24.6	33.2	57	70.7	140.4	1211	15.7	20.8	24.4	33.7	57.5	71.5	138
1156	15.6	20.5	24.6	33.2	57	70.9	139.9	1212	15.1	21.1	25.4	33.5	57.4	71.5	138.2
1157	14.9	19.5	25.1	32.9	57	71.1	139.8	1213	14.3	20.4	23.6	33.3	58.1	71.7	138.5
1158	15	20.5	24.5	33.2	57.7	70.8	139.6	1214	15.8	21	24.1	33.3	57.7	71.5	139.1
1159	15.8	20.4	24.2	33	57.9	70.7	139	1215	15.4	21.1	25.3	33.3	57.5	71.3	138.8
1160	14.8	19.5	25.3	32.6	57.1	71	138.9	1216	14.4	20.2	24.5	32.8	58.6	71.4	139.4
1161	14.7	20.4	24.5	33.2	57.4	70.8	139	1217	15.8	21	24.4	33.5	57.6	71.8	139.2
1162	16.2	20.7	23.7	33	57.5	70.8	138.7	1218	15	20.8	25.2	33.6	57.9	71.5	139.1
1163	15	20.7	24.9	32.7	57.2	71.4	138.7	1219	14.7	20.1	24.8	33	58.4	72.2	139
1164	15	20.6	24.3	33.2	57.1	71.1	138.8	1220	15.7	20.9	23.9	33.7	57.7	71.7	138.9
1165	16.3	20.7	24.2	32.6	57.1	70.7	139	1221	15.3	20.4	25.2	33.7	58.4	71.7	138.7
1166	14.5	19.8	25.6	33.1	57	71.1	139.1	1222	14.7	19.6	24.8	33.1	58.2	71.4	139.2
1167	13.9	21	24.3	33.7	56.6	71	139.3	1223	15.6	20.9	24.5	33.3	57.6	71.2	139
1168	16.1	20.9	24	33	57.2	71.2	139.3	1224	15.7	20.9	25.1	33.3	57.9	71.7	139
1169	14.8	19.7	25.7	33.3	56.9	70.9	139.2	1225	14.6	20	24.8	33.3	58.5	71.9	139.5
1170	13.8	20.6	24.3	33.9	57.1	71	139.4	1226	15.4	20.9	24.6	33.5	59.4	71.8	139.6
1171	15.4	20.6	24.6	33.7	57.3	71.1	139.2	1227	15.6	20.3	25.4	33.6	59.4	71.9	139.3
1172	14.9	19.7	25	33.1	57	71.1	139.3	1228	14.5	19.8	24.5	33.2	59.2	71.9	139.9
1173	14	21	24.5	33.9	57.2	71.2	139.7	1229	15	20.8	24.3	33.7	59.6	71.5	140.6
1174	15.3	20.3	25.2	33.4	57	71.1	139.7	1230	16	20.5	25.4	33.5	59.2	71.5	140.2
1175	15.3	19.7	25.4	33.5	57.6	70.9	139.6	1231	14.7	19.8	24.6	33.3	59.3	71.6	139.9
1176	13.9	21.8	24.8	33.6	57.1	70.9	139.7	1232	15.4	21.1	24.3	33.6	59.5	71.3	139

Data for Figure 3-8 (Cont'):

Time (s)	Current signal (pA)							Time (s)	Current signal (pA)						
	C0	C1	C2	C3	C4	C5	C6		C0	C1	C2	C3	C4	C5	C6
1233	16.3	20.4	25.2	33.9	59.4	71.4	139.3	1289	14.6	21.6	24.7	33.8	58.1	71.8	139.3
1234	14.7	20	24.4	33.9	59.7	71.3	138.7	1290	15.3	20.8	25.6	33.9	59.3	71.7	139.5
1235	15.3	21.2	24.3	33.6	59.2	71.3	138.9	1291	16.2	20.4	24.9	33.7	59.2	72	139.3
1236	16.5	20.5	25.5	34	59	71.5	139.4	1292	14.6	21.4	24.5	33.6	59.5	71.9	139.4
1237	14.3	20	24.4	33.3	59.5	71.3	139.8	1293	15.3	20.5	25.3	33.9	59.2	71.8	139.2
1238	15.1	21.3	24.5	33.6	59.7	71.3	138.9	1294	16	20.5	25.1	33.7	58.9	72	139.5
1239	16.2	20.6	25.5	33.7	59.2	71	138.3	1295	15.2	21.6	24.3	33.4	58.7	71.9	139.7
1240	14.7	20	24.4	33.4	59.4	71.2	137.7	1296	14.5	20.9	25.3	34.2	59.5	71.8	140.3
1241	14.8	20.7	24.3	33.4	59.8	71.3	137.4	1297	16.6	19.8	24.9	34	59.3	71.8	140
1242	16.1	20.3	25.2	33.8	59.3	71.1	137.9	1298	14.9	21.1	24.6	33.9	59.5	72	139.7
1243	15.1	20.3	24.2	33.6	59.5	71.1	137	1299	14.7	20.7	25.2	34.3	59.3	71.9	139.7
1244	14.9	21	24.6	33.7	59.1	71	137.2	1300	16.4	19.9	24.7	33.9	58.9	72.2	139.8
1245	16.4	20.9	25.3	33.9	59.4	70.9	137.5	1301	14.5	21.2	24.1	33.9	59.7	72.1	139.7
1246	14.8	20.4	24.9	33.6	59.6	70.9	138.5	1302	15.2	21	25.5	34.2	59.1	72.4	139.8
1247	14.6	21.4	24.2	33.7	59.9	70.6	139.4	1303	16.4	20.6	24.7	34.1	59.1	72.1	139.9
1248	16.8	20.8	25.3	33.8	59.1	71.7	139.6	1304	14.8	20.9	24.5	34	59.3	72	140.1
1249	15.1	20.2	24.6	33.4	59.6	71.6	139.2	1305	14.5	21.3	25.6	34.6	59	72.1	140.3
1250	14.6	22	24.3	33.4	59.6	71.2	139.1	1306	16.8	20.8	25	34	59.3	72.2	139.8
1251	16.2	21.3	25	33.4	59.1	71.6	139	1307	14.4	21.1	24.8	34.1	59.1	71.9	139.7
1252	14.9	20.2	24.7	33.1	59.4	71.3	138.7	1308	14.7	21.2	25.5	34.6	59.6	71.9	139.1
1253	14.9	22	24.7	33.6	59.3	71.2	139.4	1309	16.3	20.3	24.6	34.1	59.4	72	139.6
1254	16.4	20.7	25.2	33.6	59.3	71.4	139.4	1310	14.9	20.8	24.9	34.2	60.6	71.9	139.3
1255	15.8	20.2	25	33.1	59.4	71.6	139.1	1311	14.9	21.4	25.8	34.6	59.5	71.8	138.7
1256	14.2	21.3	24.6	34	59.6	71.3	139.2	1312	16.7	20.5	24.9	34.2	59.3	71.9	139
1257	16.5	20.4	25.3	33.9	61	71.5	139.4	1313	14.4	20.5	24.7	33.9	59.4	71.6	139
1258	15	20.6	24.8	33.6	59	71.3	139.7	1314	14.4	21.1	25.7	34.7	59.2	71.9	139.2
1259	14.4	21.6	24.3	33.6	58.2	71.2	139.5	1315	16.4	20.6	25	33.9	59.7	72.1	139.4
1260	15.6	20.6	25	33.8	59.8	72.7	139.6	1316	14.3	20.6	25	33.7	59.5	72	139.2
1261	14.8	19.7	24.7	33.6	59.2	72.9	139.4	1317	14.5	21.6	25.6	33.9	59.5	72	138.6
1262	14.1	21.9	24.9	33.6	58.9	72.8	138.9	1318	16.3	20.6	25.3	34.2	60.1	71.8	138.6
1263	16	20.4	25.4	33.5	59.9	72.7	139.4	1319	15	20.5	24.6	33.7	60.1	72.1	138.8
1264	14.8	19.9	24.4	32.9	59	72.4	139.1	1320	14.3	21.9	25.7	34	59	71.9	138.9
1265	13.6	21.3	23.9	33.7	60.1	72.5	138.8	1321	16.4	20.7	24.9	34.2	59.2	71.6	138.5
1266	16.2	20.6	25.4	33.2	59.6	72.3	138	1322	15	20.1	24.6	34	59.2	72.2	138.9
1267	14.7	20.4	24.5	32.9	58.7	72	137.7	1323	14.5	22	25.1	34	59.3	72.3	138.9
1268	13.7	21.8	24	33.7	59.3	72.1	137.6	1324	16.6	20.5	24.6	34.8	59.9	71.8	138.1
1269	15.6	20.1	25.4	33.8	59.8	72.6	137.8	1325	14.9	20.9	24.7	33.8	59.5	72.3	138
1270	14.9	20.1	24.5	33.6	59.5	72.2	138.1	1326	14.3	21.8	24.9	33.7	59.3	72.3	137.9
1271	13.9	21.9	24.7	33.5	59.1	72.1	138.3	1327	16.1	21.1	25.1	34.9	59.3	72.3	138.4
1272	15.7	20.4	25.5	33.5	59.4	72.4	138.1	1328	14.4	19.9	24.8	33.7	59.7	72.7	138.3
1273	14.5	20	24.5	33.3	59.5	71.9	138.5	1329	14.3	21.8	25.1	34	59.2	72.9	138.2
1274	14.2	21.4	24.1	33.9	59.5	71.8	138.8	1330	16.4	20.7	24.7	34.6	58.8	72.9	138.9
1275	15.8	20.6	25.3	33.9	59.8	71.8	138.8	1331	14.8	19.8	24.7	33.6	59.5	73	138.4
1276	15	20.4	24.7	33.3	59.3	71.8	138.7	1332	13.6	21	25	33.7	59.3	73.1	138.2
1277	14.1	21.7	24.6	33.7	59.5	71.5	139	1333	16.5	20.2	24.6	34.6	59.6	73.2	138.2
1278	15.4	20.4	25.3	33.8	59.6	71.8	138.9	1334	15.1	19.9	25	34.2	59.7	72.8	137.8
1279	15.4	20.1	24.2	33.4	59.6	71.9	138.9	1335	13.9	20.9	25	33.6	59.1	72.9	137.6
1280	14.4	21.9	24.3	33.1	59.5	71.9	138.9	1336	15.7	20.8	24	34.6	59.1	73	137.8
1281	15.8	20.4	25.3	33.8	58.9	71.6	139.4	1337	14.9	20	25	33.8	59.1	73	137.6
1282	15.5	20.3	24.9	33.5	59.7	71.8	139	1338	14.2	20.8	24.7	33.2	59.3	73.1	137.4
1283	14.6	21.9	24.6	33.7	59.2	71.6	139.1	1339	15.9	21.1	24.6	34.9	59.5	73.1	138
1284	15.3	20.5	25.2	33.7	59.2	71.6	139.1	1340	15.4	20.5	24.6	33.7	59.1	72.8	138.6
1285	15.4	20.7	24.9	33.8	59.5	72.1	139.2	1341	14.5	21.1	24.5	33.4	58.9	72.8	138.9
1286	14.8	21.9	24.7	33.7	58.2	72.3	139.7	1342	16.5	21.8	24.6	34.5	59.2	73.2	138.9
1287	15.3	20.9	25.3	34.2	59.1	71.9	139.3	1343	15.8	20.8	25.8	33.9	59.7	72.7	138.7
1288	15.9	20.8	24.9	33.8	58.8	71.8	139.3	1344	15	20.9	24.6	33.7	59.5	72.5	139.1

Data for Figure 3-8 (Cont'):

Time (s)	Current signal (pA)							Time (s)	Current signal (pA)						
	C0	C1	C2	C3	C4	C5	C6		C0	C1	C2	C3	C4	C5	C6
1345	16.4	21.1	24.4	34.6	58.5	72.8	139	1401	15.9	20.5	24.7	34.1	59.1	73.3	139.1
1346	15.7	21.1	25.5	34.1	59.4	72.6	139.1	1402	14.8	21	25	35	59.1	73	139.3
1347	14.8	21.2	24.8	33.5	59.7	72.7	139.8	1403	14.9	21.4	25.1	34	58.8	73.2	139.8
1348	16	21.2	24.8	34.3	59.5	72.4	140.3	1404	16.4	20.6	24.9	34.5	59.4	73.3	139.4
1349	15.4	20.4	25.6	33.8	59	72.5	140.2	1405	15.1	21.4	24.6	35.1	59.3	73.2	139.5
1350	15.3	20.8	24.9	33.9	59.6	72.4	140.8	1406	15.3	21.7	25.2	34	59	73.2	139.8
1351	15.9	21.3	24.9	34.1	59.1	72.5	140.8	1407	16.7	20.7	24.9	34.1	59.4	72.9	139.8
1352	15.3	20.5	26	33.6	59.4	72.4	140.9	1408	14.7	21.1	25.3	34.8	58.8	73	140.3
1353	14.7	20.4	25.1	33.1	59.6	72.9	140.6	1409	15.1	21.2	25.2	33.7	59.3	73.1	140.3
1354	15.6	21.1	25.1	34.3	58.6	72.7	140.7	1410	16.5	21	24.6	33.3	60.2	73.2	140.5
1355	16	20.5	26.1	33.8	58.9	72.5	140.2	1411	14.8	21.5	24.9	34.6	59.5	73	140.4
1356	14.9	20.8	24.9	33.5	59.4	72.7	140.1	1412	15	21.3	24.8	34.2	59.3	73.2	140.6
1357	15.2	21.5	24.9	34.3	58.7	72.6	140.1	1413	17.1	20.7	24.2	34.1	60.2	73.4	140
1358	15.8	21.1	25.7	33.7	58.6	72.4	140	1414	15.1	21.1	24.3	34.6	59.4	73.2	140.3
1359	14.9	20.4	25.4	33.7	59.1	72.9	139.9	1415	15.1	21.7	24.8	34.1	60	73.6	140.1
1360	15.6	22	24.8	34.2	58.6	73.1	140.2	1416	17.1	20.3	24.2	34	59.5	73	139.9
1361	15.6	20.8	25.7	33.7	58.8	72.6	140.7	1417	15.2	20.8	24.3	34.9	59.3	72.8	139.9
1362	15	20.5	24.8	33.4	59.3	72.9	140.5	1418	14.9	21.3	24.5	34.2	59.9	72.9	139.1
1363	14.7	21.9	24.6	34.7	58.8	73	139.8	1419	16.6	20.6	24.6	33.9	60.6	73	138.1
1364	16.1	20.6	25.4	34.2	59.4	72.7	139.2	1420	15.1	20.6	25.2	34.8	60	73	138.2
1365	15	20.5	25	33.4	59.5	72.9	139.1	1421	14.9	20.9	24.7	33.8	60.1	73.1	137.6
1366	14.6	21.8	25.3	34.2	58.8	73.5	139.3	1422	16.3	20.5	24.2	33.3	60.5	73	137.5
1367	16.1	21	25.4	33.6	59.5	73.2	138.4	1423	15.2	20.6	25	34.4	59.6	73.1	137.5
1368	14.4	20	25	33.2	58.7	73	138.6	1424	14.5	21.2	24.7	34	59.4	73.3	137.9
1369	14.8	21.4	24.5	34.4	59.1	73.4	138.7	1425	16	20.6	24.8	34	60.1	73	137.7
1370	16.3	20.6	25.6	33.8	59.7	73.5	138.8	1426	15.4	20.8	25.4	34.2	59.4	72.9	137.7
1371	15	20	24.7	33.5	59.2	73.3	138.6	1427	14.7	21.8	25.1	34.5	59.8	73	137.7
1372	14.3	21.3	24.6	34.5	59.6	73.3	138.6	1428	16.3	21.1	24.8	33.8	60.7	72.9	137.6
1373	16.8	20.5	25.2	33.5	59.9	73	138.6	1429	15.1	21	26.1	35	60.1	72.6	137.7
1374	15.1	19.4	25.1	33.6	58.1	73	138.3	1430	14.7	22.1	25	33.8	59.8	72.7	138.2
1375	14.7	21.6	24.6	34.3	58.9	73.5	138.4	1431	15.7	20.8	24.5	33.7	60.3	72.5	138.5
1376	16.3	20.2	25.2	33.9	59.4	73.7	138.4	1432	15	21	25.5	33.9	59.6	72.5	138.3
1377	14.7	19.9	25	33.7	61.5	73.7	138.1	1433	14.2	21.9	24.7	33.9	59.6	72.3	138.7
1378	14	20.8	24.3	33.7	60.1	73.4	138.3	1434	15.1	21.6	25.2	33.6	60.2	72.2	139
1379	16.2	20.8	25.5	33.7	59.7	73.3	138.1	1435	15.9	20.6	25.9	34.2	59.5	72.3	139
1380	14.8	19.8	24.7	33.5	59	73.3	138.3	1436	14.4	21.4	25.2	34.3	60.1	72.7	139.1
1381	14.3	21.3	24.9	34.2	59.4	73.5	138.3	1437	15.2	20.8	24.6	33.9	60.2	72.9	139.2
1382	15.9	21.3	25.3	34	60.2	73.7	138.3	1438	16.3	20.8	25.9	34.6	59.7	72.5	139.5
1383	14.8	20.2	25	33.1	59.6	73.7	140.5	1439	14.7	21.8	25.1	34.4	59	72.4	139.4
1384	13.8	21	25.1	34.5	59.4	73.7	139.4	1440	15.7	20.5	25	33.5	60.3	72.6	139.7
1385	15.6	20.8	25.5	34	59.2	73.5	138.7	1441	16	21.1	25.7	34.3	59.7	72.8	139.4
1386	15.3	20.4	25	33.6	58.9	73.9	137.9	1442	15.1	21.7	25	34.2	60.1	72.7	139.8
1387	14.6	21.6	24.8	34.2	59.5	73.6	137.4	1443	15.5	20.9	25.2	33.8	59.9	72.8	140.5
1388	15.5	21.2	25.4	33.7	60	73.5	137.3	1444	16.2	20.5	25.8	33.7	59.5	72.7	140.6
1389	15.1	20.3	25.3	33.9	59.3	73.4	137.8	1445	14.9	21.3	25.1	34.2	60.3	72.9	140.3
1390	15	21.3	25	34.5	59.1	73.8	137.4	1446	15.4	20.9	24.8	33.6	60.2	72.8	140.5
1391	15.7	21.3	25.4	34	58.9	73.6	137.3	1447	16.6	20.6	25.7	34	59.4	72.9	140.6
1392	15.4	20.4	24.7	33.6	59.1	73.2	137.3	1448	14.8	21.7	25	34	58.7	72.8	140.4
1393	14.6	20.9	25.1	35.1	58.8	73.3	138.1	1449	16.1	20.7	25.2	34.2	60.4	72.8	140.6
1394	15.1	21.4	25.2	34.2	58.4	73.4	138	1450	16.3	20.9	25.4	34.2	59.4	73.1	140.6
1395	15.6	20	25.4	33.4	58.9	73.6	138	1451	14.6	21.9	25.1	34.1	59.4	73	140.5
1396	14.7	21.1	25	34.3	59.3	73.3	138	1452	15	20.7	25.3	34.1	60.3	73	140.4
1397	15.1	21	25.2	33.7	58.3	73.3	137.7	1453	16.8	20.8	25.1	33.9	59.4	73	140.1
1398	16.1	20.5	24.9	34	58.8	73.5	138.1	1454	14.6	21.9	25	33.9	60.7	73.3	140.1
1399	14.4	21.1	24.5	35.2	59.1	73.3	138.5	1455	15.4	20.8	25.3	33.8	60	73.5	139.7
1400	15.4	20.7	25.2	34.3	59.6	73.4	139	1456	16.5	20.8	25.1	33.5	60	72.7	140

Data for Figure 3-8 (Cont'):

Time (s)	Current signal (pA)							Time (s)	Current signal (pA)						
	C0	C1	C2	C3	C4	C5	C6		C0	C1	C2	C3	C4	C5	C6
1457	14.9	21.6	24.6	33.8	60.3	72.9	140.3	1479	14.4	21.3	25.5	34.7	59.7	72.2	137.5
1458	14.8	21.1	25.2	33.9	60.2	73.2	140.2	1480	15.8	21.5	24.8	34.8	60.2	72.5	137.9
1459	16.6	20.8	24.9	33	60	73.1	140.2	1481	15.7	21.8	25.2	35.3	60.1	72.1	137.4
1460	14.8	21.8	24.7	34.3	60.1	73.3	140	1482	14.5	21.2	25.2	34.8	59.9	72.1	137.7
1461	14.6	21	25.3	34	60.2	73.4	139.4	1483	15.3	21.4	25.3	34	59.7	72.1	137.5
1462	16.5	20.5	25.2	33.7	60.4	73	139.2	1484	16.4	21.9	25.3	35.4	60.9	71.9	137.1
1463	15.1	22	25.4	34.4	60.6	73.1	139.4	1485	14.7	20.3	25.4	34.6	59.8	71.9	137.3
1464	14.7	21.3	25.3	33.8	59.9	72.7	139.1	1486	15.3	21.7	25.4	34.7	60.1	71.9	137.2
1465	16.1	21.6	25.1	33.5	59.9	72.6	139.2	1487	16	21	25	35.4	60.8	71.7	137.3
1466	15.5	21.9	24.8	35.7	59.5	72.6	139.2	1488	14.7	20.1	25.3	34.7	59.4	71.7	137.2
1467	14.7	21.3	25.8	35.8	60	72.6	139.4	1489	15.3	21.4	25	34.7	59.2	71.4	137.5
1468	16.1	21.7	25.3	36.1	60	72.5	139.3	1490	16.5	21.1	24.4	35.4	60.1	71.4	137.7
1469	15.3	22.4	24.3	35.2	59.9	72.6	138.8	1491	14.4	20.3	24.9	34.8	60.3	71.3	137.5
1470	14.3	22.2	26.1	35.9	59.9	72.8	138.5	1492	15.3	21.9	24.9	34.5	60.1	71.3	137.9
1471	15.9	21.5	25.1	35.4	59.9	72.6	138.4	1493	16.7	20.8	24.4	35.4	61	71.6	138.3
1472	14.9	22.5	24.9	34.6	59.8	72.4	138.1	1494	15	20.6	24.5	34.9	60	71	139.3
1473	14.7	21.7	24.7	35.2	59	72.9	137.4	1495	14.5	21.1	24.4	35.3	60.3	71.1	139.1
1474	15.2	21.7	25.6	34.6	59.5	72.3	137.4	1496	16.7	20.8	24.1	35.5	60.5	71.2	138.5
1475	15.4	22	25.6	35.3	59.4	72.2	137.1	1497	15.4	22.5	24.7	35.1	60.9	71.2	138.4
1476	14.5	21	25	35.2	59.5	71.9	136.8	1498	15.3	21.9	24.3	35.7	60.5	71.2	138.6
1477	15.6	21.5	25.7	35.2	59.6	72.6	137.4	1499	16.4	22	24.2	35.8	60.4	71	138.4
1478	15.8	21.9	24.9	35.3	60	72.4	137	1500	15	22.3	24.3	35.6	60.7	71.6	138.4

***: C0 to C6 denote for concentrations of NH_2Cl as follows:**

Level	C0	C1	C2	C3	C4	C5	C6
NH_2Cl (mg/L as Cl_2)	0.0	1.1	2.2	4.1	8.7	11.9	26.2

Data for Figure 3-9:

Influent NH_2Cl (mg/L as Cl_2)	Effluent NH_2Cl (mg/L as Cl_2)	Average NH_2Cl (mg/L as Cl_2)	Signal (pA)
0.0	0.0	0.0	15.4
1.2	1.1	1.1	21.4
2.3	2.1	2.2	25.1
4.3	3.9	4.1	34.6
8.8	8.5	8.6	60.0
12.1	11.6	11.9	72.4
26.3	26.0	26.2	138.8

Data for Figure 3-10:

NH_2Cl (mg/L as Cl_2)	Signal (pA)
0.0	43.5
1.1	49.0
2.2	53.8
4.0	62.1
8.4	75.9
12.4	92.6
28.0	159.4

Data for Figure 3-11:

NH_2Cl (mg/L as Cl_2)	Signal (pA)				
	Test 1	Test 2	Test 3	Test 4	Average
0.0	2.0	3.0	3.0	4.0	3.0
1.3	5.0	7.0	8.0	6.0	6.5
2.5	8.0	9.0	10.0	8.0	8.8
4.5	14.0	14.0	17.0	15.0	15.0
8.5	24.0	24.0	33.0	29.0	27.5
11.0	34.0	32.0	37.0	39.0	35.5

Appendix C – Data for Figures in Chapter 4

Data for Figure 4-1 (PVC):

PVC slide			
Distance from Substratum (μm)	NH_2Cl (mg/L as Cl_2)		
	Test 1	Test 2	Average
1000	5.3	5.3	5.3
950	5.3	5.3	5.3
900	5.2	5.3	5.2
850	5.2	5.3	5.2
800	5.1	5.3	5.2
750	5.2	5.2	5.2
700	5.2	5.3	5.2
650	5.3	5.3	5.3
600	5.2	5.2	5.2
550	5.2	5.1	5.2
500	5.2	5.2	5.2
450	5.1	5.2	5.2
400	5.1	5.3	5.2
350	5.2	5.2	5.2
300	5.2	5.2	5.2
250	5.2	5.2	5.2
200	5.2	5.2	5.2
150	5.1	5.2	5.2
100	5.2	5.1	5.2
50	5.1	5.2	5.1
0	5.1	5.1	5.1

Data for Figure 4-1 (PC):

Distance from substratum (μm)	PC slide NH_2Cl (mg/L as Cl_2) Test 1	Test 2	Average
1000	6.0	6.0	6.0
950	6.0	6.0	6.0
900	5.9	6.0	5.9
850	5.9	6.0	6.0
800	5.9	5.9	5.9
750	5.9	5.9	5.9
700	5.9	5.9	5.9
650	5.9	6.0	5.9
600	5.9	6.0	5.9
550	5.9	5.9	5.9
500	5.8	5.9	5.9
450	5.8	5.9	5.8
400	5.8	5.9	5.9
350	5.8	5.8	5.8
300	5.8	5.8	5.8
250	5.8	5.8	5.8
200	5.8	5.8	5.8
150	5.8	5.8	5.8
100	5.8	5.7	5.8
50	5.8	5.8	5.8
0	5.8	5.7	5.8

Data for Figure 4-1 (Concrete):

Concrete slide			
Distance from substratum (μm)	NH_2Cl (mg/L as Cl_2)		
	Test 1	Test 2	Average
1000	5.7	5.8	5.8
950	5.7	5.9	5.8
900	5.8	5.9	5.8
850	5.8	5.8	5.8
800	5.8	5.9	5.8
750	5.8	5.8	5.8
700	5.7	5.8	5.8
650	5.6	5.9	5.7
600	5.5	5.8	5.7
550	5.5	5.8	5.6
500	5.3	5.8	5.6
450	5.2	5.7	5.4
400	5.1	5.6	5.3
350	5.0	5.6	5.3
300	5.0	5.4	5.2
250	4.9	5.3	5.1
200	4.8	5.1	5.0
150	4.9	5.1	5.0
100	4.8	5.0	4.9
50	4.8	5.0	4.9
0	4.7	5.0	4.9

Data for Figure 4-2:

Distance from substratum (μm)	NH_2Cl (mg/L as Cl_2)		
	Test 1	Test 2	Average
1000	7.9	8.3	8.1
950	7.9	8.3	8.1
900	8.0	8.3	8.1
850	7.9	8.2	8.1
800	7.8	8.1	8.0
750	7.6	7.8	7.7
700	7.4	7.3	7.3
650	7.0	6.8	6.9
600	6.6	6.4	6.5
550	6.2	5.9	6.0
500	5.8	5.6	5.7
450	5.5	5.2	5.3
400	5.2	5.0	5.1
350	5.0	4.7	4.8
300	4.8	4.4	4.6
250	4.6	4.1	4.3
200	4.3	3.9	4.1
150	4.0	3.7	3.8
100	3.9	3.4	3.7
50	3.6	3.2	3.4
0	3.5	3.1	3.3

Data for Figure 4-3:

Distance from substratum (μm)	Signal (pA)	
	Microelectrode #1	Microelectrode #2
1000	3.1	14.3
950	3.0	14.2
900	3.0	14.2
850	3.0	14.1
800	3.1	13.9
750	2.9	13.7
700	3.0	13.6
650	3.0	13.5
600	2.8	13.3
550	2.8	13.4
500	2.8	13.3
450	3.0	13.3
400	2.9	13.2
350	2.7	13.2
300	2.7	13.0
250	2.8	12.8
200	2.7	12.7
150	2.9	12.6
100	2.8	12.6
50	2.6	12.6
0	2.7	12.6

Data for Figure 4-4:

Distance from substratum (μm)	NH_2Cl (mg/L as Cl_2)		
	15 min	45 min	65 min
1000	6.2	5.6	5.3
950	6.1	5.6	5.1
900	6.1	5.5	5.0
850	6.1	5.4	4.8
800	5.9	5.3	4.6
750	5.8	5.1	4.4
700	5.6	4.9	4.1
650	5.3	4.7	3.8
600	4.9	4.5	3.6
550	4.5	4.2	3.4
500	4.0	3.8	3.1
450	3.4	3.4	2.8
400	2.8	3.1	2.7
350	2.1	2.9	2.5
300	1.4	2.6	2.4
250	0.8	2.3	2.3
200	0.2	2.0	2.3
150	0.0	1.8	2.2
100	0.0	1.6	2.2
50	–	1.5	2.1
0	–	1.4	2.1

Data for Figure 4-5:

Distance from substratum (μm)	NH_2Cl (mg/L as Cl_2) 10 min	20 min	40 min	70 min
1000	24.7	21.7	22.4	23.0
950	24.5	21.6	22.3	23.1
900	24.4	21.3	22.3	23.1
850	24.3	21.1	22.2	23.1
800	24.2	20.9	22.2	23.1
750	24.0	20.8	22.1	23.1
700	23.7	20.3	22.0	23.0
650	23.4	20.0	21.9	23.0
600	23.1	19.7	21.7	23.0
550	22.7	19.3	21.6	23.0
500	22.2	19.0	21.2	22.8
450	21.5	18.5	20.8	21.9
400	20.7	17.7	20.0	21.2
350	18.4	16.6	19.3	20.9
300	17.2	16.0	17.9	19.8
250	16.8	14.5	17.2	18.8
200	15.8	13.5	16.5	17.2
150	14.9	13.3	15.6	16.7
100	15.0	13.2	15.5	15.9
50	14.3	13.2	15.4	16.3
0	13.5	12.6	14.9	15.4

Data for Figure 4-6:

Distance from substratum (μm)	NH_2Cl (mg/L as Cl_2) 10 min	20 min	30 min	45 min
1000	6.2	6.0	6.0	5.9
950	6.2	6.0	6.0	5.8
900	6.2	6.0	6.0	5.9
850	6.2	6.0	5.9	5.9
800	6.2	6.0	5.9	5.9
750	6.2	6.0	5.9	5.8
700	6.2	6.0	5.9	5.8
650	6.2	6.0	5.9	5.8
600	6.2	6.0	5.9	5.8
550	6.2	6.0	5.9	5.8
500	6.2	6.0	5.8	5.8
450	6.2	5.9	5.8	5.7
400	6.2	5.9	5.8	5.7
350	6.2	5.9	5.7	5.7
300	6.2	5.8	5.7	5.6
250	6.2	5.7	5.7	5.6
200	6.1	5.4	5.7	5.4
150	6.0	5.3	5.7	5.3
100	5.8	5.2	5.3	5.3
50	5.6	4.8	5.0	5.1
0	5.2	4.6	4.8	5.0

Data for Figure 4-7:

Distance from substratum (μm)	NH_2Cl (mg/L as Cl_2) 5 min	15 min	20 min
1000	8.0	7.6	7.5
950	8.0	7.6	7.5
900	8.0	7.6	7.5
850	8.0	7.6	7.5
800	8.0	7.6	7.5
750	8.0	7.6	7.5
700	8.0	7.6	7.4
650	8.0	7.6	7.4
600	8.0	7.5	7.4
550	8.0	7.5	7.4
500	8.0	7.5	7.4
450	8.0	7.4	7.4
400	7.9	7.4	7.4
350	7.9	7.3	7.4
300	7.8	7.2	7.3
250	7.6	7.1	7.2
200	7.4	7.0	7.0
150	7.0	6.8	7.2
100	6.6	6.5	6.6
50	6.1	6.3	6.3
0	5.1	6.0	6.1

Appendix D – Data for Figures in Chapter 5

Data for Figure 5-2:

Time (days)	NO_2^- (mg/L)	NO_3^- (mg/L)	Time (days)	NO_2^- (mg/L)	NO_3^- (mg/L)
0	0.004	0.35	186	0.005	0.20
9	0.005	0.56	188	0.006	0.21
15	0.004	0.28	191	0.007	0.19
20	0.004	0.29	195	0.006	0.16
22	0.003	0.10	198	0.005	0.17
29	0.004	0.19	202	0.005	0.06
35	0.007	0.26	205	0.005	0.19
37	0.007	0.26	209	0.001	0.18
41	0.003	0.17	212	0.002	0.18
44	0.006	0.23	216	0.004	0.17
50	0.005	0.25	219	0.004	0.20
58	0.004	0.19	223	0.001	0.19
62	0.003	0.19	226	0.002	0.14
65	0.003	0.20	230	0.001	0.16
69	0.004	0.23	233	0.002	0.19
72	0.005	0.27	237	0.002	0.14
76	0.006	0.18	240	0.002	0.15
80	0.005	0.17	244	0.003	0.15
83	0.004	0.16	247	0.004	0.18
86	0.005	0.17	251	0.005	0.14
91	0.005	0.20	258	0.004	0.23
94	0.004	0.17	261	0.002	0.08
97	0.005	0.18	265	0.003	0.13
100	0.004	0.11	268	0.019	0.18
113	0.010	0.21	270	0.010	0.12
117	0.006	0.16	272	0.020	0.17
121	0.005	0.17	275	0.035	0.16
125	0.006	0.17	279	0.002	0.17
128	0.005	0.25	282	0.006	0.17
132	0.009	0.19	286	0.005	0.14
135	0.008	0.18	289	0.009	0.18
139	0.005	0.27	293	0.008	0.14
142	0.008	0.17	298	0.008	0.13
146	0.008	0.20	300	0.009	0.15
149	0.006	0.17	303	0.009	0.16
153	0.005	0.16	308	0.016	0.12
157	0.006	0.20	310	0.021	0.15
160	0.005	0.19	314	0.022	0.16
163	0.006	0.18	317	0.041	0.12
167	0.004	0.25	321	0.044	0.12
171	0.004	0.14	324	0.032	0.14
174	0.004	0.17	329	0.051	0.15
177	0.003	0.23	336	0.041	0.15
181	0.004	0.21	345	0.026	0.13
183	0.002	0.29	352	0.019	0.10

Data for Figure 5-3:

Time (days)	Nitrifying microorganisms (MPN/mL)	HPC Log_{10}(cfu/mL)
0	ND*	6.01
9	ND	5.67
17	ND	5.73
21	ND	6.70
29	ND	5.90
34	ND	5.13
43	ND	4.28
55	ND	5.01
62	ND	4.94
69	ND	5.02
80	ND	4.77
87	ND	5.05
99	ND	5.53
106	ND	4.70
113	ND	3.90
121	ND	3.92
128	ND	4.86
135	ND	4.74
144	ND	4.31
151	ND	4.01
158	3	5.11
165	ND	4.62
172	ND	4.93
179	ND	5.37
207	ND	4.57
242	ND	3.71
249	ND	5.37
256	2	4.98
263	23	5.74
270	2	4.87
277	4	5.54
284	ND	4.67
291	ND	5.02
298	ND	4.70
305	ND	4.77
312	ND	4.71
319	ND	4.90
326	ND	4.64
337	ND	4.61

*ND: not detected. Detection limit = 2 MPN/mL.

Data for Figure 5-4:

Distance from substratum (μm)	NH_4^+-N (mg/L)	NO_3^--N (mg/L)	DO (mg/L)	pH
600	0.17	0.14	7.21	7.40
570	0.17	0.14	7.21	7.40
540	0.17	0.14	7.21	7.41
510	0.17	0.14	7.20	7.41
480	0.17	0.14	7.20	7.41
450	0.17	0.14	7.20	7.41
420	0.17	0.14	7.20	7.42
390	0.17	0.14	7.20	7.42
360	0.17	0.14	7.20	7.43
330	0.17	0.15	7.20	7.44
300	0.16	0.15	7.20	7.45
270	0.16	0.15	7.18	7.46
240	0.16	0.15	7.17	7.46
210	0.16	0.15	7.15	7.47
180	0.16	0.15	7.15	7.48
150	0.16	0.16	7.15	7.49
120	0.16	0.16	7.13	7.50
90	0.15	0.16	7.10	7.51
60	0.15	0.16	7.06	7.51
30	0.16	0.16	7.01	7.52
0	0.15	0.16	6.98	7.53

Data for Figure 5-5:

Distance from substratum (μm)	NH_4^+-N (mg/L)	NO_3^--N (mg/L)	DO (mg/L)	pH
600	0.55	0.16	6.08	8.62
570	0.53	0.17	6.06	8.68
540	0.53	0.19	6.05	8.73
510	0.52	0.21	6.06	8.79
480	0.52	0.23	6.06	8.83
450	0.51	0.25	6.05	8.87
420	0.50	0.26	6.06	8.91
390	0.48	0.28	6.05	8.94
360	0.47	0.30	6.04	8.97
330	0.44	0.32	6.02	9.00
300	0.43	0.34	5.99	9.02
270	0.41	0.36	5.95	9.05
240	0.41	0.37	5.90	9.07
210	0.40	0.37	5.80	9.09
180	0.38	0.38	5.65	9.11
150	0.38	0.39	5.49	9.12
120	0.37	0.39	5.30	9.13
90	0.36	0.39	5.04	9.15
60	0.36	0.39	4.68	9.15
30	0.35	0.39	4.45	9.16
0	0.35	0.39	4.30	9.17

Data for Figure 5-6:

Distance from substratum (μm)	NH_4^+-N (mg/L)	NO_3^--N (mg/L)	DO (mg/L)	pH
600	0.50	0.20	7.65	9.66
570	0.49	0.20	7.65	9.66
540	0.49	0.20	7.64	9.67
510	0.48	0.21	7.63	9.67
480	0.48	0.22	7.63	9.68
450	0.48	0.22	7.62	9.66
420	0.47	0.23	7.60	9.68
390	0.47	0.24	7.58	9.69
360	0.47	0.25	7.52	9.67
330	0.47	0.26	7.39	9.69
300	0.46	0.26	7.19	9.73
270	0.45	0.28	6.93	9.71
240	0.45	0.29	6.63	9.69
210	0.45	0.30	6.32	9.71
180	0.43	0.31	5.99	9.72
150	0.41	0.31	5.81	9.70
120	0.40	0.32	5.63	9.73
90	0.38	0.32	5.53	9.74
60	0.36	0.33	5.46	9.73
30	0.32	0.33	5.40	9.73
0	0.29	0.33	5.35	9.74

Appendix E – Data for Figures in Chapter 6

Data for Figure 6-3:

Depth under biofilm surface (μm)	DO (mg/L)	
	From biofilm surface toward substratum	Retreating back to biofilm surface
0	6.98	7.41
20	6.77	6.95
40	6.47	6.66
60	6.33	6.59
80	6.26	6.57
100	6.23	6.56
120	6.20	6.53